UNITED STATES DEPARTMENT OF THE INTERIOR

GEOLOGICAL SURVEY

TEST AND CALIBRATION OF THE DIGITAL WORLD-WIDE STANDARDIZED SEISMOGRAPH

by

Jon Peterson

and

Charles R. Hutt

Open-File Report 82-1087

1982

CONTENTS

		Page
1.	BACKGROUND	1
2.	BRIEF DESCRIPTION OF THE DWWSS SYSTEM	5
	2.1 General	5
	2.2 Amplifier Assembly	5
	2.3 Digital Recording System	8
3.	DWWSS SYSTEM TRANSFER FUNCTIONS	14
	3.1 General	14
	3.2 DWWSS Short-Period Transfer Functions	16
	3.2.1 General	16
	3.2.2 Short-Period (Benioff) Seismometer Transfer Function	16
	3.2.3 DWWSS Short-Period Amplifier	26
	3.2.4 Short-Period Digital System Transfer Function	29
	3.2.5 Short-Period Analog System Transfer Function	36
	3.2.6 Special Short-Period Digital System Transfer Function	39
	3.3 DWWSS Long-Period Transfer Functions	50
	3.3.1 General	50
	3.3.2 Seismometer-Preamplifier Transfer Function	50
	3.3.3 DWWSS Long-Period Analog System Transfer Function	51
	3.3.4 DWWSS Long-Period Digital System Transfer Function	58
	3.4 Intermediate-Period Transfer Function	63
4.	DWWSS CALIBRATION	75
	4.1 General	75
	4.2 Short-Period Calibration	78
	4.3 Long-Period Calibration	80
	4.4 Intermediate-Period Calibration	82
	4.5 DWWSS Calibration Stability	88
	4.6 Analysis of the Step Response	100
	4.6.1 General	100
	4.6.2 Fourier Transformation	103
	4.6.3 Least-Squares Fitting of the Step Response	105

CONTENTS CON'T

Page

5. DWWSS NOISE CHARACTERISTICS 121
   5.1 General 121
   5.2 DWWSS Short-Period Noise 122
   5.3 Intermediate-Period Noise 122
   5.4 Long-Period Noise 129
6. LINEARITY AND DISTORTION 142
   6.1 General 142
   6.2 Short-Period Test Results 146
   6.3 Intermediate-Period Test Results 151
   6.4 Long-Period Test Results 161
   6.5 Conclusions 161
7. REFERENCES 169

TABLES

Page

Table 1.1 List of DWWSSN stations 2
2.1 DWWSS digital header format 12
3.1 Nominal DWWSS short-period instrument parameters 23
3.2 Poles and zeros of trial seismometer transfer functions 24
3.3 Computed relative amplitude and phase in degrees for trial seismometer transfer functions 25
3.4 Differences between mean measured amplitude and phase and computed amplitude and phase for the DWWSS short-period amplifier using design parameters 31
3.5 The mean of measured short-period amplitudes taken from six DWWSS stations compared with amplitudes computed from the nominal short-period digital transfer function 32
3.6 Nominal DWWSS short-period digital system transfer function poles and zeros for an input of earth displacement 34
3.7 Poles, zeros, and sensitivity constants for short-period analog transfer functions for an input of displacement 38
3.8 Computed relative amplitude and phase angle for transfer functions: TFA25, TFA200, and TFW25 40

TABLES CON'T

		Page
Table 3.9	DWWSS special short-period instrument parameters	44
3.10	Poles, zeros, and sensitivity constant for nominal DWWSS special short-period digital system transfer function	47
3.11	Differences between Jamestown measured amplitudes and computed amplitudes	49
3.12	DWWSS long-period seismometer parameters	53
3.13	Differences between mean measured amplitude and phase and computed amplitude and phase for the DWWSS galvanometer driver	56
3.14	Poles, zeros, and sensitivity constant for the nominal DWWSS long-period analog system	57
3.15	The mean of measured DWWSS long-period analog amplitudes taken from 15 DWWSS systems compared with amplitudes computed from the nominal DWWSS long-period transfer function	59
3.16	Differences between mean measured amplitude and phase and computed amplitude and phase for the DWWSS long-period filter	64
3.17	Poles, zeros, and sensitivity constant for the DWWSS long-period digital system transfer function	65
3.18	The mean of measured DWWSS long-period digital amplitudes taken from 19 vertical and horizontal components compared with amplitudes computed from the nominal transfer function .	66
3.19	Differences between mean measured amplitude and phase and computed amplitude and phase for the DWWSS intermediate-period filter	71
3.20	Poles, zeros, and sensitivity constant for the nominal DWWSS intermediate-period transfer function	72
3.21	The mean of measured DWWSS intermediate-period amplitudes taken from 19 components compared with amplitudes predicted using the nominal transfer function	73
4.1	Magnifications, calibrating currents, and nominal peak amplitudes of the step response at the operating DWWSSN stations	76
4.2	Calibration constants used in the DWWSS system	77

1. BACKGROUND

During the past decade there has been steady progress in the modernization of the global seismograph network operated by the U.S. Geological Survey (USGS). The World-Wide Standardized Seismograph Network (WWSSN) has been augmented by new stations with advanced instrumentation, including the Seismic Research Observatories (SRO) and the modified High-Gain Long-Period (ASRO) stations. One goal in the modernization effort has been to improve signal resolution in the long-period band. A second goal has been to generate a global digital data base to support contemporary computer-based analysis and research.

In 1976, a Panel on Seismograph Networks was established by the Committee on Seismology of the National Academy of Sciences to review progress in network seismology and recommend actions that would lead to an improved global data base for seismology. One recommendation in the Panel report (Engdahl, 1977) called for upgrading selected WWSSN stations by the installation of digital recorders. This was viewed as an economical way of expanding the digital network, which had proven itself to be a very promising new tool for earthquake and explosion research. Funds for the development and assembly of 15 digital recorders were provided to the USGS by the Defense Advanced Research Projects Agency and an *ad hoc* panel of scientists was convened by the Committee on Seismology to advise the USGS on the selection of stations to be upgraded and on data recording requirements. A total of 19 digital World-Wide Standardized Seismograph (DWWSS) systems will be operational when all are installed. The additional systems were made available through purchase by the USGS and other organizations; for example, the University of Bergen purchased and installed a DWWSS-type recorder and agreed to furnish the USGS with the data. A list of operational and planned DWWSS network stations is given in Table 1.1.

As one might expect, the digital recorder turned out to be somewhat more sophisticated than the original concept. It was decided to record three components of long-period data continuously, three components of intermediate-period data in an event mode, and the vertical-component short-period data in and event mode (with the capability of adding short-period horizontal channels in the future). Special amplifiers were developed for use with the WWSS seismometers, and a 16-bit fixed-point analog-to-digital converter was chosen

Station	Location	Operating Organizations	Operational Date
AFI	Afiamalu, Western Samoa	Geophysics Division, D.S.I.R, New Zealand	15 May 1981
BDF	Brasilia, Brazil	University of Brasilia	8 June 1982
BER	Bergen, Norway	University of Bergen	10 August 1981
COL	College, Alaska	U.S. Geological Survey	6 January 1982
GDH	Godhavn, Greenland	Geodetic Institute, Denmark	26 August 1982
HON	Ewa Beach, Hawaii	National Weather Service	(1983)
JAS	Jamestown, California	University of California	1 October 1980
KEV	Kevo, Finland	University of Helsinki	14 October 1981
LEM	Lembang, Indonesia	Meteorological & Geophysical Institute	2 June 1982
LON	Longmire, Washington	University of Washington	1 October 1980
QUE	Quetta, Pakistan	Pakistan Meteorological Department	(1983)
SBA	Scott, Antarctica	Geophysics Division, D.S.I.R., New Zealand	(1984)
SCP	State College, Pennsylvania	Penn State University	29 January 1981
SLR	Silverton, South Africa	S.A. Geological Survey	24 October 1981
TAIF	Taif, Saudi Arabia	Directorate-General of Mineral Resources	(1983)
TAU	Hobart, Tasmania	University of Tasmania	10 June 1981
TOL	Toledo, Spain	Geophysical Observatory	3 November 1981
ZRN	Zaria, Nigeria	Ahmadu Bello University	(1983)

Table 1.1.--List of DWWSSN stations. Anticipated operational dates are shown in brackets.

to provide increased resolution (as opposed to a 16-bit gain-ranged encoder). The microprocessor-based digital recording systems were developed and assembled at the USGS Albuquerque Seismological Laboratory (ASL) and ASL-based technicians began installation at WWSSN stations in 1980.

The current and proposed locations of the DWWSSN stations, together with other stations in the Global Digital Seismograph Network (GDSN), are shown on the map in Figure 1.1. A system was operated at Albuquerque for about 18 months, serving as a test bed for evaluation studies. Although the network hardware has been available for some time, the installation of the DWWSSN has proceeded slowly. The National Science Foundation supported installation of six stations and the USGS is funding installation of most of the others; however, the network completion date is conjectural because of funding uncertainties.

The DWWSSN stations are supported with supplies and technical assistance from ASL (subject to availability of funds). Data recorded on magnetic tapes are mailed to ASL where they are reviewed for quality, then merged with other GDSN station data on the network-day tapes. Hoffman (1980) provides a description of the network-day tape format. Zirbes and Buland (1981) have developed and published user software for reading and interpreting the day tapes.

This report will serve several purposes. One is to provide nominal system transfer functions and calibration information that are needed in the analysis of DWWSSN data. A second purpose is to report on an evaluation of operating characteristics (calibration stability, noise levels, and linearity) that may limit the usefulness of the data and to determine if modifications may be needed to improve the data. It is not an exhaustive study in this respect. We continue to depend mostly on data user feedback to point out deficiencies and we solicit comments whenever anomalies are observed in the data.

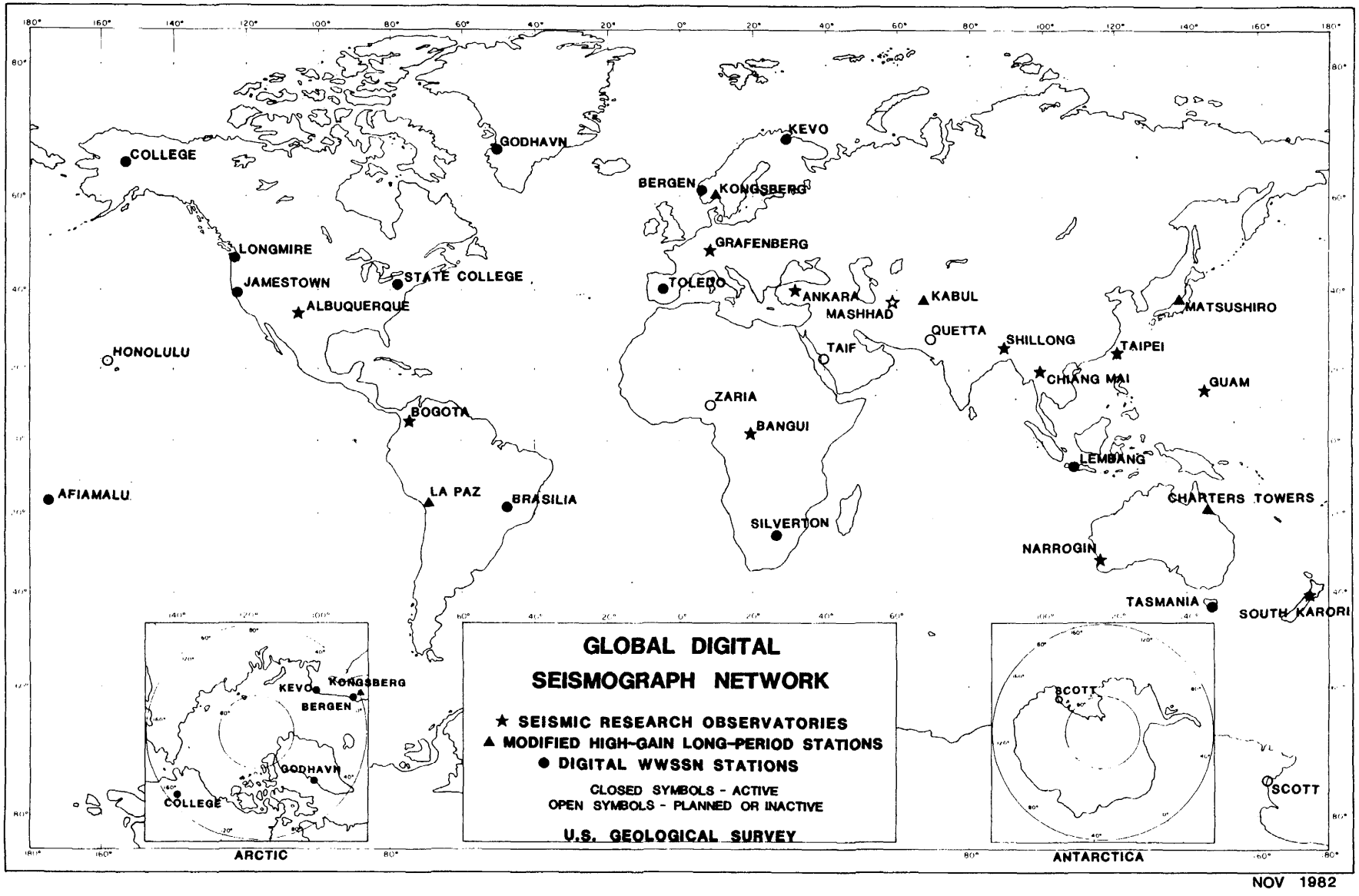

Figure 1.1.--Map locations of GDSN stations, including operational and planned DWWSSN stations.

2. BRIEF DESCRIPTION OF THE DWWSS SYSTEM

2.1 General

The DWWSS equipment was designed to interface with existing instrumentation used at WWSSN stations without interfering with the production of analog seismograms. Some changes in the analog recording have been necessary, but, for the most part, they have improved the quality of the seismograms. A block diagram of the DWWSS system is shown in Figure 2.1. The two major new components that have been installed at each DWWSSN station are the amplifier assembly and the digital recording system.

The WWSS Benioff seismometers have not been modified for use in the DWWSS system, nor have any other components of the short-period photographic recording system, except for adding a connector on the control box. The WWSS Sprengnether long-period seismometers have been modified in that the original 500-ohm signal coil and calibration coil have been replaced by two 5,000-ohm signal coils wired in series to increase the voltage sensitivity for digital recording. The calibration coil is wound on one of the signal coils. The higher impedance signal coils are not suitable as current sources for driving the WWSS long-period galvanometers; hence, suitably shaped and conditioned signals are derived from the preamplifiers and used to drive .75-second galvanometers to produce the long-period seismograms. This has an added advantage in that the long-period control boxes have been eliminated. These are known to be significant noise sources that often cause "trace stacking" on the seismograms at stations where temperature is not well controlled.

2.2 Amplifier Assembly

The amplifier assembly used in the DWWSS system was designed and manufactured by Teledyne Geotech, Inc. of Garland, Texas. The assembly (see Figure 2.2) consists of three wideband preamplifiers, three intermediate-period (IP) filters, three long-period (LP) filters, one short-period (SP) amplifier/filter combination, and a regulated power supply, all housed in an insulated and shielded enclosure. The inputs to the preamplifiers are derived from the vertical (Z), north (N), and east (E) long-period seismometers. The preamplifiers have a fixed voltage gain of 25 in the signal path used to drive the filters. They also provide signals from a low impedance current source to

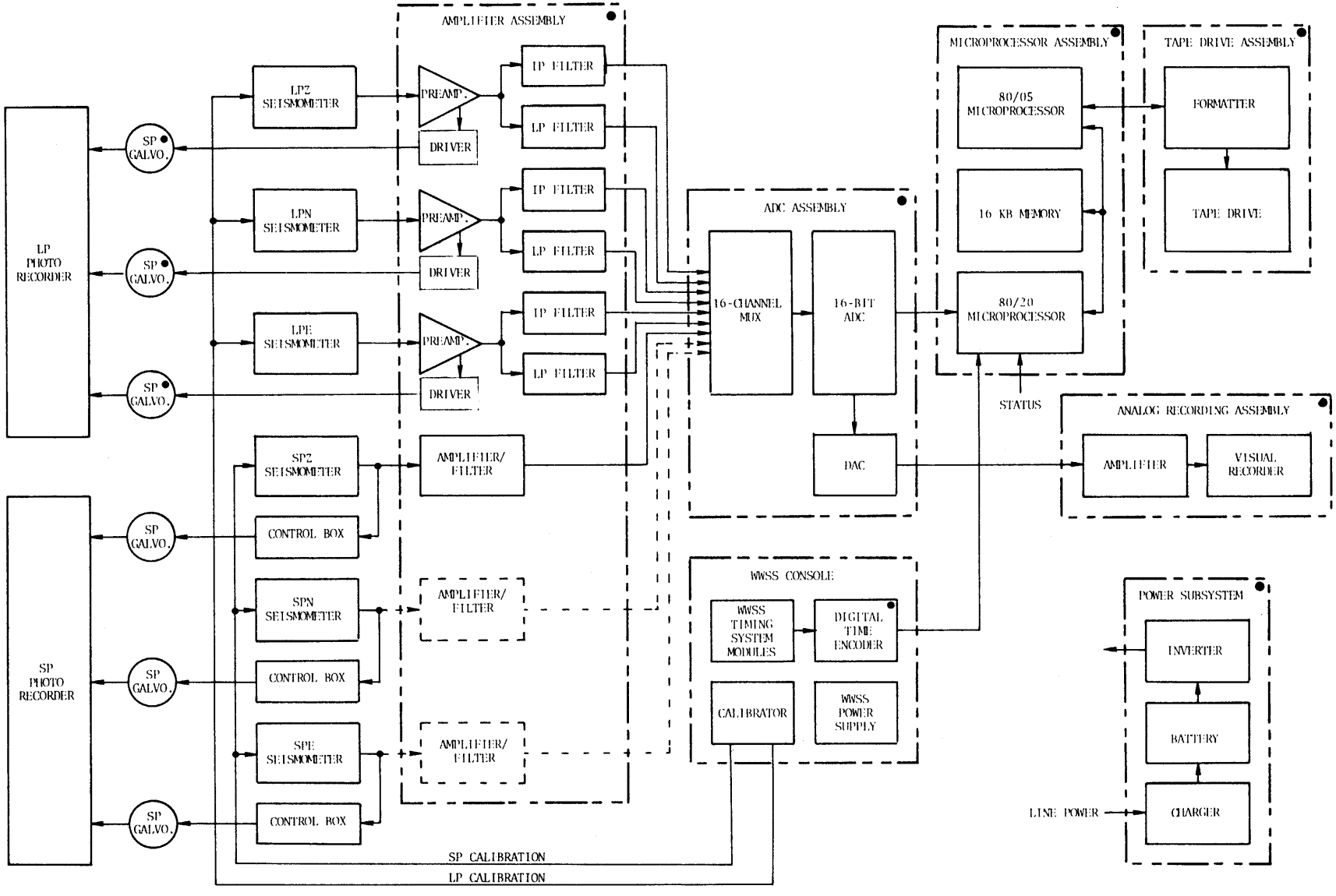

Figure 2.1.--Simplified block diagram of the DWWSS system. The bullets designate new equipment that is attached to the WWSS instrumentation.

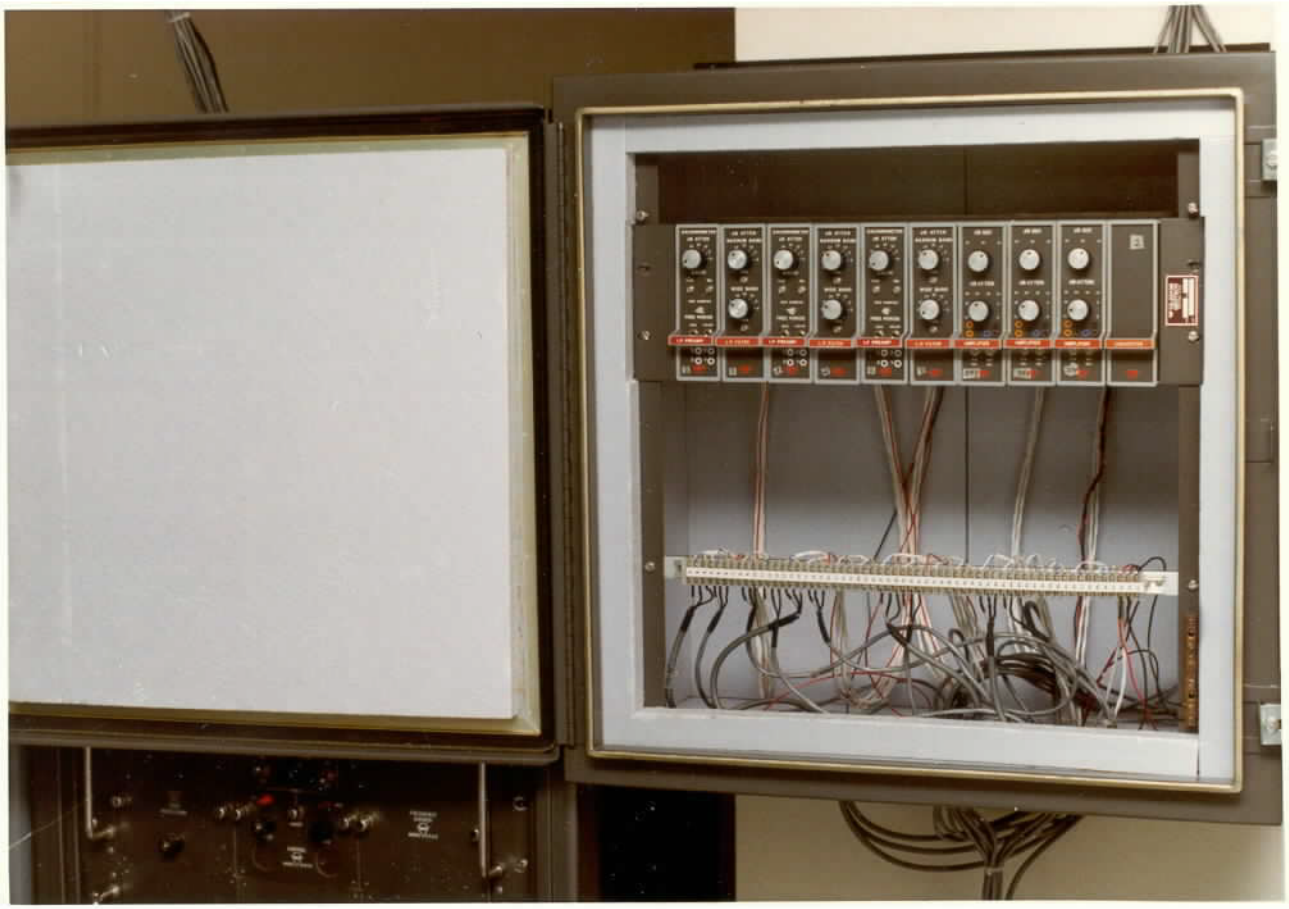

Figure 2.2.--DWWSS amplifier assembly. Three SP amplifiers are shown in this photograph although only one is normally used.

drive the galvanometers used to produce the analog seismograms. These signals are shaped by 100-second period high-pass filters to simulate the standard WWSS LP response. Controls are available to adjust photographic magnification to standard settings and to measure seismometer and galvanometer free periods. The preamplifier generates a TTL-compatible digital output signal when saturated, which is recorded as a clip-level flag in the header of the digital records.

The IP filter has a flat response from about 1 to 300 seconds period. Together with the seismometer, the response is approximately flat to an input of earth velocity from 1 to 15 seconds period. The filter has step and trim attenuators used to set the recorded sensitivity to a standard value. The LP narrowband filter, together with the seismometer, produces a response that is similar to the SRO LP response, peaking at 25 - 30 seconds period. The LP filter has step and trim attenuators and generates a TTL-compatible digital signal output when saturated. More detailed descriptions of the IP and LP filter response characteristics are given in Section 3.

The short-period amplifier is a modified version of the Teledyne Geotech Model 42.21 amplifier. The modification provides a low-pass filter corner at .75 seconds period to simulate the WWSS SP galvanometer so that the DWWSS short-period amplitude response matches the WWSS amplitude response. Normally, only one SP amplifier is provided and it is connected to the vertical-component seismometer. However, the DWWSS system can accommodate two additional SP channels for recording horizontal data. The SP amplifier is connected directly across the seismometer terminals in parallel with the control boxes. Although the amplifier input resistance is high compared with other circuit resistances, some modifications to the system transfer function are necessary to compensate for the circuit change (see Section 3.).

2.3 Digital Recording System

The digital recording system, designed at the Albuquerque Seismological Laboratory by H.E. Clark (1982, Digital Recording System For DWWSSN Stations, in prep.), consists of an analog-to-digital converter (ADC) assembly, a microprocessor assembly, tape-drive assembly, analog recording assembly, and power subsystem. The electro-mechanical programmer in the WWSS console is replaced by a new digital time encoder that generates a formatted time code for digital recording, timing signals for the WWSS recorders, and a visual display of the

Figure 2.3.--DWWSS digital recording system.

time of day for the station operator.

The amplified and filtered signals, having peak values of 10 volts, are sampled sequentially by a 16-channel multiplexer (MUX), then converted to 16-bit data words (15-bit fixed-point word plus a sign bit) by the ADC. Short-period signals are sampled 20 times each second, intermediate-period signals 10 times each second, and long-period signals once each second. The long-period data are recorded continuously, but only events detected in the short- and intermediate-period signals are recorded.

System control and recording functions, including event detection, reside in the software of the microprocessor assembly. The assembly consists of two 8-bit microprocessors and 16 kilobytes (Kb) of random access memory (RAM) wired on a common bus. One of the microprocessors contains the operating software for controlling the ADC, event detection, and data formatting; the second microprocessor is used primarily to clock the data into the tape recorder. The software is written on programmable read-only memories (PROMS), and the program can be replaced or modified by replacing the PROMs, which are mounted on plug-in sockets. The RAM serves as a buffer in formatting the data records prior to recording and for storing pre-event intermediate- and short-period data. The RAM holds two long-period records, three intermediate-period records, and three short-period records. This corresponds in time to 660 seconds of long-period data, 99 seconds of intermediate-period data, and 148.5 seconds of short-period data (49.5 seconds if three short-period channels are recorded.

The SP event detector operates on the vertical-component short-period signal. The peak-to-trough (PT) values of the signal are averaged over a short-term interval (adjustable from 8 to 32 PT values) and a long-term interval (adjustable from 64 to 128 PT values). Events in the signal are detected when the short-term average exceeds a turn-on threshold based on the long-term average. The turn-on algorithm is similar to the one used in the SRO system except that only PT amplitude values are averaged to reduce the memory required. Intermediate-period turn on is based on a simple threshold detector. Turn off occurs when the short-term average falls below the turn-on threshold over a preset delay time. The scaling factors, short-term averaging time, long-term averaging time, and intermediate-period threshold are set and adjusted at the station to optimize the event detection for local conditions. The current

event detector will be replaced by a new, more sophisticated event detection algorithm developed by J.N. Murdock and C.R. Hutt (1982, A Seismic Signal Onset and Phase Detector, in prep.).

The digital data are recorded on a nine-track synchronous magnetic tape recorder in IBM-compatible, 2's complement binary format with odd parity at a density of 1600 characters per inch. Tape length is 1200 feet, so a full tape will hold approximately 121 megabits of formatted data. With long-period data recorded continuously, and assuming that intermediate-period data are recorded 15% of the time, and short-period data are recorded 5% of the time, a reel of tape will record for about 10 days. The number of records on the tape is accumulated in a counter, and an alarm operates when the tape is 80% full and requires changing. This is rarely needed, as a routine has been established to change tapes at weekly intervals.

The data are recorded in 2,000-byte (1,000 data word) records. The first 20 bytes of a record, called the header, contain information and the next 1980 bytes contain data. There are separate records for the long-, intermediate-, and short-period data, and they can be differentiated by the sampling rate that is specified in the header. Separate components are multiplexed into each record; that is, the first three data words in a long-period record will contain the vertical, north, and east components in that order. The record header contains the station identification code, sampling rate, time of year to the nearest 10 milliseconds, number of channels being recorded, eight flag bits, event detector parameters, and an unspecified block of six bytes. The format of the header is given in Table 2.1. The format of the DWWSS data, as written on the network-day tapes, is described by Hoffman (1980).

A visual, heated-stylus drum recorder is furnished with each digital recording system. Analog signals for the recorder are derived from a digital-to-analog converter (DAC) that can be switched to monitor any of the channels for verifying operation of the amplifiers, filters, and ADC. In normal day-to-day operation, the recorder may be used to continuously record any channel selected by the station operator.

Operating parameters for the digital recording system are set on a digi-switch located on the front panel. Switchable parameters include channel selection for analog recording, event detection constants, and the tape recording mode (number of channels and continuous or event mode). A master key

BYTE 1:	10's Station ID	1's Station ID	(BCD)
BYTE 2:	10's Sample Rate	1's Sample Rate	(BCD)
BYTE 3:	1's Year	100's Days	(BCD)
BYTE 4:	10's Days	1's Days	(BCD)
BYTE 5:	10's Hours	1's Hours	(BCD)
BYTE 6:	10's Minutes	1's Minutes	(BCD)
BYTE 7:	10's Seconds	1's Seconds	(BCD)
BYTE 8:	100's Milliseconds	10's Milliseconds	(BCD)
BYTE 9:	10's No. of Channels	1's No. of Channels	(BCD)
BYTE 10:	Bit 0 (LSB) not specified		
	Bit 1-3 = Z, N, E amplifier saturation (set)		
	Bit 4 = event on (set)		
	Bit 5-6 not specified		
	Bit 7 = calibration on (set)		
BYTE 11:	Digiswitch No. 1		(hexadecimal)
BYTE 12:	Digiswitch No. 2		(hexadecimal)
BYTE 13:	Digiswitch No. 3		(hexadecimal)
BYTES 14-20:	Not specified.		

Note 1: Bit 4 in BYTE 10 is set only for short- and intermediate-period records.

Note 2: Digiswitch settings indicate event detection constants.

Note 3: Station ID numbers of 60 to 79 indicate DWWSSN format.

Table 2.1--DWWSS digital header format.

switch must be activated to initiate a new command so that the parameters cannot be changed inadvertently.

During normal operation, the digital recording system requires about 300 watts of power. The power subsystem consists of a charger, battery, and inverter. As originally designed, it has a backup capacity of about one hour if line power fails. As funds become available, the power subsystems are being upgraded with a backup capacity of about eight hours.

The components of the digital recording system, except for the digital time encoder, are contained in a single rack, which is normally located adjacent to the WWSS console. The amplifier assembly is separate and its location depends on the station layout.

3. DWWSS SYSTEM TRANSFER FUNCTIONS

3.1 General

A system transfer function describes the linear transformation of a signal between input and output. In seismic data analysis, it provides the key needed to remove the instrument response and recover information in terms of earth motion. A general expression for a seismograph in the Laplace domain is

$$R(s) = F(s) \cdot H(s)$$

where R(s) represents the recorded output, F(s) represents the force acting on the inertial mass, and H(s) is the system transfer function. If the forcing function is earth motion

$$F(s) = -MX(s)s^2 = -MV(s)s = -MA(s)$$

where X(s), V(s), and A(s) represent earth displacement, velocity, and acceleration, respectively, and M is the inertial mass. For a calibrating force applied through an electromagnetic calibrator attached to the mass

$$F(s) = G_c I(s)$$

where I(s) represents the current through the calibrator and G_c is the electrodynamic constant.

A general expression in the time domain for a seismograph is

$$r(t) = f(t) * h(t) \qquad (* = \text{convolution})$$

where r(t) is the time function of the recorded waveform, f(t) is the input of force, and h(t) is the system impulse response. Of particular interest in the development and testing of transfer functions are the waveforms that result from calibration. In the DWWSS system, sine-wave calibrations are used during installation and step functions are applied daily. For the sine-wave calibration

$$f(t) = G_c i_c \sin\omega t$$

where i_c is the peak calibrating current. For the step input

$$f(t) = \begin{cases} 0 & t \leq 0 \\ G_c i_c & t > 0 \end{cases}$$

Often, parameters in the transfer function can be fine-tuned by fitting synthetic waveforms to the recorded waveforms that result from calibration.

Transfer functions are usually represented by a ratio of polynomials in the Laplace domain as

$$H(s) = K_o \cdot \frac{s^m + a_{m-1}s^{m-1} + \ldots + a_2 s^2 + a_1 s + a_o}{s^n + b_{n-1}s^{n-1} + \ldots + b_2 s^2 + b_1 s + b_o} \qquad n \geq m$$

where K_o is a lumped sensitivity constant. On the GDSN network-day tapes, the transfer functions are tabulated by listing the roots of the denominator (poles), the roots of the numerator (zeros), and a constant that normalizes the computed amplitude to unity at a stated reference period. Absolute magnitudes for any period can then be determined from the product of the transfer function (converted to the frequency domain), its normalizing constant, and a listed sensitivity constant that is given in units of digital counts per micrometer of earth displacement at the normalizing period.

The transfer functions for the DWWSS system are derived in this report as follows. First, component transfer functions are developed based on a parametric analysis of component design. Magnitude and phase data computed from the trial transfer function often are compared with steady-state amplitude and phase measurements to insure that the modeling is correct and parameter values are accurately assigned. The system transfer function is derived from the product of the component transfer functions. At this point, damping and sensitivity values are adjusted by fitting synthetic calibration waveforms to required specification in much the same way as the installation personnel make the actual adjustments at the station. Finally, the system transfer function is fitted to mean values of sine-wave calibration data taken from all of the operating systems during their installation. The result is a "nominal" system transfer function that is listed on the network-day tape. It is possible that nominal transfer functions will be modified in the future so that the listed roots fit calibration data taken from individual components, especially if it appears that instrument parameters are drifting.

3.2 DWWSS Short-Period Transfer Functions

3.2.1 General

In the WWSS short-period seismograph, the coils of a Benioff variable-reluctance seismometer are connected to a 0.75 sec galvanometer through a control box that provides controls for attenuation and damping. In the DWWSS system, an amplifier has been placed across the seismometer terminals in parallel with the control box. The input resistance of the amplifier is high (4,000 ohms) compared to the other circuit resistances. Nevertheless, some adjustments to damping and attenuation are needed to compensate for the change in circuit resistance. With the amplifier connected, the seismometer damping is adjusted so that the seismometer-galvanometer combination produces an overshoot ratio of 1/17 (the same as for the WWSS) in response to a step of force applied through the calibration coil. Analog magnification is adjusted to standard values for the WWSS based on the peak amplitude of a step response recorded on the analog channel. These adjustments are interdependent and affect the values of important parameters in the transfer function.

3.2.2 Short-Period (Benioff) Seismometer Transfer Function

The derivation of a transfer function for the DWWSS Benioff seismometer is complicated by the high inductance of the signal coil, which generates a pole at mid band that cannot be ignored, and by the fact that there are two voltage generators in the circuit -- the seismometer and the galvanometer. An equivalent circuit for the seismometer-galvanometer combination is illustrated in Figure 3.1.

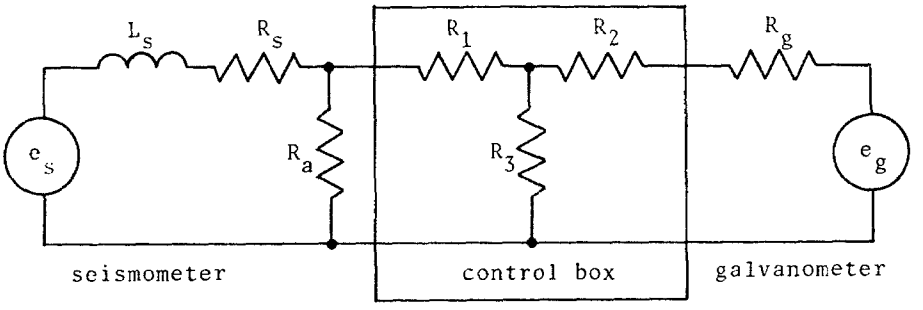

Figure 3.1.--Equivalent circuit for the DWWSS short-period seismograph.

In the figure

L_s = inductance of seismometer coil

R_s = resistance of seismometer coil

R_a = input resistance of SP amplifier

R_g = resistance of galvanometer coil

R_1, R_2, R_3 are equivalent T-network resistances of control box

In general, R_1, R_2, and R_3 are unknown, although their values can be computed from input and output measurements taken on the control box. Using the notation $R_1//R_2$ to mean "R_1 parallel with R_2" = $R_1R_2/(R_1+R_2)$, let

R_{11} = total resistance seen by the seismometer

$= R_s+R_a//(R_1+R_3//(R_2+R_g))$

R_{22} = total resistance seen by galvanometer

$= R_2+R_g+R_3//(R_1+R_a//R_s)$

R_x = forward resistance looking into control box with galvanometer connected

$= R_1+R_3//(R_2+R_g)$

R_y = resistance seen by galvanometer when seismometer is out of the circuit

$= R_2+R_g+R_3//(R_1+R_a)$

i_{ss} = current in seismometer circuit due to voltage generated in the seismometer

i_{sa} = current into amplifier due to seismometer voltage

i_{sg} = current through galvanometer coil due to seismometer voltage

i_{gg} = current through galvanometer due to galvanometer voltage

i_{gs} = current in seismometer coil due to galvanometer voltage

i_{ga} = current into amplifier due to galvanometer voltage

and define the following parameters

α = ratio of seismometer inductance to total resistance in seismometer circuit

$= L_s/R_{11}$

κ_{cb} = forward current gain through control box

$= R_3/(R_2+R_3+R_g)$

κ_{sg} = forward current gain between seismometer and galvanometer

$= i_{sg}/i_{ss}$

Summation of voltage drops in the three-loop network shown in Figure 3.1 leads to the following Laplace subsidiary equations for currents flowing in the network due to the voltage generated in the seismometer coil:

$$I_{ss}(s) = \frac{E_s(s)}{R_{11}(\alpha s+1)} \tag{3.1}$$

$$I_{sg}(s) = \frac{R_a \kappa_{cb} I_{ss}(s)}{R_a+R_x} = \kappa_{sg} I_{ss}(s) \tag{3.2}$$

$$I_{sa}(s) = \frac{R_x I_{ss}(s)}{R_a+R_x} \tag{3.3}$$

and due to the voltage generated in the galvanometer coil:

$$I_{gg}(s) = \frac{E_g(s)\alpha s}{R_y(\alpha s+1)} + \frac{E_g(s)}{R_{22}(\alpha s+1)} \tag{3.4}$$

$$I_{gs}(s) = \frac{\kappa_{sg} E_g(s)}{R_{11}(\alpha s+1)} \tag{3.5}$$

$$I_{ga}(s) = \frac{\kappa_{sg}(\alpha s+R_s/R_{11})E_g(s)}{R_a(\alpha s+1)} \tag{3.6}$$

A block diagram of the DWWSS short-period seismograph, showing signal paths and boxes representing elemental transfer functions, is shown in Figure 3.2. In the diagram, F(s) represents an arbitrary input forcing function, either earth motion or calibration, R(s) represents the signal deflection on a photographic record, and $E_i(s)$ represents a voltage into the amplifier. The first summing junction represents the inertial mass of the seismometer. The three forces acting on the mass are due to F(s), electromagnetic damping, $F_d(s)$, and the reaction of the galvanometer, $F_r(s)$. (The function argument, s, has been left out of the transfer functions in the figure to save space.)

The transfer function labeled H_1 converts the relative mass-frame motion

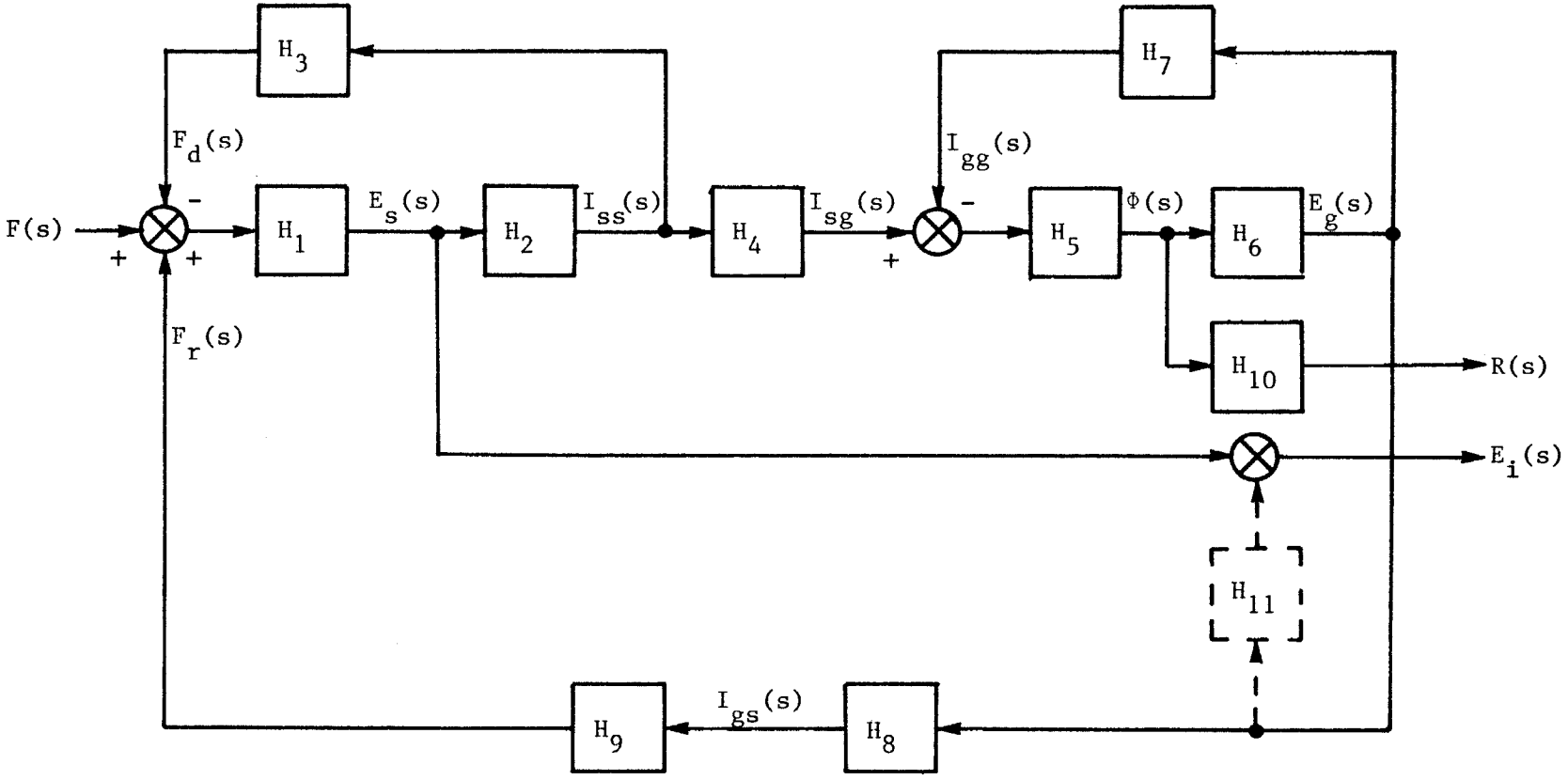

Figure 3.2.--Block diagram of signal paths in the DWWSS short-period seismograph.

in the seismometer to a voltage across the seismometer coil

$$H_1 = \frac{G_s s}{M(s^2 + 2\lambda_{so}\omega_s s + \omega_s^2)}$$

where G_s is the electrodynamic constant of the signal transducer, ω_s is the natural angular frequency of the seismometer, and λ_{so} is the open-circuit (air) damping ratio of the seismometer.

The transfer function labeled H_2 is found from equation 3.1.

$$H_2 = \frac{I_{ss}(s)}{E_s(s)} = \frac{1}{R_{11}(\alpha s+1)}$$

The current flowing in the seismometer signal coil generates a damping force equal to $G_s \cdot I_{ss}(s)$. Therefore,

$$H_3 = G_s$$

The transfer function labeled H_4 equals $I_{sg}(s)/I_{ss}(s)$. By an earlier definition,

$$H_4 = \kappa_{sg}$$

The transfer function labeled H_5 represents the galvanometer, which converts the current through the coil to an angular displacement, $\Phi(s)$.

$$H_5 = \frac{G_g}{K_g(s^2 + 2\lambda_{go}\omega_g s + \omega_g^2)}$$

where G_g is the electrodynamic constant of the galvanometer, K_g is the coil moment of inertia, ω_g is the natural angular frequency of the galvanometer, and λ_{go} is the open-circuit damping ratio.

The voltage generated when the galvanometer coil is in motion is equal to the product of the coil angular velocity and the electrodynamic constant.

$$H_6 = \frac{E_g(s)}{\Phi(s)} = G_g s$$

An expression for the current flowing in the galvanometer circuit due to $E_g(s)$ was derived in the circuit analysis (equation 3.4).

$$H_7 = \frac{I_{gg}(s)}{E_g(s)} = \frac{\alpha s}{R_y(\alpha s+1)} + \frac{1}{R_{22}(\alpha s+1)}$$

A small fraction of the current generated in the galvanometer circuit flows through the seismometer coil. From equation 3.5,

$$H_8 = \frac{I_{gs}(s)}{E_g(s)} = \frac{\kappa_{sg}}{R_{11}(\alpha s+1)}$$

The current, $I_{gs}(s)$, generates a force on the mass of the seismometer proportional to the electrodynamic constant of the signal coil, so

$$H_9 = \frac{F_r(s)}{I_{gs}(s)} = G_s$$

The transfer function labeled H_{10} represents the optical lever between the galvanometer mirror and the photographic recorder.

$$H_{10} = 2r_o$$

where r_o is the distance between the mirror and the drum.

A fraction of the galvanometer voltage will appear at the input to the amplifier. From equation 3.6,

$$H_{11} = \frac{I_{ga}(s)R_a}{E_g(s)} = \frac{\kappa_{sg}(\alpha s+R_s/R_{11})}{\alpha s+1}$$

This path is shown dashed in Figure 3.2 because it will be ignored. For nominal circuit values and instrument parameters, and computed for an angular displacement of 1 radian at a frequency of 1 Hz,

$$I_{ga}(s)/I_{sa}(s) \simeq 6 \times 10^{-4}$$

The signal into the amplifier from the galvanometer is more than 60 dB below the signal level into the amplifier due to the seismometer.

The seismometer transfer function that relates a voltage into the amplifier as a function of an external force applied to the mass has the form

$$\frac{E_i(s)}{F(s)} = \frac{H_1(1+H_5H_6H_7)}{(1+H_1H_2H_3)(1+H_5H_6H_7) - H_1H_2H_4H_5H_6H_8H_9}$$

By inserting the parametric expressions for the elemental transfer functions and rearranging slightly, we get

$$\frac{E_i(s)}{F(s)} = \frac{\frac{G_s s}{M} \cdot \left(s^2+2\lambda_{go}\omega_g s+\omega_g^2 + \frac{\alpha G_g^2 s^2}{K_g R_y(\alpha s+1)} + \frac{G_g^2 s}{K_g R_{22}(\alpha s+1)}\right)}{\left((s^2+2\lambda_{so}\omega_s s+\omega_s^2)(\alpha s+1) + \frac{G_s^2 s}{MR_{11}}\right)\left(s^2+2\lambda_{go}\omega_g s+\omega_g^2 + \frac{\alpha G_g^2 s^2}{K_g R_y(\alpha s+1)} + \frac{G_g^2 s}{K_g R_{22}(\alpha s+1)}\right) - \frac{G_s^2 \kappa_{sg}^2 G_g^2 s^2}{MK_g R_{11}^2(\alpha s+1)}} \qquad (3.7)$$

If the reaction of the galvanometer voltage on the seismometer (the negative term in the denominator) can be ignored, the seismometer transfer function will reduce to the much simpler form

$$\frac{E_i(s)}{F(s)} = \frac{G_s s/M}{(s^2 + 2\lambda_{so}\omega_s s + \omega_s^2)(\alpha s+1) + \frac{G_s^2 s}{MR_{11}}} \quad \text{volts/newton} \qquad (3.8)$$

If not, separate transfer functions will be needed for each magnification setting since the negative term is a function of control box attenuation.

The full and reduced expressions for the transfer function can be compared quantitatively by inserting values for parameters and computing amplitude and phase over the period band of interest. The nominal instrument parameters for the DWWSS short-period seismograph are listed in Table 3.1. The circuit parameters R_{11}, R_{22}, R_y, and κ_{sg} vary as a function of seismograph magnification. For magnification settings of 25,000 and 200,000, these parameters were measured and found to be (in one test system) as listed below.

	--25,000--	--200,000-
R_{11}	176.6 ohms	174.0 ohms
R_{22}	159.0 ohms	152.0 ohms
R_y	159.0 ohms	162.5 ohms
κ_{sg}	.0310	.2400

The poles and zeros of the transfer functions for magnifications of 25,000 (TF25) and 200,000 (TF200) are listed in Table 3.2. These were derived from equation 3.7 using the parameters given above. Also listed in Table 3.2 are the poles and zeros for the reduced transfer function (TFR) derived from equation 3.8. Amplitude and phase values computed from the three transfer functions are listed in Table 3.3, together with differences between results obtained from the full expression for the transfer function and the reduced expression.

Parameter	Value	Units
M	107.5	kilograms
R_s	64.6	ohms
L_s	6.8	henrys
G_s	350.0	volt-seconds/meter
ω_s	6.283	radians/second
λ_{so}	.0088	
K_g	1.7×10^{-10}	kilogram-meters^2
R_g	77.5	ohms
G_g	6.68×10^{-4}	newton-meters/ampere
ω_g	8.378	radians/second
λ_{go}	.020	
R_a	4000	ohms
r_o	1.0	meter
G_c	2.0	newtons/ampere

Table 3.1.--Nominal DWWSS short-period instrument parameters.

Trial Transfer Functions for SP Seismometer

	TF25	TF200	TFR
Poles:	s = -4.029 ± 6.373j	-3.599 ± 6.428j	-4.033 ± 6.370j
	s = -18.07	-14.97 ± 5.886j	-18.03
	s = -9.182	-5.054	
	s = -7.558	-25.57	
	s = -25.94		
Zeros:	s = -9.260	-12.27	
	s = -7.580	-6.204	
	s = -25.97	-23.60	
	s = 0	0	0

Table 3.2.--Poles and zeros of trial seismometer transfer functions: TFR (reduced transfer function), TF25 (25,000 magnification), and TF200 (200,000 magnification). Input is a force acting on the mass and output is a voltage at the input to the amplifier.

	TFR		TF25				TF200			
PERIOD (SECONDS)	AMPLITUDE (RELATIVE)	PHASE (DEG.)	AMPLITUDE (RELATIVE)	DIFF. (PERCENT)	PHASE (DEG.)	DIFF. (DEG.)	AMPLITUDE (RELATIVE)	DIFF. (PERCENT)	PHASE (DEG.)	DIFF. (DEG.)
0.10	.03988	-156.6	.03959	0.7	-156.7	0.1	.03848	3.8	-156.8	0.2
0.15	.08638	-145.5	.08578	0.7	-145.6	0.1	.08334	3.5	-145.8	0.3
0.20	.14650	-134.9	.14550	0.7	-135.1	0.2	.14190	3.4	-135.2	0.3
0.30	.29550	-115.4	.29380	0.6	-115.6	0.2	.28550	3.4	-115.6	0.2
0.40	.46840	-97.4	.46620	0.5	-97.6	0.2	.45050	3.8	-97.7	0.3
0.50	.65030	-79.8	.64790	0.4	-80.1	0.3	.62500	3.9	-80.7	0.9
0.60	.82070	-62.2	.81850	0.3	-62.5	0.3	.79510	3.1	-63.6	1.4
0.80	1.02300	-27.9	1.02200	0.1	-28.2	0.3	1.01900	0.4	-29.1	1.2
1.00	1.00000	-0.3	1.00000	---	-0.6	0.3	1.00000	---	-0.1	0.2
1.50	.71090	36.2	.71170	0.1	36.0	0.2	.69310	2.5	37.1	0.9
2.00	.52360	51.8	.52450	0.2	51.6	0.2	.50650	3.3	52.2	0.4
3.00	.34090	65.5	.34160	0.2	65.4	0.1	.32980	3.2	65.6	0.1
5.00	.20150	75.6	.20200	0.2	75.5	0.1	.19560	2.9	75.5	0.1
10.00	.10000	82.9	.10030	0.3	82.8	0.1	.09734	2.7	82.8	0.1
20.00	.04993	86.5	.05007	0.3	86.4	0.1	.04862	2.6	86.4	0.1
40.00	.02496	88.2	.02502	0.3	88.2	0.0	.02430	2.6	88.2	0.0
60.00	.01664	88.8	.01668	0.2	88.8	0.0	.01620	2.6	88.8	0.0

Table 3.3.--Computed relative amplitude and phase in degrees for trial seismometer transfer functions: TFR (reduced transfer function), TF25 (25,000 magnification), and TF200 (200,000 magnification). Differences are with respect to TFR; amplitude differences in percent, phase differences in degrees.

Clearly, the differences are negligible between the reduced transfer function and the transfer function for a magnification of 25,000, and this would be true for any magnifications less than 25,000. The amplitude differences between the reduced transfer function and the transfer function for a magnification of 200,000 are less than 4% over the measured band. While this error is not negligible, it is not large enough to justify separate seismometer transfer functions in developing a nominal (average) system transfer function, which is fitted to the mean value of all calibration data. If separate system transfer functions are derived and listed for individual components of the DWWSSN in the future, it may be appropriate to account for seismometer response as a function of magnification setting. Until then, the reduced seismometer transfer function will be used to describe all of the DWWSSN short-period (Benioff) seismometers. Seismometer response to earth displacement, computed using the reduced transfer function, is shown graphically in Figure 3.3.

3.2.3 DWWSS Short-Period Amplifier

The short-period amplifier used in the DWWSS system is a modified version of the Teledyne Geotech Model 42.21 amplifier and is fully described in its accompanying manual (Teledyne Geotech, 1980a). A block diagram of the amplifier is shown in Figure 3.4. The frequency dependent transfer characteristics of the amplifier are established by three filters. There is a second-order high-pass filter, cornered at .01 Hz, to eliminate offset and a second-order low-pass filter, cornered at 25 Hz, to reduce high frequency noise at the input. The in-band response is shaped by a second-order low-pass filter having a corner period at 0.75 sec and a damping ratio of 1.0. This filter simulates the response of the WWSS short-period galvanometer so that the DWWSS short-period digital channel will have a response similar to the WWSS short-period seismograph.

The transfer function for the amplifier, based on design parameters (given in Figure 3.4), is

$$\frac{E_i(s)}{E_o(s)} = \frac{1.751 \times 10^6 G_{spa} s^2}{(s^2+.08884s+.003948)(s^2+222.1s+24680)(s^2+16.83s+70.94)} \qquad (3.9)$$

where G_{spa} is the preamplifier gain. The roots of the polynomials are listed below.

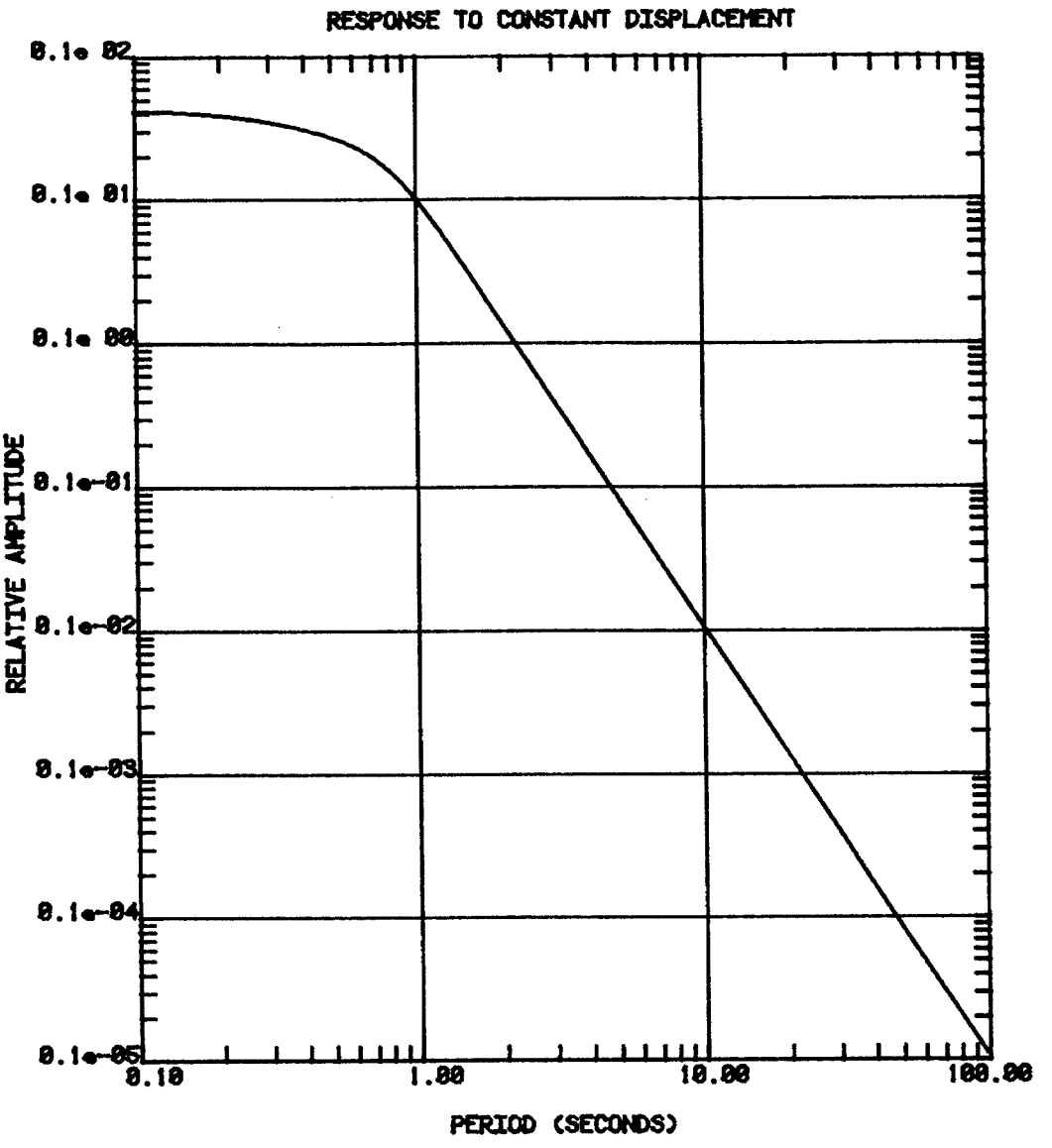

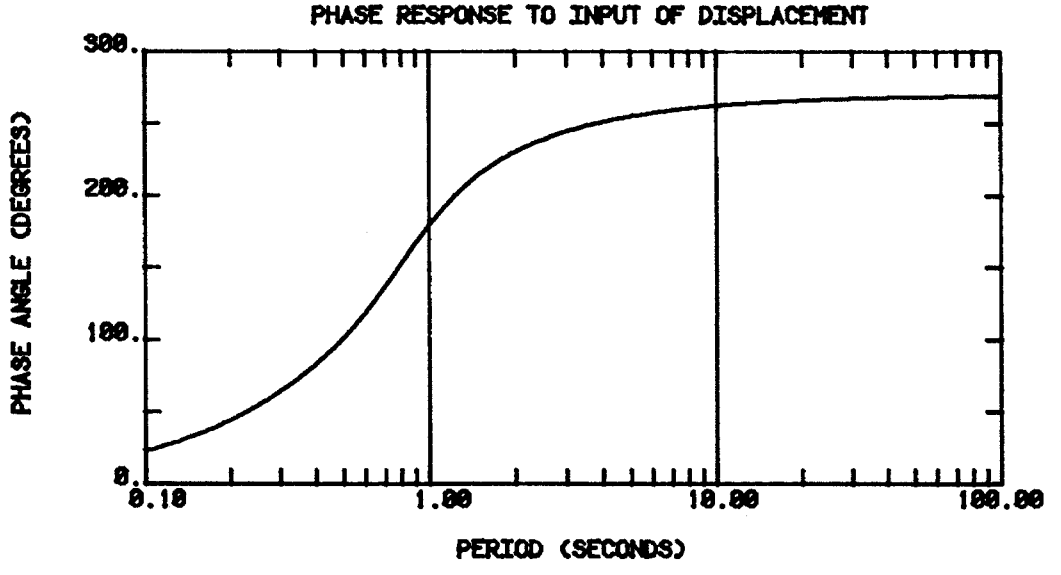

Figure 3.3.--Relative amplitude and phase angle of the DWWSS short-period seismometer (Benioff) computed from the reduced transfer function (TFR).

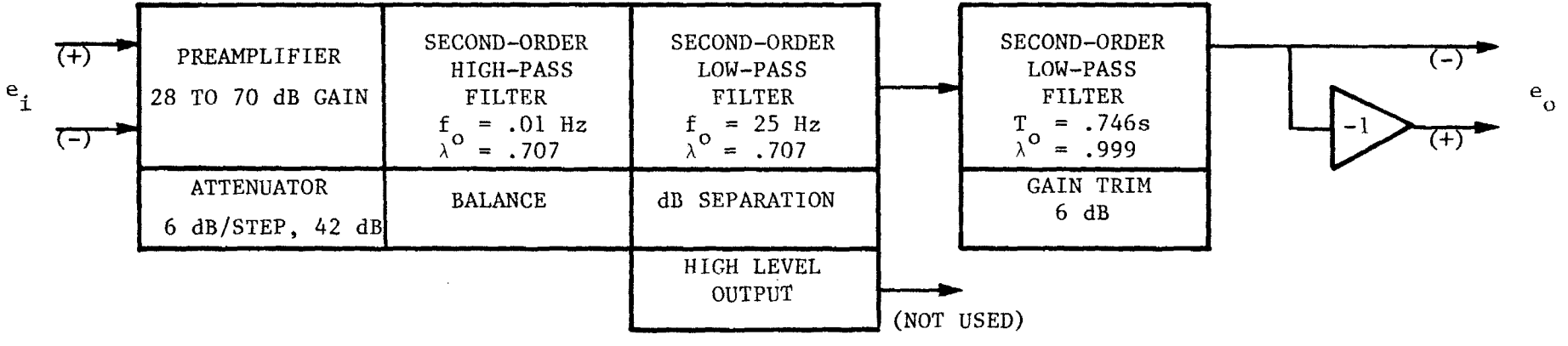

Figure 3.4.--Block diagram of DWWSS short-period amplifier showing active components (after Teledyne Geotech, 1980a).

Poles: $s = -.04442 \pm .04444j$ Zeros: $s^2 = 0$

$s = -111.10 \pm 111.10j$

$s = -8.4150 \pm .35700j$

Computed amplitude and phase vs. period are shown in Figure 3.5.

Steady-state amplitude and phase measurements were made on 11 short-period amplifiers. These measurements, and all similar laboratory measurements described in this report, were taken using a two-channel digital oscilloscope. The 12-bit digitizer in the oscilloscope permits a measurement precision of .05%. The phase angle is computed from the phase delay between input and output waveforms. During the tests the digitizing rate is set such that 512 samples per cycle are recorded, so that the precision of the phase measurements is 0.7^{o}. In both amplitude and phase measurements, the precision is affected by the presence of noise and is generally less at the band edges where signal-to-noise ratios are lower.

The amplifier measurements showed very slight differences between units. In the band from 0.1 to 60 seconds period, maximum amplitude deviation from the mean was 2% and the maximum phase deviation from the mean was 6.4^{o}, both maximums occurring at the band edges. The differences between the mean measured amplitudes and phase angles and the computed amplitudes and phase angles, using the transfer function above, are shown in Table 3.4 for the period band from 0.1 to 10 sec. Agreement is excellent, so no attempt was made to achieve a better fit between measured and computed data by adjusting parameter values in the transfer function.

3.2.4 Short-Period Digital System Transfer Function

A transfer function for the DWWSS SP digital system, in units of volts per meter, is derived from the product of the seismometer transfer function (equation 3.8), the amplifier transfer function (equation 3.9), and $-Ms^2$, which converts a displacement of the seismometer frame to a force on the mass.

Relative amplitudes computed from the system transfer function are compared in Table 3.5 with the mean measured amplitudes taken from six DWWSS systems. The scatter in the measured data is to be expected as the measurements are taken in the presence of noise. Also, the magnifications at these stations varied from 12,500 to 200,000, and, as we have shown, this affects the seismometer response to some small extent. In adjusting the system transfer function

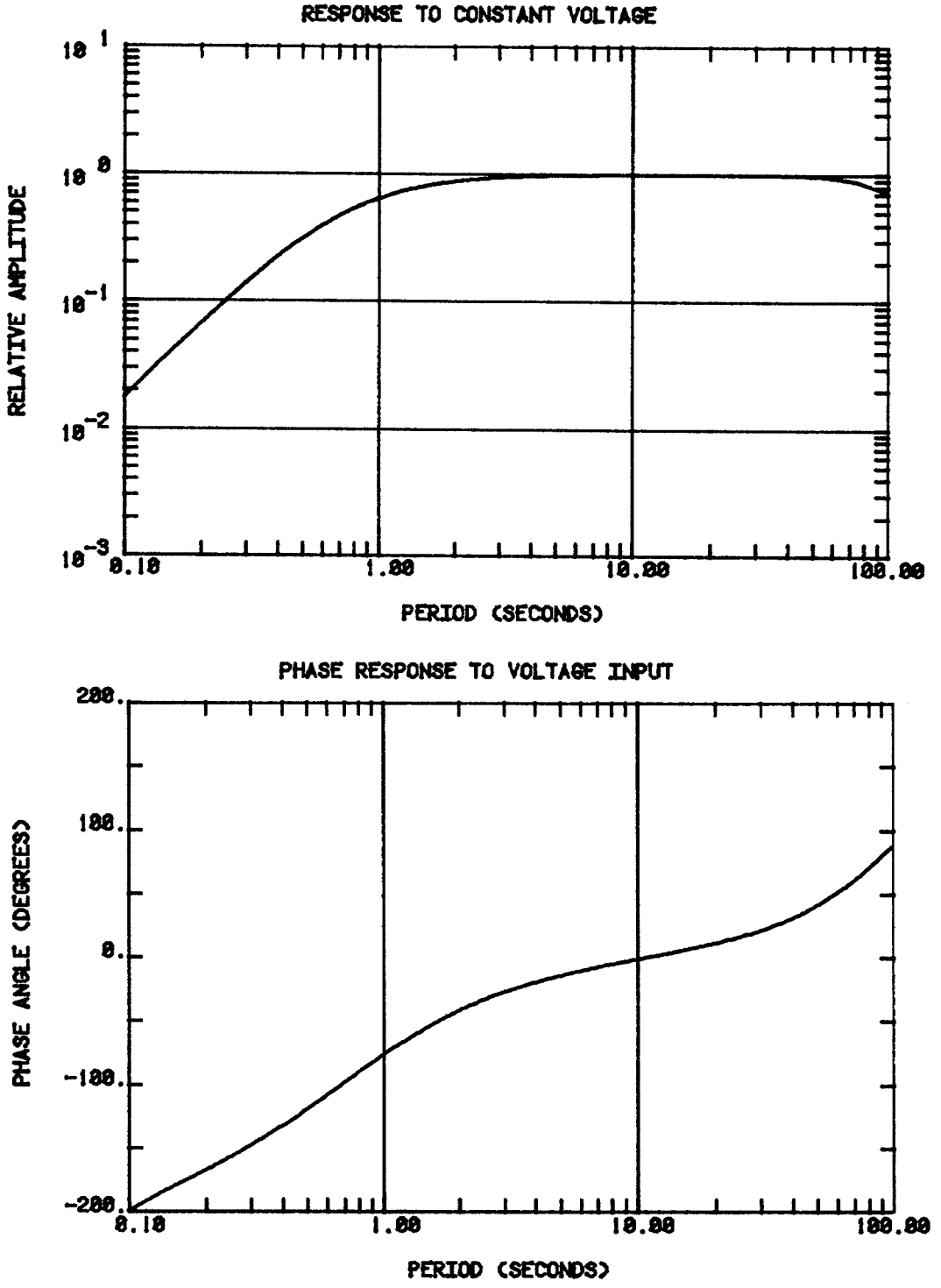

Figure 3.5.--Amplitude and phase response characteristics of DWWSS short-period amplifier using design parameters.

PERIOD (SECONDS)	MEASURED AMPLITUDE (RELATIVE)	COMPUTED AMPLITUDE (RELATIVE)	DIFFERENCE (PERCENT)	MEASURED PHASE ANGLE (DEGREES)	COMPUTED PHASE ANGLE (DEGREES)	DIFFERENCE (DEGREES)
0.198	0.1036	0.1027	0.8	-158.7	-166.7	8.0
0.331	0.2579	0.2570	0.3	-137.1	-141.7	4.6
0.497	0.4806	0.4805	0.0	-115.7	-118.8	3.1
0.661	0.6889	0.6876	0.2	-99.0	-101.3	2.3
0.793	0.8293	0.8294	0.0	-88.1	-89.9	1.8
0.994	1.0000	1.000	0.0	-74.4	-76.2	1.8
1.243	1.1480	1.1490	0.1	-62.2	-63.5	1.3
1.655	1.3000	1.2990	0.1	-48.1	-49.1	1.0
1.987	1.3710	1.3690	0.1	-40.2	-41.2	1.0
2.482	1.4350	1.4330	0.1	-32.4	-32.7	0.3
4.971	1.5280	1.5280	0.0	-13.2	-13.7	0.5
9.947	1.5520	1.5530	0.1	0.4	-0.8	1.2

Table 3.4.--Differences between mean measured amplitude and phase and computed amplitude and phase for the DWWSS short-period amplifier using design parameters.

PERIOD (SECONDS)	MEAN MEASURED AMPLITUDE (RELATIVE)	STANDARD DEVIATION (PERCENT)	COMPUTED AMPLITUDE (RELATIVE)	DIFFERENCE (PERCENT)
0.2	0.3718	1.3	0.3841	3.2
0.3	0.7111	2.1	0.7242	1.8
0.4	1.0240	2.5	1.0440	1.9
0.5	1.2840	2.3	1.2900	0.5
0.6	1.4260	1.8	1.4270	0.1
0.7	1.4580	0.9	1.4390	1.3
0.8	1.3570	0.9	1.3410	1.2
1.0	1.0000	-	1.0000	-
1.5	0.3902	2.1	0.3972	1.8
2.0	0.1777	3.5	0.1815	2.1
3.0	.05587	3.9	.05666	1.4
4.0	.02397	4.3	.02433	1.5
5.0	.01246	4.5	.01256	0.8
6.0	.007316	4.7	.007301	0.2
8.0	.003068	4.9	.003094	0.8
10.0	.001602	5.1	.001587	0.9

Table 3.5.--The mean of measured short-period amplitudes taken from six DWWSS stations compared with amplitudes computed from the nominal short-period digital transfer function (poles and zeros listed in Table 3.6).

to fit the mean of measured points, it was found that a good fit could be obtained by letting G_s equal 342 volt-seconds/meter, rather than its design value of 350 given in Table 3.1. This was the only parameter adjusted.

The poles and zeros for the nominal DWWSS short-period digital transfer function are listed in Table 3.6. Computed response functions are plotted in Figure 3.6. When the amplitude response computed from the transfer function (not normalized as in the figure) is multiplied by the constant K_o (given in the table), the product will be in units of digital counts per meter of displacement.

$$K_o = \frac{G_s}{\alpha} \cdot K_{spa} \cdot G_{spa} \cdot K_{adc} = 1.123 \times 10^{17}$$

where $\alpha = L_s/R_{11} = .03851$ seconds/radian

$G_s = 342$ volt-seconds/meter (seismometer electrodynamic constant)

$K_{spa} = 1.751 \times 10^6$ (SP amplifier constant)

$K_{adc} = 3277$ digital counts/volt (ADC constant)

The sensitivity of the seismograph is set by adjusting the preamplifier gain (G_{spa}). Nominal gain is 2204 volts/volt.

The time response of a seismograph to an impulse of force on the inertial mass is given by

$$h(t) = \mathcal{L}^{-1}\{K_i \cdot H(s)\}$$

where K_i is a lumped constant of the transfer function for an input of force.

$$K_i = \frac{G_s}{\alpha M} \cdot K_{spa} \cdot G_{spa} \cdot K_{adc} = 1.045 \times 10^{15}$$

Impulse responses are computed in this report by taking the inverse fast Fourier transform (FFT) of the Fourier components of the transfer function. The step response, g(t), can be computed from

$$g(t) = f_s(t) * h(t)$$

where $f_s(t) = G_c I_c$ when applied and 0 otherwise. However, it is usually faster to compute the step response from

$$g(t) = \mathcal{L}^{-1}\{G_c I_c \cdot K_i \cdot H(s)/s\}$$

Poles	Zeros
$s = -4.033 \pm 6.370j$	$s^3 = 0$
$s = -18.03$	
$s = -.04442 \pm .04444j$	$s^2 = 0$
$s = -111.10 \pm 111.10j$	
$s = -8.4150 \pm .35700j$	

$$K_o = 1.123 \times 10^{17}$$

Table 3.6.--Nominal DWWSS short-period digital system transfer function poles and zeros for an input of earth displacement. When the transfer function is evaluated at a specific frequency and multiplied by K_o, the result will be in units of digital counts per meter of earth displacement.

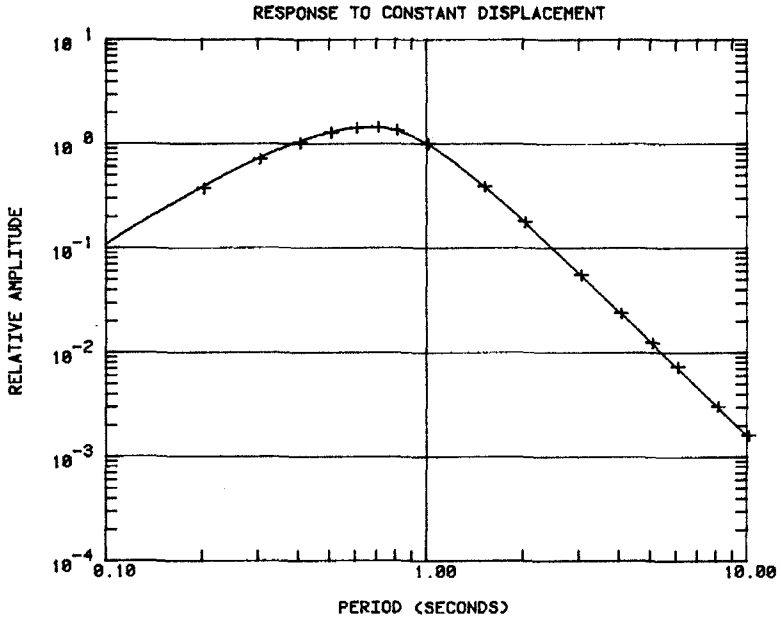

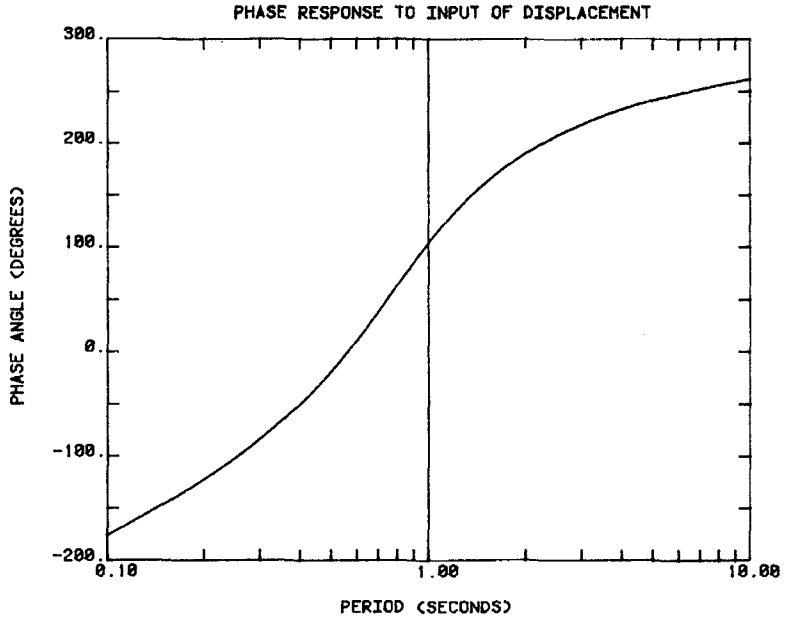

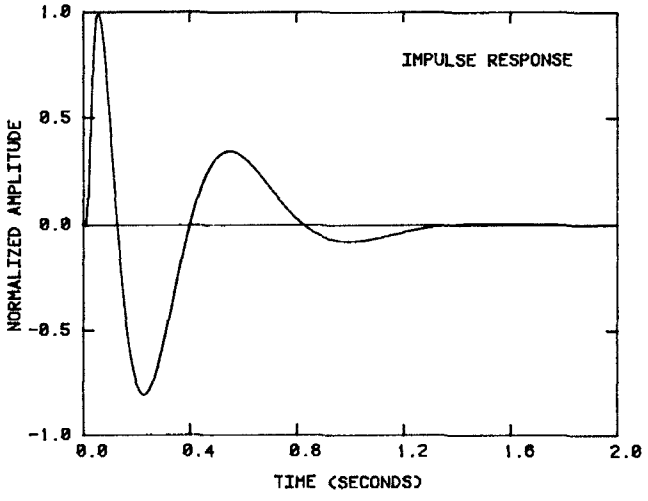

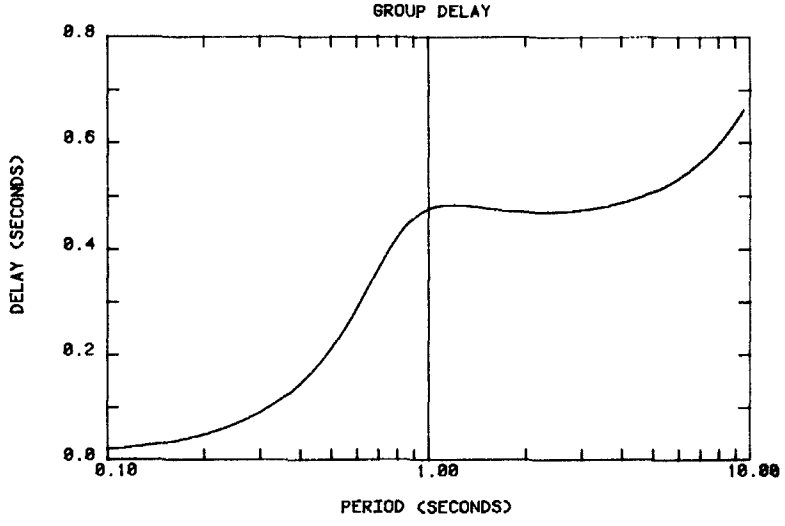

Figure 3.6.--Response functions computed for the DWWSS short-period digital channel from the nominal transfer function (poles and zeros listed in Table 3.6). The crosses on the amplitude curve represent the mean values of the measured data.

using the procedures for computing an impulse response. The current used in step calibration depends on the magnification of the analog record. This practice was established in the WWSSN so that the amplitude of the step response will be the same (44 mm) on all seismograms. Hence, the recorded amplitudes in the digital records will vary depending on system magnification since the digital sensitivity is constant at all DWWSSN stations. For a system operating with a magnification of 25,000, the current step is 6.4 ma and, for nominal system parameters, the step response will appear as shown in Figure 3.7 with a peak amplitude of 17,600 digital counts. The high-pass filter is responsible for the long time constant.

3.2.5 Short-Period Analog System Transfer Function

The differences between the DWWSS short-period seismograms and the WWSS short-period seismograms, in terms of response characteristics, are slight, negligible considering the limited precision of the analog data. Nevertheless, for completeness, it is appropriate to define these differences and provide a transfer function for the DWWSS seismograms.

From Figure 3.2, using block diagram algebra, the transfer function for analog recording has the form

$$\frac{R(s)}{F(s)} = \frac{H_1H_2H_4H_5H_{10}}{(1 + H_1H_2H_3)(1 + H_5H_6H_7)}$$

By inserting system parameters and rearranging slightly, we get

$$\frac{R(s)}{F(s)} = \frac{\frac{2r_oG_sG_g\kappa_{sg}s}{MR_{11}K_g}}{\left\{(s^2+2\lambda_{so}\omega_s s+\omega_s^2)(\alpha s+1) + \frac{G_s^2 s}{MR_{11}}\right\}\left\{s^2+2\lambda_{go}\omega_g s+\omega_g^2 + \frac{\alpha G_g^2 s^2}{K_gR_y(\alpha s+1)} + \frac{G_g^2 s}{K_gR_{22}(\alpha s+1)}\right\} - \frac{G_s^2\kappa_{sg}^2G_g^2s^2}{MK_gR_{11}^2(\alpha s+1)}} \qquad (3.10)$$

Again, the transfer function is dependent on system magnification since this determines the value of the reactive term in the denominator. The poles and zeros of the transfer function for magnifications of 25,000 and 200,000 are listed in Table 3.7 together with the sensitivity constants that establish the proper absolute magnification values. In this case,

$$K_o = \frac{2r_oG_sG_g\kappa_{sg}}{L_sK_g}$$

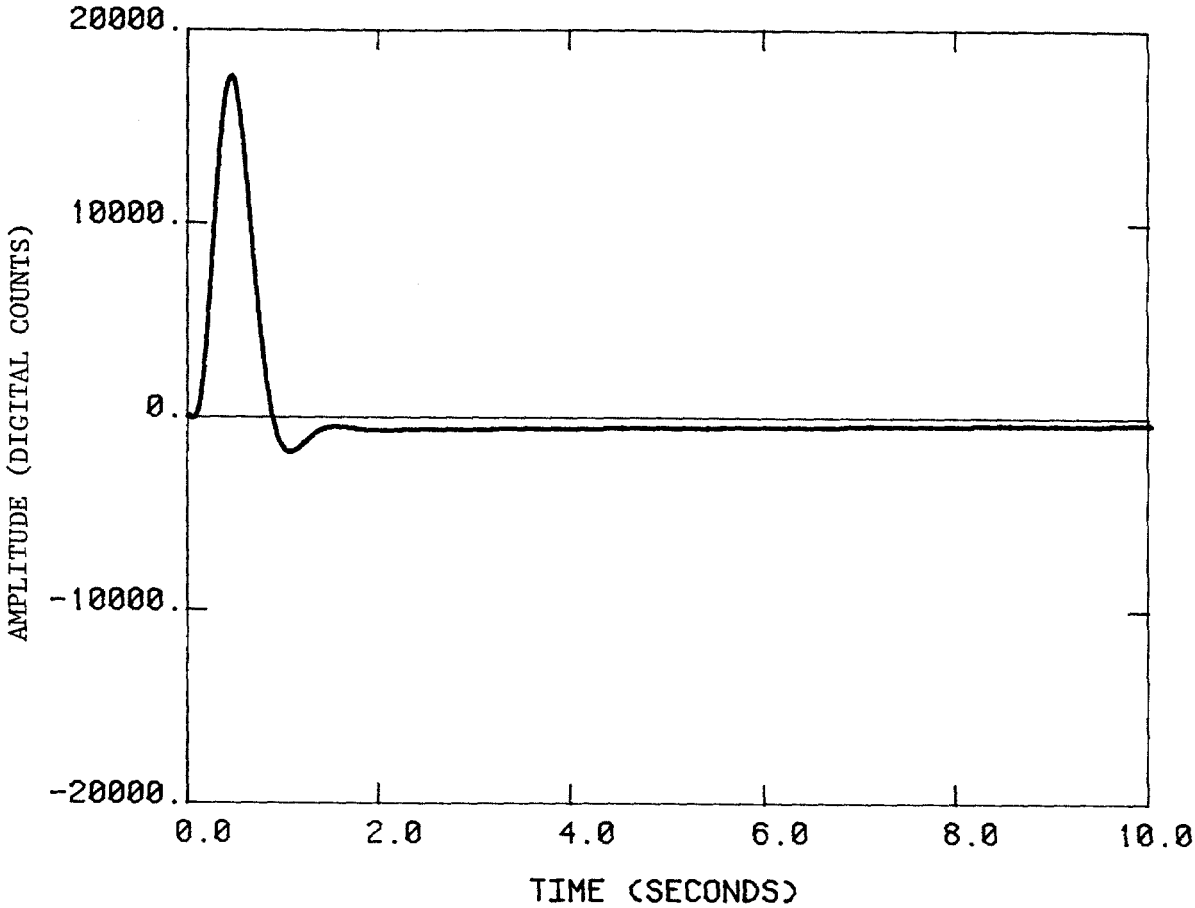

Figure 3.7.--Step response computed for a DWWSS short-period digital system where the analog magnification is 25,000. Calibration current used is 6.4 ma.

SP Analog System Transfer Functions

	TFA25	TFA200	TFW25
Poles:	s = -4.026 ± 6.373j	-3.599 ± 6.428j	-4.004 ± 6.373j
	s = -18.07	-14.97 ± 5.886j	-18.20
	s = -9.182	-5.054	-9.754
	s = -7.558		-7.196
Zeros:	s = 0	0	0
	s = 0	0	0
	s = 0	0	0
K_o =	1.128×10^7	8.938×10^7	1.144×10^7

Table 3.7.--Poles, zeros, and sensitivity constants for short-period analog transfer functions for an input of displacement. TFA25 and TFA200 are for the DWWSS system operated at magnifications of 25,000 and 200,000 at one second; TFW25 is the WWSS SP seismograph operated at a magnification of 25,000 at one second. When the transfer function is evaluated at a specific frequency and multiplied by K_o, the result will be the magnification at that frequency.

Values computed for κ_{sg} are .0286 for the magnification of 25,000 and .225 for the magnification of 200,000. Also listed in Table 3.7 are the poles, zeros, and sensitivity constant for a nominal WWSS short-period seismograph operated at a magnification of 25,000 at 1 second period. They were computed from equation 3.10 letting $R_y = R_{22} = 158$ (as measured in the WWSS system) and adjusting R_{11} and κ_{sg} to produce a synthetic step response amplitude of 44 mm and an overshoot ratio of 1/17, as specified for both the WWSS and DWWSS systems. R_{11} was found to have the value of 177.5 ohms and κ_{sg} was found to have the value .0283.

Amplitude and phase angle differences between the three transfer functions given in Table 3.7 are listed in Table 3.8. Clearly, the differences over the period band from .2 to 20 seconds are negligible and need not be considered during an analysis of DWWSS analog seismograms.

The amplitude and phase characteristics of the DWWSS short-period analog signals are plotted in Figure 3.8 using the TFA transfer function. A step response computed using this transfer function (less two zeros to account for the input of force) is shown in Figure 3.9.

3.2.6 Special Short-Period Digital System Transfer Function

DWWSS-type recording systems have been installed at two sites (Jamestown, California, and Bergen, Norway) and will be installed at a third (Taif, Saudi Arabia) where WWSS systems are not operated. The short-period seismometer used is a Teledyne Geotech Model S-13 and there is no galvanometric recording. The seismometer is connected directly to the DWWSS short-period amplifier through a series resistance that is used to control damping (see Figure 3.10). Parameter values for the seismometer and coupling circuit are listed in Table 3.9. Two of these parameters are adjusted during installation. The natural period of the seismometer is adjusted to 1.0 second and the damping ratio is set to the specified value by adjusting R_d such that the step response, measured at the output of the preamplifier, has an overshoot ratio of 1/17. The location of the inductive pole for this seismometer is far out of band (about 450 Hz) and can safely be ignored.

A block diagram showing elements of the seismometer circuit is provided in Figure 3.11. In the diagram, R_{11} represents the total circuit resistance ($R_s + R_d + R_a$) and $E_i(s)$ represents the voltage at the input to the preamplifier.

PERIOD (SECONDS)	TFA25 AMPLITUDE (RELATIVE)	TFA25 PHASE (DEG.)	TFA200 AMPLITUDE (RELATIVE)	TFA200 DIFF. (PERCENT)	TFA200 PHASE (DEG.)	TFA200 DIFF. (DEG.)	TFW25 AMPLITUDE (RELATIVE)	TFW25 DIFF. (PERCENT)	TFW25 PHASE (DEG.)	TFW25 DIFF. (DEG.)
0.20	.3788	-105.1	.3815	0.7	-105.0	0.1	.3823	0.9	-104.6	0.5
0.30	.7142	-71.0	.7161	0.3	-70.2	0.2	.7182	0.6	-70.5	0.5
0.40	1.0070	-41.6	.9972	1.0	-40.5	1.1	1.0100	0.3	-41.1	0.5
0.50	1.2510	-11.9	1.2260	2.0	-11.3	0.6	1.2520	0.1	-11.5	0.4
0.60	1.3900	16.0	1.3630	2.0	15.9	0.1	1.3900	0.0	16.3	0.3
0.80	1.3330	64.6	1.3300	0.3	64.4	0.2	1.3330	0.0	64.9	0.3
1.00	.9965	106.0	.9965	---	106.6	0.6	.9965	---	106.2	0.2
1.50	.3842	164.0	.3759	2.2	164.7	0.7	.3837	0.1	164.2	0.2
2.00	.1801	190.3	.1756	2.5	190.4	0.1	.1797	0.2	190.5	0.2
3.00	.05456	217.7	.05356	1.8	217.3	0.4	.05445	0.2	217.8	0.1
5.00	.01222	238.5	.01208	1.1	238.1	0.4	.01220	0.2	238.6	0.1
10.00	.001555	254.2	.001543	0.8	254.0	0.2	.001551	0.2	254.3	0.1
20.00	.0002102	261.9	.0002089	0.6	261.8	0.1	.0002098	0.2	261.9	0.0

Table 3.8.--Computed relative amplitude and phase angle for transfer functions: TFA25 (DWWSS SP at 25,000 magnification), TFA200 (DWWSS SP at 200,000 magnification), and TFW25 (WWSS SP at 25,000 magnification). Response is with respect to earth displacement, amplitudes are normalized at one second period. Differences are with respect to TFA25; amplitude differences in percent, phase differences in degrees.

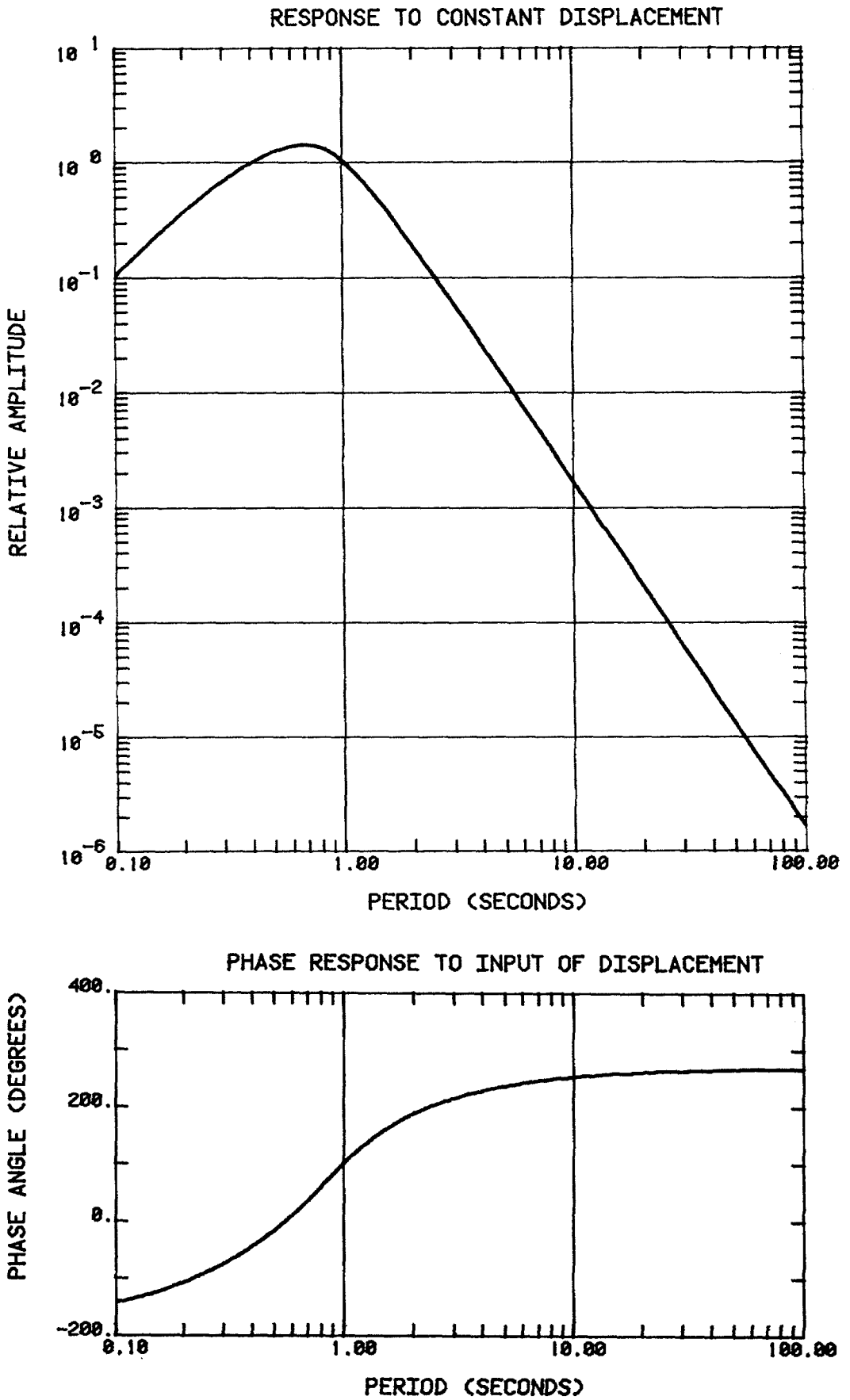

Figure 3.8.--Relative amplitude and phase angle of the DWWSS short-period analog recording system computed from transfer function TFA25.

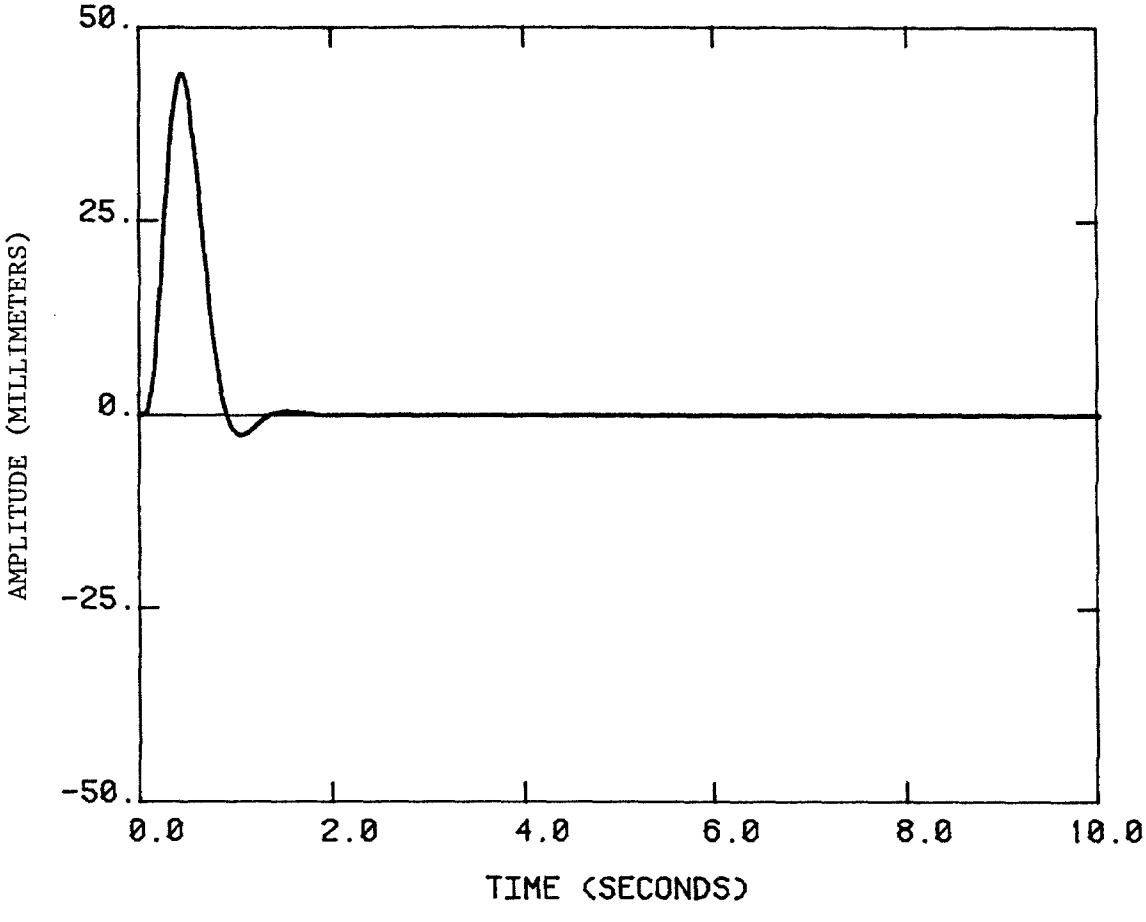

Figure 3.9.--Step response computed for the DWWSS short-period analog system using the transfer function TFA25. Peak amplitude is 44 mm.

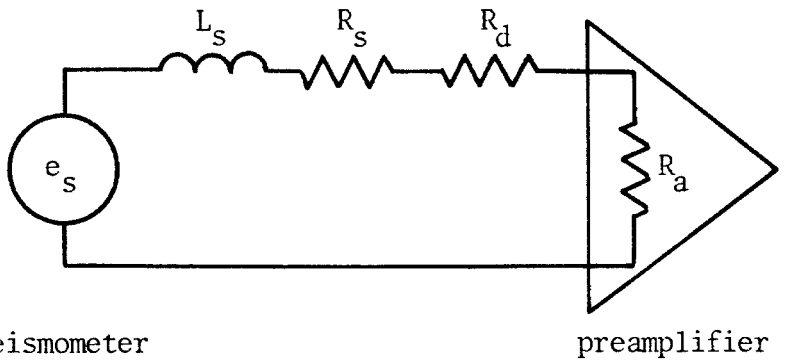

Figure 3.10.--Equivalent circuit for the DWWSS special short-period seismometer and preamplifier.

Parameter	Value	Units
M	5.0	kilograms
R_s	3600	ohms
L_s	3.33	henrys
G_s	629	volt-seconds/meter
ω_s (adjusted)	6.283	radians/second
λ_s (adjusted)	.671	
R_d (approx.)	2000	ohms
R_a	4000	ohms

Table 3.9.--DWWSS special short-period instrument parameters.

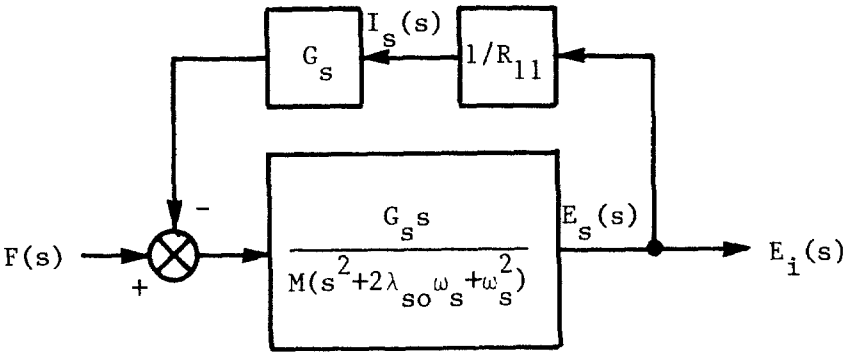

Figure 3.11.--Block diagram of special short-period seismometer.

The transfer function is readily derived from the block diagram as

$$\frac{E_i(s)}{F(s)} = \frac{G_s s/M}{s^2 + 2\lambda_{so}\omega_s s + \omega_s^2 + G_s^2 s/MR_{11}} \quad \text{volts/newton}$$

or, in more simplified form,

$$\frac{E_i(s)}{F(s)} = \frac{G_s s/M}{s^2 + 2\lambda_s \omega_s s + \omega_s^2} \quad \text{volts/newton} \tag{3.11}$$

if we combine air and electromagnetic damping terms so that

$$\lambda_s = \lambda_{so} + \frac{G_s^2}{2\omega_s MR_{11}}$$

The transfer function for the special short-period digital system is the product of equation 3.11 and the short-period amplifier transfer function (equation 3.9). The poles, zeros, and sensitivity constant for this transfer function to an input of earth displacement are listed in Table 3.10. The sensitivity constant is computed from

$$K_o = G_s \cdot K_{spa} \cdot G_{spa} \cdot K_{adc} \quad \text{digital counts/meter}$$

The gain is adjusted to provide an output of 10,000 digital counts per micrometer at 1.0 second period. For nominal values, G_{spa} = 1612 volts/volt. Response functions computed from the nominal transfer function are plotted in Figure 3.12.

The transfer function was tested by comparing computed amplitude values with amplitudes measured at the Jamestown station. The results are shown in Table 3.11. The fact that the computed amplitudes are higher than the measured amplitudes at longer periods and lower at shorter periods would indicate that the seismometer period was slightly lower than 1.0 second when the measurements were made.

Special SP Digital System Transfer Function

Poles	Zeros
$s = -4.2160 \pm 4.6590j$	$s^3 = 0$
$s = -8.4150 \pm .35700j$	$s^2 = 0$
$s = -111.10 \pm 111.10j$	
$s = -.04442 \pm .04444j$	

$$K_o = 5.817 \times 10^{15}$$

Table 3.10.--Poles, zeros, and sensitivity constant for the nominal DWWSS special short-period digital system transfer function for an input of earth displacement. When the transfer function is evaluated at a specific frequency and multiplied by the constant, the result will be in units of digital counts per meter at that frequency.

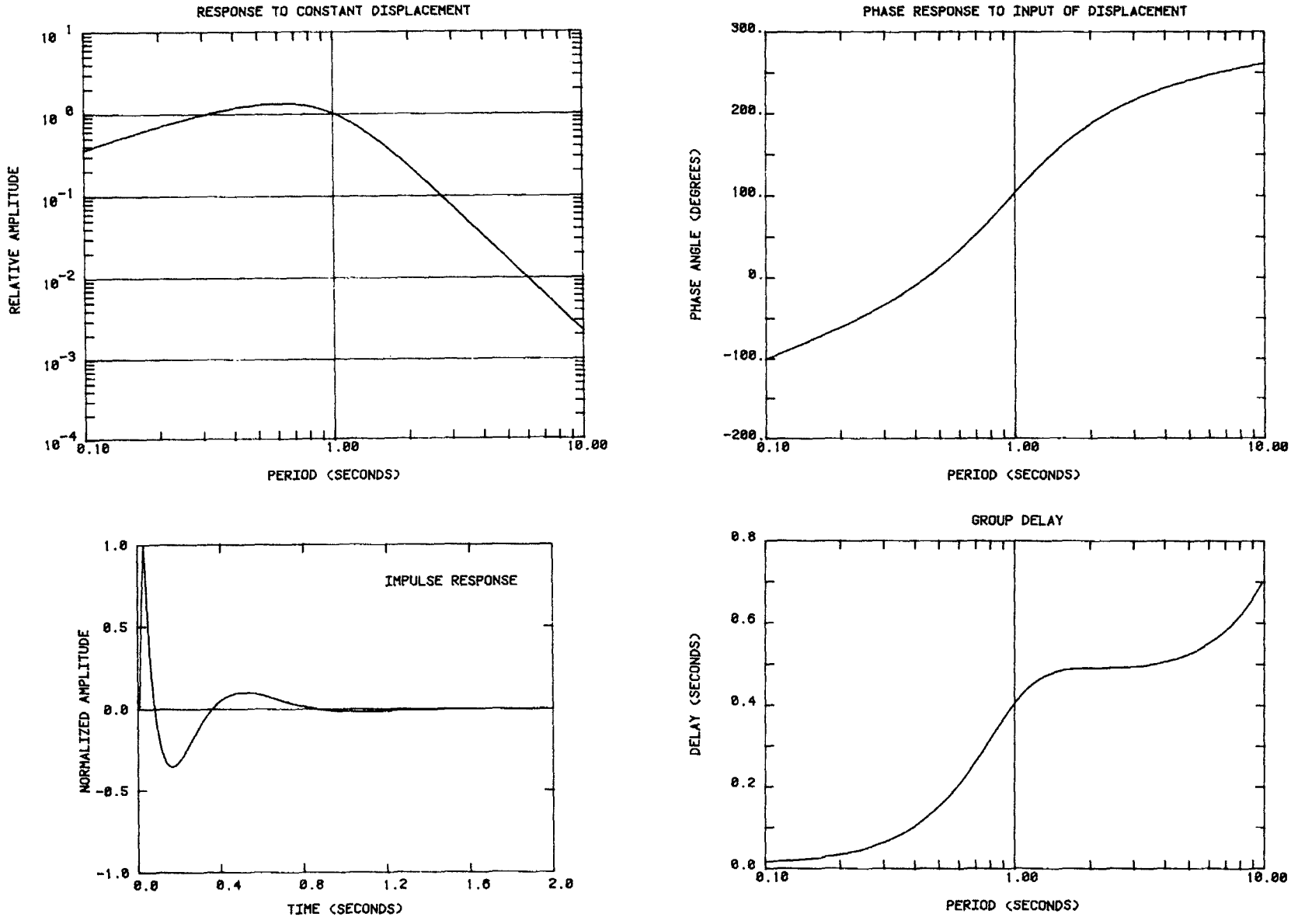

Figure 3.12.--Response functions computed for the DWWSS special short-period digital channel from the nominal transfer function (poles and zeros listed in Table 3.8).

PERIOD (SECONDS)	MEASURED AMPLITUDE (RELATIVE)	COMPUTED AMPLITUDE (RELATIVE)	DIFFERENCE (PERCENT)
0.200	.7143	.7017	1.8
0.400	1.2010	1.1170	2.6
0.500	1.3050	1.2870	1.4
0.600	1.3490	1.3300	1.4
0.800	1.2480	1.2340	1.2
1.000	1.0000	1.0000	-
1.500	.4686	.4710	0.5
2.000	.2187	.2276	3.9
3.000	.07023	.07316	4.0
4.000	.03034	.03165	4.1
5.000	.01568	.01638	4.3
6.000	.009131	.009538	4.3
8.000	.003872	.004047	4.3
10.000	.001972	.002077	5.1

Table 3.11.--Differences between Jamestown measured amplitudes and computed amplitudes using the poles and zeros listed in Table 3.9.

3.3 DWWSS Long-Period Transfer Functions

3.3.1 General

Several changes are made in the WWSS long-period seismograph when the digital recorders are installed in order to improve the quality of the recorded data, both analog and digital. The 500-ohm seismometer coils are replaced by two 5000-ohm coils wired in series to increase signal levels, and the control boxes are eliminated to remove a known noise source. In the DWWSS long-period systems, the seismometers are connected directly to the preamplifiers whose outputs, in turn, are connected to galvanometer drivers, long-period filters, and intermediate-period filters. The WWSS 100-second galvanometers are replaced by .75-second galvanometers and these are used to produce the long-period photographic records.

The long-period seismometers used at the three stations that do not have WWSS systems are Teledyne Geotech Model SL-210 (vertical component) and Model SL-220 (horizontal component). Although the instrument constants differ from those of the WWSS seismometers, the system transfer characteristics are identical when the proper sensitivity adjustments are made.

The long-period seismometers are rotational rather than translational, so the general expression for the seismograph is

$$R(s) = T(s) \cdot H(s)$$

where T(s) is a torque applied about the hinge. For an input of earth motion,

$$T(s) = -Mr_{cm}X(s)s^2 = -Mr_{cm}V(s)s = -Mr_{cm}A(s)$$

where r_{cm} is the distance from the hinge to the center of mass. And, for an input of calibration,

$$T(s) = G_c r_{cm} I(s)$$

Note that the calibrator constant is referenced to the center of mass rather than the position of the calibration coil (equivalent to G* in the WWSS system).

3.3.2 Seismometer-Preamplifier Transfer Function

The long-period seismometer is operated at a period of 15 seconds with the damping ratio adjusted to .88 of critical to match the operating parameters of the WWSS. The seismometer is actively coupled to a preamplifier. Active

coupling is used to improve signal-to-noise ratio by reducing the noise in the damping circuit (Teledyne Geotech, 1980b). The coupling circuit includes a two stage low-pass filter, but the locations of the poles are well out of band (60 Hz and 1350 Hz) for both the intermediate and long periods; hence, direct, passive coupling will be assumed in developing a transfer function. The preamplifier has a gain of 25 and a flat response throughout the period band of interest.

The block diagram shown in Figure 3.13 represents the seismometer-preamplifier combination. K_s is the pendulum moment of inertia about the hinge, and R_{11} is the total resistance in the circuit (sum of the seismometer coil resistances and the preamplifier input resistance). The preamplifier input resistance can be adjusted and this is the method used to set the seismometer damping. Block diagram algebra yields the following transfer function for the seismometer-preamplifier combination.

$$\frac{E_{po}(s)}{T(s)} = \frac{G_{pa}G_s s/K_s}{s^2 + 2\lambda_{so}\omega_s s + \omega_s^2 + G_s^2/K_s R_{11}} \quad \text{volts/newton-meters}$$

As in the previous case (equation 3.11), this may be simplified to

$$\frac{E_{po}(s)}{T(s)} = \frac{G_{pa}G_s s/K_s}{K_s(s^2 + 2\lambda_s\omega_s s + \omega_s^2)} \quad \text{volts/newton-meters}$$

where the parameters λ_s and ω_s are adjusted to specified values. Nominal values for the instrument parameters are listed in Table 3.12. The values for R_s and G_s vary from instrument to instrument and therefore the sensitivities vary between instruments. However, overall system sensitivity is standardized by adjustments of gain in subsequent stages.

3.3.3 DWWSS Long-Period Analog System Transfer Function

A block diagram illustrating the components used in the DWWSS long-period analog recording channel is shown in Figure 3.14. The output of the preamplifier, $E_{po}(s)$, is shaped and conditioned in a galvanometer driver, which produces a suitable, low-level current for driving the galvanometer. The driver also has attenuators needed to set the recording magnification to one of the standard WWSS magnifications. Since the seismometer and galvanometer are decoupled by the driver, the system response characteristics are not dependent

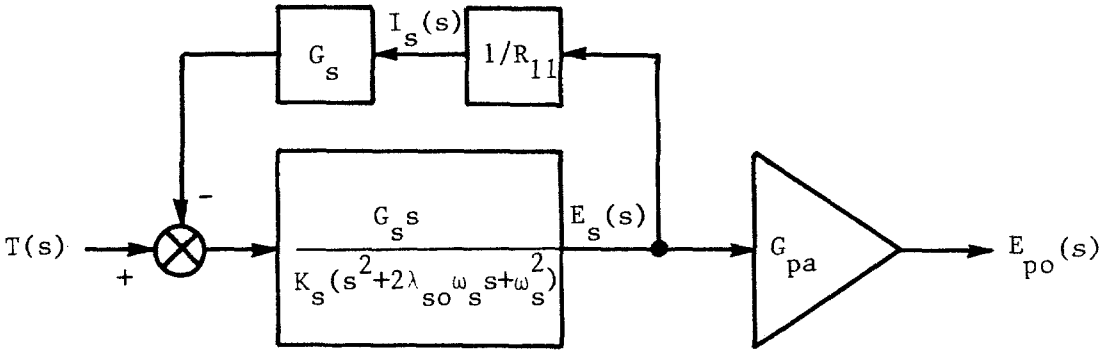

Figure 3.13.--Block diagram of DWWSS long-period seismometer and preamplifier combination.

Parameter	Value		Units
	Vertical	Horizontal	
M	11.2	10.7	kilograms
K_s	1.229	1.331	kilogram-meters^2
r_{cm}	.3078	.3454	meters
R_s (average)	9,807	9,807	ohms
L_s	1.16	1.16	Henrys
G_s (average)	176	189	volt-seconds/radian
λ_{so}	.0172	.0709	
λ_s	.88	.88	
ω_s	.4189	.4189	radians/second
R_{11} (approx.)	30,000	30,000	ohms
G_c (effective)	.0560	.0535	newtons/ampere
r_c	.3480	.3556	meters

Table 3.12.--DWWSS long-period seismometer parameters.

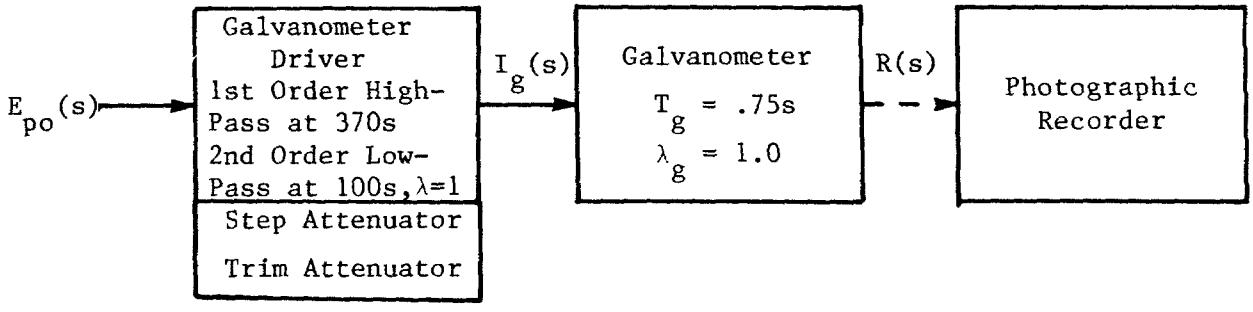

Figure 3.14.--Filter and recording components of the DWWSS long-period analog channel.

on the magnification setting.

The galvanometer driver has a first-order high-pass design corner at 370 seconds to eliminate offset and a critically-damped second-order low-pass design corner at 100 seconds to simulate the response of the WWSS long-period galvanometer. Steady-state measurements on the galvanometer drivers indicate that the high-pass corner is nearer 300 seconds and a better fit to a trial transfer function is achieved by letting the low-pass corner be at 99 seconds. With these modified parameters, the transfer function for the galvanometer driver is

$$\frac{I_g(s)}{E_{po}(s)} = \frac{K_{gd}G_{gd}s}{(s^2 + .1269s + .004028)(s + .02094)} \quad \text{amperes/volt} \qquad (3.13)$$

where K_{gd} is the driver filter constant and G_{gd} is the gain. Relative amplitude and phase angles computed from this transfer function are compared with measured magnitude and phase taken from 35 galvanometer drivers in Table 3.13. The match is excellent.

The recording galvanometer is critically damped and has a natural period of 0.75 seconds (it is a standard WWSS SP galvanometer). Its transfer function is

$$\frac{R(s)}{I_g(s)} = \frac{2r_oG_g}{K_g(s^2 + 16.76s + 70.18)} \quad \text{meters/ampere} \qquad (3.14)$$

where R(s) represents the recorded deflection and r_o is the distance from the mirror to the recording surface. Values for G_g and K_g are given in Table 3.1.

The analog system transfer function is derived from the product of the seismometer-preamplifier transfer function (equation 3.12), equation 3.13, and equation 3.14. The poles, zeros, and a sensitivity constant for the analog system are listed in Table 3.14 for an input of earth displacement. The sensitivity constant, K_o, is computed for a magnification of 1500 at 15 seconds period; its value will change proportionately for other magnifications.

$$K_o = \frac{Mr_{cm}G_{po}G_sK_{gd}G_{gd}2r_oG_g}{K_sK_g} \quad \text{meters/meter}$$

PERIOD (SECONDS)	MEASURED AMPLITUDE (RELATIVE)	COMPUTED AMPLITUDE (RELATIVE)	DIFFERENCE (PERCENT)	MEASURED PHASE ANGLE (DEGREES)	COMPUTED PHASE ANGLE (DEGREES)	DIFFERENCE (DEGREES)
2.488	.001290	.001323	2.5	-174.9	-176.6	1.7
4.967	.005220	.005264	0.8	-172.2	-173.3	1.1
9.960	.02124	.02100	1.1	-165.4	-166.6	0.2
14.89	.04623	.04632	0.2	-159.0	-160.1	1.1
19.91	.08132	.08133	0.0	-152.5	-153.5	1.0
24.82	.1236	.1236	0.0	-146.9	-147.1	0.2
29.87	.1739	.1741	0.1	-141.1	-140.7	0.4
39.76	.2895	.2887	0.3	-128.5	-128.7	0.2
49.67	.4181	.4160	0.5	-117.0	-117.3	0.3
59.28	.5446	.5428	0.3	-106.5	-107.0	0.5
79.24	.7932	.7915	0.2	-87.6	-87.9	0.3
99.50	1.0000	1.0000	-	-70.9	-71.4	0.5
159.30	1.3340	1.3360	0.1	-35.6	-35.8	0.3
249.2	1.3850	1.3930	0.6	-3.7	-3.6	0.1
499.00	1.0380	1.0390	0.1	37.0	36.5	0.5
996.8	.6032	.5983	0.8	62.4	61.9	0.5

Table 3.13.--Differences between mean measured amplitude and phase and computed amplitude and phase for the DWWSS galvanometer driver.

LP Analog System Transfer Function

Poles	Zeros
$s = -.37700 \pm .18270j$	$s^3 = 0$
$s = -8.3770$	
$s = -8.3770$	
$s = -.06347$	
$s = -.06347$	
$s = -.02094$	$s = 0$

$$K_o = 8.149 \times 10^4$$

Table 3.14.--Poles, zeros, and sensitivity constant for the nominal DWWSS long-period analog system for an input of earth displacement and a magnification of 1500 at 15 seconds period. When the transfer function is evaluated at a specific frequency and multiplied by the constant, the result will be the magnification at that frequency. For other magnification settings, change the constant K_o proportionately.

where K_{gd} = .004028. G_{gd} is adjusted to produced the desired magnification. For a magnification of 1500 at 15 seconds period, $G_{gd} = 2.085 \times 10^{-4}$ amperes/volt.

Amplitudes computed from the system transfer function are compared with the mean of measured data taken from 15 DWWSS systems in Table 3.15. A seismometer damping ratio of 0.9, rather than the nominal 0.88, is used in the transfer function as this provides a better fit between measured and computed response data. Agreement is excellent except at short periods where calibration signal-to-noise ratio is very low. In Figure 3.15, the response functions computed from the system transfer function are illustrated and compared with response functions computed from the standard WWSS transfer function for a magnification of 1500. Step responses are compared in Figure 3.16.

3.3.4 DWWSS Long-Period Digital System Transfer Function

DWWSS long-period signals for digital recording are derived from the seismometer and preamplifier, then shaped in a long-period filter to produce a long-period response peaking at about 30 seconds period. The active stages in the filter are illustrated in Figure 3.17. A preamplifier at the input of the filter provides a gain of 10. Response shaping is performed in subsequent stages that contain three second-order low-pass filters. Design parameters are listed in Figure 3.17. The filter has switch selectable attenuation from 0 to 42 dB, in 6 dB steps, and 6 dB of trim attenuation. However, all of the DWWSS systems are set at the same recording sensitivity; the trim attenuator is used to compensate for differences in seismometer sensitivity.

Steady-state amplitude and phase measurements were made on 23 of the long-period filters. The best computed fit to mean measured values was achieved by setting the high-pass corner at 294 seconds, the first-order low-pass corner at 9.6 seconds, and the second-order low-pass corner at 22.8 seconds with a damping ratio of 1.015. For these parameter values, the long-period filter transfer function can be written as follows:

$$\frac{E_o(s)}{E_{po}(s)} = \frac{G_{lpf}K_{lpf}s^2}{(s^2 + .5594s + .07594)^3(s + .6545)(s + .02140)^2} \text{ volts/volt} \quad (3.15)$$

where G_{lpf} is the filter gain (adjusted) and $K_{lpf} = 2.866 \times 10^{-4}$. Amplitude and phase values computed from this transfer function are compared with mean

PERIOD (SECONDS)	MEAN MEASURED AMPLITUDE (RELATIVE)	STANDARD DEVIATION (PERCENT)	COMPUTED AMPLITUDE (RELATIVE)	DIFFERENCE (PERCENT)
5.0	.5894	6.1	.5604	4.9
6.0	.6782	4.5	.6555	3.4
8.0	.8287	2.5	.8106	2.2
10.0	.9210	1.8	.9168	0.5
15.0	1.0000	-	1.0000	-
20.0	.9312	0.6	.9350	0.4
25.0	.8161	1.1	.8267	1.3
30.0	.7225	1.8	.7183	0.6
40.0	.5409	2.3	.5401	0.1
60.0	.3190	2.7	.3185	0.2
80.0	.1986	3.0	.1981	0.3
100.0	.1285	3.1	.1283	0.1
200.0	.02292	3.6	.02261	1.3

Table 3.15.--The mean of measured DWWSS long-period analog amplitudes taken from 15 DWWSS systems compared with amplitudes computed from the nominal DWWSS long-period analog transfer function (poles and zeros listed in Table 3.14).

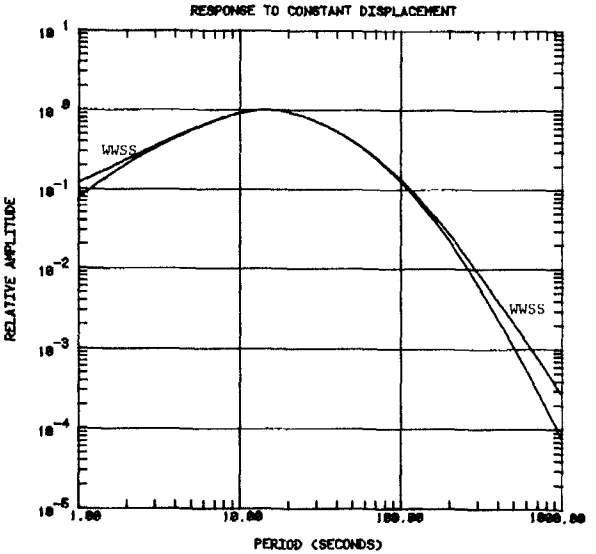

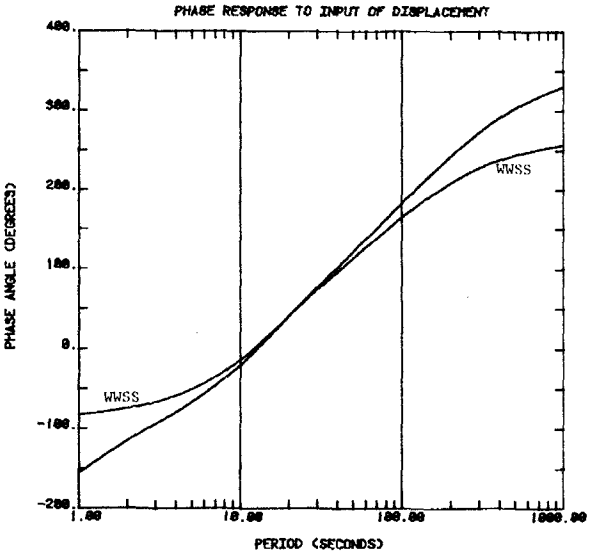

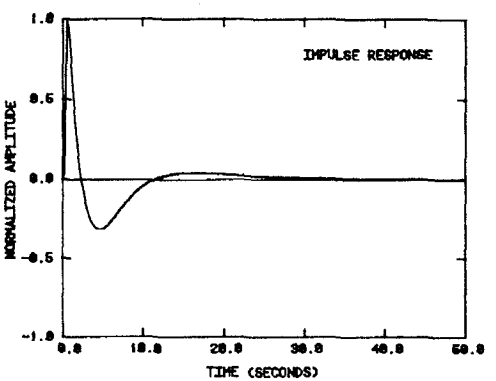

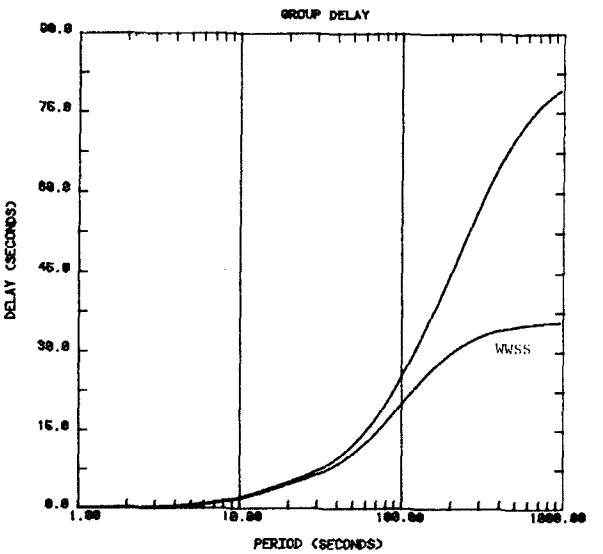

Figure 3.15.--Response functions computed for the DWWSS long-period analog channel from the nominal transfer function (poles and zeros listed in Table 3.14). Curves labeled WWSS were computed from the WWSS long-period transfer function.

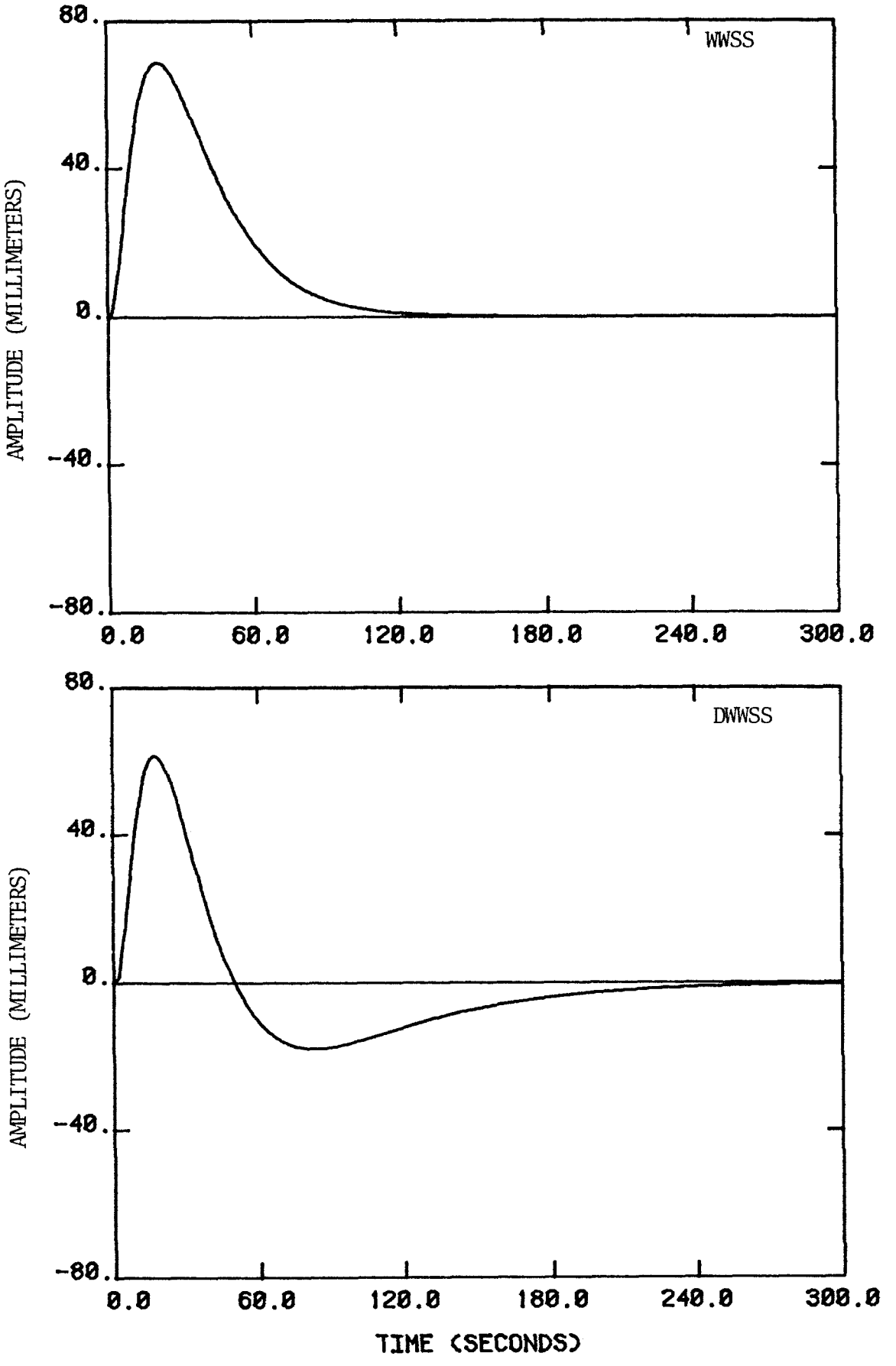

Figure 3.16.--Step responses of the WWSS (upper plot) and DWWSS (lower plot) long-period analog systems for an input of .4 milliamperes when operating at a magnification of 1,500.

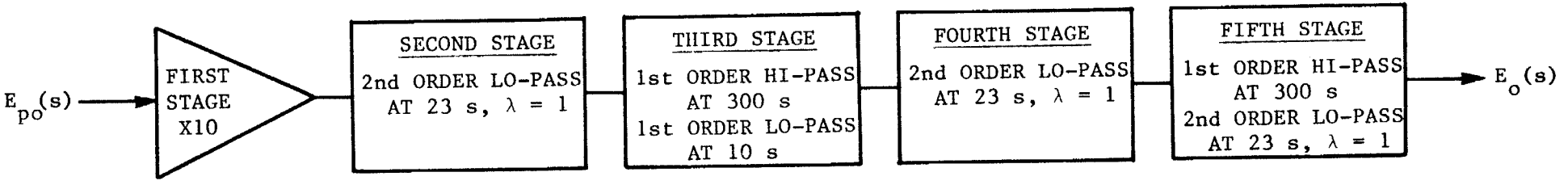

Figure 3.17.--Block diagram of active components in the DWWSS long-period filter (after Teledyne Geotech, 1980c)

measured values in Table 3.16. Over the period band from 10 to 1000 seconds, the maximum standard deviation of the measured data was 2.1% in amplitude and 3.5^{o} in phase.

The nominal system transfer function for the complete long-period digital system is derived from the product of equations 3.12 and 3.15. The poles, zeros, and sensitivity constant for an input of earth displacement are listed in Table 3.17. In this case, the sensitivity constant is derived as follows:

$$K_o = \frac{Mr_{cm} G_s G_{pa} K_{lpf} G_{lpf} K_{adc}}{K_s} \quad \text{digital counts/meter}$$

For nominal parameter values, the gain of the long-period filter, G_{lpf}, is 1188 volts/volt for the vertical components and 1119 volts/volt for the horizontal components.

Amplitudes computed from the nominal transfer function are compared in Table 3.18 with mean measured amplitudes taken from 19 vertical and horizontal DWWSS systems. Although there is considerable scatter in the measurements, the agreement between the mean values and computed values is excellent. Response functions computed from the DWWSS long-period digital transfer function are illustrated in Figure 3.18. The step response, computed from the transfer function, is shown in Figure 3.19.

3.4 DWWSS Intermediate-Period Transfer Function

The intermediate-period digital response is designed to be relatively flat to an input of earth velocity between 1 and 15 seconds period, essentially the long-period seismometer output. Signals are derived from the long-period seismometer, amplified in the preamplifier, shaped in an intermediate-period filter, then digitized and recorded on tape in an event mode.

The active stages of the intermediate-period filter are shown in Figure 3.20. The first stage is a second-order low-pass filter with a corner at 1 second. This combines with a second-order low-pass filter in the third stage to approximate a four-pole Butterworth response with a corner at 1 second. Nominal design values for the parameters are provided in Figure 3.20. The best fit between computed and measured data is achieved by setting the corner of the third stage low-pass filter to .996 seconds and the corners of the high-pass filters at 298 seconds. With these values, the transfer function for

PERIOD (SECONDS)	MEASURED AMPLITUDE (RELATIVE)	COMPUTED AMPLITUDE (RELATIVE)	DIFFERENCE (PERCENT)	MEASURED PHASE ANGLE (DEGREES)	COMPUTED PHASE ANGLE (DEGREES)	DIFFERENCE (DEGREES)
4.97	.00005628	.00005607	0.4	-525.1	-525.9	0.8
9.93	.003720	.003743	0.6	-436.9	-437.7	0.8
14.9	.02818	.02851	1.2	-366.3	-367.1	0.8
19.9	.09054	.09139	0.9	-311.9	-311.0	0.9
24.8	.1866	.1857	0.5	-267.1	-267.3	0.2
29.9	.3020	.3011	0.3	-231.0	-230.8	0.2
39.7	.5198	.5171	0.5	-178.3	-178.5	0.2
49.7	.6934	.6910	0.4	-140.5	-140.8	0.3
59.1	.8096	.8077	0.2	-113.9	-114.3	0.4
79.2	.9503	.9479	0.2	-73.7	-74.2	0.5
99.3	1.0000	1.0000	-	-46.1	-46.8	0.6
159.1	.9502	.9530	0.3	4.7	3.8	0.9
248.5	.7434	.7468	0.5	47.5	46.4	1.1
497.5	.3322	.3380	1.7	102.4	101.8	0.6
995.0	.1039	.1053	1.4	138.4	138.6	0.2

Table 3.16.--Differences between mean measured amplitude and phase and computed amplitude and phase for the DWWSS long-period filter.

LP Digital System Transfer Function

Poles	Zeros
$s = -.37700 \pm .18270j$	$s^3 = 0$
$s = -.23180$	
$s = -.32760$	
$s = -.23180$	
$s = -.32760$	
$s = -.23180$	
$s = -.32760$	
$s = -.65400$	
$s = -.02140$	$s = 0$
$s = -.02140$	$s = 0$

$$K_o = 1.378 \times 10^7$$

Table 3.17.--Poles, zeros, and sensitivity constant for the DWWSS long-period digital system transfer function for an input of earth displacement. When the transfer function is evaluated at a specific frequency and multiplied by the constant, the result is in units of digital counts per meter of displacement at that frequency.

PERIOD (SECONDS)	MEAN MEASURED AMPLITUDE (RELATIVE)	STANDARD DEVIATION (PERCENT)	COMPUTED AMPLITUDE (RELATIVE)	DIFFERENCE (PERCENT)
8.0	.05463	16.8	.05224	4.4
10.0	.1355	3.4	.1350	0.4
15.0	.5011	2.7	.4991	0.4
20.0	.8536	1.9	.8458	0.9
25.0	1.0000	-	1.0000	-
30.0	1.002	1.4	.9899	1.2
40.0	.7735	1.9	.7719	0.2
50.0	.5423	3.1	.5425	0.0
60.0	.3749	3.4	.3752	0.1
80.0	.1874	3.1	.1876	0.1
100.0	.1025	3.6	.1018	0.6
200.0	.01127	3.4	.01109	1.6

Table 3.18.--The mean of measured DWWSS long-period digital amplitudes taken from 19 vertical and horizontal components compared with amplitudes computed from the nominal transfer function (poles and zeros listed in Table 3.17).

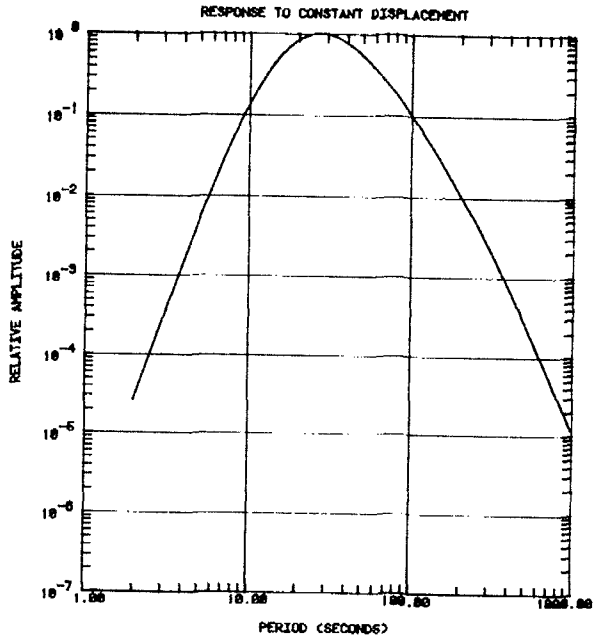

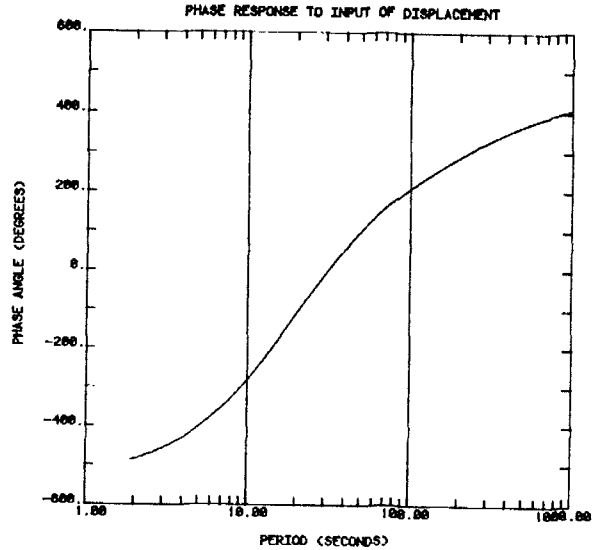

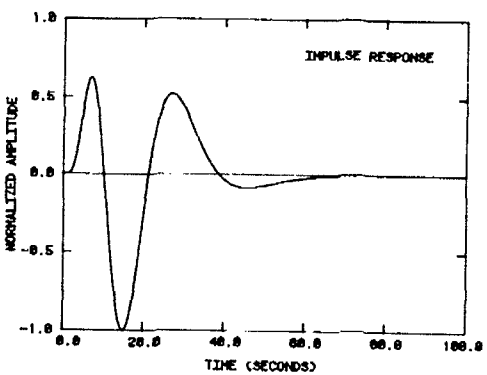

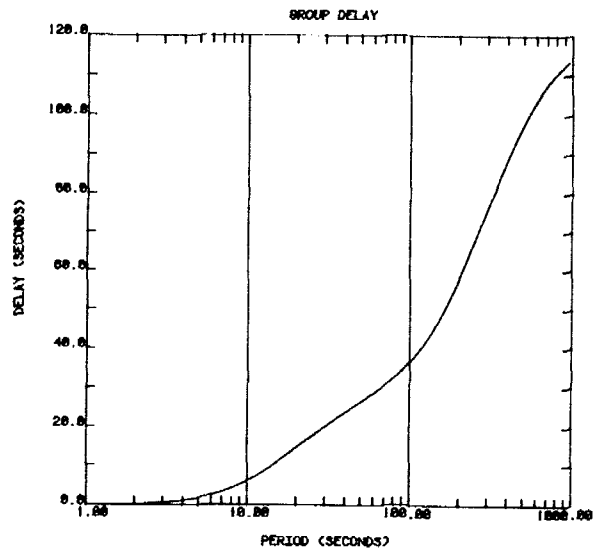

Figure 3.18.--Response functions computed for the DWWSS long-period digital channel from the nominal transfer function (poles and zeros listed in Table 3.17). The Nyquist period is 2 seconds.

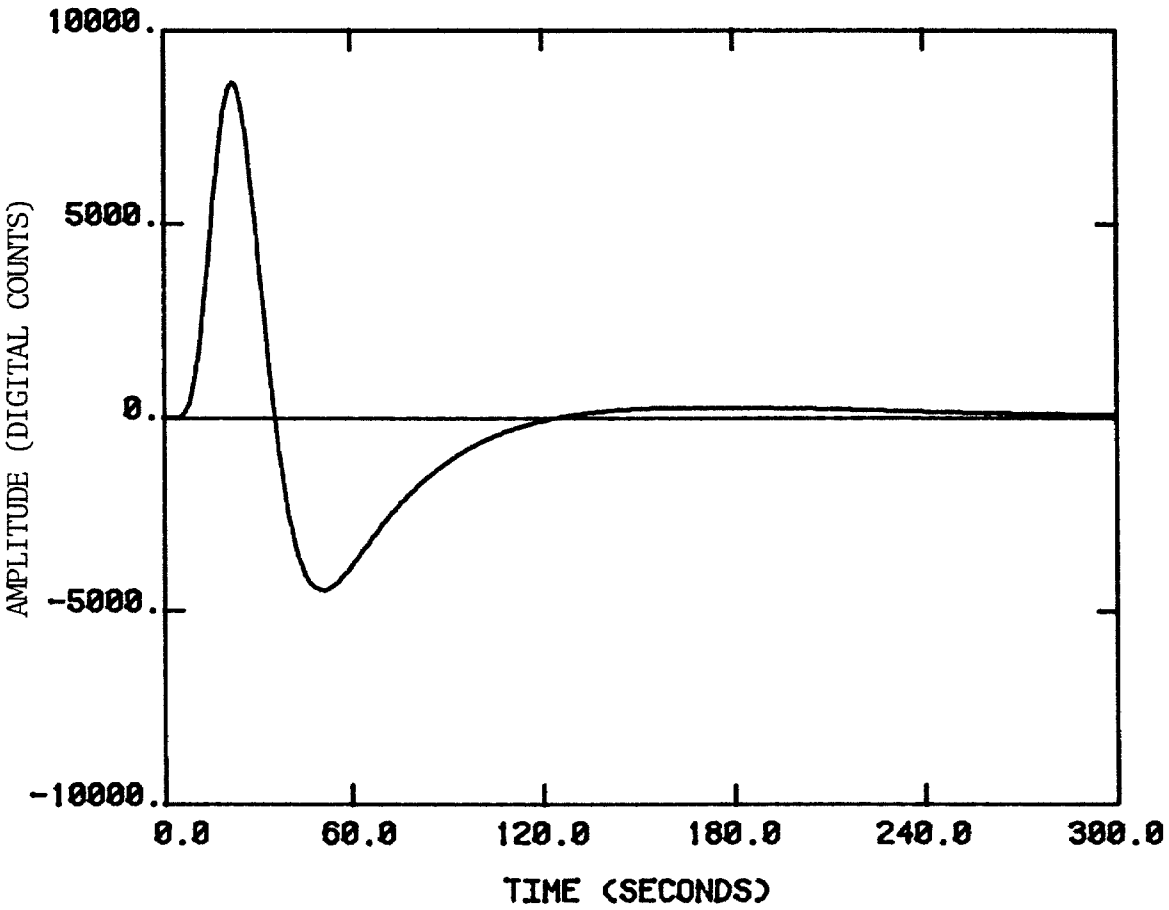

Figure 3.19.--Step response computed for the DWWSS long-period digital channel for an input of .2 milliamperes.

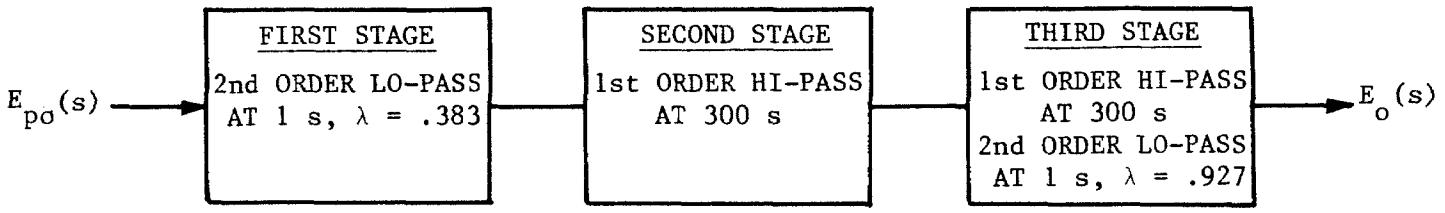

Figure 3.20.--Block diagram showing components of the DWWSS intermediate-period filter (after Teledyne Geotech, 1980c).

the intermediate-period filter can be written

$$\frac{E_o(s)}{E_{po}(s)} = \frac{K_{ipf}G_{ipf}s^2}{(s^2+4.813s+39.48)(s^2+11.70s+39.80)(s+.02108)^2} \text{ volts/volt} \quad (3.16)$$

where G_{ipf} is the gain of the filter (adjustable) and $K_{ipf} = 1.571 \times 10^3$. Steady-state amplitude and phase measurements were made on 23 intermediate-period filters. Maximum standard deviation over the band from 0.2 to 1000 seconds was 1.7% in amplitude and 3^o in phase, so the variation between filters is very small. The mean measured values are compared in Table 3.19 with computed values. Agreement is excellent.

The transfer function for the DWWSS intermediate-period system is derived from the product of equations 3.12 and 3.16. The resulting poles, zeros, and sensitivity constant are listed in Table 3.20 for an input of earth displacement. In this case, the value of the sensitivity constant is obtained from

$$K_o = \frac{Mr_{cm}G_sG_{pa}K_{ipf}G_{ipf}K_{adc}}{K_s} \quad \text{digital counts/meter}$$

For nominal parameter values, the gain of the filter, G_{ipf}, is .6998 for the vertical component and .6589 for the horizontal component. At a period of 1 second, the value of the transfer function is adjusted to 125 digital counts per micrometer of displacement.

Amplitudes computed using the IP transfer function are compared in Table 3.21 with the mean of measured amplitudes obtained from 19 intermediate-period components. The differences are less than 2% except at the shortest period where the calibration signal-to-noise level is very low. Response functions computed from the IP transfer function are illustrated in Figure 3.21.

PERIOD (SECONDS)	MEASURED AMPLITUDE (RELATIVE)	COMPUTED AMPLITUDE (RELATIVE)	DIFFERENCE (PERCENT)	MEASURED PHASE ANGLE (DEGREES)	COMPUTED PHASE ANGLE (DEGREES)	DIFFERENCE (DEGREES)
0.198	.001766	.001732	1.9	-329.7	-329.9	0.2
0.331	.01370	.01351	1.4	-308.6	-309.2	0.6
0.496	.06887	.06763	1.8	-281.8	-282.2	0.4
0.661	.2132	.2089	2.0	-251.7	-252.2	0.5
0.792	.4134	.4081	1.3	-224.5	-225.2	0.7
0.994	.7826	.7763	0.8	-179.8	-180.6	0.8
1.244	1.030	1.025	0.5	-135.6	-136.0	0.4
1.660	1.103	1.101	0.2	-95.0	-95.4	0.4
2.480	1.113	1.110	0.2	-60.5	-60.9	0.4
4.980	1.112	1.111	0.1	-28.2	-28.3	0.1
9.950	1.111	1.110	0.1	-11.1	-11.2	0.1
14.90	1.111	1.109	0.2	-4.2	-4.3	0.1
19.90	1.108	1.107	0.1	-0.5	0.1	0.6
24.80	1.104	1.104	0.0	3.7	3.5	0.2
29.90	1.100	1.101	0.1	6.7	6.5	0.2
39.80	1.094	1.092	0.2	11.9	11.5	0.4
49.70	1.083	1.082	0.1	16.2	15.9	0.3
59.30	1.070	1.069	0.1	19.9	20.0	0.1
79.30	1.038	1.038	0.0	28.0	27.9	0.1
99.60	1.000	1.000	-	36.0	35.5	0.5
159.6	.8628	.8639	0.1	55.6	55.4	0.2
249.4	.6568	.6539	0.4	79.5	79.2	0.3
498.3	.2899	.2929	1.0	117.1	117.9	0.8
997.3	.09092	.09115	0.3	146.6	146.6	0.0

Table 3.19.--Differences between mean measured amplitude and phase and computed amplitude and phase for the DWWSS intermediate-period filter.

IP Digital System Transfer Function

Poles	Zeros
$s = -.37700 \pm .18270j$	$s^3 = 0$
$s = -2.4070 \pm 5.8040j$	
$s = -5.8480 \pm 2.3660j$	
$s = -.02108$	$s = 0$
$s = -.02108$	$s = 0$

$$K_o = 4.434 \times 10^{10}$$

Table 3.20.--Poles, zeros, and sensitivity constant for the nominal DWWSS intermediate-period transfer function for an input of earth displacement. When the transfer function is evaluated at a specific frequency and multiplied by the constant, the result will be in units of digital counts per meter of displacement at that frequency.

PERIOD (SECONDS)	MEAN MEASURED AMPLITUDE (RELATIVE)	STANDARD DEVIATION (PERCENT)	COMPUTED AMPLITUDE (RELATIVE)	DIFFERENCE (PERCENT)
0.5	.1845	16.3	.1777	3.7
0.6	.3026	3.4	.3046	0.7
0.8	.6763	3.0	.6717	0.7
1.0	1.0000	-	1.0000	-
1.5	.9127	1.7	.9211	0.9
2.0	.6916	2.2	.6995	1.1
3.0	.4625	1.3	.4609	0.4
4.0	.3392	1.3	.3390	0.1
6.0	.2143	1.6	.2136	0.3
8.0	.1470	2.3	.1480	0.7
10.0	.1065	3.1	.1071	0.6
15.0	.05174	3.8	.05240	1.3
20.0	.02767	3.1	.02798	1.1
25.0	.01609	2.8	.01616	0.4
30.0	.009951	2.7	.009987	0.4
40.0	.004529	3.0	.004482	1.0
60.0	.001384	3.8	.001365	1.4
80.0	.0005735	2.0	.0005687	0.8
100.0	.0002871	2.0	.0002828	1.5

Table 3.21.--The mean of measured DWWSS intermediate-period amplitudes taken from 19 components compared with amplitudes predicted using the nominal transfer function (poles and zeros listed in Table 3.20).

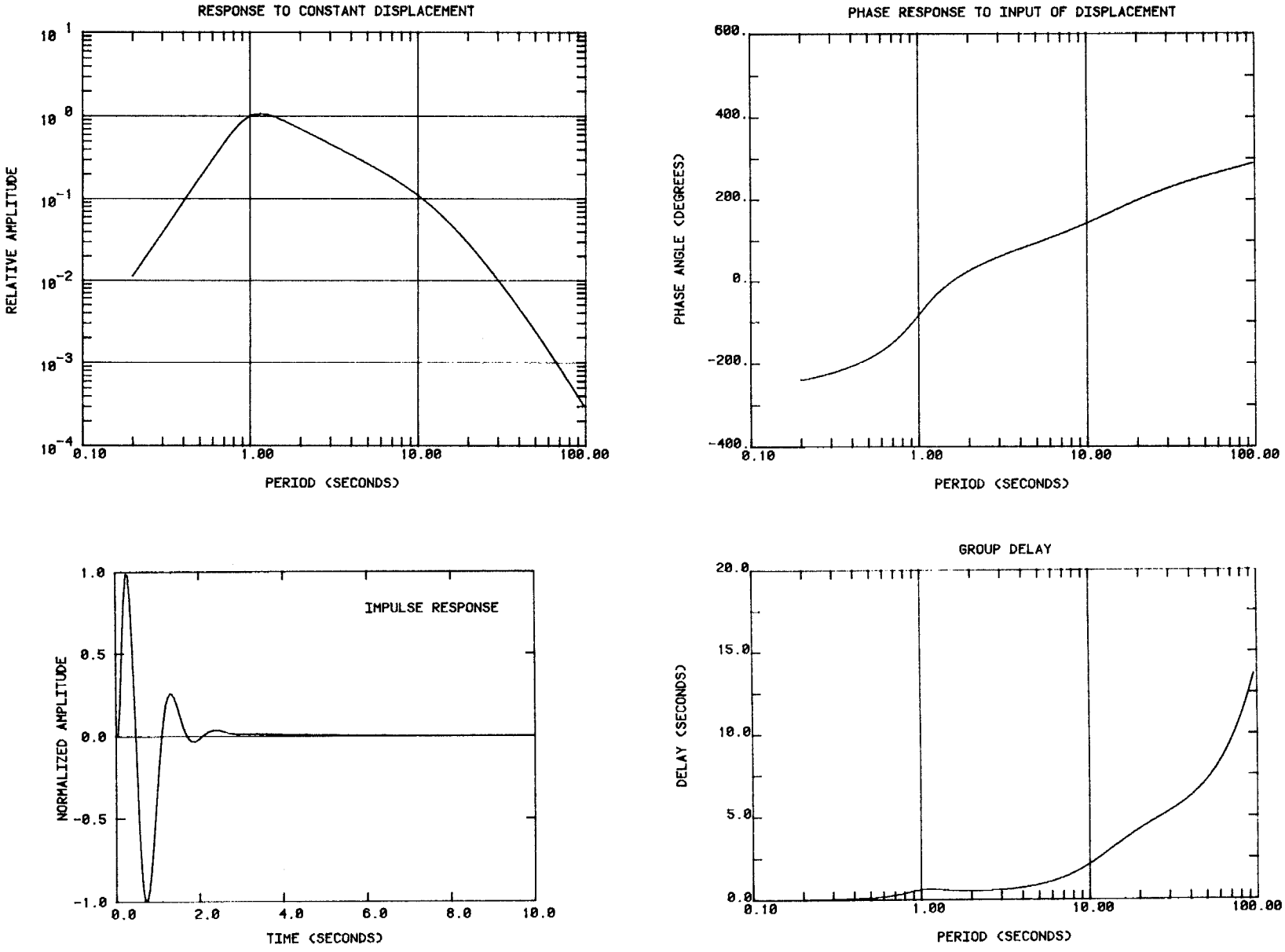

Figure 3.21.--Response functions computed for the DWWSS intermediate-period digital system from the nominal IP transfer function (poles and zeros listed in Table 3.20). The Nyquist period is 0.2 seconds.

4. DWWSS CALIBRATION

4.1 General

The development of the system transfer function is part of the calibration process, usually the first step. It has been treated separately in this report because of its scope and complexity. In this section on calibration we will review the field test and analysis procedures used to validate and refine the system transfer functions.

An important part of the calibration takes place during the installation of the seismograph. Instrument parameters are adjusted to proper values and those that are not adjustable are measured. In general, the procedures used to install and calibrate the WWSS systems are repeated during the installation of the added equipment used in the DWWSS system, although some additional tests are necessary. The procedures are prescribed in an installation report form prepared by C.R. Hutt (1980, Digital World-Wide Standardized Seismograph Network Installation Report). Most of the tests are recorded, either on the seismograms or the digital tapes, or on both. The completed form with its attached records becomes the station installation report. These reports are filed at the Albuquerque Seismological Laboratory. Most of the calibration procedures used during installation are repeated during maintenance visits by ASL personnel and the maintenance reports are also kept on file. Maintenance visits should be repeated at six-month intervals, but this will depend on the availability of funds.

Daily calibration of the DWWSS system consists of a step of force applied to the seismometer mass through an electromagnetic calibrator, the same procedure that is used with the WWSS systems. The recorded step response provides the information needed to monitor calibration stability and general system performance. It also contains information that is potentially useful in generating precise transfer functions for individual recorded components. At present, the analysis of calibration step responses is performed manually. In time, these procedures will be automated as part of the routine data review process at ASL. The magnifications and calibration currents used at the DWWSSN stations are listed in Table 4.1. Calibration constants are listed in Table 4.2. The use of these constants will be explained later in the text.

Station	SP Magnification (@ 1 sec)	SP Cal. Current (ma)	Nominal Peak SP Step Amplitude		LP Magnification (@15 sec)	LP Cal. Current (ma)	Nominal Peak LP Step Amplitude	
			Analog (mm)	Digital (counts)			Analog (mm)	Digital (counts)
AFI	12,500	6.4	22	17,600	750	0.4	31	17,400
BDF	100,000	1.6	44	4,400	1,500	0.4	62	17,400
BER	---	1.5	--	8,750	---	0.24	--	10,440
COL	100,000	1.6	44	4,400	1,500	0.4	62	17,400
GDH	25,000	6.4	44	17,600	1,500	0.4	62	17,400
JAS	---	0.8	--	4,670	---	0.1	--	4,350
KEV	25,000	6.4	44	17,600	1,500	0.4	62	17,400
LEM	25,000	6.4	44	17,600	750	0.4	31	17,400
LON	100,000	1.6	44	4,400	1,500	0.4	62	17,400
SCP	50,000	3.2	44	8,800	1,500	0.4	62	17,400
SLR	50,000	3.2	44	8,800	1,500	0.4	62	17,400
TAU	25,000	6.4	44	17,600	750	0.4	31	17,400
TOL	25,000	6.4	44	17,600	1,500	0.4	62	17,400

Table 4.1.--Magnifications, calibrating currents, and nominal peak amplitudes of the step response at the operating DWWSSN stations. BER and JAS do not have WWSS analog recorders. Maximum step calibrating current is limited to 6.4 ma for the short-period and 0.4 ma for the long-period systems to prevent overdriving the digital recorder.

	WWSS	TG
Calibrator Electrodynamic Constants: (newtons/ampere)		
SP G_c	2.0	.1975
LPZ G_c	.0560	.01
LPH G_c	.0535	.01
Analog Calibration Constants: (newtons/meter)		
SP K_{pm} @ 1 sec	7300	---
LPZ K_{pm} @ 15 sec	.542	---
LPH K_{pm} @ 15 sec	.518	---
Digital Calibration Constants: (newton-counts/meter^2)		
SP K_{pd} @ 1 sec	7300	338
LPZ K_{pd} @ 25 sec	.645	.1149
LPH K_{pd} @ 25 sec	.616	.1149

Table 4.2.--Calibration constants used in the DWWSS system. The column labeled WWSS refers to the WWSS seismometers used at most DWWSSN stations; the column labeled TG refers to Teledyne Geotech seismometers used at JAS, BER, and TAIF.

Some of the DWWSS calibration procedures are likely to be changed, based on the results of this study. Not all of the information that is needed to fully describe the operating system is obtained during installation and maintenance, calibration drive levels used in the WWSS system are not necessarily the best for digital recording, and analysis of the calibration data is inhibited to some extent by the procedures now used. Because of the importance of calibration in the analysis of high-resolution digital data, most would agree that the calibration of DWWSS systems should be tailored for digital data analysis even though this might change the traditional calibration format of the analog seismograms.

4.2 Short-Period Calibration

The following procedures are used to calibrate the DWWSS short-period system during installation.

Step 1. The free period of each seismometer is adjusted to 1.0 second and recorded on a test record.

Step 2. The electrodynamic constant of each calibrator is adjusted to 2.0 newtons/ampere by positioning a small magnet in the calibrator such that

$$G_c = \frac{y_i mg}{y_w i_c} = 2.0 \text{ newtons/ampere}$$

where y_i is the peak amplitude of the current step response, y_w is the peak amplitude of a "weight lift" step response, m is the mass of the test weight, and g is the acceleration of gravity. Normally, a 1.0 gram mass and a current of 4.9 ma are used in the test; then, when the deflections are equal, G_c is adjusted properly. This test is also recorded.

Step 3. The magnification of the seismogram at a period of 1.0 second is set to its proper level by applying a current step and adjusting the control box attenuator such that

$$\text{Magnification @ 1 sec} = \frac{7300 y_i}{G_c i_c}$$

The magnifications and calibration currents used at the DWWSSN stations are listed in Table 4.1. The magnifications conform to the discrete settings specified for the WWSSN. The calibration constant, 7300 newtons/meter, was

determined empirically for the WWSS system in shake table tests (the nominal system transfer function yields 7110 newtons/meter, but the measured value will continue to be used). During the adjustment of magnification, the seismograph overshoot ratio is set to 1/17 by adjusting the seismometer damping control.

Step 4. The sensitivity of the short-period digital recording is set to 10,000 digital counts per micrometer at a period of 1 second by driving the calibrator with a sine wave having a peak-to-peak amplitude of 8.488 ma. The equivalent peak-to-peak earth displacement, x_p, is found from the relationship

$$x_p = \frac{G_c i_c}{M\omega^2} = 4.0 \times 10^{-6} \text{ meters}$$

The adjustment is made by setting the step and trim attenuators on the short-period amplifier to produce 40,000 digital counts peak to peak.

Step 5. The final step during installation of the short-period seismograph is the recording of calibration sine waves at 16 specified frequencies from 0.1 to 5.0 Hz using a constant input of 8.488 ma.

Daily calibration consists of the application and removal of a current step repeated several times in succession. The currents used are listed in Table 4.1. The amplitude of the digitally recorded step response will vary depending on the analog system magnification. The specified current steps will produce equal amplitudes (44 mm) on the analog seismograms for magnifications of 25,000 and greater. A step current of 6.4 ma will produce a peak amplitude of 17,600 digital counts (nominal) and proportionately lower amplitudes for the other currents used. The calibrations are applied manually, just after the seismograms are changed (usually early morning, local time). When the calibrations are applied, a flag is set in the digital record.

The digital sensitivity or magnification may not be set precisely at its nominal value. The magnification (M_o) and digital sensitivity (DS) at a period of 1.0 second can be determined from the peak amplitude of the step response using the following relationships.

$$M_o = \frac{K_{pm} y_m}{G_c i_c} \text{ meters/meter at reference period} \qquad (4.1)$$

$$DS = \frac{K_{pd} y_d}{G_c i_c} \text{ digital counts/meter at reference period} \qquad (4.2)$$

where y_m and y_d are the peak recorded amplitudes of the step response in meters and digital counts, respectively, and K_{pm} and K_{pd} are the calibration constants for analog and digital calibration listed in Table 4.2. It must be pointed out, however, that there are other factors beside the system sensitivity that affect the amplitude of the step response. In the case of the WWSS Benioff seismometer, the electrodynamic constant of the calibrator is sensitive to mass position, which varies with temperature. Small changes in short-period step response amplitude are more likely due to mass position drift than to a change in the operating sensitivity of the seismograph. If significant change occurs in the amplitude of the short-period step response, either abruptly or in steady drift, a weight lift should be made to determine if the change has been in signal sensitivity or calibration sensitivity.

4.3 Long-Period Calibration

The following procedures are used to calibrate the long-period system during the installation of the digital recorder.

Step 1. The air-damped period of each seismometer is adjusted to 15 seconds and records are made of the free period. The natural period, T_n, is related to the damped period, T_d, by the expression

$$T_n = (1-\lambda_d^2)^{\frac{1}{2}} T_d$$

where λ_d is the damping ratio. For the air damping ratios (λ_{so}) given in Table 3.12, the natural periods will be 14.998 seconds for the vertical seismometer and 14.96 seconds for the horizontal seismometer. These values both fall within the prescribed limits for period adjustment, which are 14.85 and 15.15 seconds.

Step 2. The air damping ratio for each seismometer is measured from the recorded free period test.

$$\lambda_{so} = \frac{\delta}{(n^2\pi^2 + \delta^2)}$$

where $\delta = \ln (y_o/y_n)$

y_o = amplitude of first peak

y_n = amplitude of nth peak

Average values of air damping measured in these tests are given in Table 3.12.

Step 3. The seismometer damping ratio is set to the value of 0.88 by adjusting the preamplifier input resistance to a value determined in the following test. A 500K ohm resistor is placed across the seismometer signal coil, the free period is recorded, and the damping ratio, λ_d, that results is computed as in Step 2. Since

$$\lambda_d = \lambda_{so} + \frac{G_s^2}{2\omega_s K_s (500000 + R_s)}$$

then

$$\frac{G_s^2}{2\omega_s K_s} = (\lambda_d - \lambda_{so})(500000 + R_s)$$

and the proper preamplifier input resistance (external damping resistance) is computed from

$$R_i = \frac{G_s^2}{2\omega_s K_s (0.88 - \lambda_{so})} \quad \text{ohms}$$

Step 4. The calibrator electrodynamic constant for each seismometer is determined from a weight lift test. In this case,

$$G_{cm} = \frac{mgr_w y_i}{i_c r_{cm} y_w} \quad \text{newtons/ampere}$$

where G_{cm} is the measured calibrator constant and r_w is the distance from the hinge to the point of weight lift. Measured values range from .08 to .13 newtons/ampere and the average value is .0933 n/a. In the DWWSS system, in order to make the calibrating force equal on all seismometers, current dividers are placed across the individual calibration coils and adjusted such that the effective calibrator constant is

$$G_c = .005M$$

for all coils. Then, for the vertical seismometer, G_{cz} = .056 n/a and for

the horizontal seismometer, G_{ch} = .0535 n/a.

Step 5. The sensitivity of the digital recording is set to 500 digital counts per micrometer at a period of 25 seconds. This is done by driving the calibrator with a 1.011 ma peak-to-peak sine-wave current (equivalent to 80 micrometers, peak to peak) and adjusting the long-period filter attenuator to produce 40,000 digital counts peak to peak on the digital record.

Step 6. The analog magnification is set by applying a sinusoidal current to the calibrator and adjusting the step and trim attenuators on the galvanometer driver. For a magnification of 1,500, the current used, 1.170 ma peak to peak, is equivalent to 33.33 micrometers of earth displacement at 15 seconds period and should result in a peak-to-peak record deflection of 50 mm. Proportionate currents are used for the other magnifications so that the record deflection will be 50 mm during the sine-wave calibration.

Step 7. Sine-wave calibrations are recorded digitally at 13 points in the period band from 8 to 500 seconds using a current of .506 ma peak to peak.

Step 8. The sine-wave calibration is repeated and recorded on the analog seismogram. In this case, the amplitude of the driving current depends on the magnification.

Daily calibration consists of a single application and removal of a current step through the calibrator. The currents used are listed in Table 4.1. As in the case of the short-period seismograph, the long-period magnification and digital sensitivity can be computed at the reference periods using equations 4.1 and 4.2 and the constants that are listed in Table 4.2. Again, caution is required because the step response amplitude can be affected by factors unrelated to changes in signal sensitivity. The step calibration is most appropriately used to monitor system stability. When significant changes in peak amplitude are observed, steps should be taken immediately to determine and correct the source of the problem.

4.4 Intermediate-Period Calibration

The intermediate-period channels are calibrated after the long-period seismometer period and damping adjustments have been made, since the signals for intermediate-period recording are derived from the long-period seismometers.

Step 1. The digital sensitivities of the intermediate-period channels are set to 125 digital counts per micrometer at a period of 1.0 second. The calibrators are driven with a peak-to-peak sinusoidal current of 78.96 ma and the proper recording level is adjusted using the trim attenuator on the intermediate-period filter. The calibration is done before the current divider is placed in the calibration circuit; hence, the equivalent earth displacement at 1 Hz is calculated individually for each seismometer using the measured electrodynamic constant

$$x_p = \frac{G_{cm} i_c}{M\omega^2}$$

Step 2. Sine-wave calibrations are recorded digitally at 19 points in the period band from 0.5 to 100 seconds using a driving current of 78.96 ma. During this test, the current divider is installed, so the effective G_c's are used to compute earth displacement.

Sine-wave calibration of the intermediate-period channels is somewhat complicated by an extraneous signal that is generated in the signal coil due to mutual inductance between the calibration coil and the signal coil. This results from the fact that the calibration coil is wound on one of the 5,000-ohm signal coils. The block diagram in Figure 4.1 illustrates a seismometer with a parallel path for a signal generated by mutual inductance. In this figure, $I_c(s)$ is the calibrating current, κ_{cd} represents the current divider attenuation (its nominal value is 0.6, although it varies from instrument to instrument), $I_{ce}(s)$ is the effective current through the calibration coil, G_{cm} is the measured calibrator electrodynamic constant, M_i is the mutual inductance, $I_{si}(s)$ is the current induced into the signal coil, R_a is the preamplifier input resistance, $E_{si}(s)$ represents the induced voltage across the preamplifier input, and the other parameters have previously been defined.

The transfer function for this configuration can be written as

$$\frac{E_o(s)}{I_c(s)} = \frac{K_1 s}{s^2 + 2\lambda_s \omega_s s + \omega_s^2} - K_2 s$$

where

$$K_1 = \frac{\kappa_{cd} G_{cm} r_{cm} G_s}{K_s} \quad \text{and} \quad K_2 = \frac{\kappa_{cd} M_i R_a}{R_{11}}$$

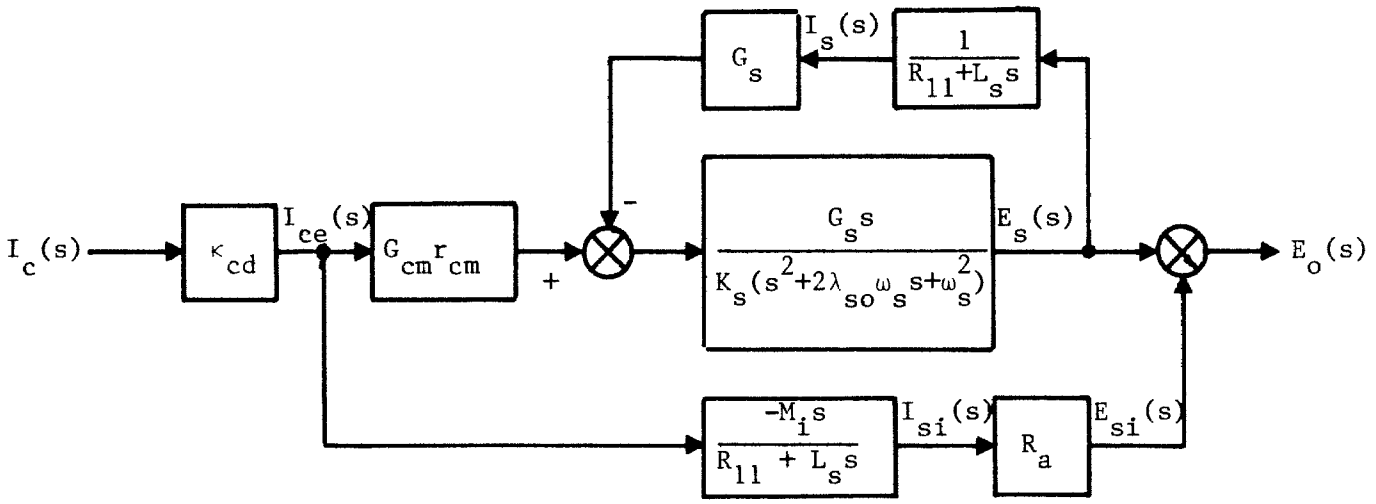

Figure 4.1.--Block diagram of a seismometer with mutual inductance between the calibration and signal coils.

The effect of self inductance in the signal coil is negligible since $L_s j\omega/R_{11}$ is less than .002 for the highest frequency of interest (5 Hz).

The mutual inductance can be determined without special test equipment in at least two ways. One way is to measure the null frequency (the point where the transfer function is zero) and compute the value of M_i.

$$M_i = \frac{K_1 R_{11}}{\kappa_{cd} R_a (\omega_s^2 - \omega_o^2 + j2\lambda_s \omega_s \omega_o)} \text{ henrys}$$

where ω_o is the angular null frequency. M_i can also be determined by blocking the mass of the seismometer and measuring the signal coil output that results from a calibration input. In this case,

$$M_i = \frac{e_p R_{11}}{K_2 i_c R_a \omega} \text{ henrys}$$

where e_p is the peak-to-peak output voltage, i_c is the peak-to-peak calibrating current, and ω is the angular driving frequency. This method was used to determine the mutual inductance in three test seismometers and the average value was found to be .01453 henrys.

The transfer function given above can be rewritten as

$$\frac{E_o(s)}{I_c(s)} = \frac{K_2 s(s^2 + 2\lambda_s \omega_s s + \omega_s^2 + K_1/K_2)}{s^2 + 2\lambda_s \omega_s s + \omega_s^2}$$

Evaluated at a frequency of 1 Hz and with κ_{cd} equal to unity (the situation that applies in Step 1), the output voltage will be 42.29 mv for a calibrating current of 78.96 ma. If M_i were zero, the output would be 52.13 mv. Hence, the correction factor is 1.102 for nominal system parameters. The correction factor will vary with each instrument and it should be determined for individual seismometers. Perhaps a preferred procedure would be to set the digital sensitivity at a lower frequency where the correction factor is known to be 1.0 for all systems.

In determining the amplitude vs. period response of the intermediate-period system (as in Step 2), the nominal value of κ_{cd} is 0.6. The amplitude and phase response characteristics computed from the transfer function above for this case are shown in Figure 4.2 and the correction factor is plotted as a function of period in Figure 4.3. The mutual inductance of the calibration

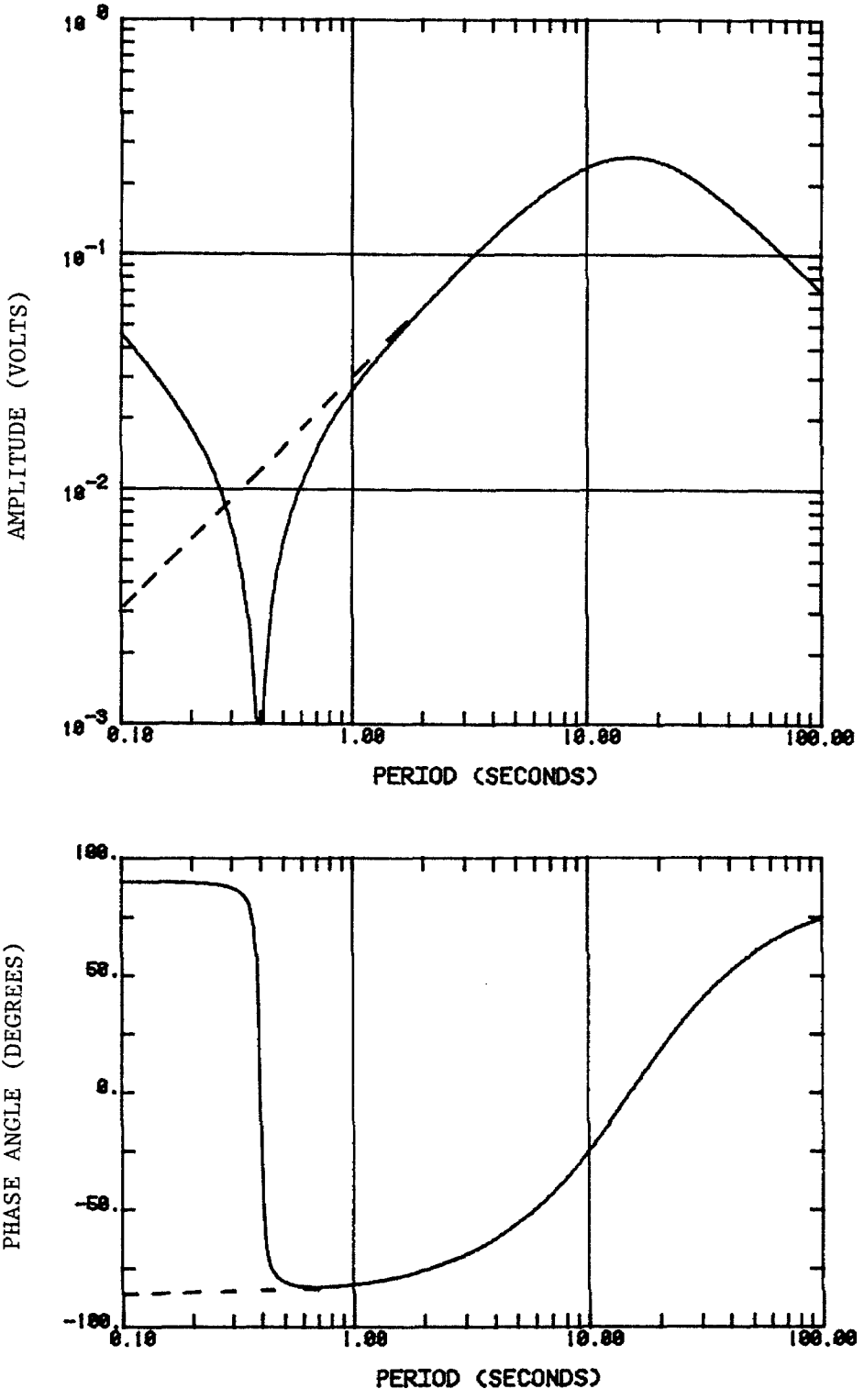

Figure 4.2.--Amplitude and phase responses of the DWWSS long-period seismometer for a calibration input of 78.96 ma peak to peak. The dashed lines illustrate responses for $M_i = 0$.

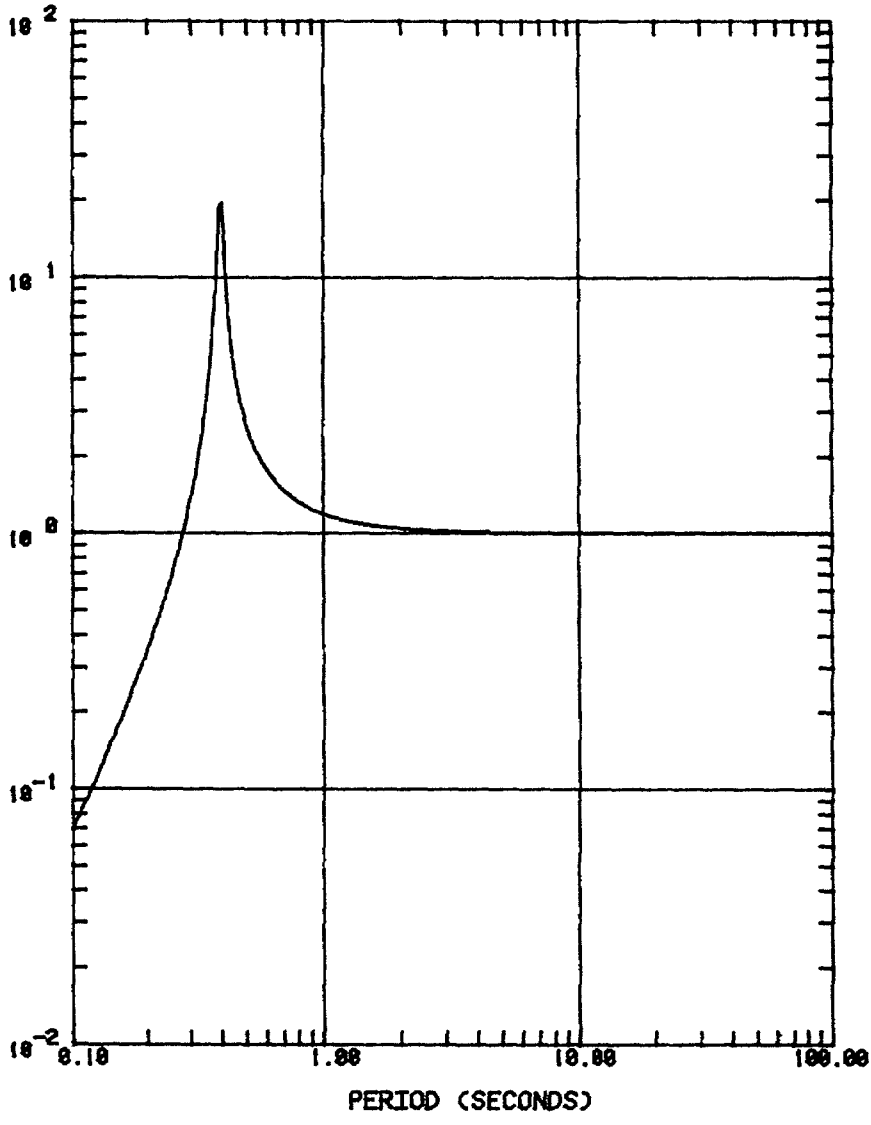

Figure 4.3.--Correction factor that must be applied to the output of a DWWSS long-period seismometer (nominal parameters) during a frequency response calibration.

and signal coils has no appreciable effect on the sine-wave or step function calibration of the long-period system.

There is essentially no means of verifying intermediate-period calibration on a day-to-day basis as the step function inputs used to calibrate the long-period systems are too small to trigger intermediate-period recording. This is a deficiency that needs to be corrected. A weekly calibration (once per tape) would be sufficient.

4.5 DWWSS Calibration Stability

The DWWSS system cannot be expected to have either the calibration accuracy or stability of digital systems, such as the SRO, that utilize modern, force-balance (inherently more stable) seismometers. However, with proper maintenance of the station equipment and diligent data review at the Albuquerque Seismological Laboratory, it should be possible to maintain data quality within acceptable limits. Realistically, one might expect an initial calibration adjustment accuracy of $\pm$ 5% in amplitude at the reference period and an amplitude stability of $\pm$ 10% between major calibration readjustments (which would include all of the calibration steps discussed in paragraphs 4.2 through 4.4). Unfortunately, the frequency of maintenance visits to the DWWSSN stations is dictated by the availability of funds rather than need, so any statement on calibration accuracy cannot be effectively guaranteed.

Parameter drift must be the principal concern with respect to DWWSS stability. Drift in the electronic components is not anticipated, based on our experience with similar electronics in other systems. However, seismometer period is subject to drift, and a change in period has more effect on system calibration than any other single parameter. The calibrator electrodynamic constant of the short-period seismometer is also known to drift. This constant is a function of mass position which is sensitive to changes in vault temperature.

The daily calibration step response provides a means of monitoring calibration stability and general system performance, and perhaps the means of computing accurate calibration data for individual components. However, to achieve maximum benefit from the step calibration, all of the systems should be calibrated with the maximum current short of overdriving the digital

recorder, if not daily, at least once per tape. This will improve the calibration signal-to-noise ratio at some stations and permit more consistent measurements to be made.

As part of the routine data review procedures at ASL, the amplitudes of calibration step responses are measured and filed with the station logs. The measurements are made on one set of step responses per tape (an interval of a week or less) selected during quiet periods. The measurements taken on State College (SCP) data over the first year of operation are plotted in Figure 4.4. This figure illustrates the results that one would hope to see from all stations. Measurement scatter is only a few percent, presumably because of a high calibration signal-to-noise ratio. The slopes of the long-period pulse amplitudes are nearly flat, -.022, +.282, and +.117 digital counts per day for the LPZ, LPN, and LPE components, respectively, based on a linear regression. This clearly indicates that the seismometer periods are not changing appreciably, nor are any other system parameters that affect either signal or calibration sensitivity. The short-period pulse amplitudes are consistent as well, although they appear to be affected by a seasonal variation, probably in vault temperature. The SCP measurements are fairly convincing evidence that the SCP data from that period of time are valid and reliable, and they are evidence that the DWWSS systems in general can produce reliable data if properly installed and serviced.

Measurements taken from other operational DWWSS stations are plotted in Figures 4.5 to 4.13. The results are mixed. The measurements from COL, KEV, and SLR look good. There is considerable scatter at several of the stations, such as BER and LON, because of high background noise, but the trend is stable. The results are erratic at several stations, such as ALQ, JAS, and TAU, where there have been operational difficulties. AFI measurements are not shown for the same reason. The step responses can be affected by several different types of malfunction. Unless the source of the problem is known, it is not possible to judge whether or not the earth signals are affected as well as the calibration pulse. In the case of the ALQ horizontal components, the malfunction was determined to be caused by small wires on the coils that were rubbing against the magnets. Since this clearly would affect the linearity of the seismometers, the data for that period of time must be considered invalid. The same difficulty is suspected at TAU. At some WWSS

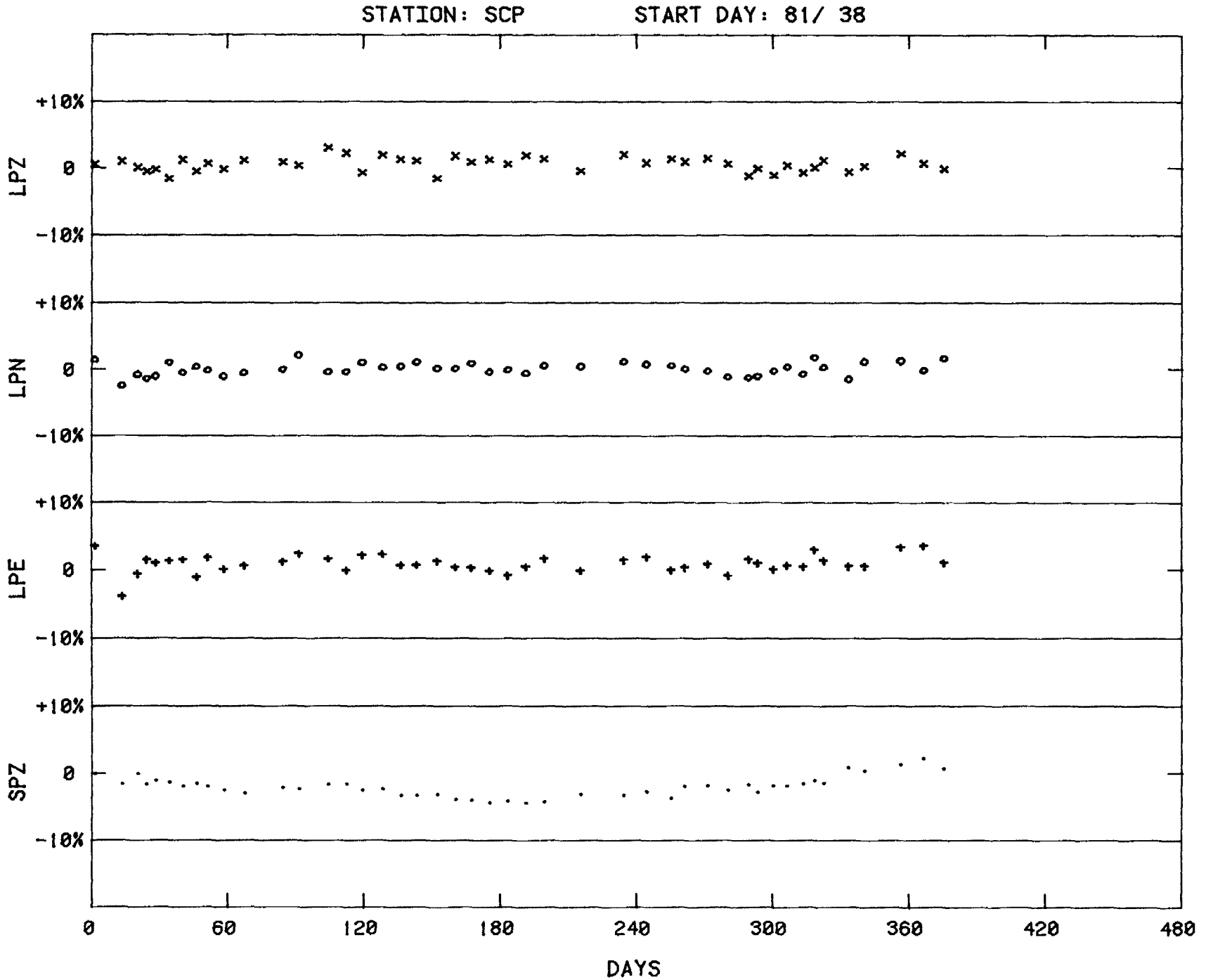

Figure 4.4.--Variation of peak step response amplitudes as a function of time at SCP.

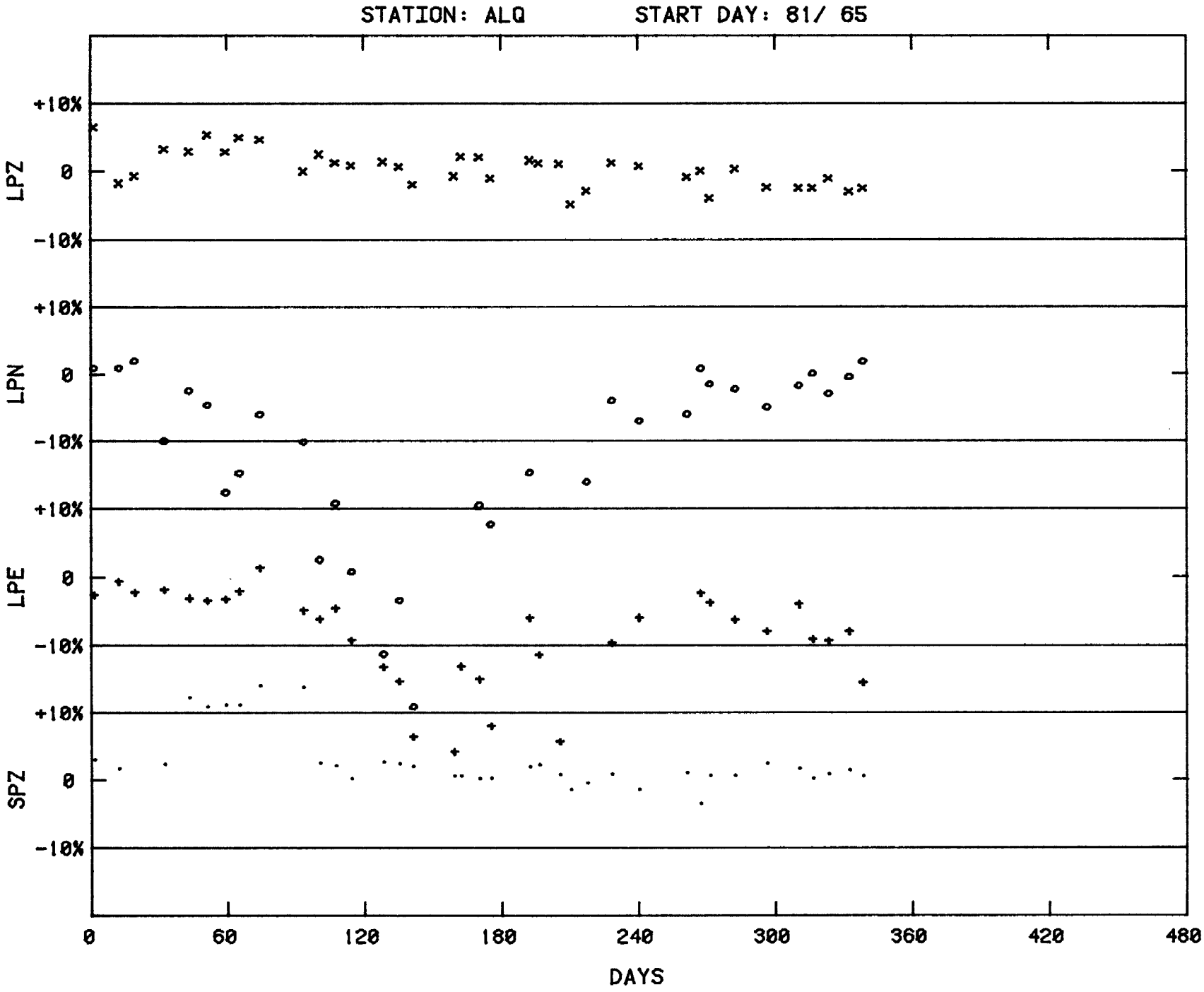

Figure 4.5.--Variation of peak step response amplitudes as a function of time at ALQ.

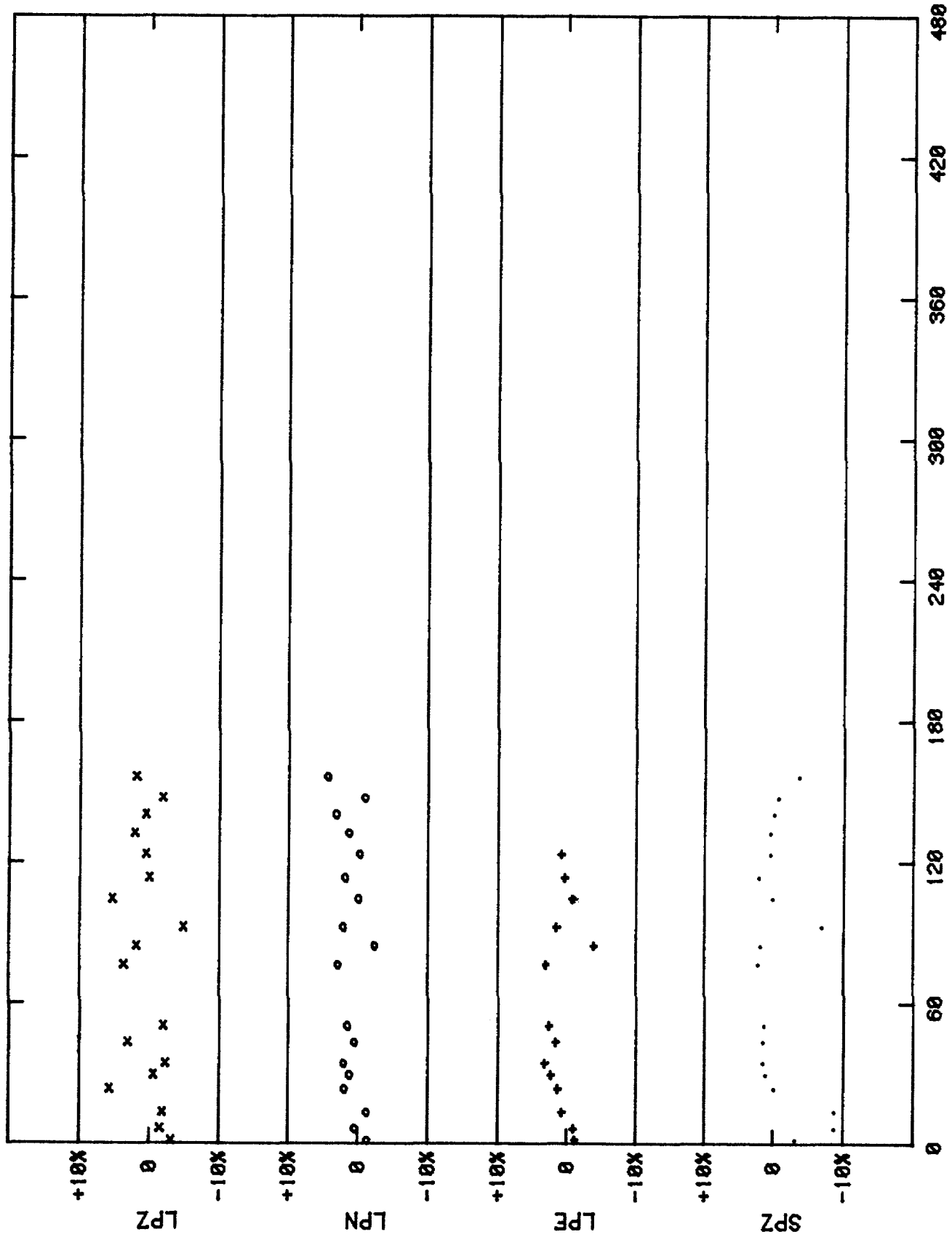

Figure 4.6.--Variation of peak step response amplitudes as a function of time at BER.

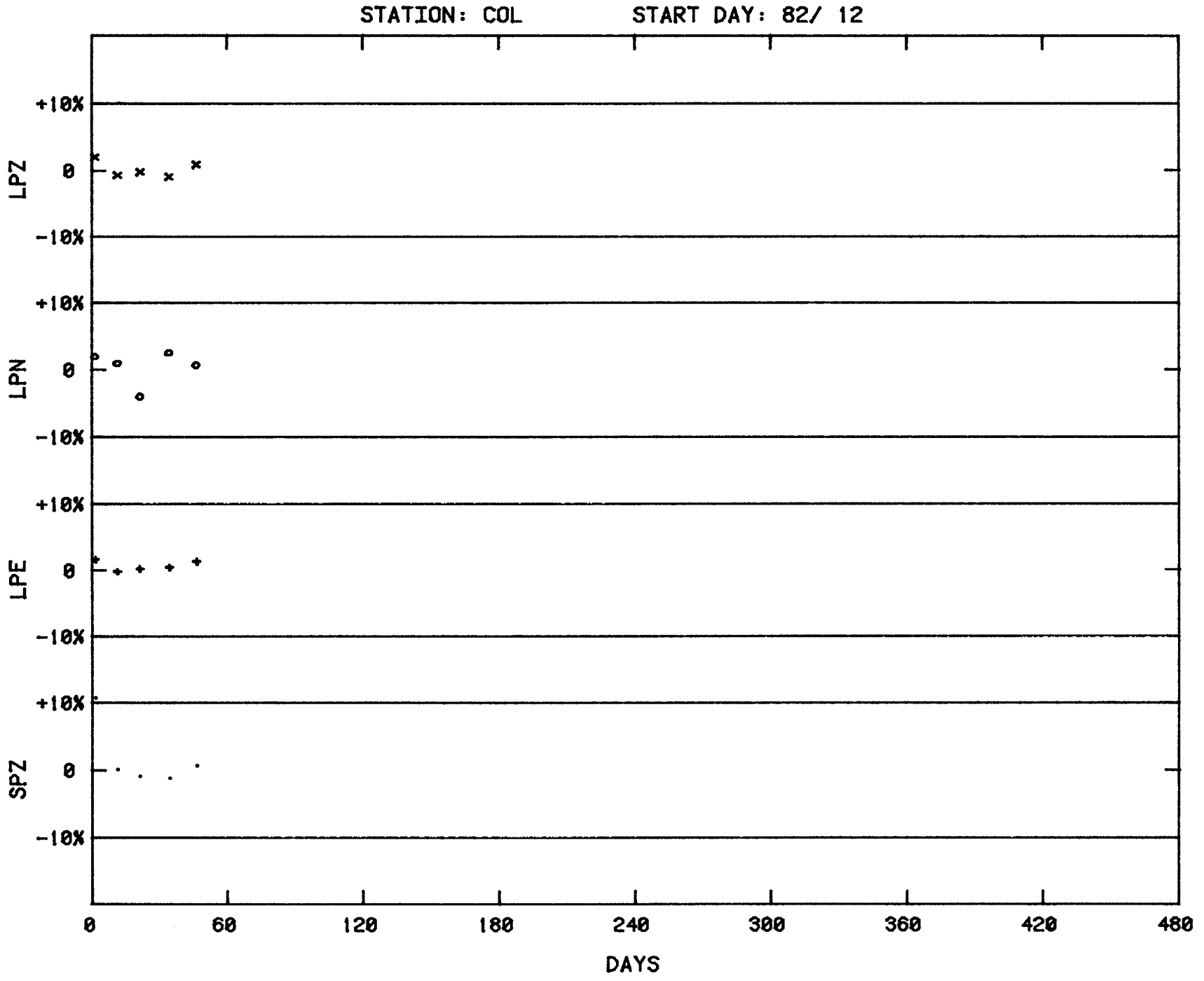

Figure 4.7.--Variation of peak step response amplitudes as a function of time at COL.

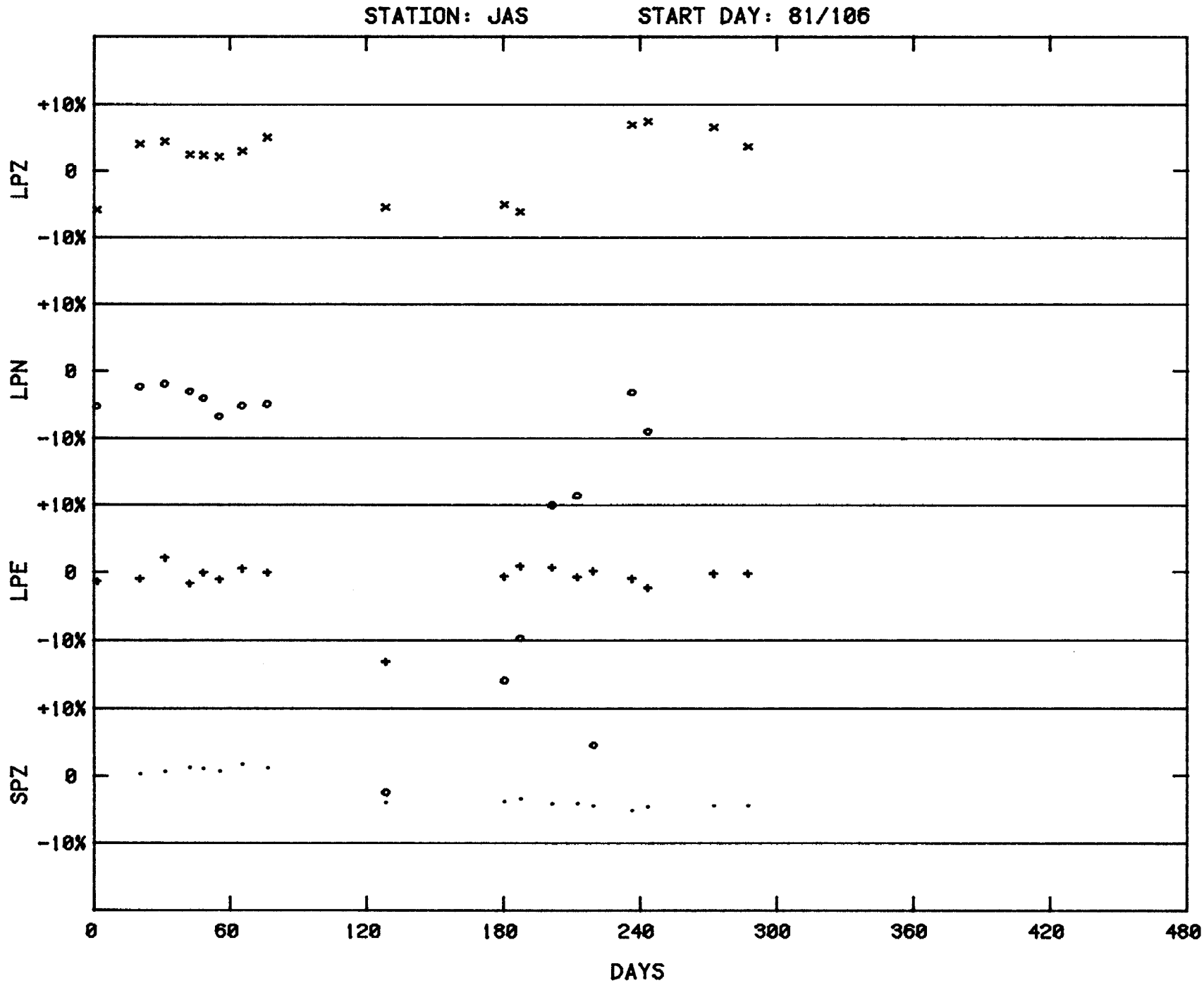

Figure 4.8.--Variation of peak step response amplitudes as a function of time at JAS.

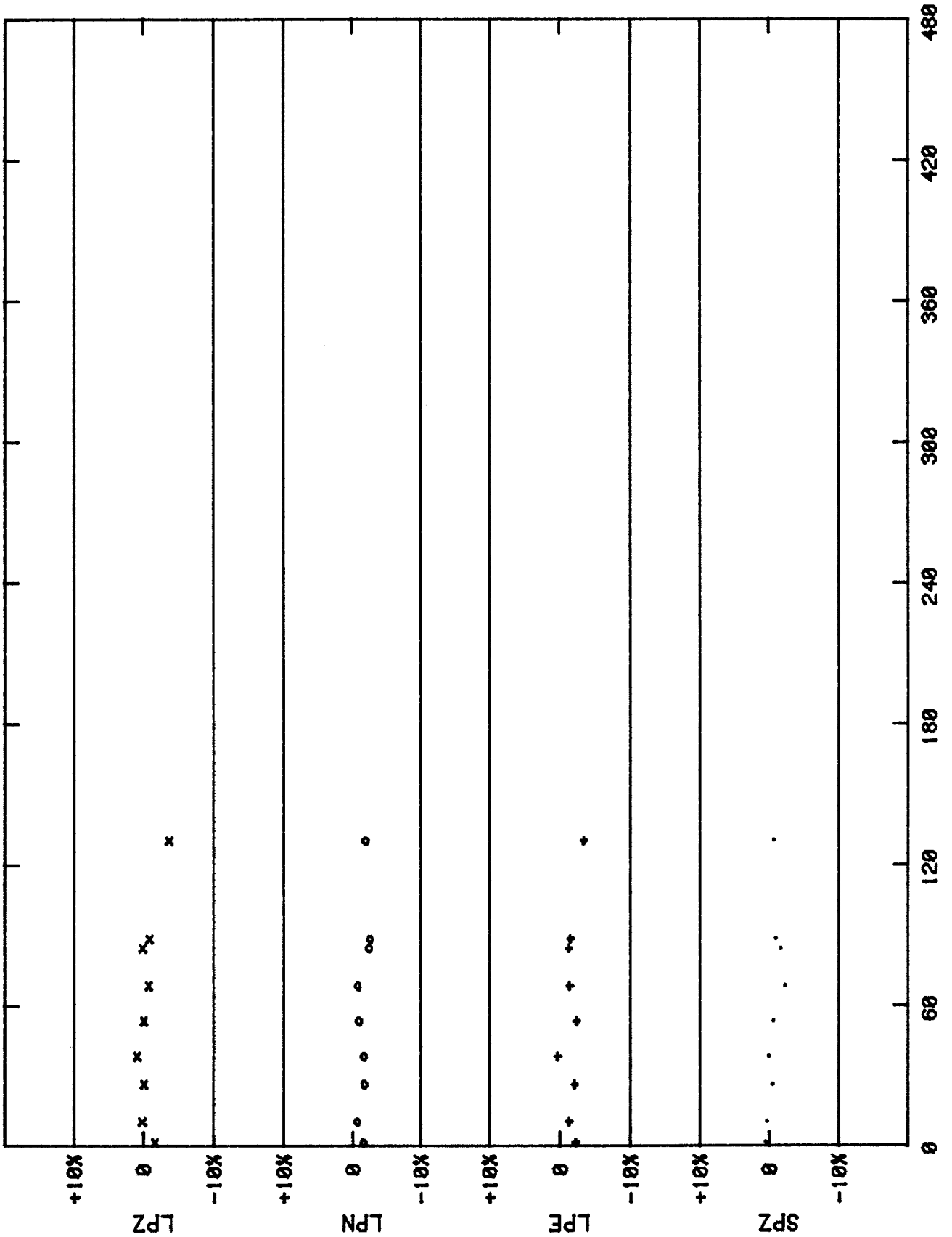

Figure 4.9.--Variation of peak step response amplitudes as a function of time at KEV.

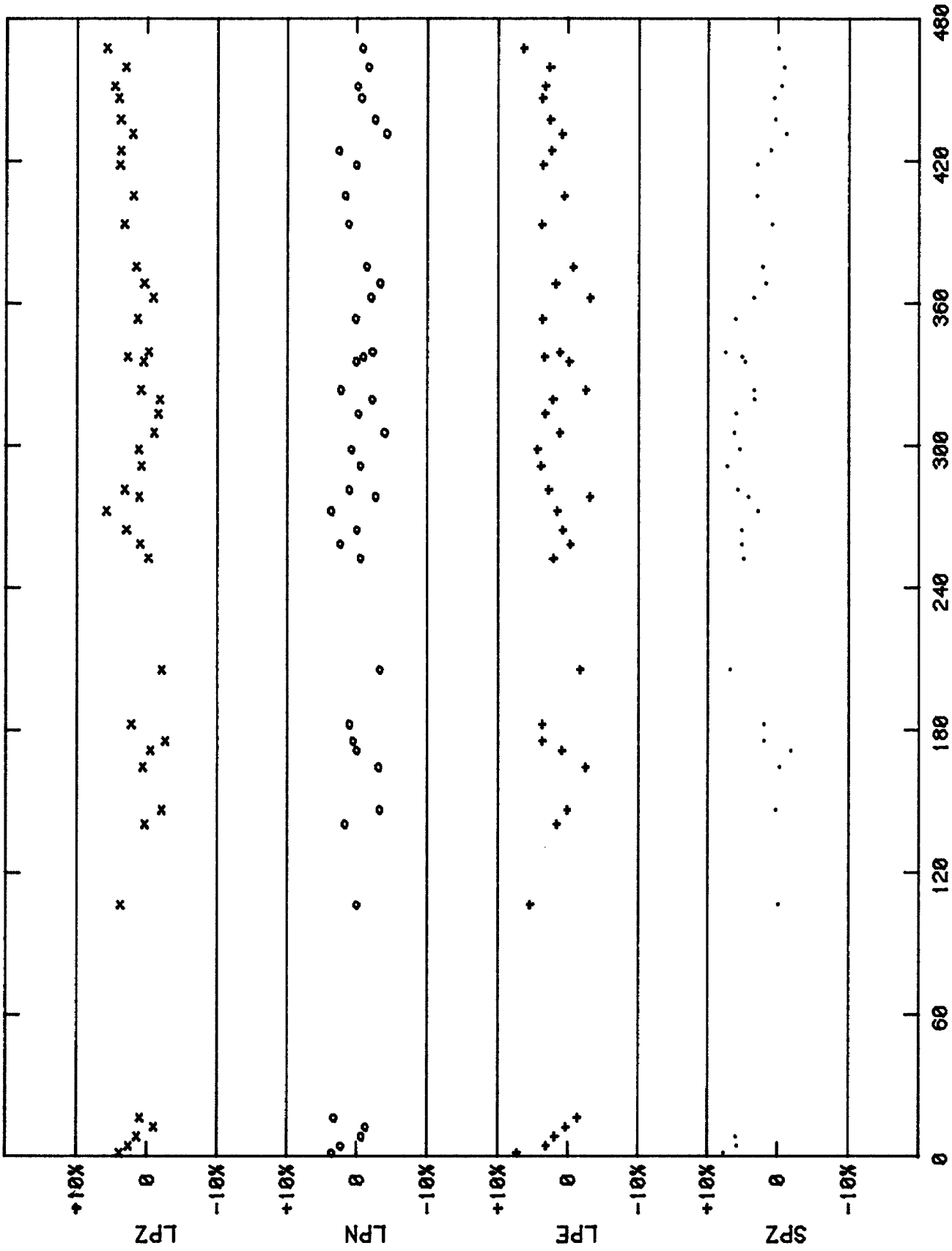

Figure 4.10.--Variation of peak step response amplitudes as a function of time at LON.

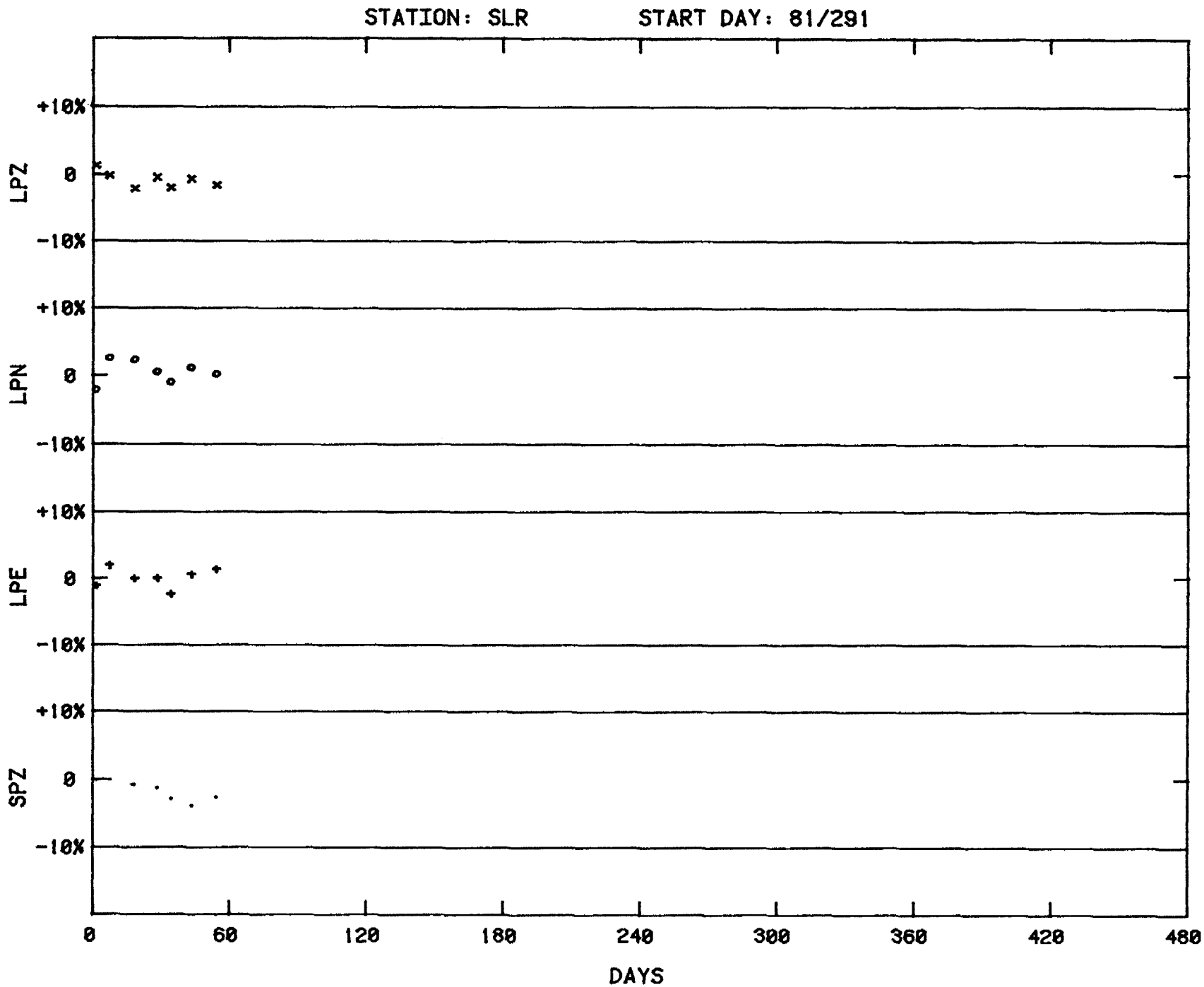

Figure 4.11.--Variation of peak step response amplitudes as a function of time at SLR.

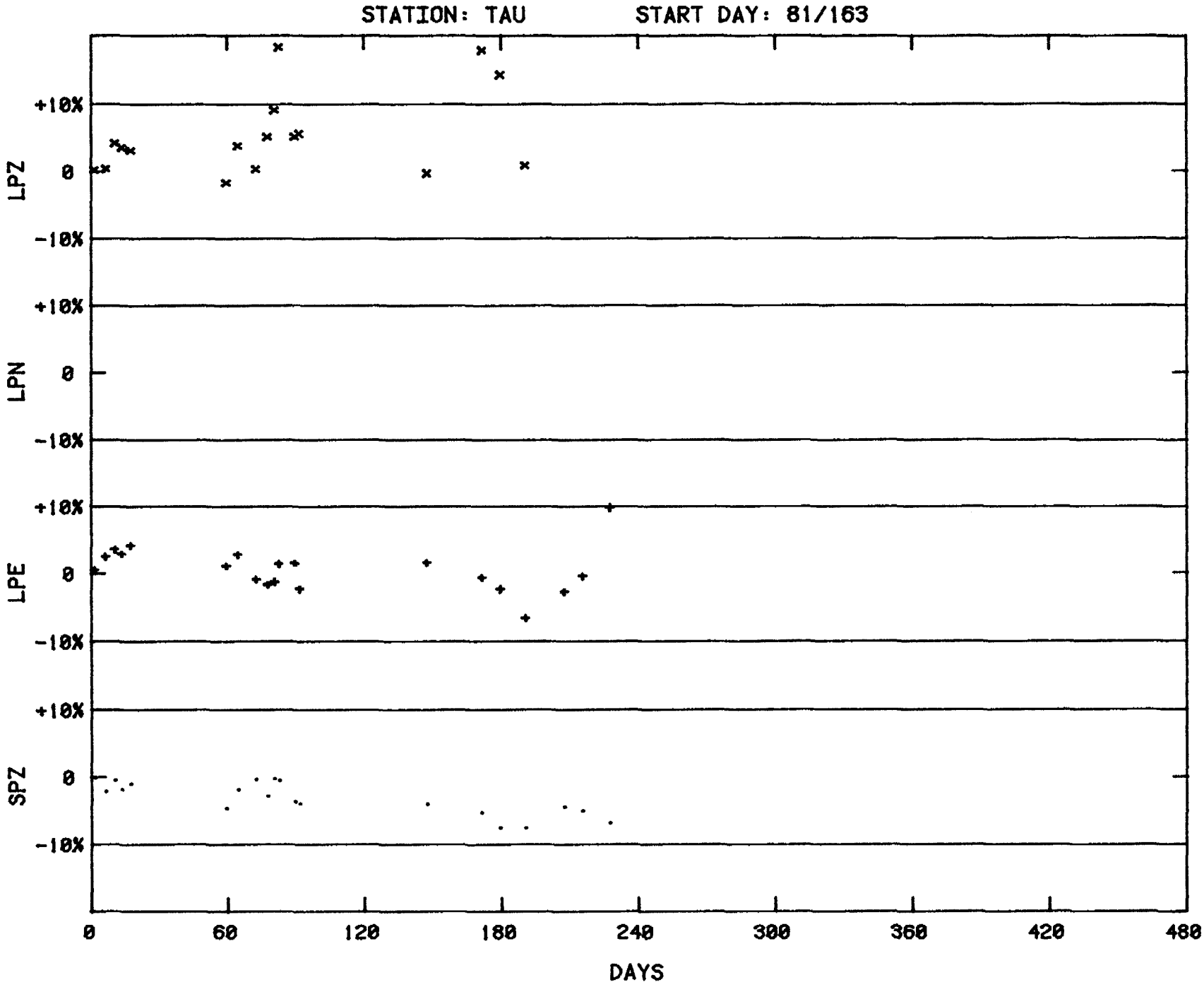

Figure 4.12.--Variation of peak step response amplitudes as a function of time at TAU.

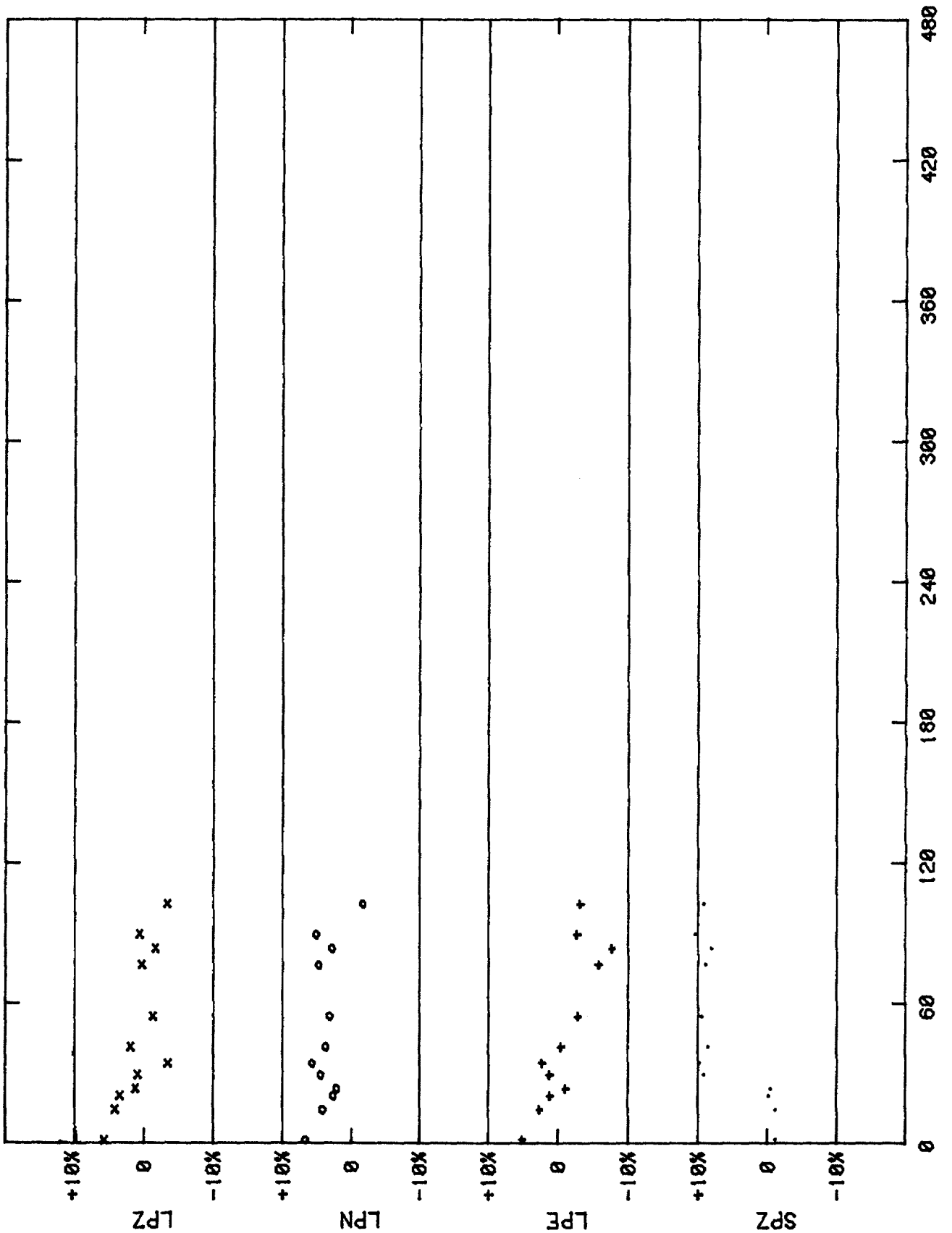

Figure 4.13.--Variation of peak step response amplitudes as a function of time at TOL.

locations, particularly in humid climates, the calibration signal has been affected by leakage. In this case, the data may still be good even though the calibration pulse is erratic. There are plans to automate the measurement and plotting of daily peak step response amplitudes, as these plots are valuable in evaluating the performance of the DWWSS systems.

4.6 Analysis of the Step Response

4.6.1 General

The step calibration is an efficient calibration technique since the step response disturbs the recording for only a short time, yet in theory it contains all of the information needed to determine the system transfer function. Several techniques have been developed for the analysis of seismograph step responses. Espinosa and others (1962, 1965) used a Fourier transform to determine the steady-state response characteristics of long-period seismographs and compiled a library of step responses that could be used as overlays to match the step responses recorded by operating systems. A series of papers (Mitchell and Landisman, 1969; Jarosch and Curtis, 1973; Mitronovas, 1976; McGonigle and Burton, 1980) deals with techniques or refinements of techniques using least-squares inversion of step responses to determine instrument parameters, particularly as applied to the WWSS long-period system. Berg and Chesley (1976) used the Fourier transform to determine steady-state response characteristics of the High-Gain Long-Period (HGLP) digital seismograph and found that the technique is improved by averaging a number of successive pulses to reduce the background noise before transforming. Based on the work cited above and the brief study of DWWSS step responses described below, it appears feasible to automate the computation of transfer functions for individual components, at least for the DWWSS long-period system. More work needs to be done and perhaps some calibration procedural changes will be needed, however, to fully exploit the DWWSS step calibration.

A set of long-period step responses recorded on the ALQ and SCP DWWSS digital recorders from the long-period channels are shown in Figures 4.14 through 4.17. The noisy ALQ waveform for day 82:049 was purposely included in the data set to test the effect of long-period (as opposed to 6-8 sec) noise in the analyses. Because of the insensitivity of the intermediate-period channels, there are no usable step responses recorded on these

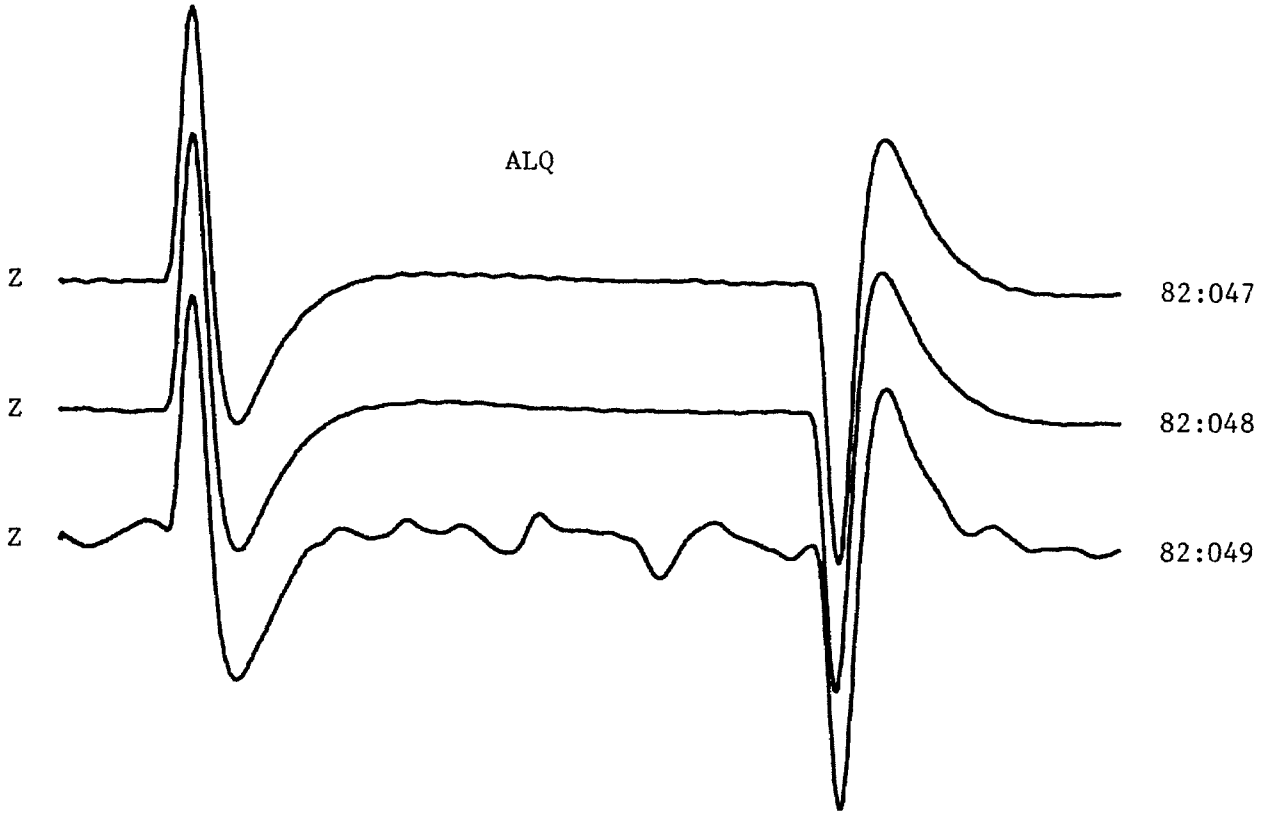

Figure 4.14.--Step calibration pulses recorded from the ALQ LPZ components for three successive days.

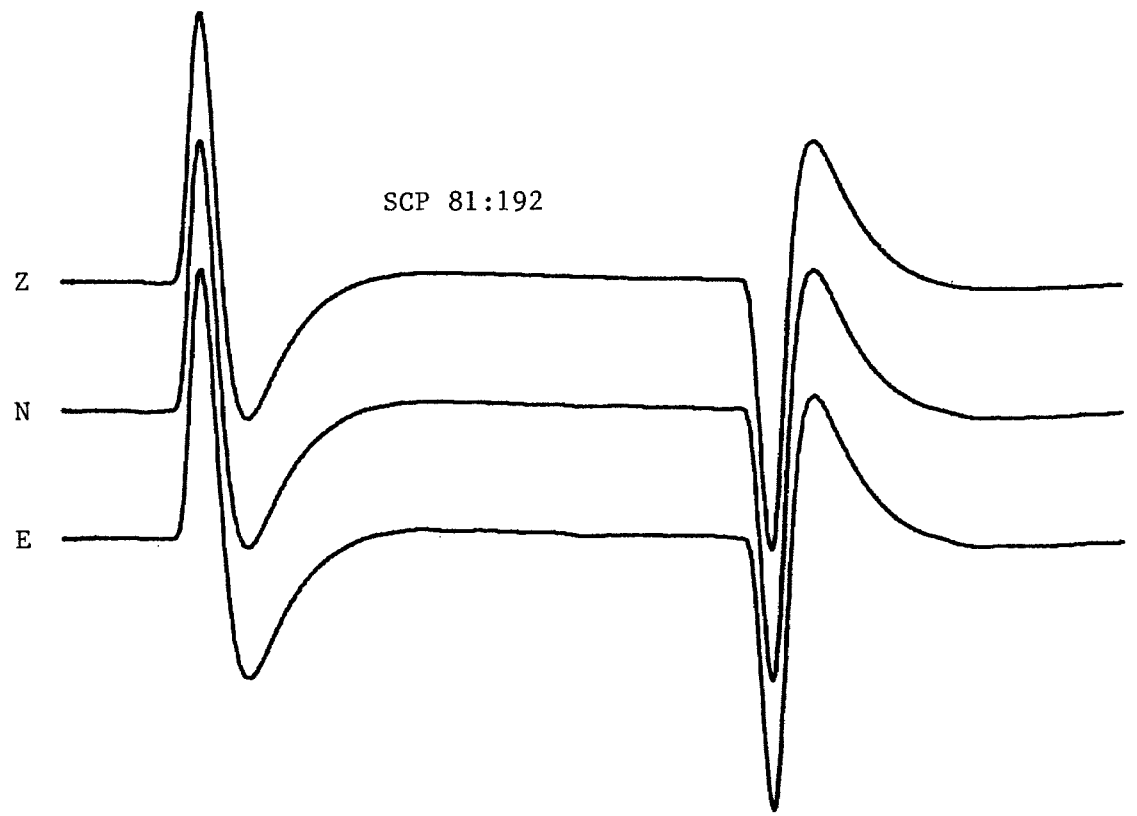

Figure 4.15.--Step calibration pulses recorded from the three SCP LP components on the same day.

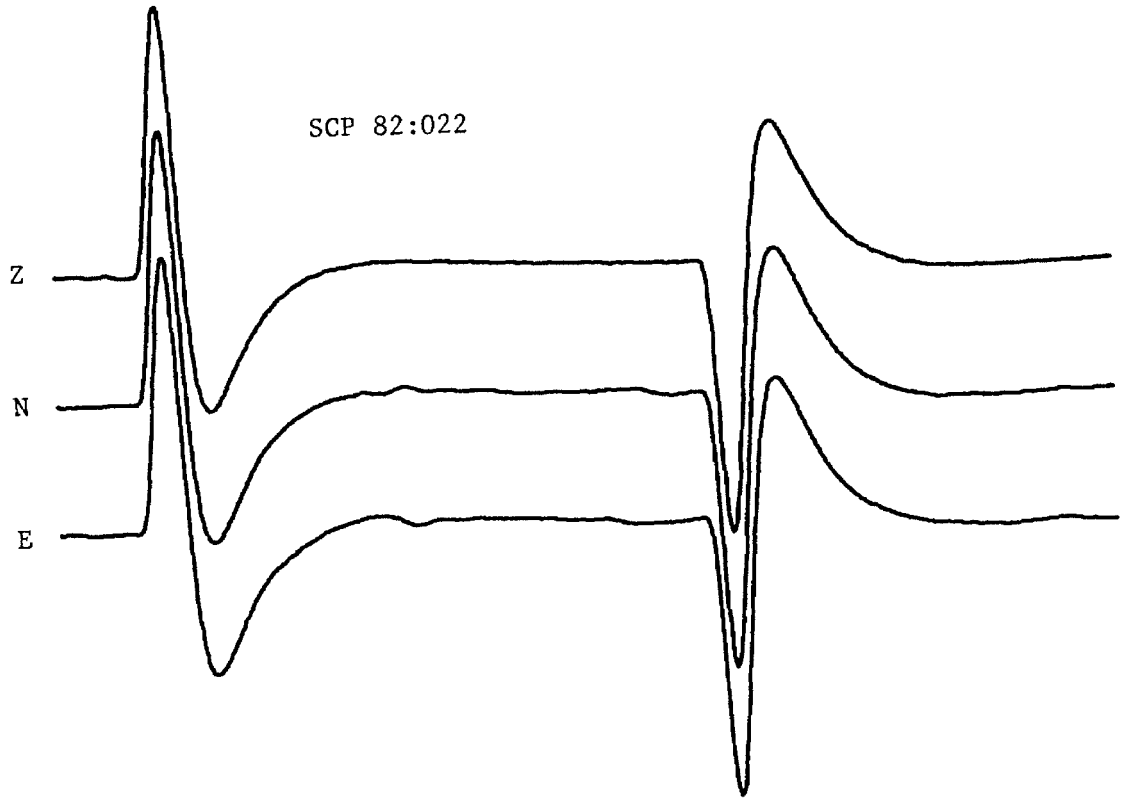

Figure 4.16.--Step calibration pulses recorded from the three SCP LP components.

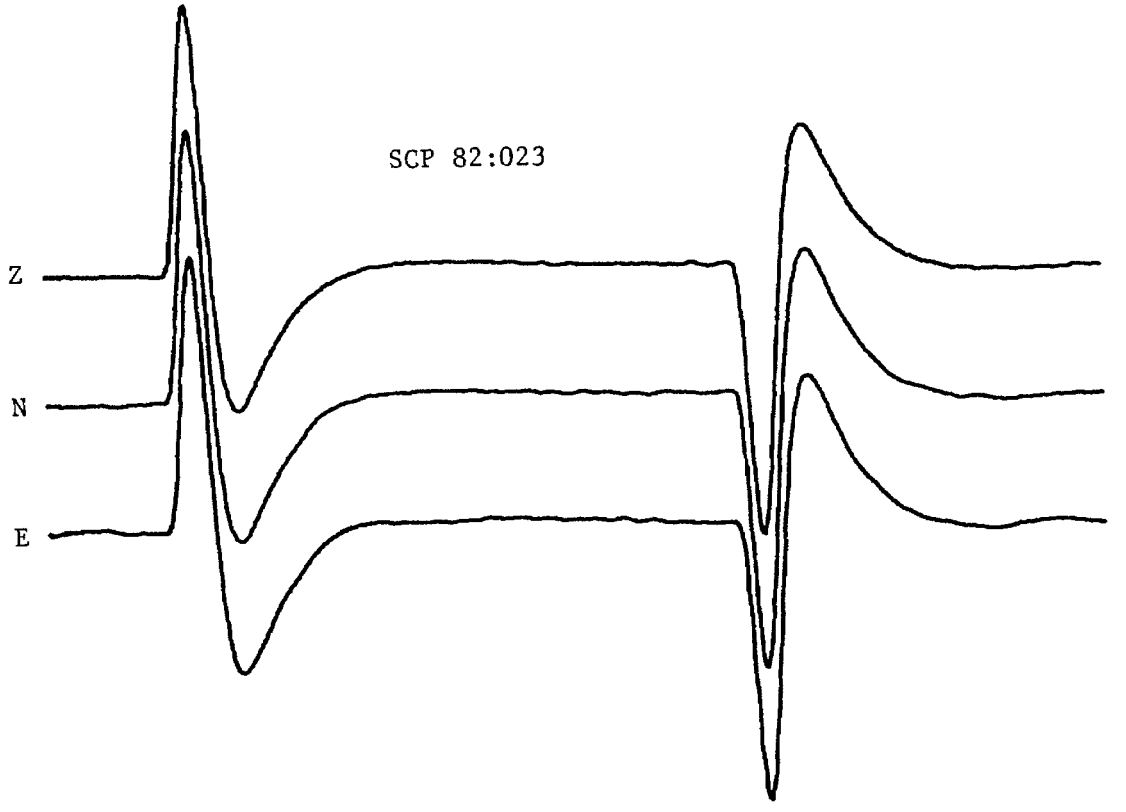

Figure 4.17.--Step calibration pulses recorded from the three SCP LP components.

channels routinely. One of the recommended changes in calibration procedure is to apply a step calibration of maximum amplitude (1.6 ma) to the long-period seismometer once each week, just before or after a tape change. Currently, the Fourier analysis of DWWSS short-period step responses is not practical because of the rapid succession of the ON and OFF pulses (see Figure 4.18). Spacing of several minutes between the SP ON and OFF pulses is another change in procedure that is recommended for implementation.

4.6.2 Fourier Transformation

By previous definition (para. 3.3.1), the general expression for the system transfer function can be written as

$$H(s) = R(s)/T(s) \quad \text{digital counts/newton-meter}$$

where

$$T(s) = G_c r_{cm} I(s) \quad \text{newton-meters (for a calibration input)}$$

$$T(s) = -Mr_{cm} X(s) s^2 \quad \text{newton-meters (for an input of earth displacement)}$$

Then, the earth displacement equivalent to the calibration input is

$$X(s) = -\frac{G_c I(s)}{Ms^2} \quad \text{meters}$$

and we can express the transfer function with respect to equivalent earth displacement during a calibration as

$$H(s) = \frac{R(s)}{X(s)} = -\frac{Ms^2}{G_c I(s)} \cdot R(s) \quad \text{digital counts/meter}$$

For a step of calibration current, $I(s) = i_c/s$, so

$$H(s) = -\frac{Ms^3}{G_c i_c} \cdot R(s)$$

The transfer function is evaluated in the frequency domain by letting $s = j\omega$, so

$$H(j\omega) = \frac{j\omega^3 M}{G_c i_c} \cdot R(s) \quad \text{digital counts/meter} \qquad (4.3)$$

where $H(j\omega)$ is the complex frequency response of the system and $R(j\omega)$ is the Fourier transform of the step response.

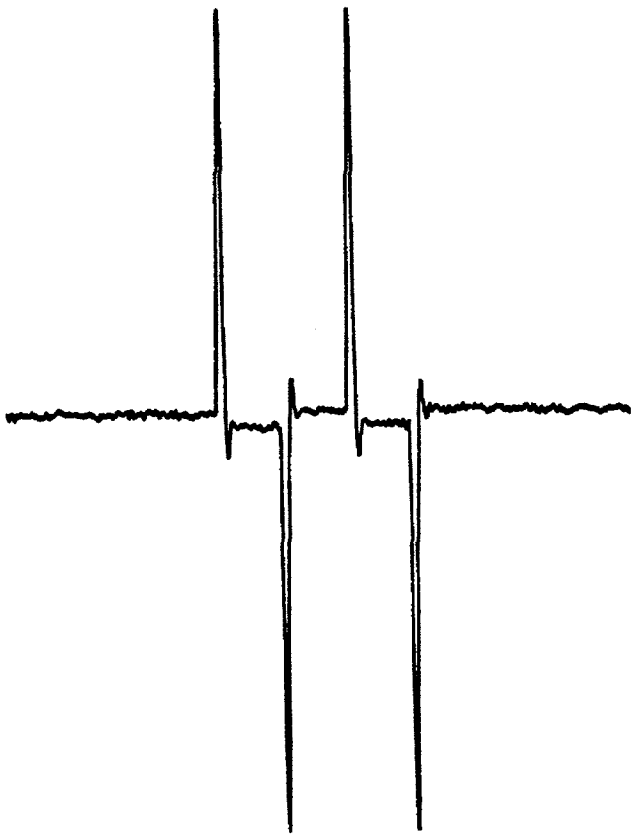

Figure 4.18.--Typical short-period calibration (two in succession) recorded at a DWWSS station (SCP). The length of the waveform is 49.5 seconds. The offset is caused by the high-pass filter time constant. To make the waveforms more suitable for analysis, several minutes of recovery is needed between the pulses.

Step response waveform data were prepared in 256 point segments and transformed using an FFT. Since the calibration onset time is unknown, it was necessary to assume an onset occurring 23 seconds before the peak recorded amplitude (the delay determined from a synthetic step response computed using the nominal system transfer function). Hence, the phase angle obtained from the transformation could be slightly in error. Amplitudes and phase angles computed from five successive SCP vertical-component step responses (days 82:020 through 82:024) are plotted in Figure 4.19. The results are consistent and close to predicted values except at the shorter periods where the signal is contaminated by microseismic noise. Similar data are plotted in Figure 4.20 for the three successive ALQ step responses shown in Figure 4.14. The poorer calibration signal-to-noise ratio increases the scatter in this case. The curve that diverges at periods above 25 seconds was computed from the noisy ALQ step response (day 82:049). The five successive SCP step responses were averaged, as suggested by Berg and Chesley (1976), then transformed. Amplitudes and phase angles are plotted in Figure 4.21. Above a period of about 12 seconds, the match between experimental and predicted response data is very good, but there is still considerable scatter in the microseismic band.

The usefulness of the step response transformation is limited because there is no direct method of transforming from the frequency domain to the Laplace domain to yield a refined system transfer function, which is the primary goal of calibration. However, it can be used as a rapid, automated check to insure that the system response falls within certain limits and it may be the most efficient way of monitoring digital sensitivity. For example, the digital sensitivity of the SCP LPZ channel, computed from the average of the five successive step response transforms, is 485 digital counts per micrometer at a period of 25 seconds with a standard deviation of only 4.82 digital counts per micrometer. This is a more precise measurement than one could obtain from a scalar measurement of peak response amplitude.

4.6.3 Least-Squares Fitting of the Step Response

The least-squares fitting of a recorded step response to synthetic step responses is potentially more useful than the Fourier transformation because the technique yields parameter values. The four principal in-band

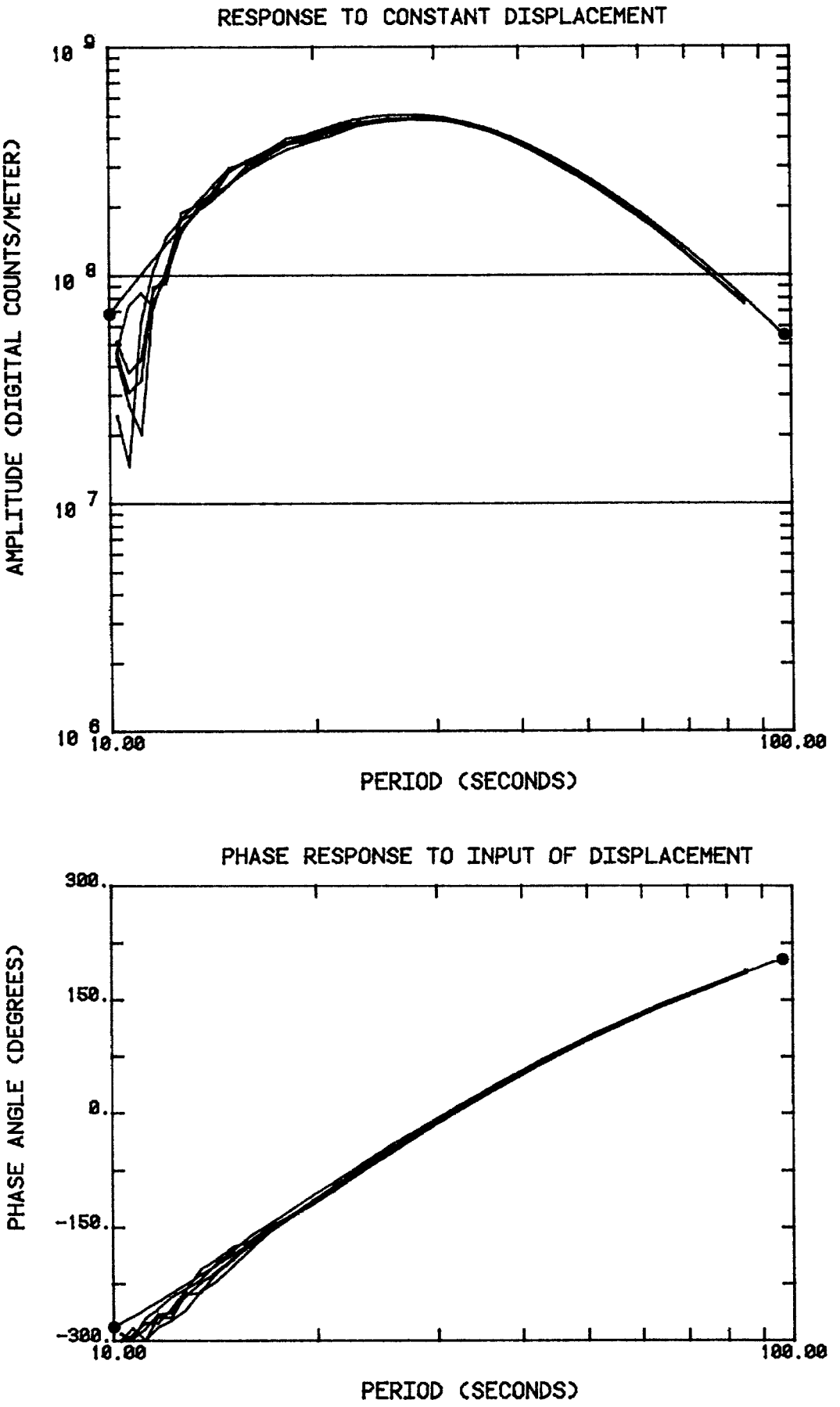

Figure 4.19.--Steady-state amplitude and phase response of the SCP LPZ component derived from the Fourier transforms of five successive daily step responses and compared with the nominal response computed from the transfer function (curves marked by bullets).

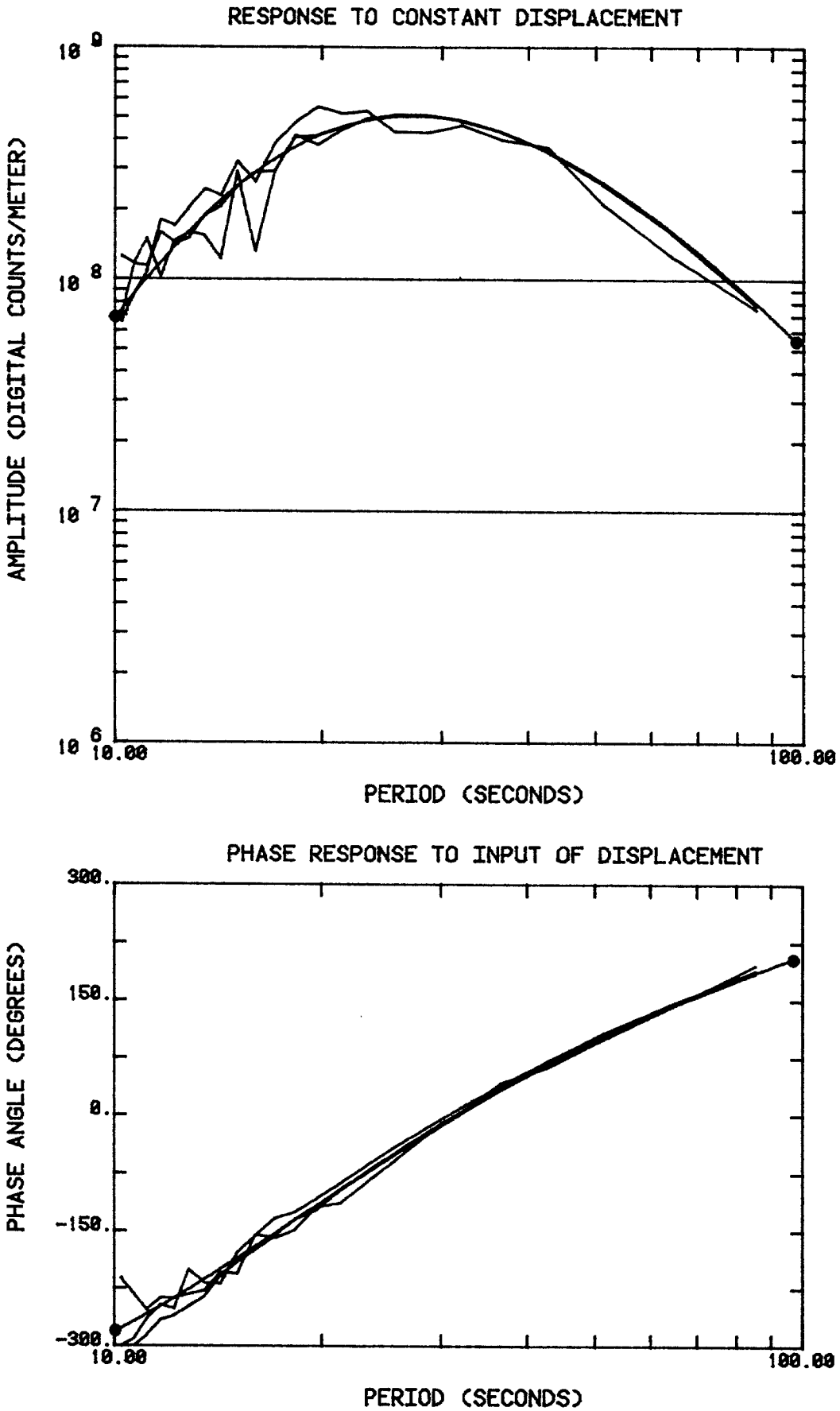

Figure 4.20.--Steady-state amplitude and phase response of the ALQ LPZ component derived from the Fourier transforms of three successive daily step responses and compared with the nominal response computed from the transfer function (curves marked by bullets).

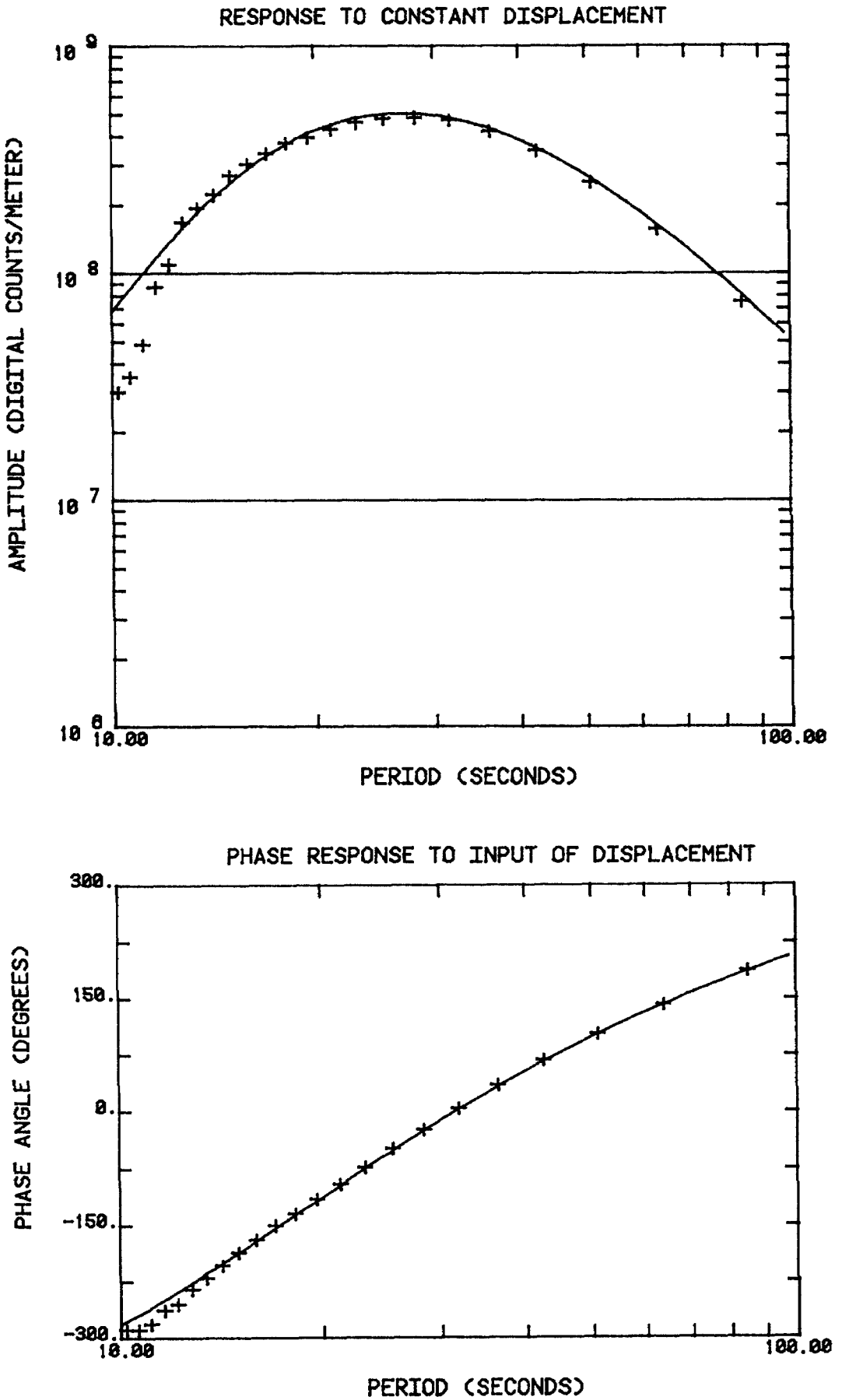

Figure 4.21.--Steady-state amplitude and phase response of the SCP LPZ component derived from the average of five successive daily step responses (+) compared with the nominal response computed from the transfer function (solid lines).

variables in the DWWSS long-period system are the seismometer period and damping, the low-pass filter corner at 22.8 seconds, and the low-pass filter corner at 9.6 seconds. Of these, the seismometer period is of primary importance because it dominates the in-band response characteristics of the system and is the most likely parameter to drift.

The effectiveness of the fitting technique in determining parameter values was tested using the step response waveforms appearing in Figures 4.14 through 4.17. The waveform data were prepared for analysis as follows. In order to achieve more accurate time alignment between the recorded and synthetic pulses, the sampling interval of the recorded waveform was shortened to .25 seconds by interpolating three additional points between each recorded sample. This was done by adding three zeros at .25 second intervals between the samples, transforming with an FFT, setting the Fourier components to zero at frequencies above the Nyquist frequency, then using an inverse FFT to reconstruct the waveform with the interpolated points. The ON pulse was then time aligned with the inverted OFF pulse and the two were averaged to produce a single pulse waveform 1024 samples in length. In practice, it was found that the averaged pulse usually yielded the most sensitive fit, although occasionally either the ON or OFF pulse produced the best results.

Synthetic pulses were generated by inserting trial parameters in the system transfer function, computing the Fourier components, then applying an inverse FFT. Files of synthetic pulses were compiled to speed the fitting, one file for each variable. Then the recorded waveform was successively matched against the synthetic waveforms stored in the file. Peak amplitudes were normalized and least-square fitting was used to achieve the best time alignment. Amplitude differences between the synthetic and recorded samples were computed, squared, and the sum of the errors squared were plotted as a function of the variable. More efficient procedures can be developed if fitting is done routinely in the future; the purpose of these tests was simply to evaluate the effectiveness of the technique with DWWSS data.

The results of matching step responses to synthetics as a function of seismometer period are shown in Figures 4.22 through 4.25 for the ALQ and SCP test data. The step responses are very sensitive to changes in seismometer period and least-squares fitting appears to be a practical way of determining seismometer period. Except for the noisy ALQ step response, the results

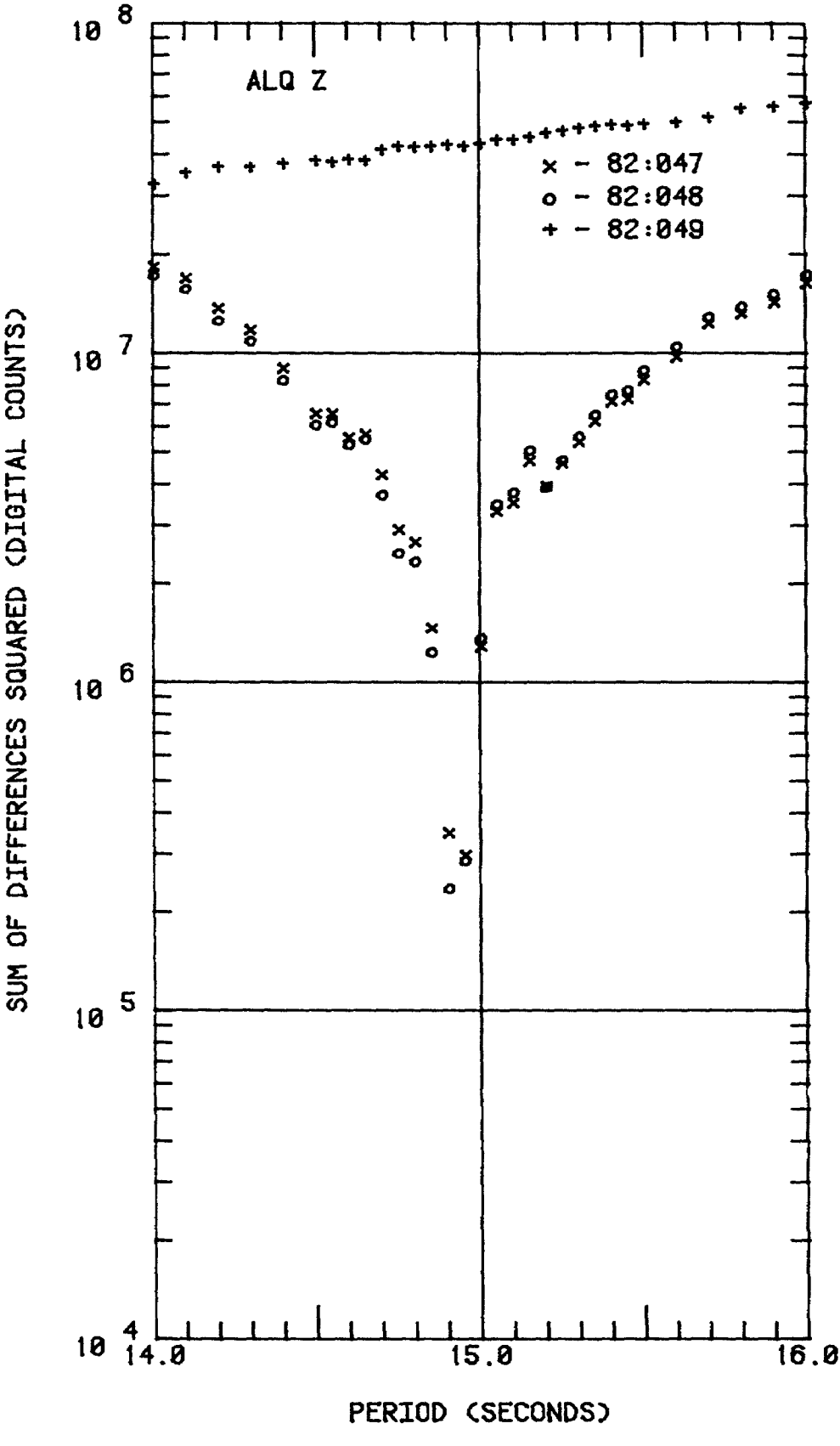

Figure 4.22.--Sum of differences squared vs. seismometer period using calibration pulses shown in figure 4.14.

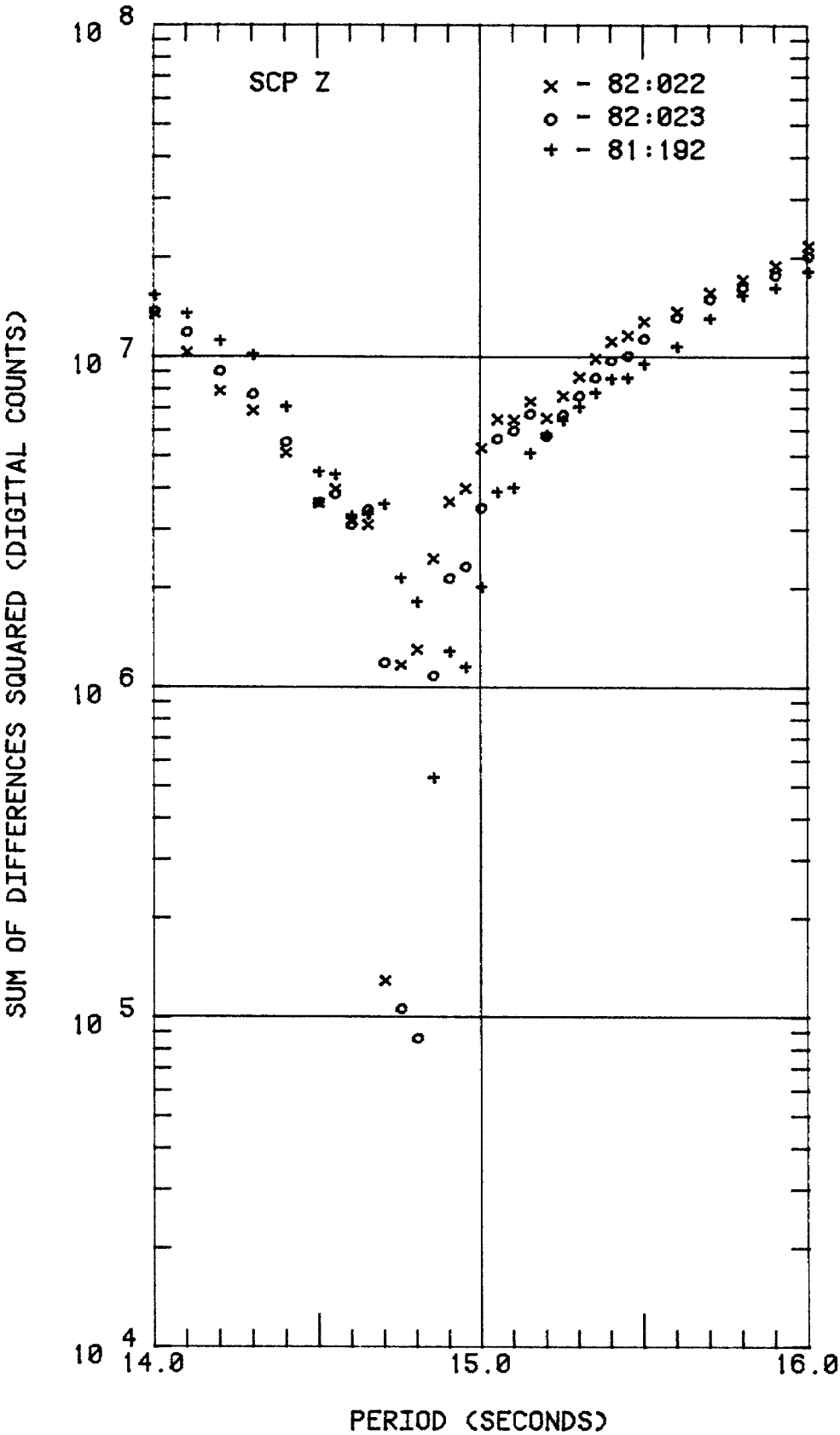

Figure 4.23.--Sum of differences squared vs. seismometer period using vertical component calibration pulses shown in Figures 4.15 through 4.17.

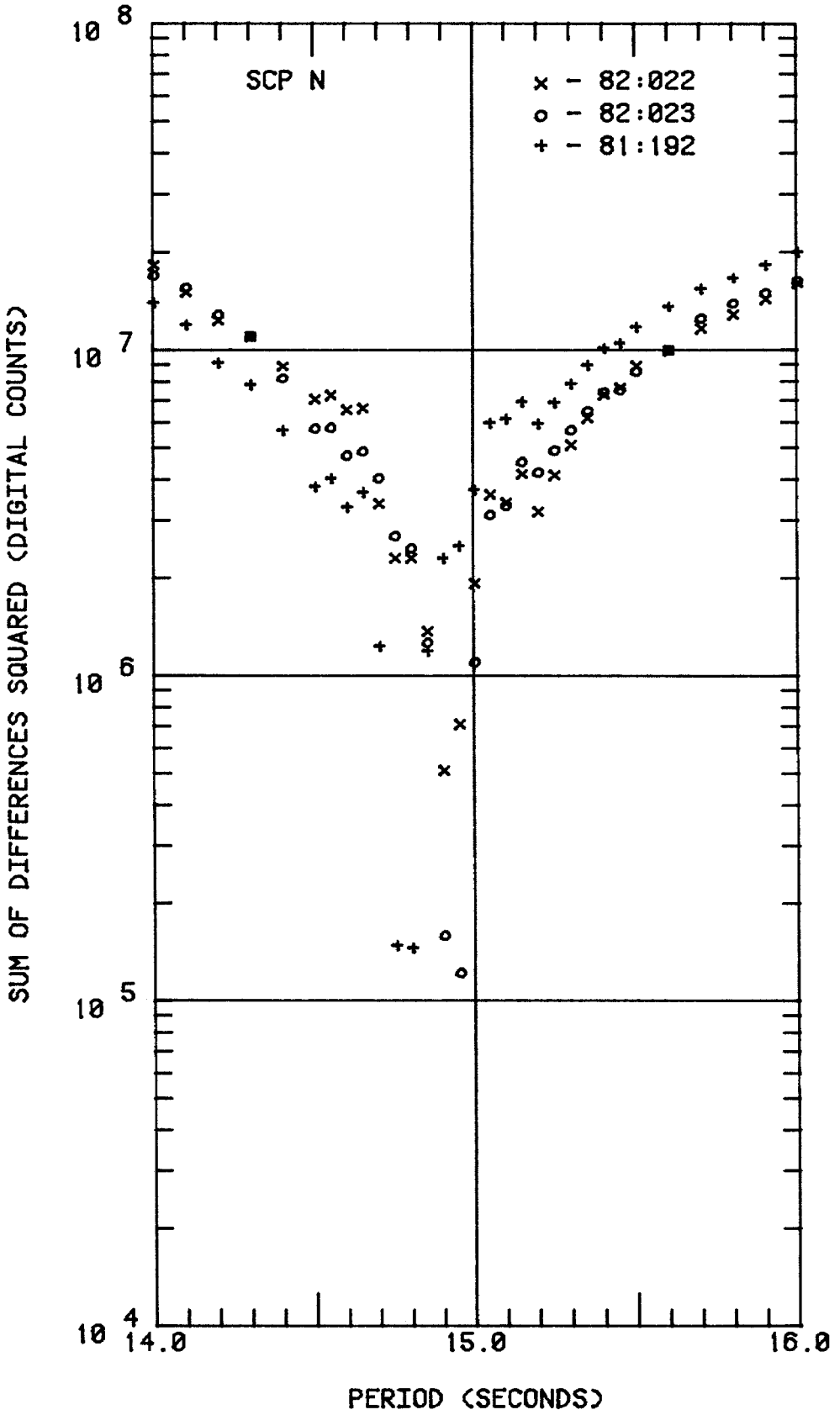

Figure 4.24.--Sum of differences squared vs. seismometer period using north component calibration pulses shown in Figures 4.15 through 4.17.

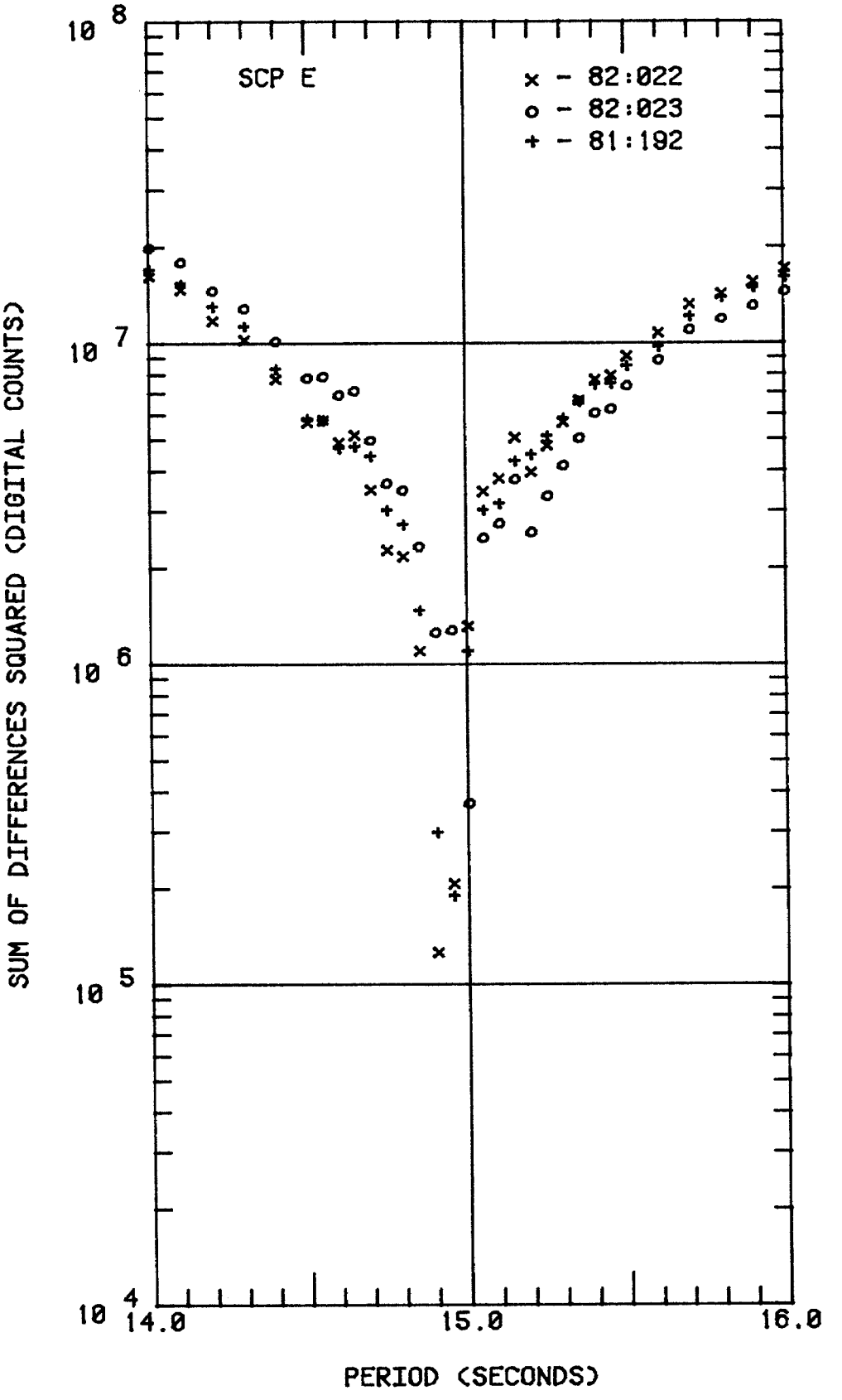

Figure 4.25.--Sum of differences squared vs. seismometer period using east component calibration pulses shown in Figure 4.15 through 4.17.

are consistent for successive days. The SCP data set includes step responses for two successive days and a step response recorded approximately six months earlier. It would appear that the vertical seismometer has drifted slightly to a shorter period, the north seismometer has drifted to a longer period, and the east seismometer has been stable over this interval. In any event, the drift has been small, which is consistent with the stability of the peak response amplitudes plotted in Figure 4.4 (the peak response amplitude is nearly proportional to the square of the period). The fact that the seismometer periods are shorter than 15 seconds can be accounted for in part by the fact that air-damped periods are measured and used for adjustment.

The results of matching step responses to synthetics computed as a function of seismometer damping are shown in Figures 4.26 through 4.29 for each set of two successive step responses. The step response is less sensitive to the magnitude of damping variation used in generating the synthetics and the results are inconsistent. Better results might be obtained if the recorded waveforms were matched to synthetics that have been generated using the period determined for the individual components during the period fit. Figures 4.30 and 4.31 show the results of matching ALQ step responses to synthetics computed as functions of the low-pass filter corners. The step response is sensitive to the corner at 22.8 seconds (and would appear to confirm its location) but relatively insensitive to the corner at 9.6 seconds.

More work is needed to verify and improve upon these experimental results. Clearly, however, the determination of seismometer period by least-squares fitting of the step responses to synthetics is feasible as a routine procedure if the signal-to-noise ratio is adequate. The technique will be of value if used only for that purpose. No attempt has been made to apply least-squares inversion to the DWWSS short-period calibration pulses. This is expected to be a more complex problem because of the increased number of critical variables in the system, their interdependence, and the effect of seismometer-galvanometer coupling.

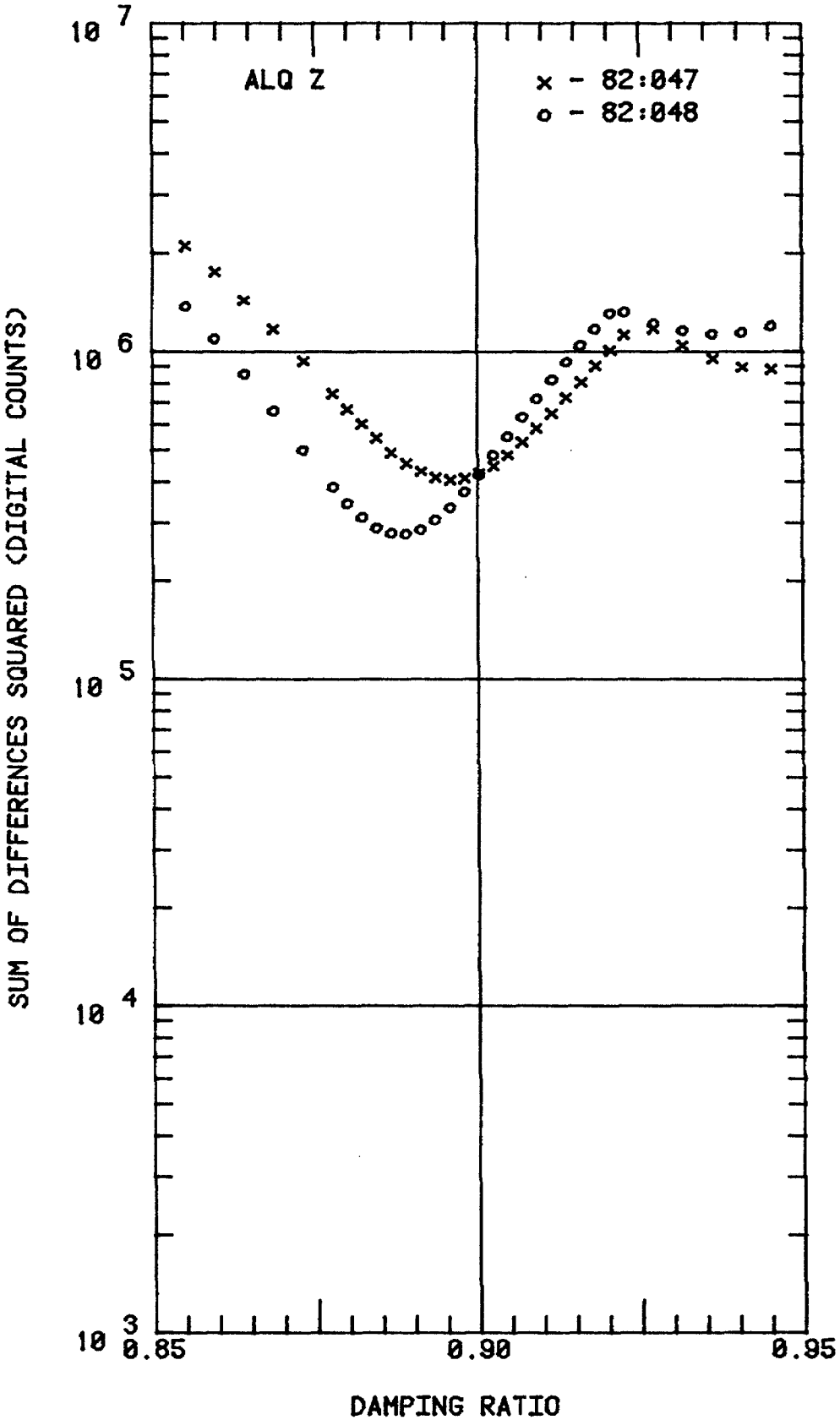

Figure 4.26.--Sum of differences squared vs. seismometer damping. ALQ LPZ data.

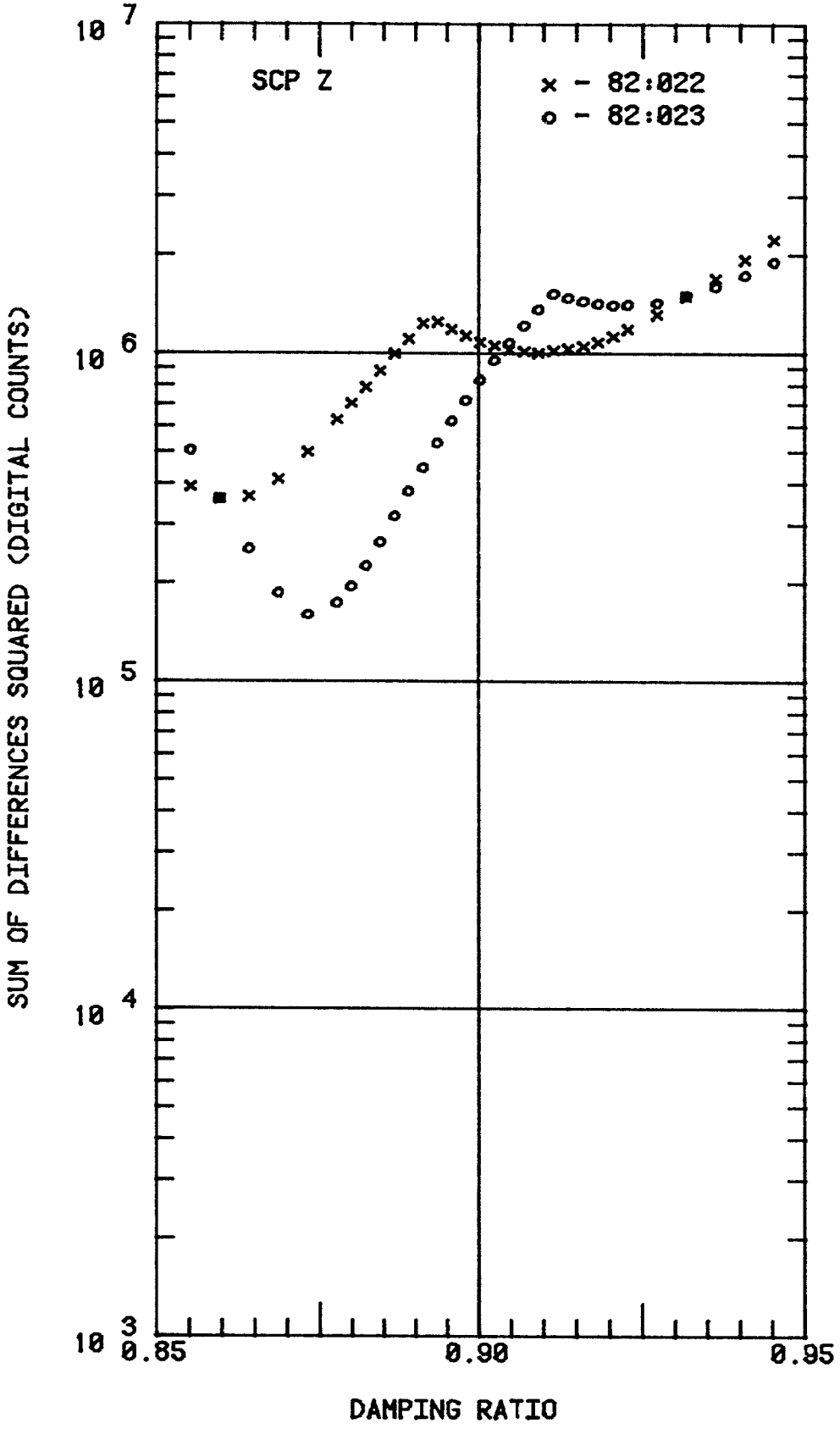

Figure 4.27.--Sum of differences squared vs. seismometer damping. SCP LPZ data.

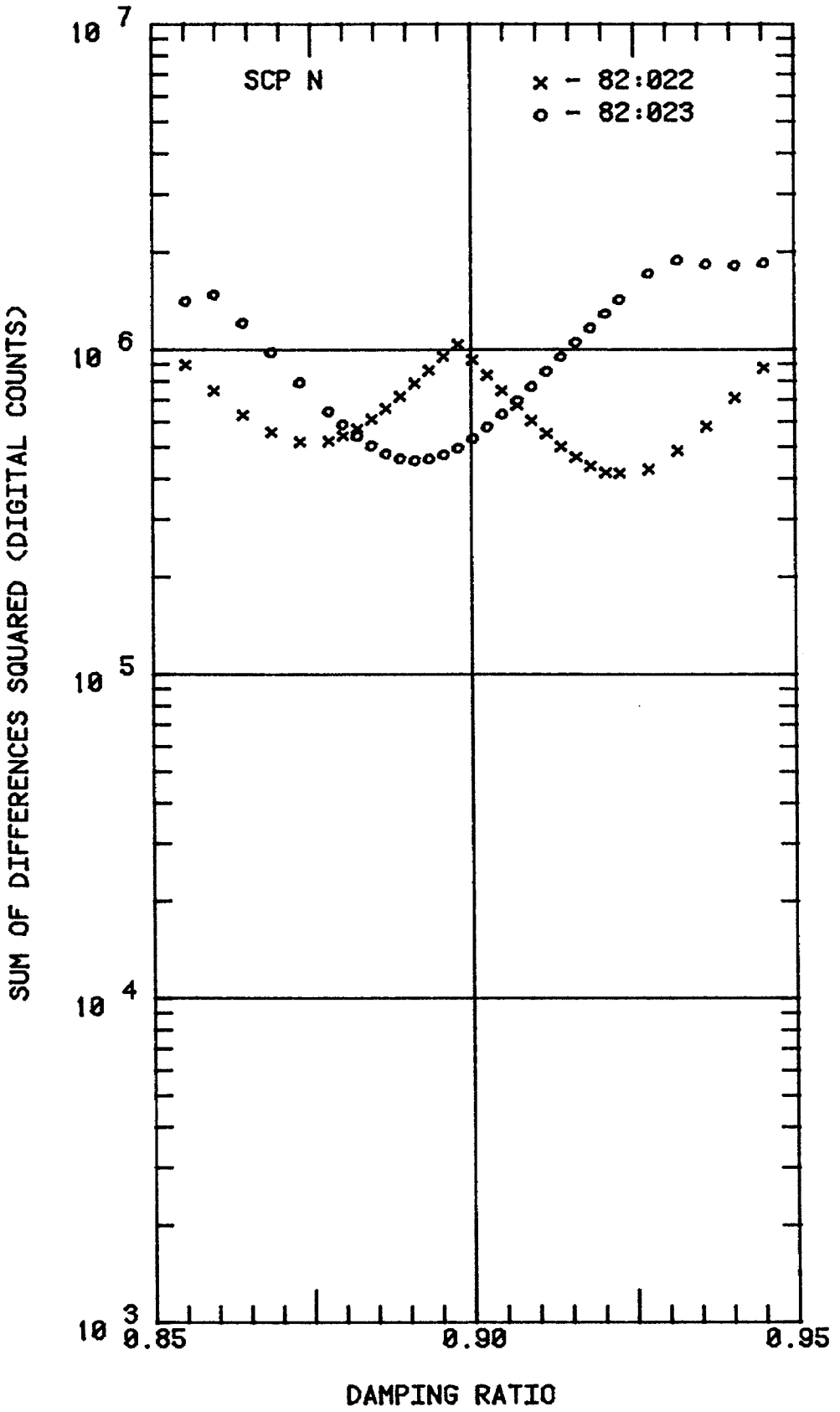

Figure 4.28.--Sum of differences squared vs. seismometer damping. SCP LPN data.

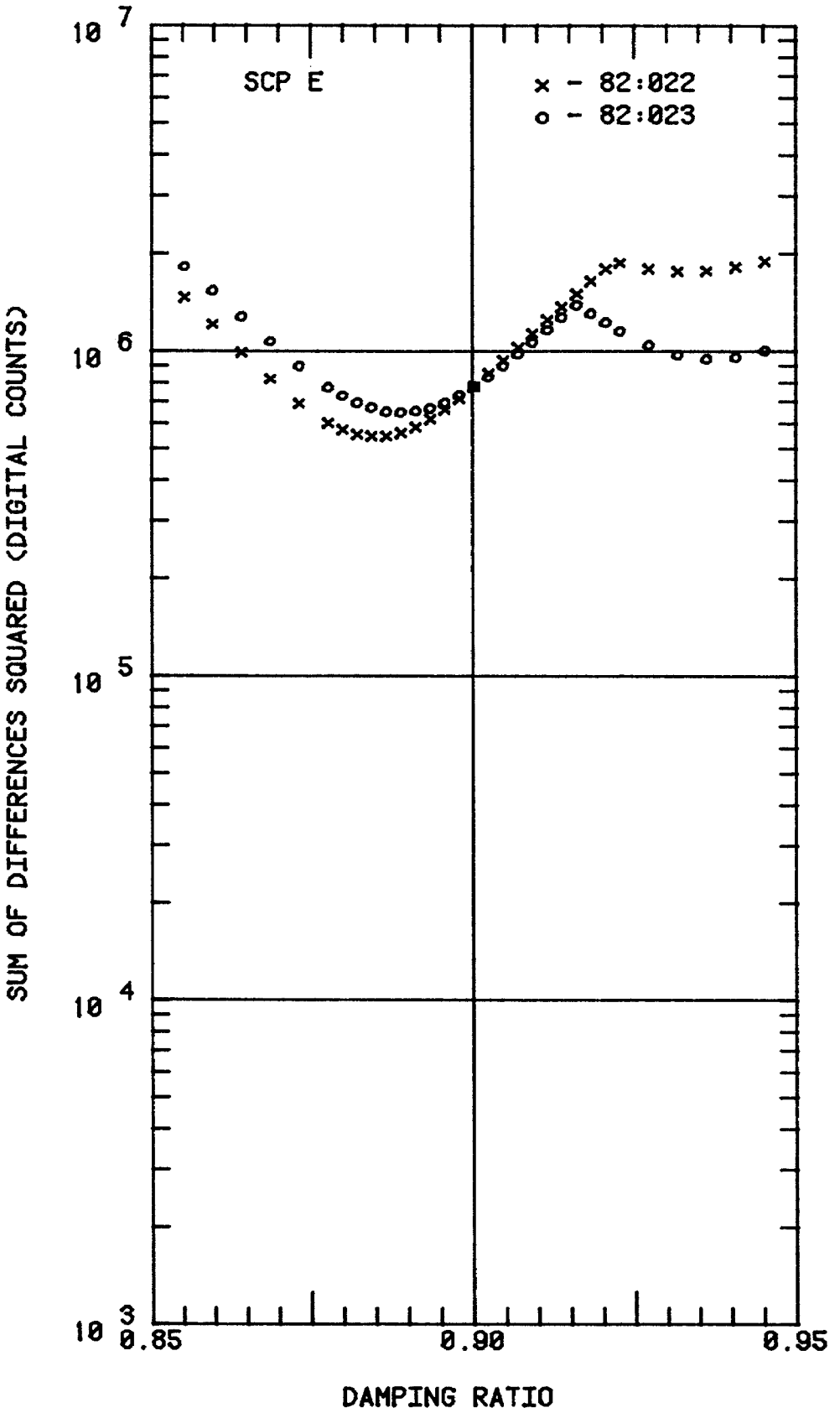

Figure 4.29.--Sum of differences squared vs. seismometer damping. SCP LPE data.

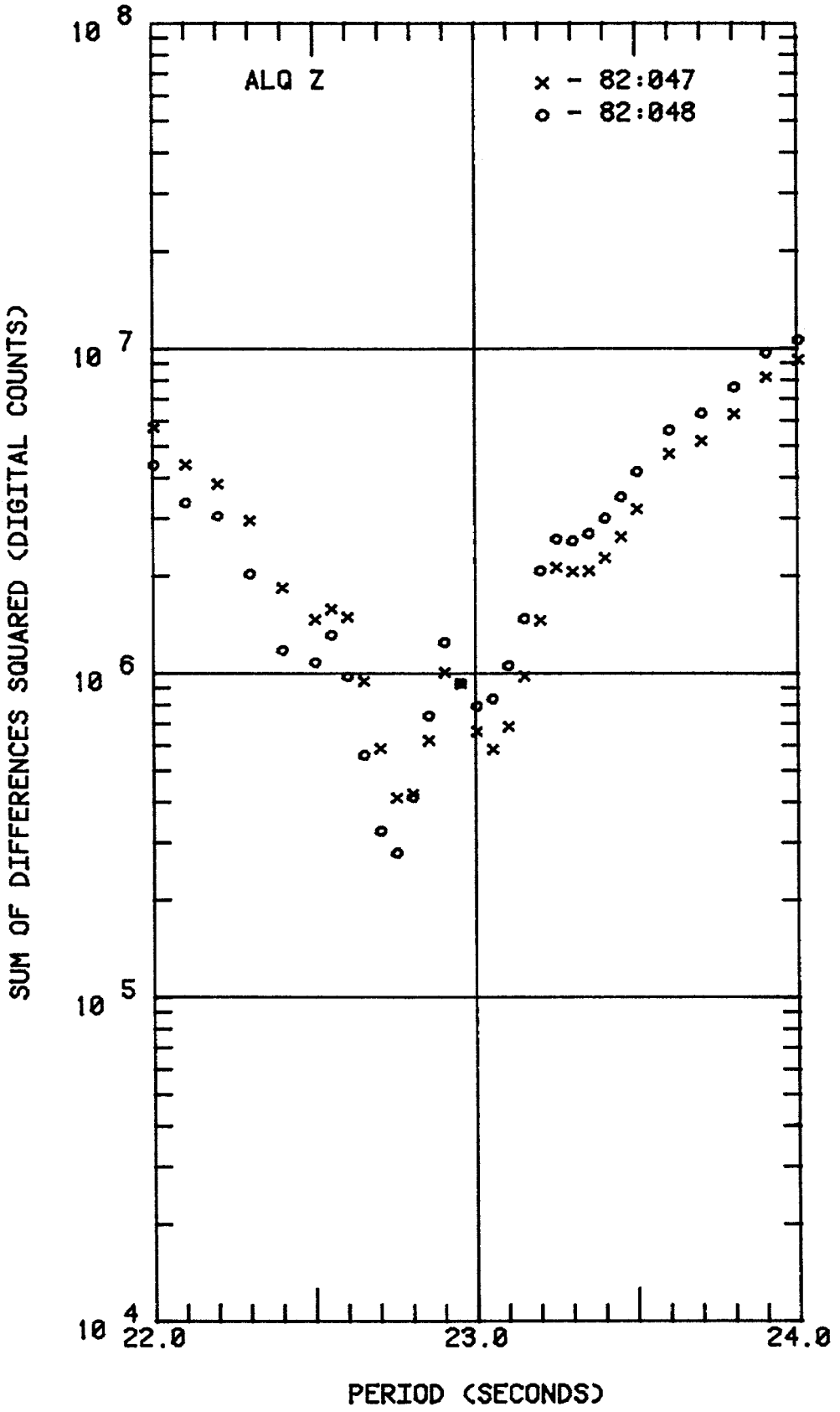

Figure 4.30.--Sum of differences squared vs. corner period of low-pass filter (nominal 22.8 sec).

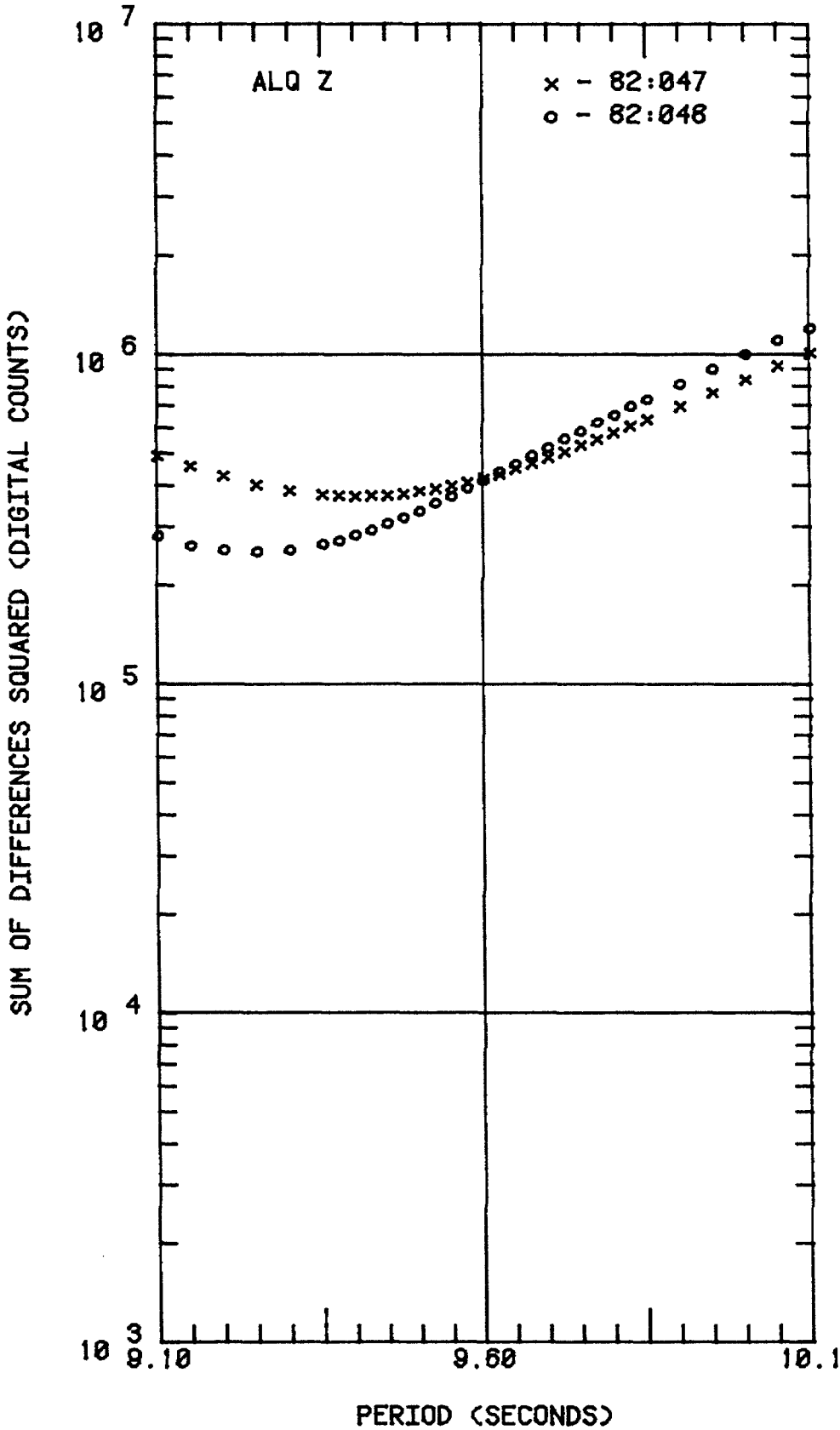

Figure 4.31.--Sum of differences squared vs. corner period of low-pass filter (nominal 9.6 sec).

5. DWWSS NOISE CHARACTERISTICS

5.1 General

The effective operating range of a seismograph is limited (for most purposes) by the recorded ambient background noise on the one hand and the clipping threshold on the other. In order to optimize the system operating range by adjusting sensitivity settings, it is necessary to know the source of the noise and its magnitude. In an optimum system, earth background noise should dominate instrument noise over the period band of interest but not to the extent that recording range is given up unnecessarily. Common sources of noise in a digital seismograph are environmental disturbances acting on the seismometers, offset and electrical noise in the analog electronics, and random fluctuations of the least-significant bit (or bits) in the analog-to-digital converter. In the DWWSS system, the last two of these noise sources can be isolated and measured. The least-count noise is measured by recording the output of the ADC with its input terminals shorted. The sum of electronic and least-count noise is measured by recording the output of the amplifier with the seismometer mass blocked. The isolation and measurement of environmental noise is not as straightforward. However, its level can be determined from coherence measurements between parallel matched components (see Stearns, 1979; Peterson and others, 1980; and Durham, 1982), and if it is the dominant source of noise, its level can be inferred from the difference between expected earth background noise level and the level of the recorded noise.

In this report, noise spectra are presented in root-mean-square (RMS) units of displacement referred to the input to the seismometer. In this way, noise from various sources can be compared on a common scale. The use of RMS values, rather than power spectral density (PSD), was chosen to provide a smoother presentation and units which can be statistically related to displacements computed from magnitude relationships. Curves representing measured RMS data were derived as follows. A single, 2048-point segment of recorded data was selected for processing. The mean value and slope were removed from the segment, a cosine-tapered window was applied, and PSD estimates were obtained using an FFT. Correction was made for instrument response using the nominal

transfer functions and sensitivity constants, and the RMS values were computed for one-half octave bands. The result is then presented in units of decibels of displacement amplitude referenced to 1 meter RMS. In the figures that follow, curves labeled 'a' represent measured least-count noise and curves labeled 'b' represent the results of blocked-mass tests. The curves labeled 'e' represent earth noise at a quiet site. The earth noise curve is a composite noise model derived from data published by Agnew and Berger (1978) for periods above 100 seconds, by Peterson (1980) for periods between 0.5 and 100 seconds, and by Li (1981) for periods below 0.5 seconds.

5.2 DWWSS Short-Period Noise

The results of noise testing on the short-period system are shown in Figure 5.1. The digital sensitivity of the DWWSS system is set to 10,000 digital counts per micrometer of displacement at a period of 1 second at all of the stations. This sensitivity was selected to insure that the least count would be about 20 dB below earth noise at a quiet site at a period of 1 second. The tests demonstrate that earth noise will predominate over a period band from about 0.3 to 10 seconds. The blocked-mass test reveals that the short-period amplifier is contributing noise, but not excessively.

A sampling of short-period noise data from each of the operating stations is shown in Figures 5.2 through 5.5. The data segments were selected in a random fashion, except to avoid earthquake signals, so they are not necessarily representative of the quietest periods. Day-night and seasonal variations can be expected. The earth noise curve is shown in each figure to provide a reference. As one would expect, the stations with the highest noise levels are situated on islands or near the coast (except for TOL). The data from Toledo appears to be dominated by cultural noise in the short-period band. At stations with persistent high noise levels, it may be appropriate to lower the recording sensitivity by 10 or 20 dB to gain a higher clipping threshold.

5.3 Intermediate-Period Noise

The sensitivity of the intermediate-period channel has been set low (125 digital counts per micrometer at 1 second) in order to record very large earthquakes without overdriving the recorder. Typical levels of noise and signals are illustrated in Figure 5.6. The background noise will be predominantly instrumental below a period of 1 second and above a period of 10 seconds.

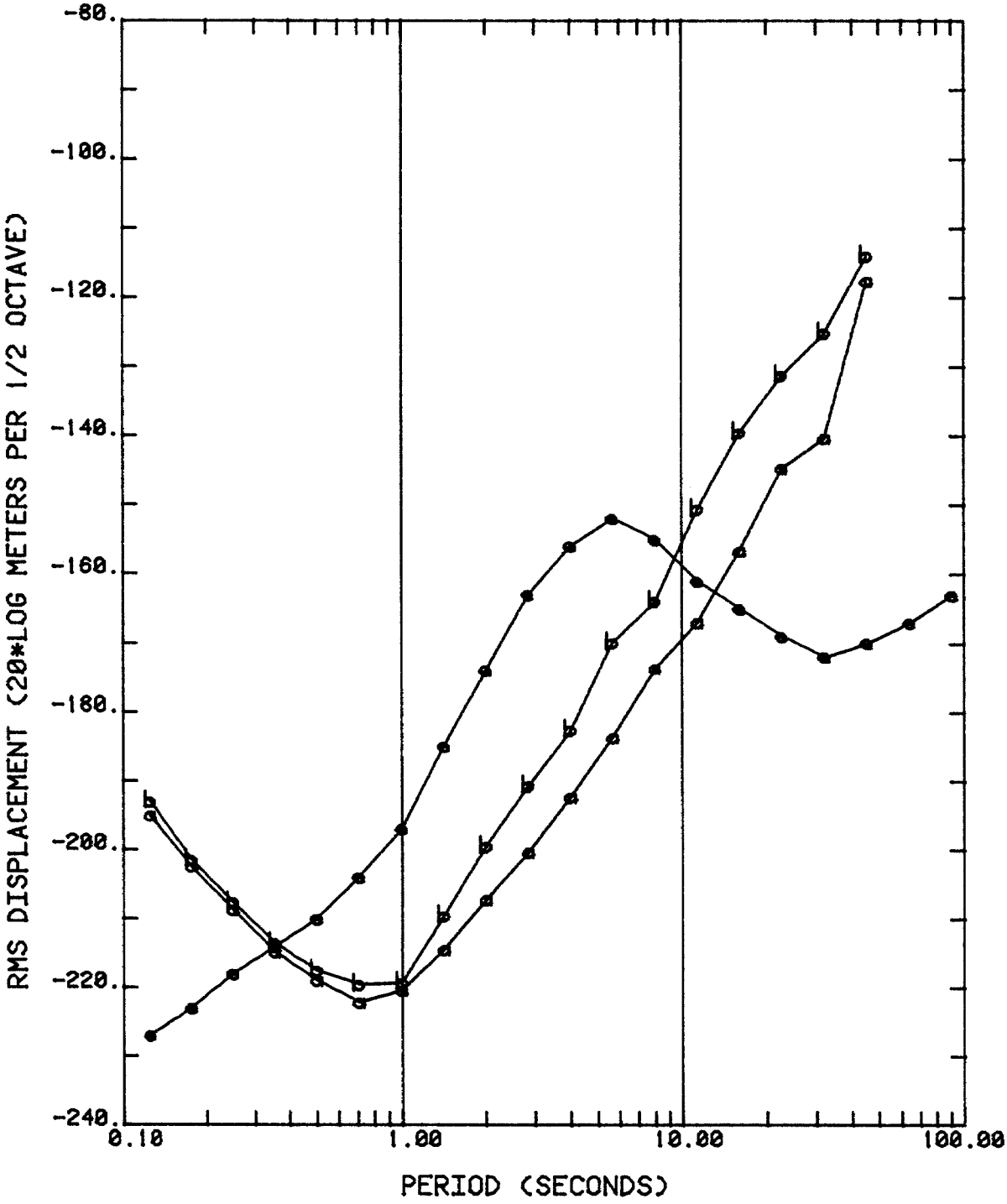

Figure 5.1.--Instrumental noise in the DWWSS short-period band compared with earth noise at a quiet site. Curve labeled 'a' represents ADC noise, curve labeled 'b' is result of blocked-mass test, and curve labeled 'e' represents earth noise at a quiet site.

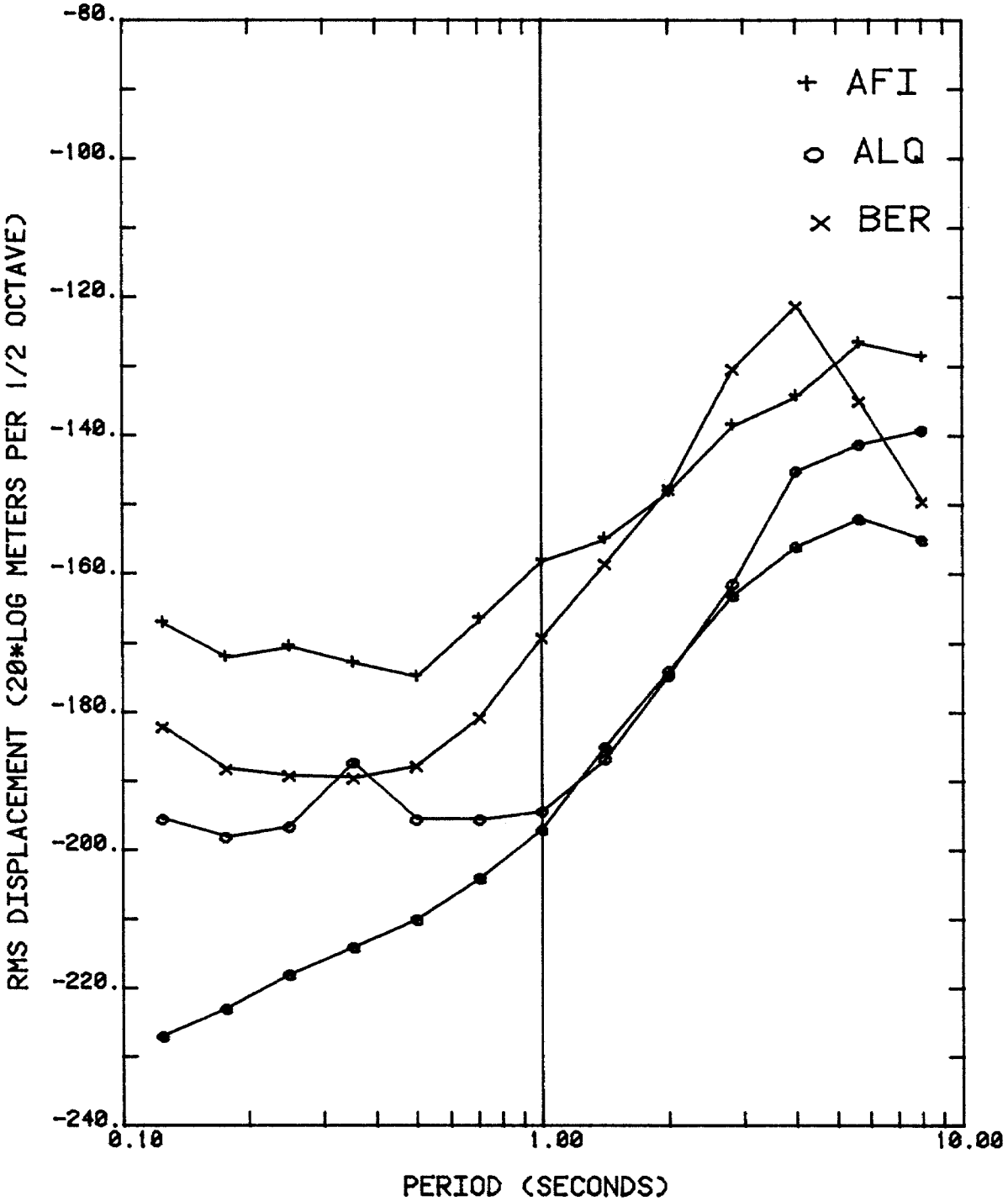

Figure 5.2.--Short-period noise spectra computed from Afiamalu, Albuquerque, and Bergen data. Curve labeled 'e' represents earth noise at a quiet site.

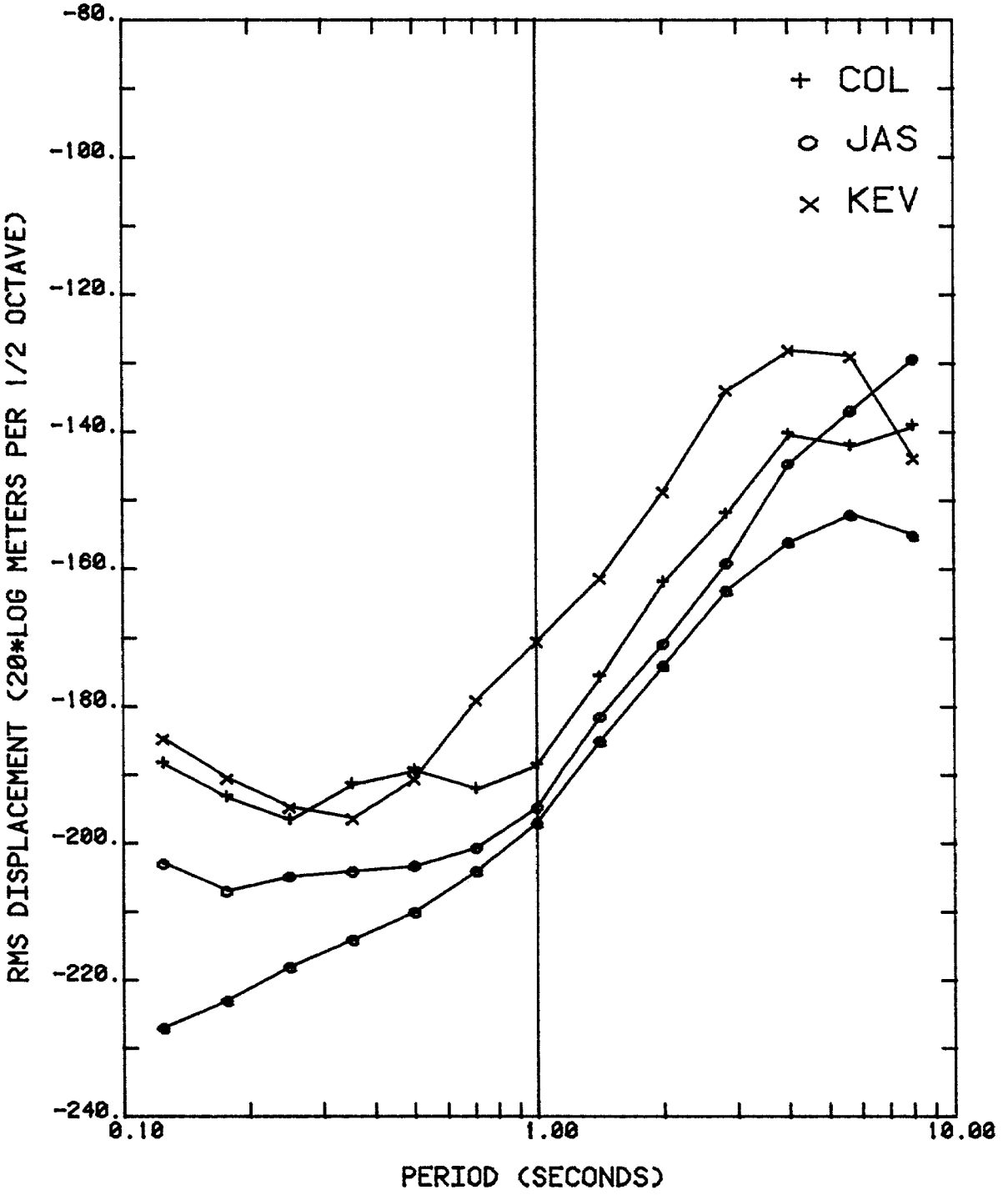

Figure 5.3.--Short-period noise spectra computed from College, Jamestown, and Kevo data. Curve labeled 'e' represents earth noise at a quiet site.

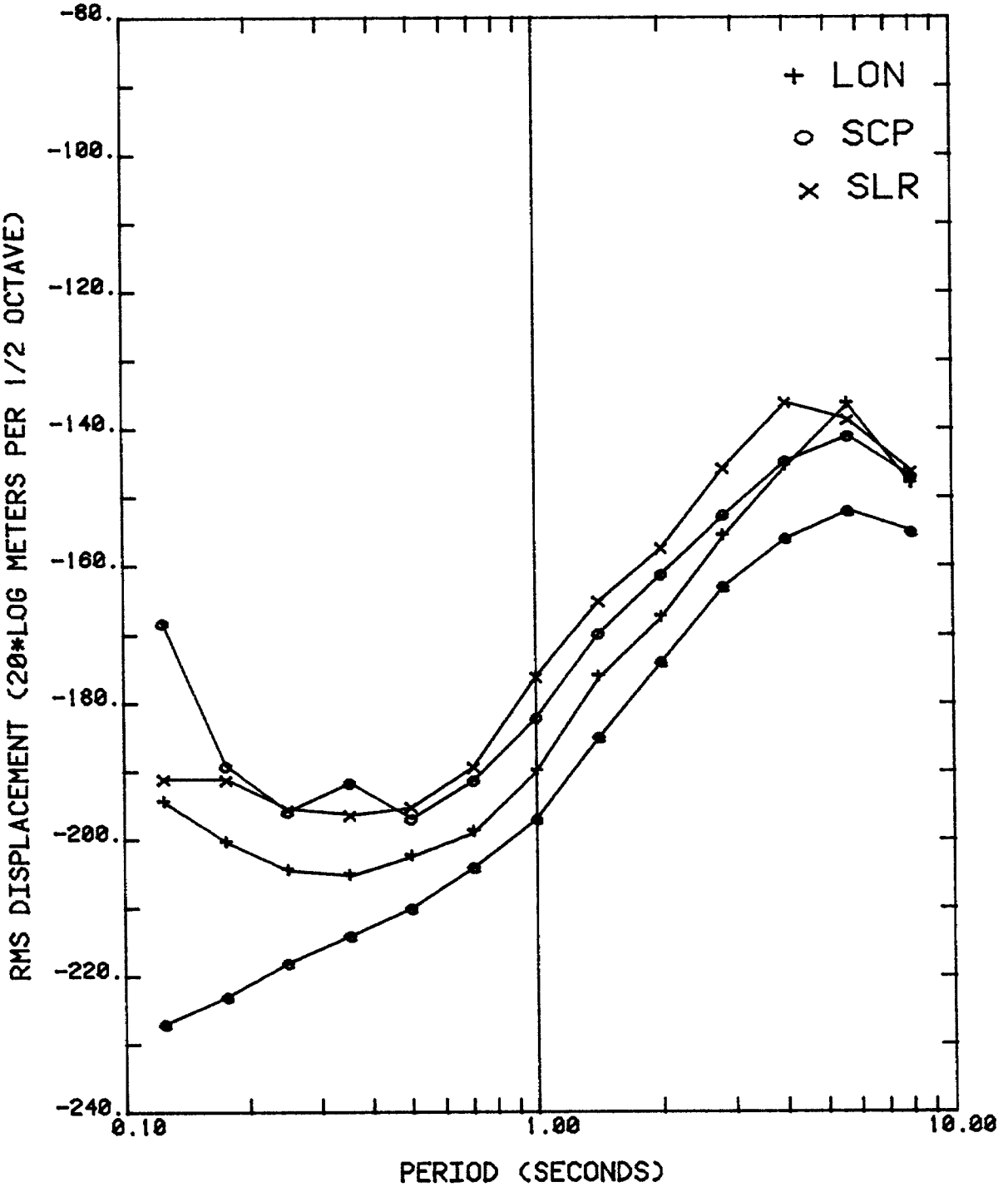

Figure 5.4.--Short-period noise spectra computed from Longmire, State College, and Silverton data. Curve labeled 'e' represents earth noise at a quiet site.

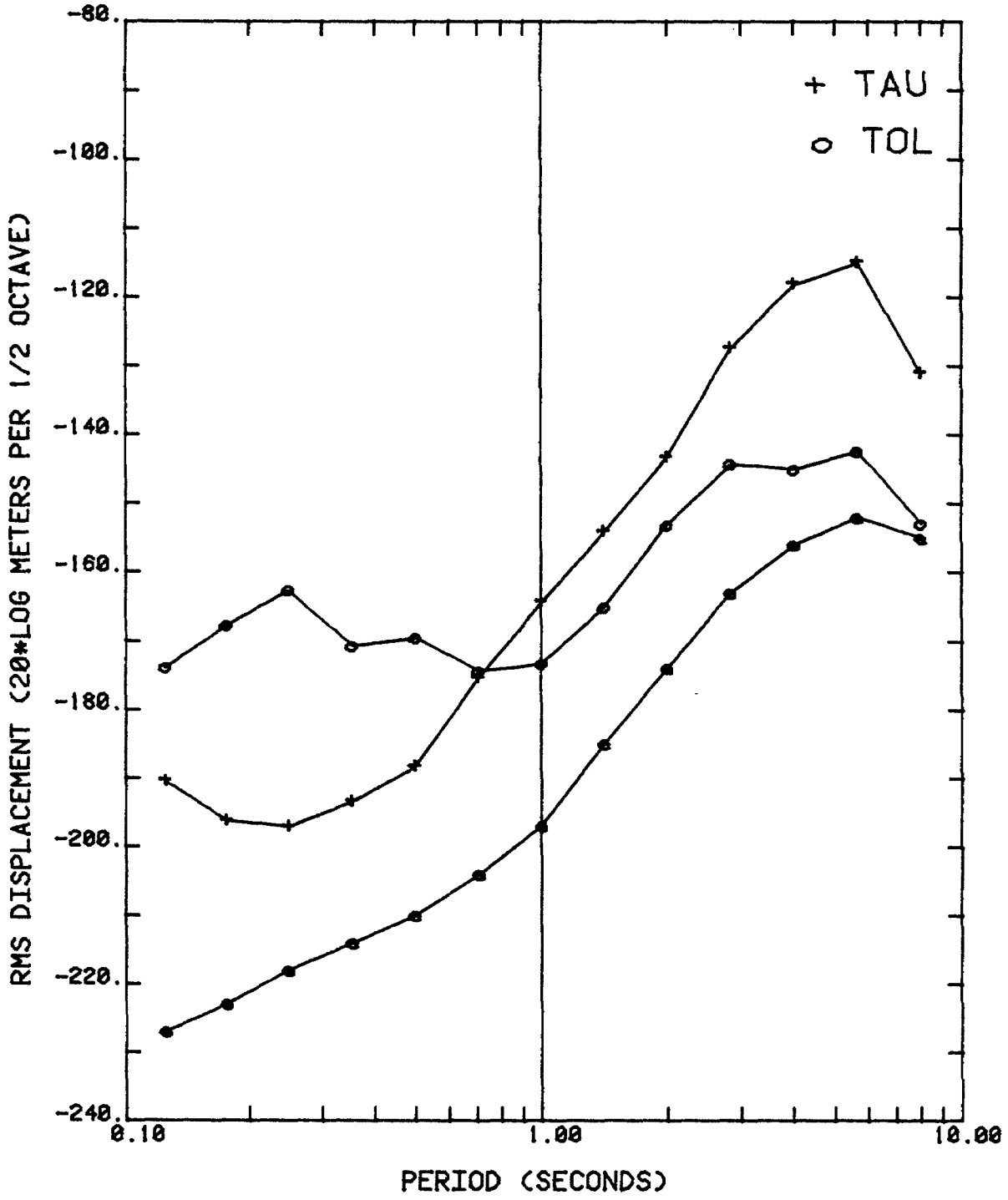

Figure 5.5.--Short-period noise spectra computed from Tasmania and Toledo data. Curve labeled 'e' represents earth noise at a quiet site.

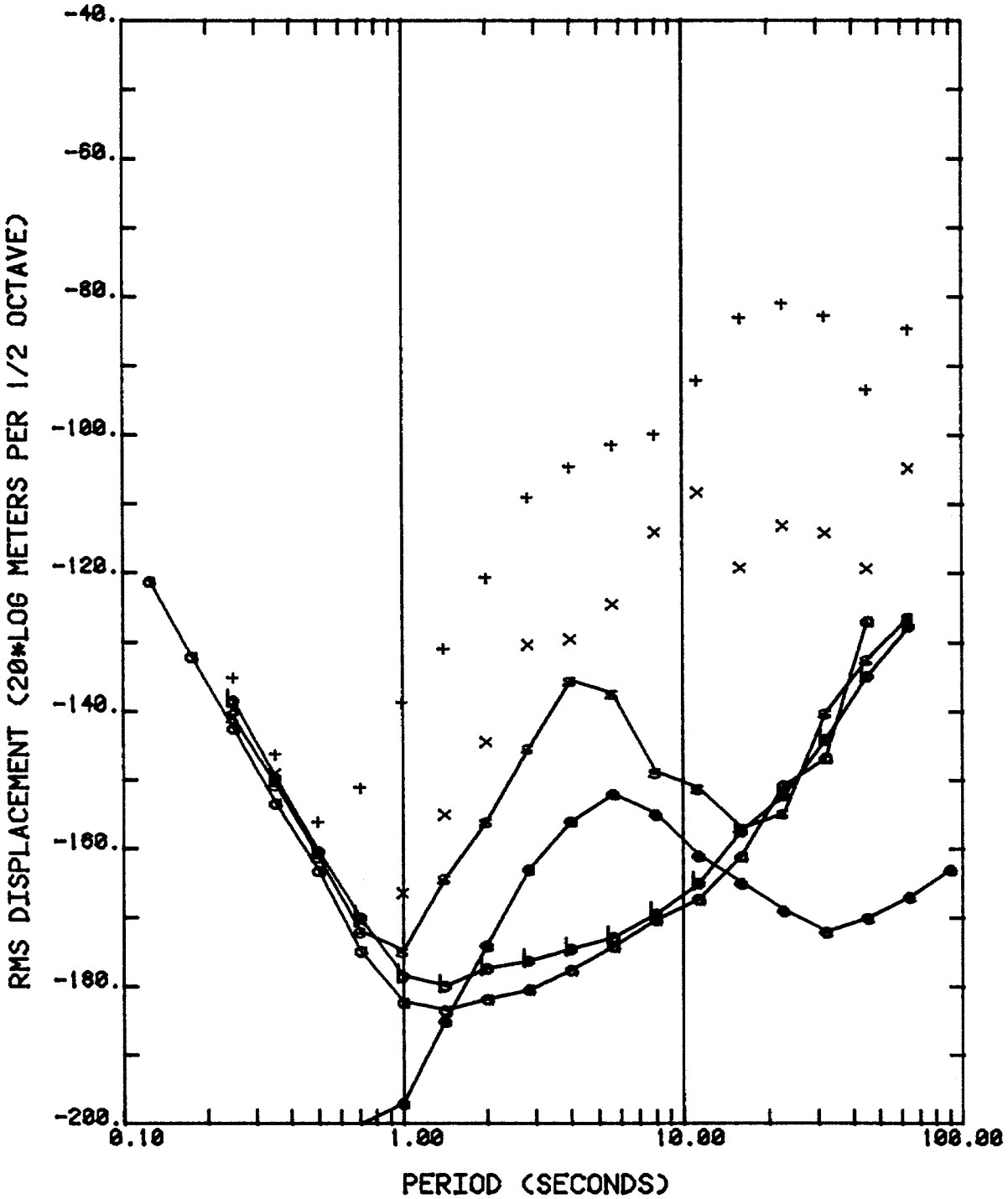

Figure 5.6.--Noise and signal spectra computed for the DWWSS intermediate-period band. Curve labeled 'a' represents ADC noise, curve labeled 'b' is result of blocked-mass test, and curve labeled 'e' represents earth noise at a quiet site. The curve labeled 's' is a spectrum of typical background recording (from SLR). The points labeled '+' and 'x' represent spectra of earthquakes recorded at ALQ.

The curve labeled 's' is a spectrum of a typical background recording on the IP channel from the SLR station. The curve labeled '+' is the spectrum of a body-wave signal recorded on the ALQ IPZ channel from an M_s 7.6 earthquake at 18°, and the curve labeled 'x' is the spectrum of a body-wave signal recorded on the ALQ IPZ channel from an M_s 7.7 earthquake at 102°.

5.4 Long-Period Noise

Based on experience with the WWSS systems, the major noise source in the long-period band (above 20 seconds) was expected to be environmental in origin. The seismometers are essentially unprotected from atmospheric disturbances and only slightly protected from temperature excursions. However, the results of the blocked-mass test, shown in Figure 5.7, reveal a very high level of electronic noise at the output of the long-period filter, and this is likely to be the dominant noise at most of the stations.

Long-period noise samples from each of the operating stations are illustrated in Figures 5.8 through 5.18. In the figures, the curves labeled '+', 'o', and 'x' represent the vertical, north, and east components, respectively, and the curve labeled 'e' is the low earth noise model. At periods below 6 seconds, resolution is limited by least-count noise because of high attenuation in the low-pass filters (to prevent aliasing). Electronic noise appears to dominate at periods above 30 seconds. However, there is considerable scatter in the curves, which may be due to differences in electronic noise levels among the filters or to environmental sources, possibly wind.

The level of electronic noise clearly degrades the DWWSS LP signals. Efforts are underway to determine the noise source and reduce the noise level. Preliminary indications are that the noise is generated in the preamplifier and that improvements can be made by replacing the input FET and increasing the gain of the first stage. The use of the single preamplifier to provide signals for both the IP and LP channels requires a dynamic range in the preamplifier that is difficult to achieve at moderate cost. The reduction of noise in the LP channel may have to be at the expense of clipping threshold in the IP channel.

If the electronic noise can be reduced significantly, it may then be useful to consider methods of reducing environmental noise. Kolesnikov and Toksoz (1981a, 1981b) have reported promising methods of extracting barometric and thermal noise from similar type seismometers.

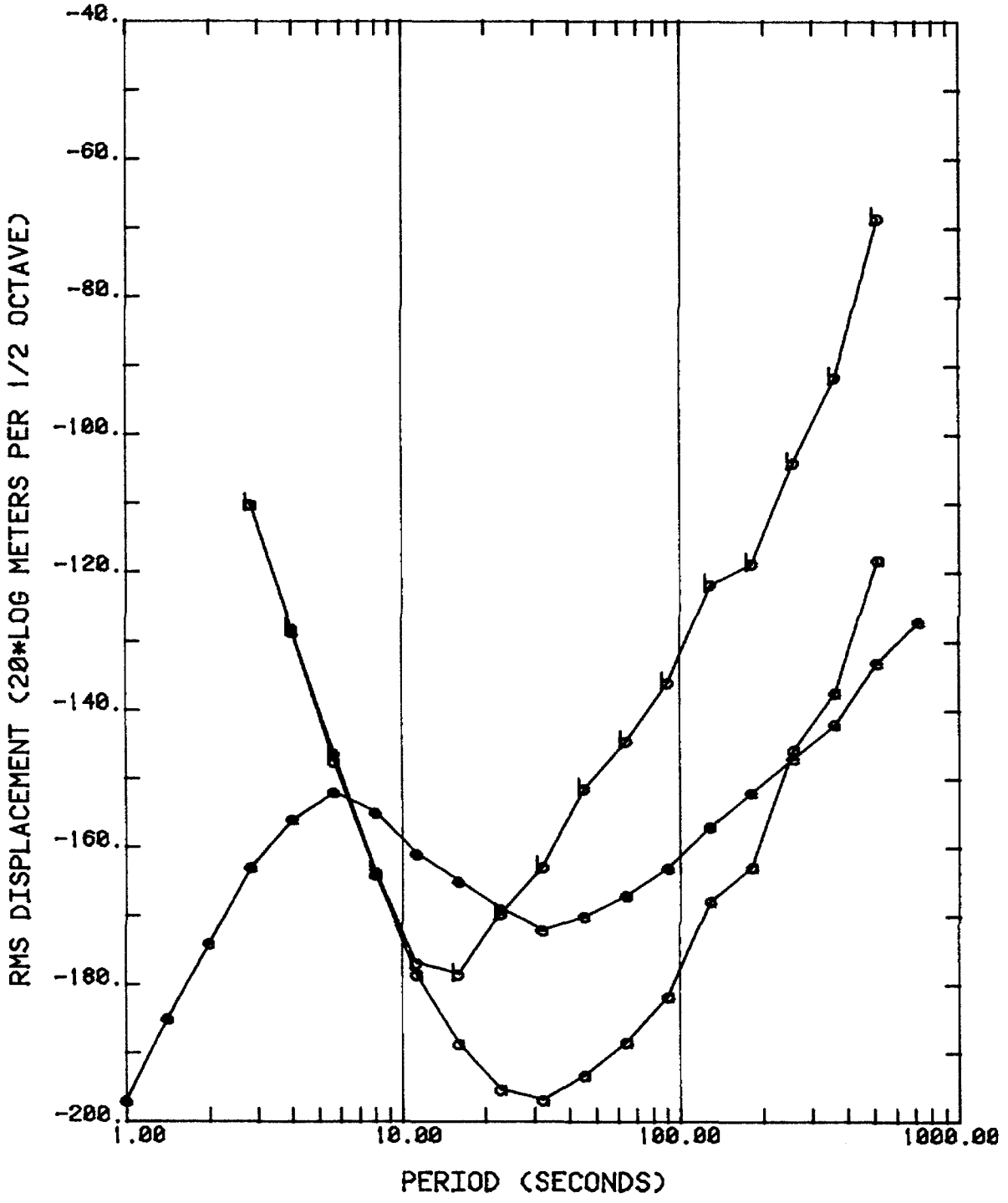

Figure 5.7.--Instrument noise spectra computed for the DWWSS long-period band compared with earth noise. Curve labeled 'a' represents ADC noise, curve labeled 'b' is the result of a blocked-mass test, and the curve labeled 'e' is the low earth noise model.

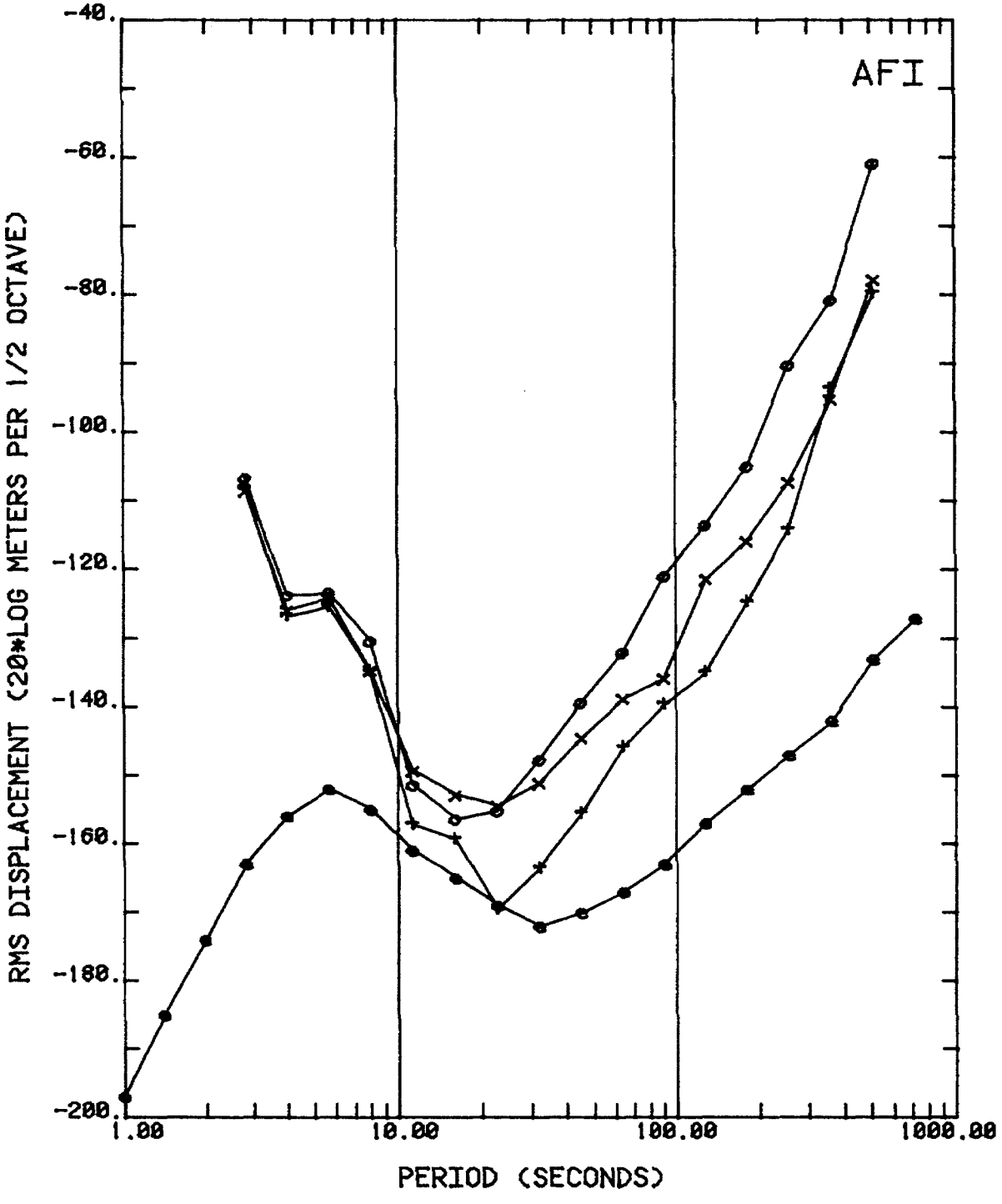

Figure 5.8.--Long-period noise spectra computed from Afiamalu data. Curves labeled '+', 'o', and 'x' represent vertical, north, and east components, and curve labeled 'e' represents the earth noise model.

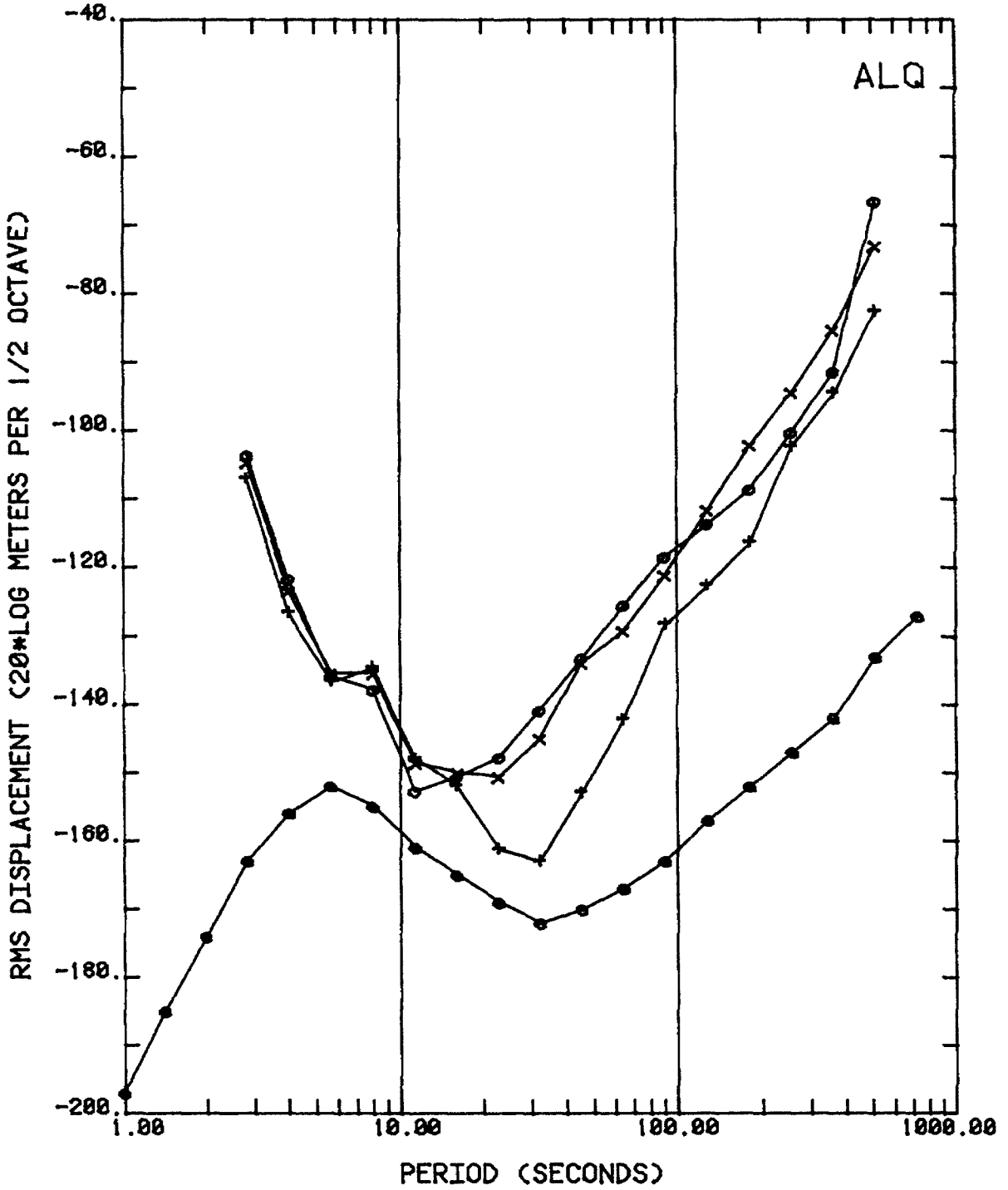

Figure 5.9.--Long-period noise spectra computed from Albuquerque data. Curves labeled '+', 'o', and 'x' represent vertical, north, and east components, and curve labeled 'e' represents the earth noise model.

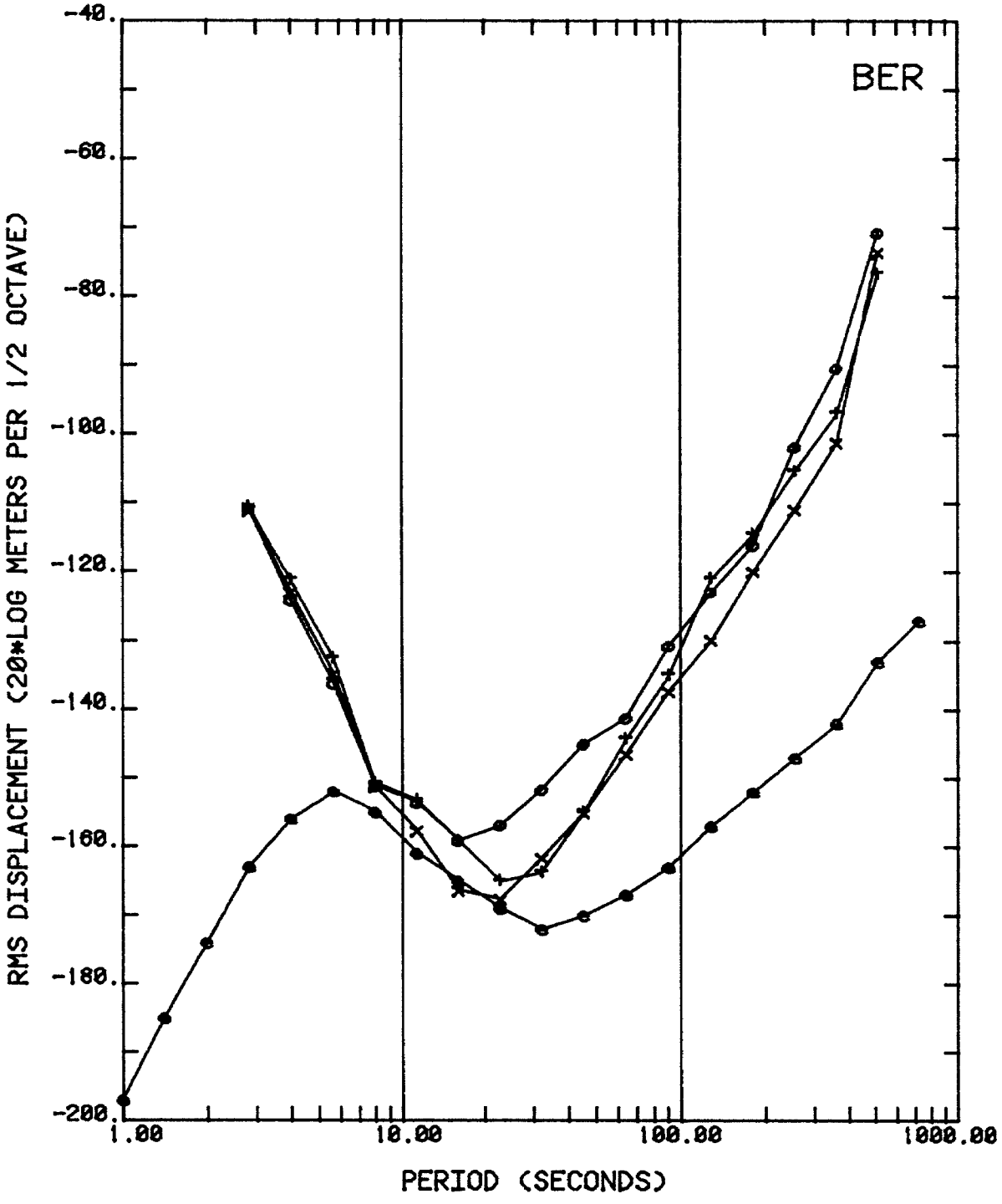

Figure 5.10.--Long-period noise spectra computed from Bergen data. Curves labeled '+', 'o', and 'x' represent vertical, north, and east components, and curve labeled 'e' represents the earth noise model.

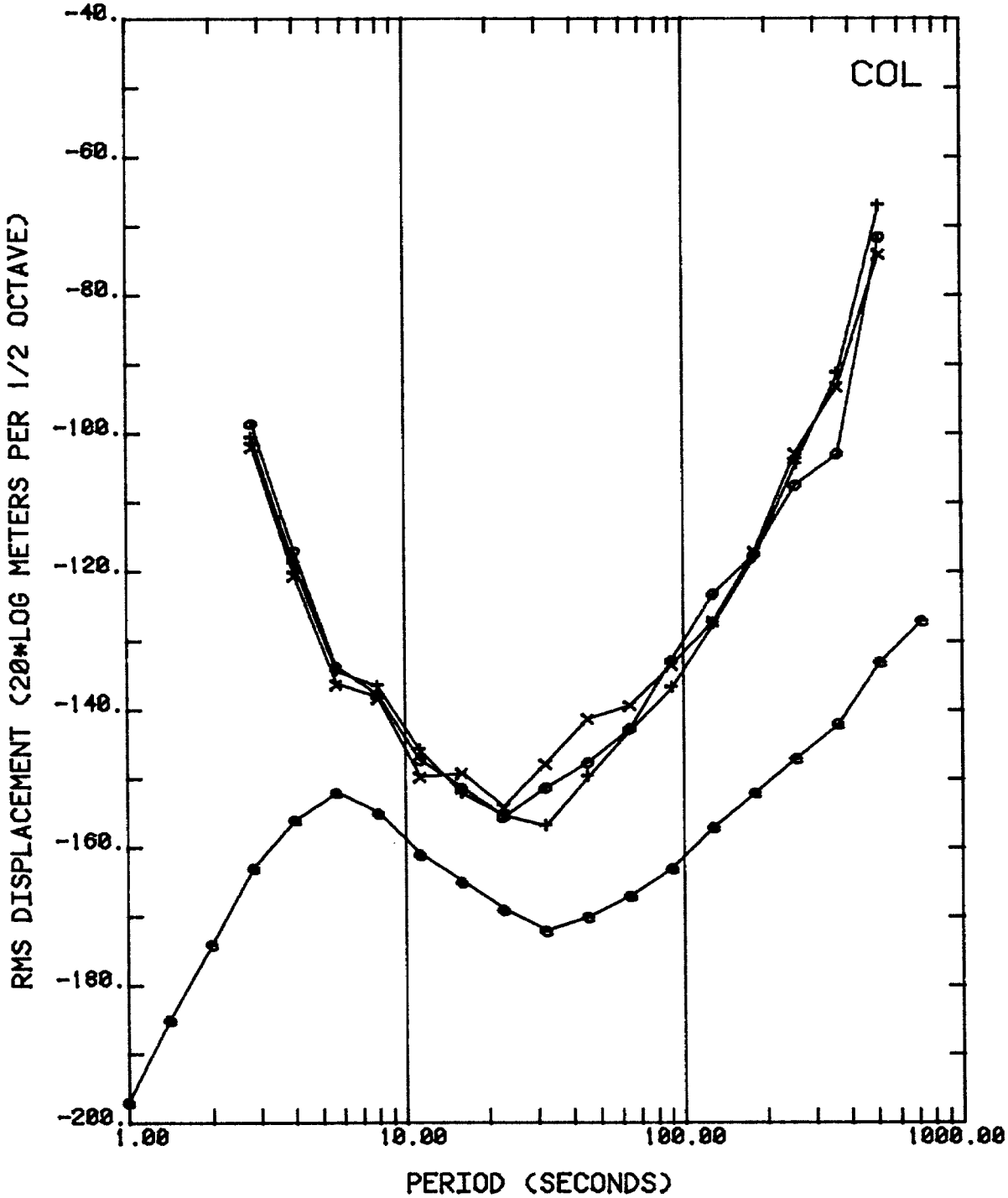

Figure 5.11.--Long-period noise spectra computed from College data. Curves labeled '+', 'o', and 'x' represent vertical, north, and east components, and curve labeled 'e' represents the earth noise model.

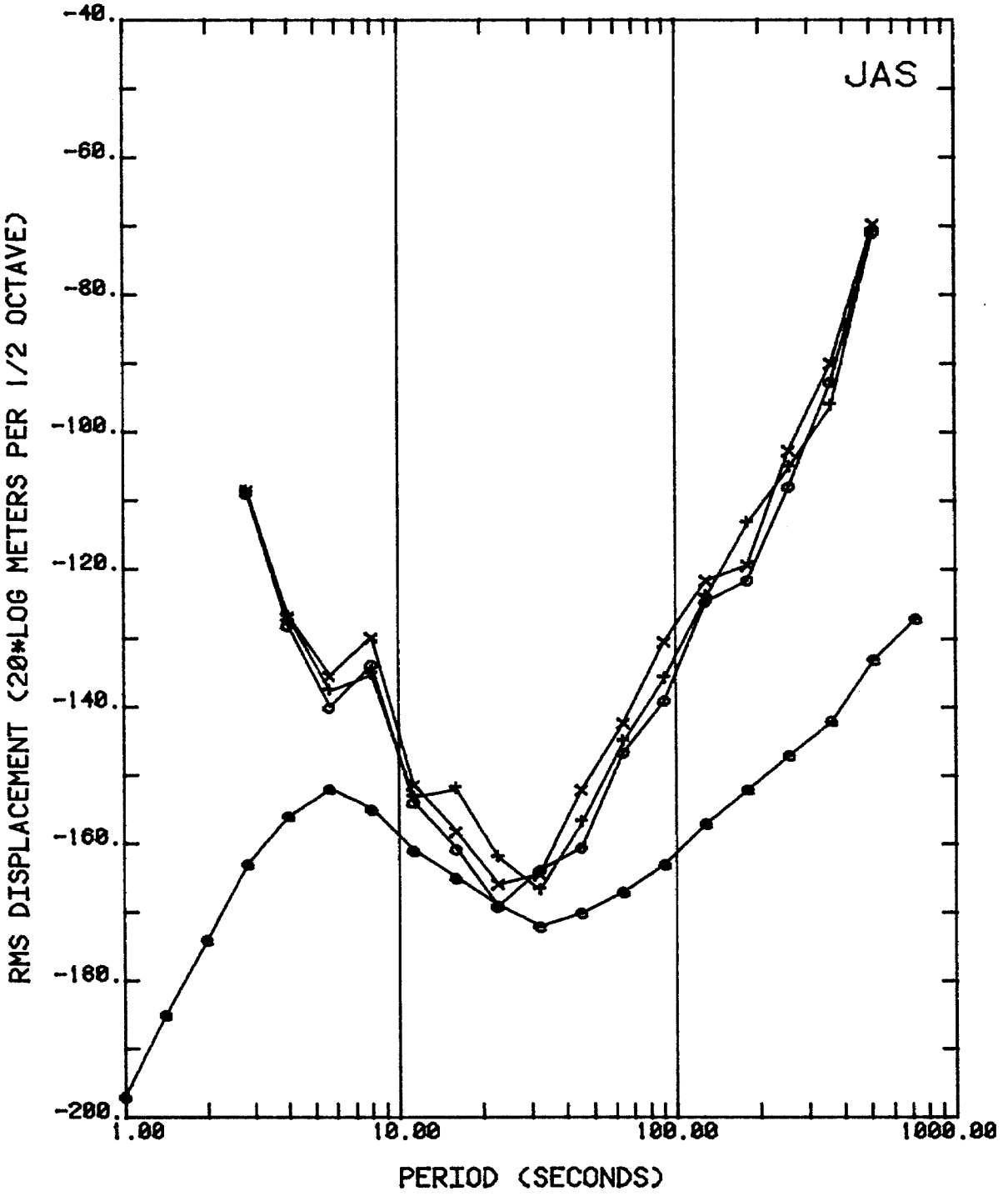

Figure 5.12.--Long-period noise spectra computed from Jamestown data. Curves labeled '+', 'o', and 'x' represent vertical, north, and east components, and curve labeled 'e' represents earth noise model.

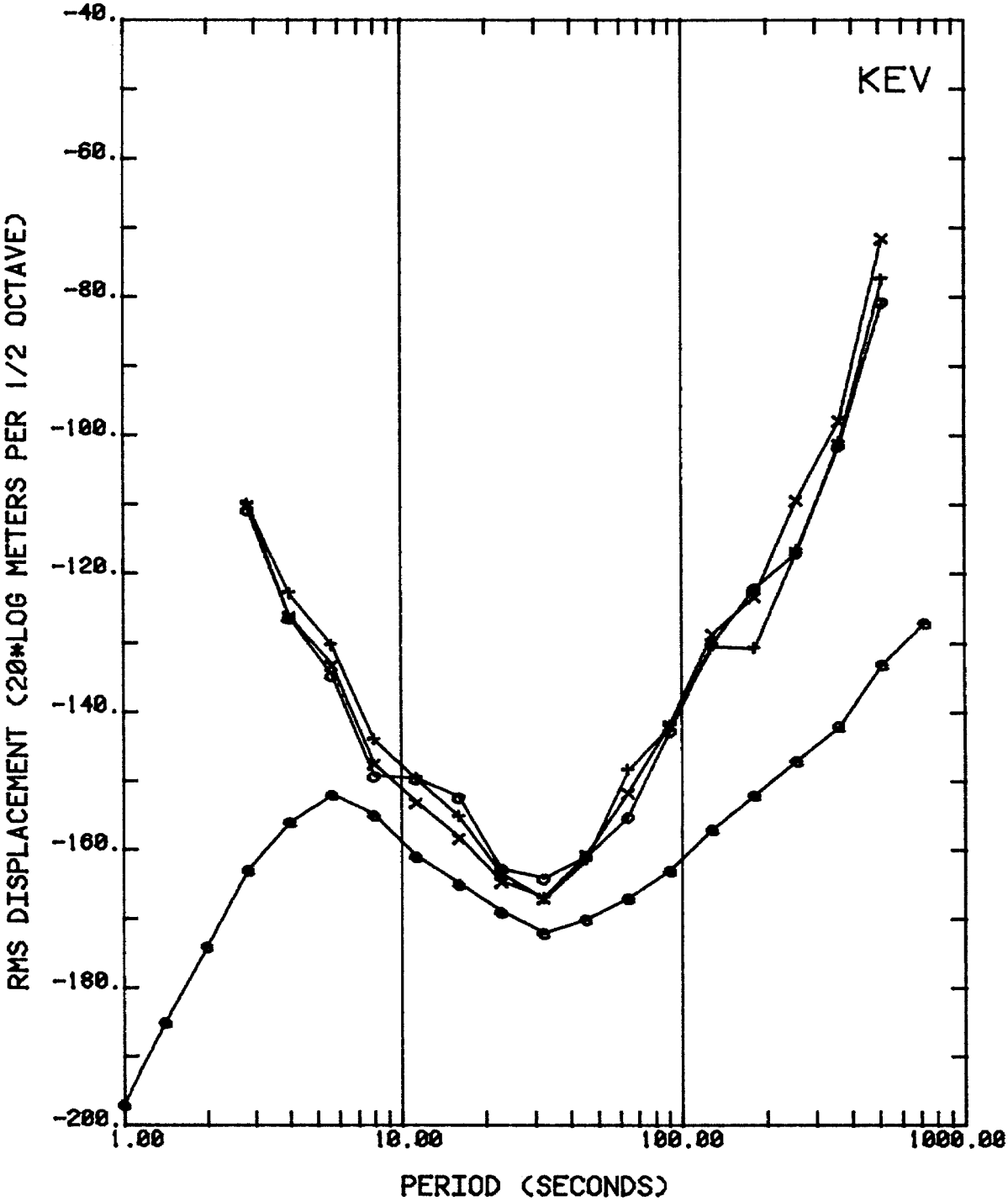

Figure 5.13.-- Long-period noise spectra computed from Kevo data. Curves labeled '+', 'o', and 'x' represent vertical, north, and east components, and curve labeled 'e' represents earth noise model.

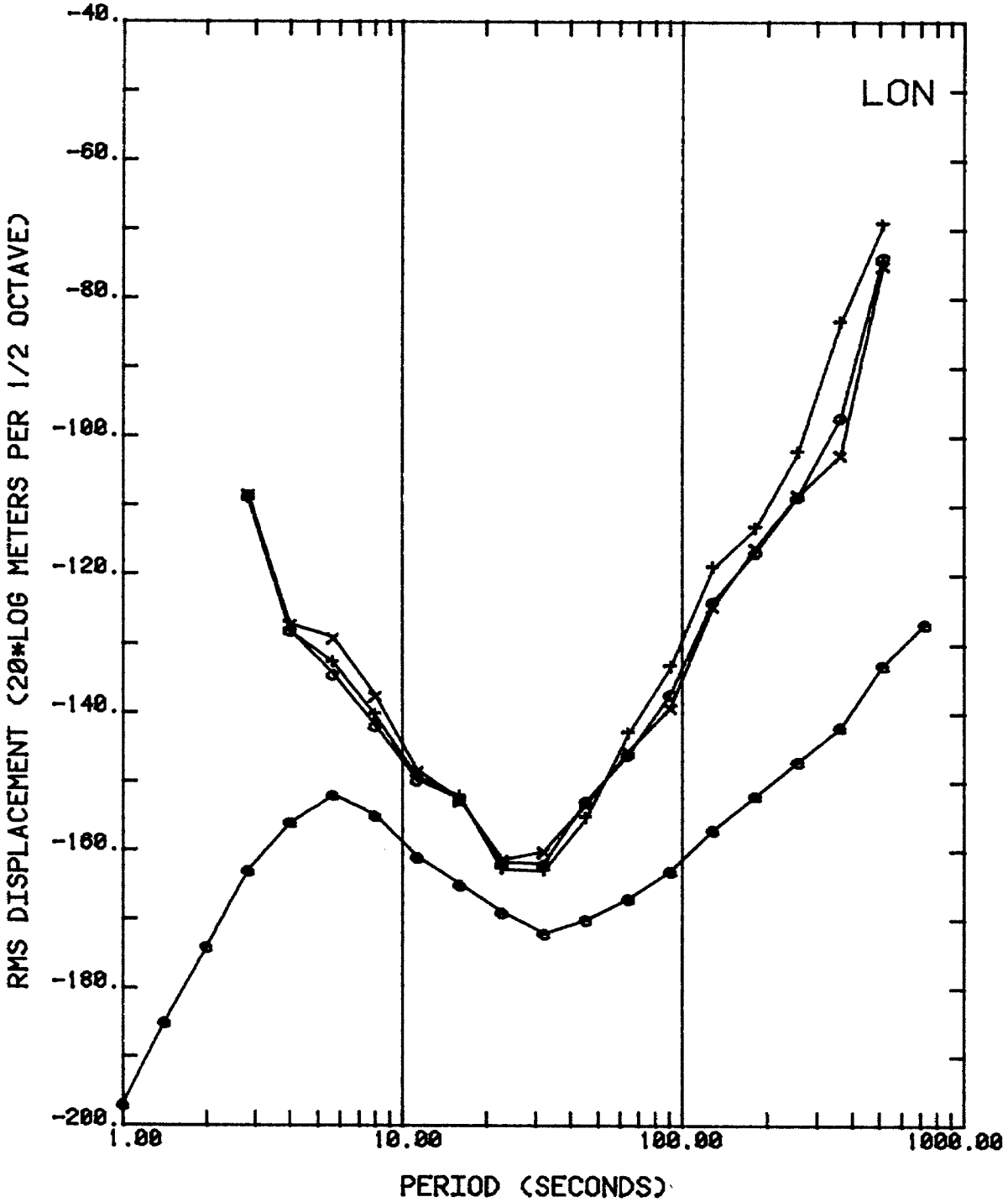

Figure 5.14.--Long-period noise spectra computed from Longmire data. Curves labeled '+', 'o', and 'x' represent vertical, north, and east components, and curve labeled 'e' represents earth noise model.

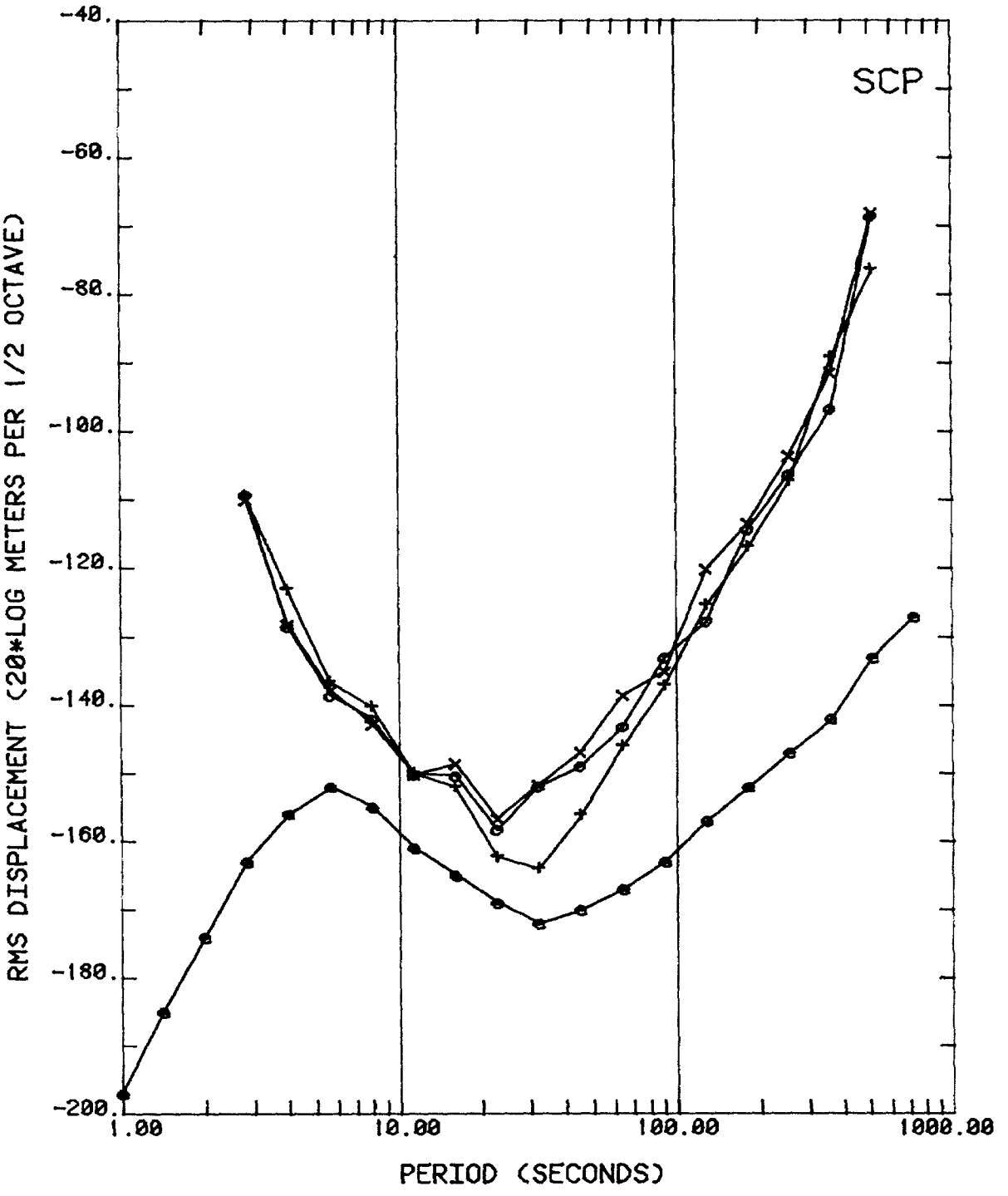

Figure 5.15.--Long-period noise spectra computed from State College data. Curves labeled '+', 'o', and 'x' represent vertical, north, and east components, and curve labeled 'e' represents earth noise model.

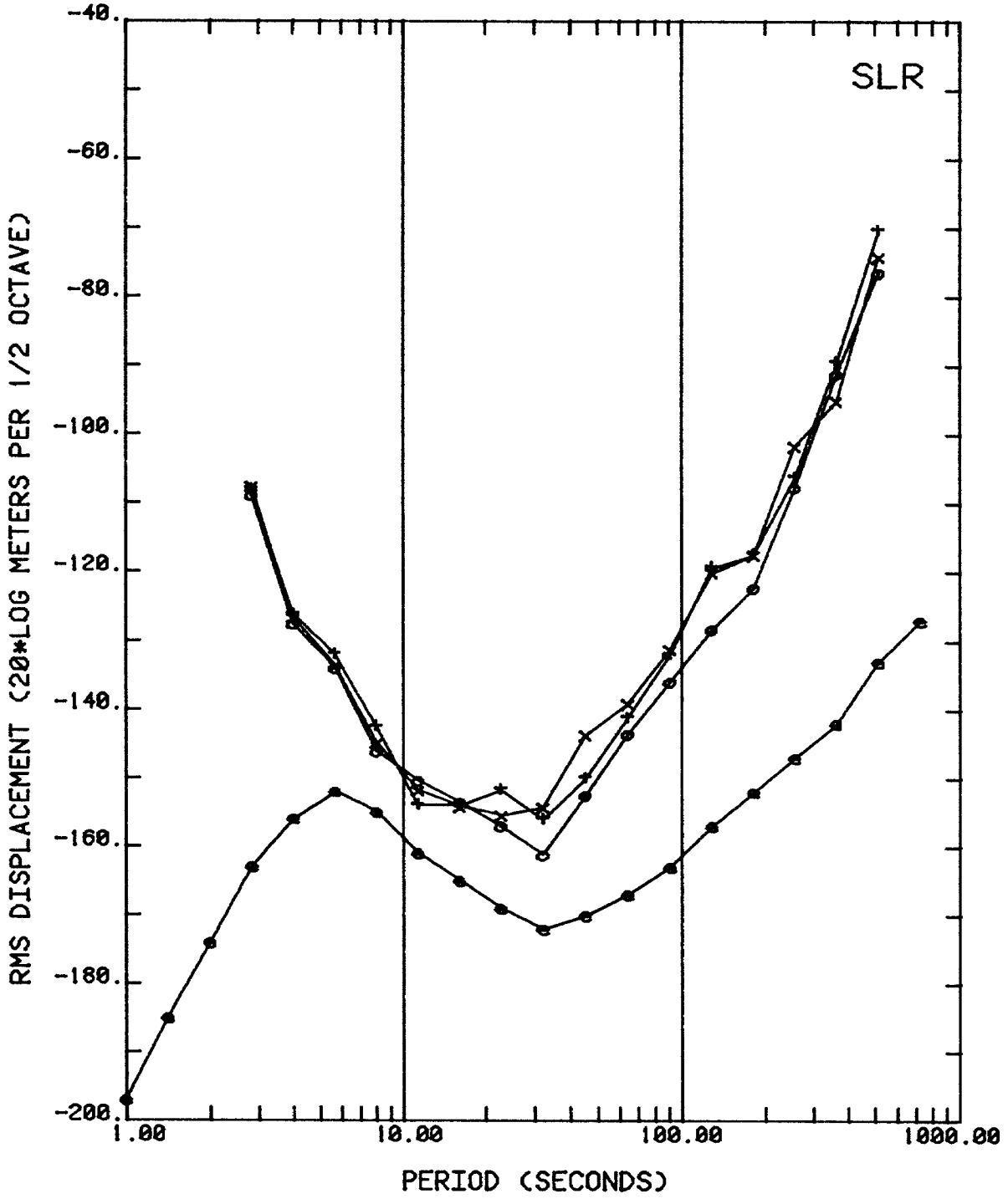

Figure 5.16.--Long-period noise spectra computed from Silverton data. Curves labeled '+', 'o', and 'x' represent vertical, north, and east components, and curve labeled 'e' represents earth noise model.

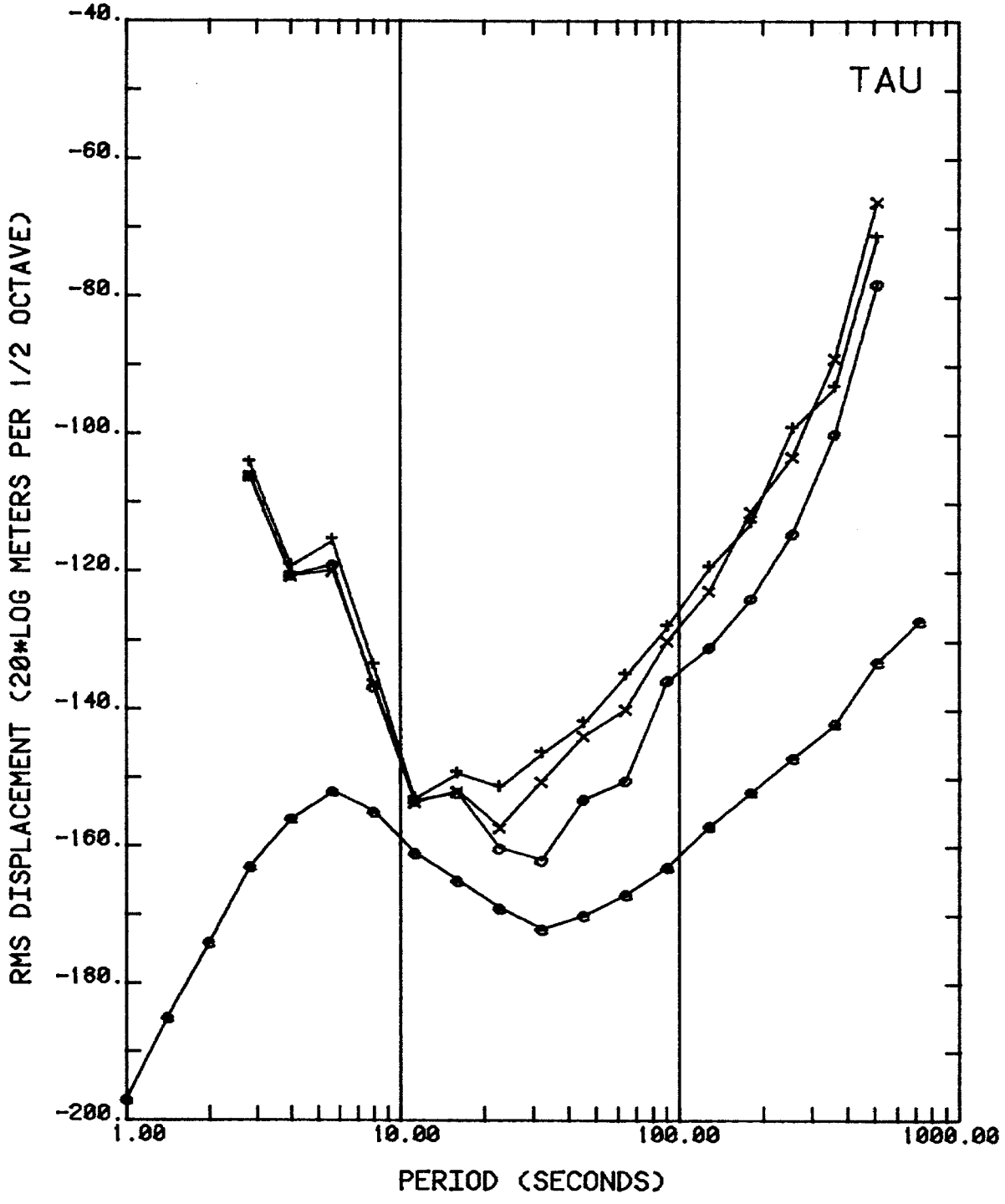

Figure 5.17---Long-period noise spectra computed from Tasmania data. Curves labeled '+', 'o', and 'x' represent vertical, north, and east components, and curve labeled 'e' represents earth noise model.

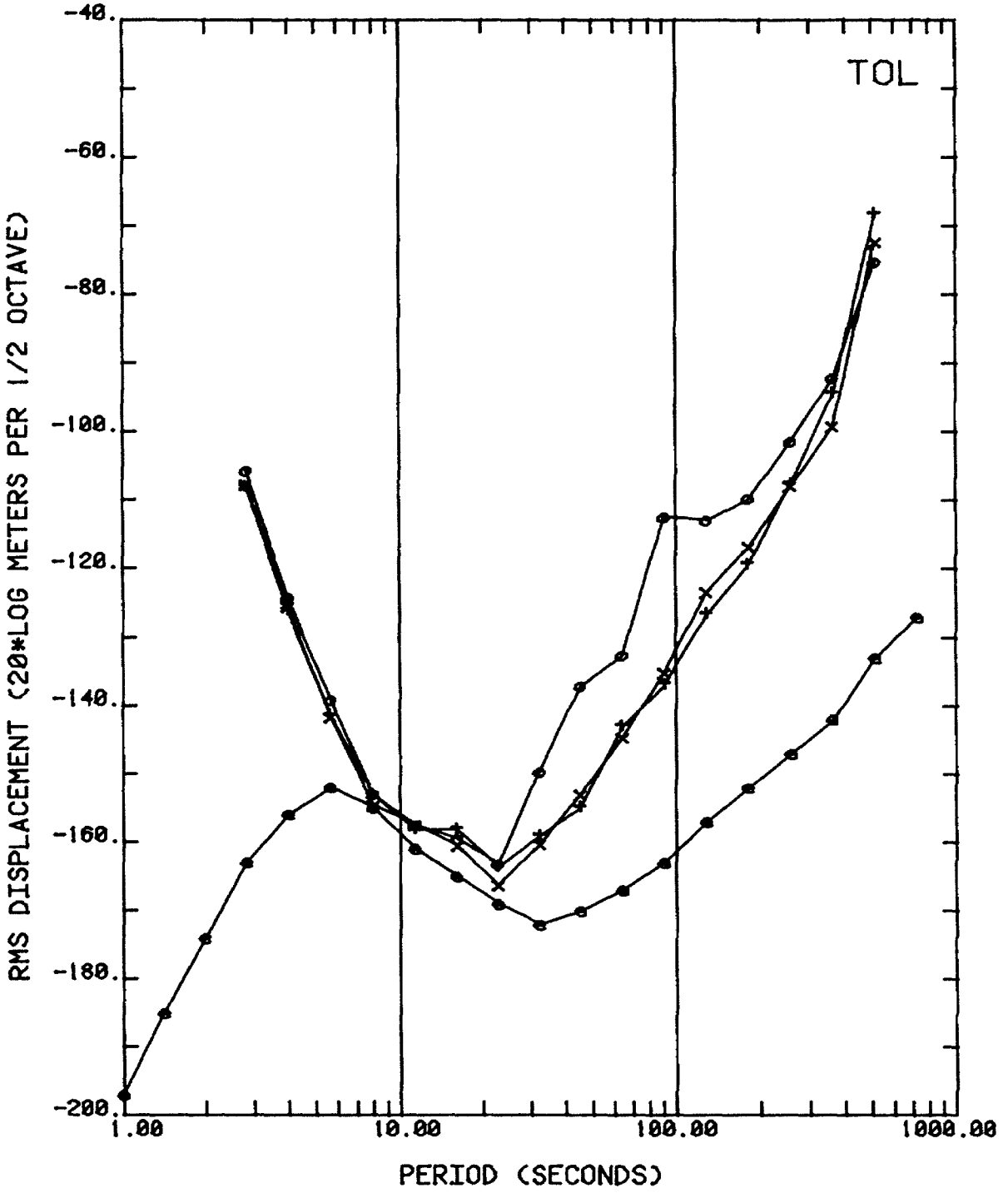

Figure 5.18.--Long-period noise spectra computed from Toledo data. Curves labeled '+', 'o', and 'x' represent vertical, north, and east components, and curve labeled 'e' represents earth noise model.

6. LINEARITY AND DISTORTION

6.1 General

All measuring systems, including seismographs, are affected by nonlinearities. From the standpoint of data analysis, the most obvious effect of a system nonlinearity is amplitude distortion, especially the catastrophic form of amplitude distortion that occurs when the system is driven beyond its operating range and "clips". Unfortunately, this condition is not always apparent from the waveform because a signal clipped in an early stage may be smoothed by subsequent filtering. For this reason, clip level sensors have been installed in the DWWSS systems and data records are flagged when the signal levels in the most sensitive stages approach to within 6 dB of full scale (see Table 2.1). Over most of the DWWSS data bands, clipping occurs in the electronics rather than the seismometers. The threshold of clipping at the input to the ADC is 10.24 volts peak, 16,384 digital counts at the output of the ADC. Amplitude distortion that occurs within the normal operating range of the DWWSS system is not a significant problem since the curvature of the input-output amplitude response curve is less than 1% at full scale.

A second important manifestation of system nonlinearity is the generation of spurious signals (distortion products) that can limit the useful operating range of the seismograph to something less than the resolution of the digital encoder. This effect of nonlinearity has become important only with the advent of high-resolution digital seismograms; hence, the causes, effects, and measurement of intermodulation distortion in seismographs are not well documented. Appropriate background theory related to nonlinear circuits is given by Russell (1962) and Sunde (1969); H.B. Durham (1979, unpublished data) considered the effect of distortion in the design of the RSTN system, and Peterson and others (1980) describe the results of tests for distortion on the SRO system.

The effects of nonlinearity in a seismograph will be considered using the simple model shown in Figure 6.1 where the output can be expressed as the power series

$$e = a_1 x + a_2 x^2 + a_3 x^3 + a_4 x^4 + \ldots\ldots$$

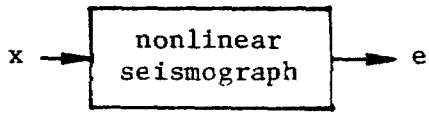

Figure 6.1

In an actual seismograph, the situation is far more complex, as the nonlinearities will occur independently in the seismometer, different stages of the amplifier/filter, and possibly in the analog-to-digital converter. However, the model above is used only to define nonlinear behaviour, not as a representation of an actual system. If the input is sinusoidal; that is, if

$$x = X\cos\omega t$$

where X is the peak value, the output will be

$$e = a_1 X\cos(\omega t)+a_2 X^2\cos^2(\omega t)+a_3 X^3\cos^3(\omega t)+a_4 X^4\cos^4(\omega t)+.....$$

An expansion of the first four terms in the series leads to the expression

$$e = A_{dc} + A_f\cos(\omega t) + A_{2f}\cos(2\omega t) + A_{3f}\cos(3\omega t) + A_{4f}\cos(4\omega t)$$

where

$$A_{dc} = \frac{a_2 X^2}{2} + \frac{3a_4 X^4}{8} \qquad \text{(DC component)}$$

$$A_f = a_1 X + \frac{3a_3 X^3}{4} \qquad \text{(first harmonic)}$$

$$A_{2f} = \frac{a_2 X^2}{2} + \frac{a_4 X^4}{2} \qquad \text{(second harmonic)}$$

$$A_{3f} = \frac{a_3 X^3}{4} \qquad \text{(third harmonic)}$$

$$A_{4f} = \frac{a_4 X^4}{8} \qquad \text{(fourth harmonic)}$$

These terms represent the peak amplitudes of the DC component and harmonics when $\cos(n\omega t) = 1$. Higher order terms in the series would generate additional harmonics and decrease or increase the amplitude of lower harmonics depending upon the sign of the coefficients. It is not often possible to measure ampli-

tudes of higher harmonics in a waveform that contains the fundamental signal. Therefore, it is convenient to express the distortion products in units of power, where $P = \frac{1}{2}A^2$, so that

$$P_f = \tfrac{1}{2}A_f^2$$

$$P_{2f} = \tfrac{1}{2}A_{2f}^2$$

and so forth. Then, if sufficient resolution exists in the recorder, it is possible to measure relative power levels of the harmonics through spectral analysis of the waveform.

A distortion level can be defined as the ratio (in decibels) of the power of the higher order harmonic to the power of the first harmonic.

$$D_{nf} = 10 \log \frac{P_{nf}}{P_f} \qquad n = 1,2,3..... \tag{6.1}$$

If only a second-order nonlinearity exists,

$$D_{2f} = 10 \log \frac{a_2^2 X^2}{4a_1^2}$$

The distortion level depends upon the value of the quadratic coefficient and the peak input amplitude. It is convenient to compute the coefficients as the ratio a_2/a_1 or, equivalently, assume that the system power gain is unity. For quadratic nonlinearity, at full scale (i.e., X = 1), the coefficient of the quadratic term, distortion level, and deviation from a linear input/output line are related by equation 6.1 as follows:

a_2/a_1	distortion level	deviation
.02	-40 dB	1%
.002	-60 dB	.1%
.0002	-80 dB	.01%

Equipment specifications for linearity are often expressed as a percentage deviation from a straight line. Ideally, the distortion level will be lower than the resolution of the digital encoder (-66 dB or less for an 11-bit encoder and -90 dB or less for a 15-bit encoder); otherwise, a large-amplitude, broadband input signal will generate broadband noise that may limit the

effective resolution of the system. There are instances where the recorded waveform may contain distortion even though the amplitude of higher harmonics is below the resolution of the digital encoder. This can occur, for example, if a signal from a nonlinear broadband system is passed through narrow band filters before digitization and recording. If the input signal consists of two or more sinusoids, an expansion of the power series will result in the generation of difference signals that can appear as resolvable noise in a recorded band that does not contain the fundamental signals. This situation exists in the SRO system; in fact, it is the basis for the two-frequency distortion test (see Peterson and others, 1980).

The measurement of nonlinearity is not as straightforward and precise as we would like it to be. The most direct approach would be to accurately measure the output of the system while driving or offsetting it through its full range, and use the result to determine the polynomial coefficients using a curve-fitting technique. In practice, this is difficult because of background noise and limits of measurement accuracy imposed by recorder resolution. A second approach is to measure the distortion that results when the system is driven by a sine wave applied through the calibration coil. This requires that the recording system have sufficient accuracy to resolve distortion products (which one might hope is not possible in a well-designed system). This approach was used with some success for the linearity tests on the DWWSS system. It is a relatively simple test to perform, but the results are not conclusive because it is not possible to differentiate between distortion that may be generated in the signal generator, the calibrator, and in the seismograph signal path. In order to isolate the distortion produced within the seismograph, an additional test was made by driving the seismometer in free period. This is a more definitive test, but in a worst-case sense because it was necessary to drive the seismometers through higher amplitudes than they are driven in normal operation. Test results are presented as PSD in units of volts^2/Hz at the input to the ADC. Data segments processed were 2048 points in length. Mean values and linear trend were removed, a cosine-tapered window applied, then the PSD estimates were obtained using an FFT. The amplitude of the sine-wave drive was adjusted to produce approximately $\pm$ 2 volts at the input to the ADC, which is 1/5 of full scale (X = .2). The tests were made on a test system. We can only hope that the results are representative of the results that

would be obtained from operating systems in the network.

6.2 Short-Period Test Results

To serve as a benchmark, the short-period background noise that appears at the input to the ADC is shown in Figure 6.2 for normal operating sensitivity. The background is predominately earth noise above a period of .25 seconds and least-count noise below .25 seconds (except for the spectral peaks at .22 and .12 seconds period, which are cultural in origin).

The PSD obtained from a waveform containing a fundamental 1 Hz sine wave is shown in Figure 6.3. The sine wave, produced in a function generator, was applied to the calibrator of the short-period vertical component Benioff seismometer. The first nine harmonics of the fundamental can be clearly identified (a fact that puts to question the common practice of assuming that harmonics higher than second order are negligible). However, it is not known where the distortion products are being generated. Figure 6.4 shows the PSD estimates obtained when the short-period seismometer is oscillating in free period. This is a very robust test of the seismometer linearity. In order to sustain the oscillation, it was necessary to place a high impedance (100K ohms) in series between the seismometer and amplifier. As a result, the seismometer had to be driven at an amplitude approximately five times the amplitude that would normally clip the system electronics. In this test the power of the even harmonics is slightly less with respect to the fundamental than in the first test, which seems to indicate that the even harmonics are being generated principally in the system electronics and that there was distortion from the function generator during the first test. The seismometer generates odd harmonics. However, when the seismometer is operating in its normal range, the level of odd harmonics is lower, as indicated in Figure 6.3. Figure 6.3 represents worst-case distortion since it includes a contribution from the function generator and perhaps the calibrator. In this figure, the ratio of second-order power to fundamental power is -68 dB. Then for full scale, the second-order distortion level would be -54 dB with respect to the fundamental. A similar free-period test was made on a Teledyne Geotech Model S-13 short-period seismometer, a type used at several of the DWWSSN stations. The results, shown in Figure 6.5, indicate that the distortion level may be slightly lower when using this seismometer.

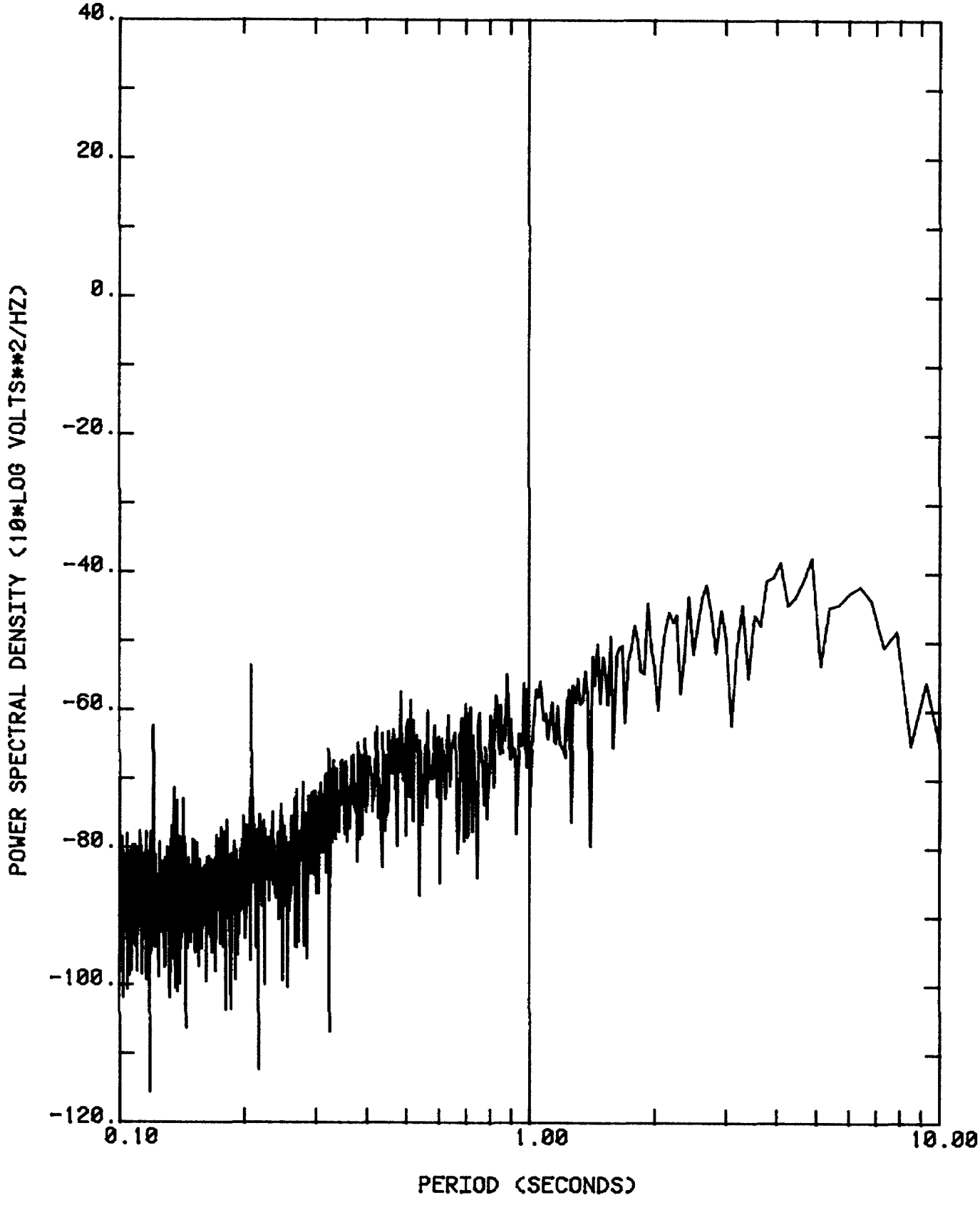

Figure 6.2.--Albuquerque test system short-period noise PSD as it appears at the input to the ADC.

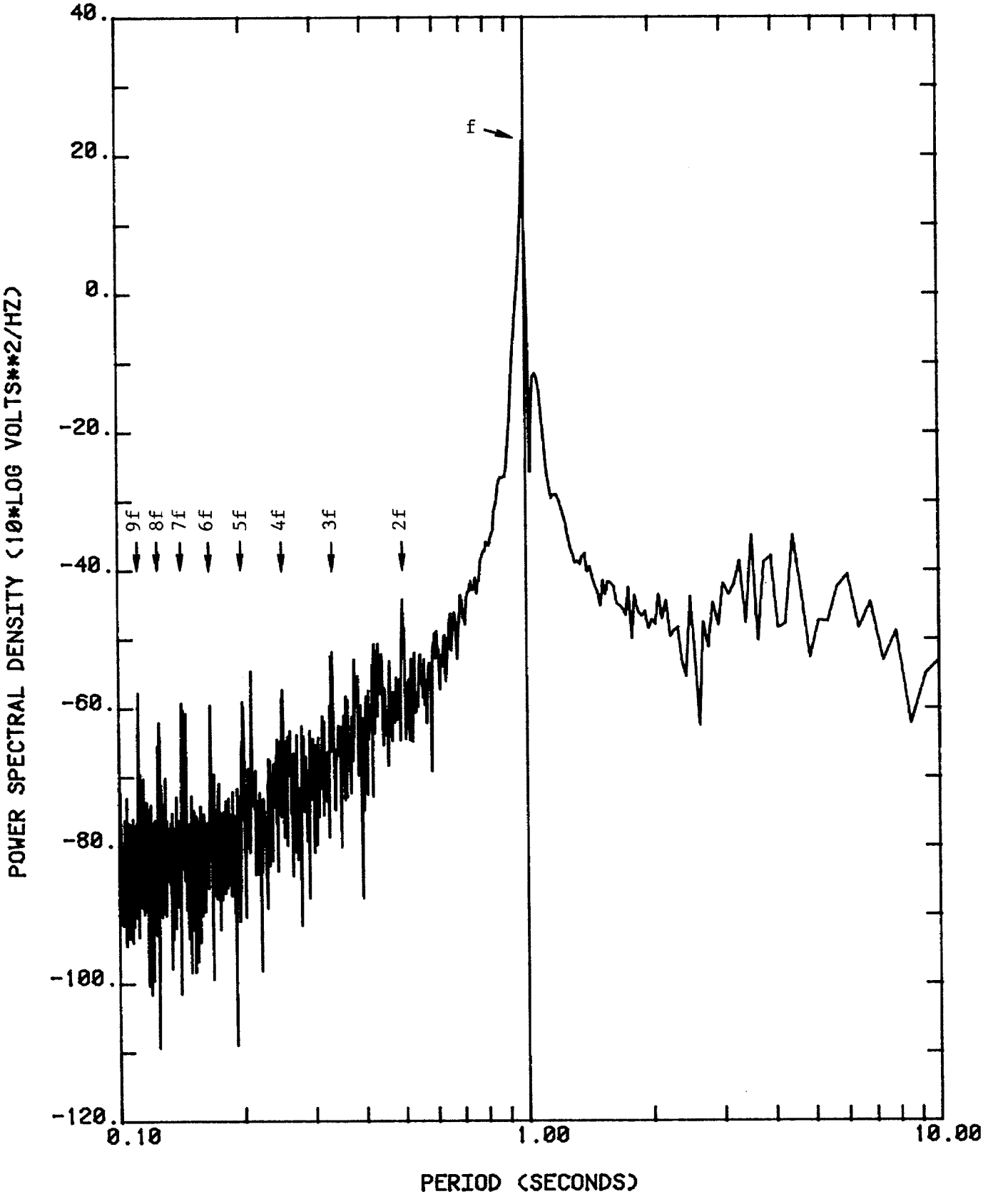

Figure 6.3.--Power spectral density computed from waveform recorded when a 1 Hz sine wave is applied through calibrator of DWWSS short-period (Benioff) system.

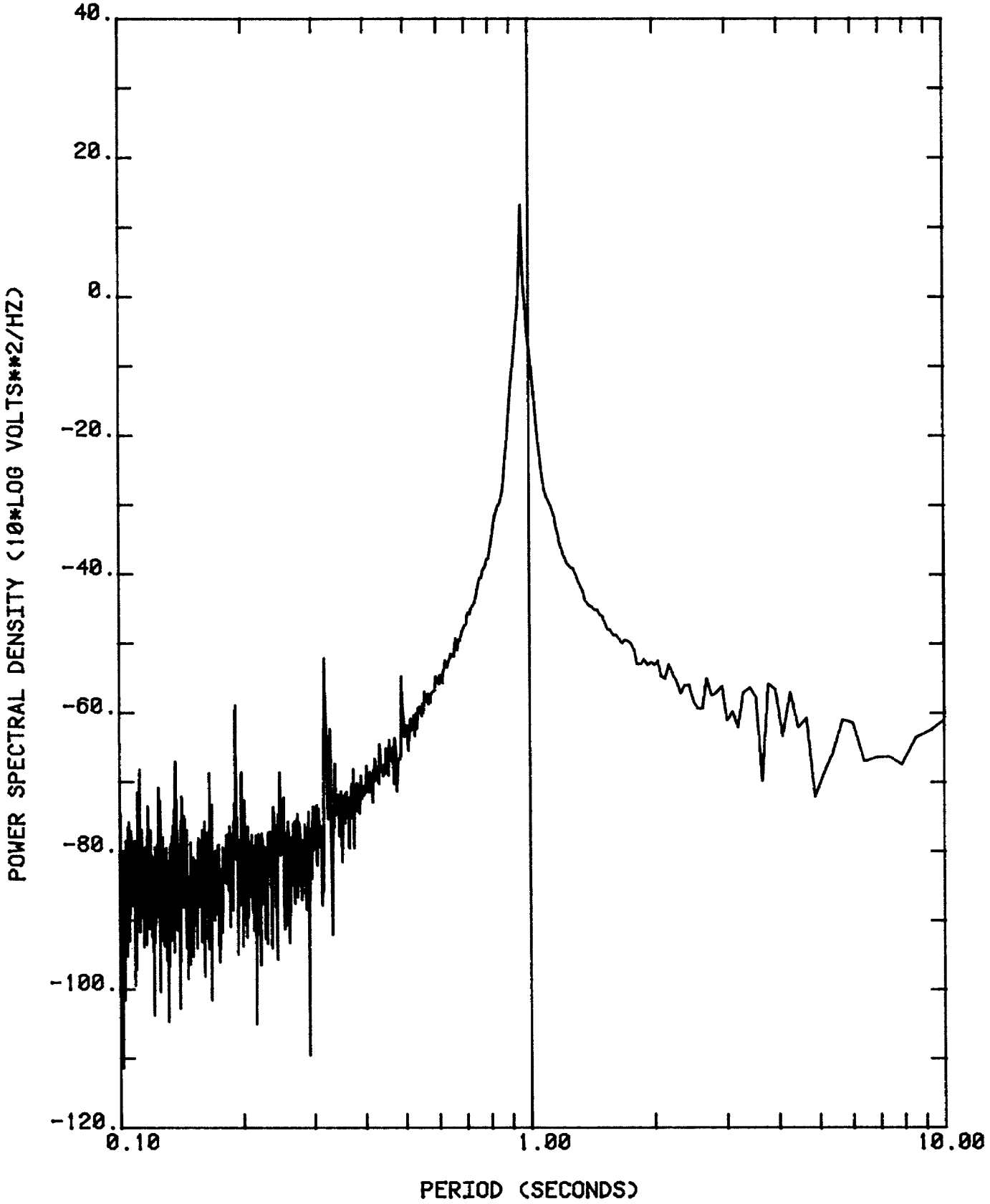

Figure 6.4.--Power spectral density computed from waveform recorded when Benioff seismometer is oscillating in free period. (Apparently, the period of the test seismometer was not precisely 1 second.)

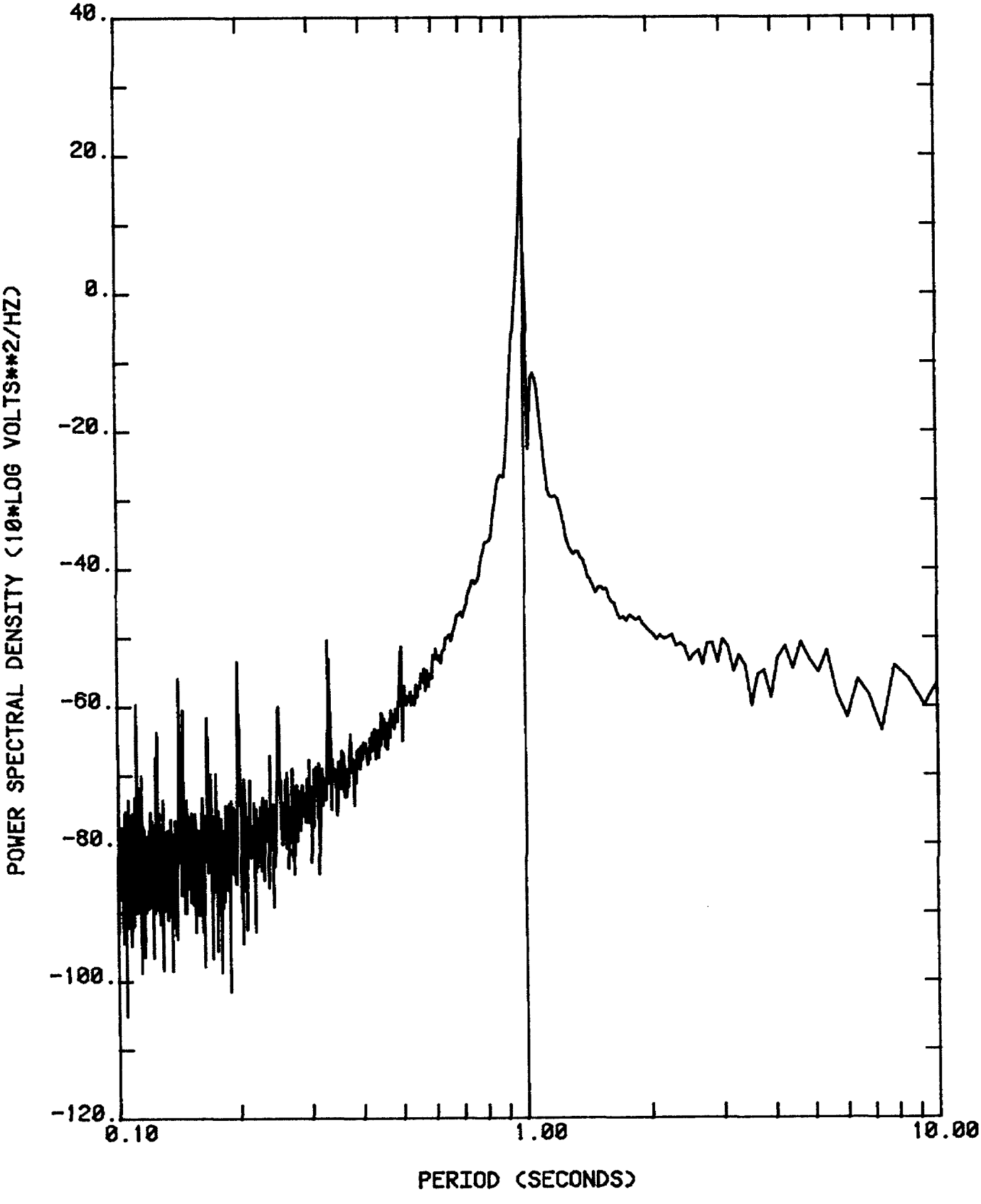

Figure 6.5.--Power spectral density computed from waveform recorded when S-13 seismometer is oscillating in free period.

6.3 Intermediate-Period Test Results

The same sequence of tests was made on the DWWSS intermediate-period channels. Typical background PSD at the input to the ADC is shown in Figure 6.6. The noise is due to random LSB oscillations below a period of about 2 seconds and to earth motion above 2 seconds. In the test data, the noise level is somewhat higher because it was necessary to increase the gain of the IP filters in order to produce the desired voltage (± 2 volts) at the input to the ADC.

PSD estimates obtained from waveforms containing a 1-Hz calibration signal are shown in Figures 6.7 through 6.9 for the three components. The second through fifth harmonics are clearly identifiable. Again, this is a worst-case demonstration because some of the distortion may not be generated in the seismograph signal circuit. In the second test, the long-period seismometers were driven in free period (15 seconds) at a large amplitude (about 1 mm peak to peak) in order to generate a sufficiently large signal through a high series impedance. Because of the relatively large air damping in the long-period seismometers, it was necessary to apply a signal from the function generator through the calibrator to sustain the oscillations. The drive signal was small in amplitude (1 ma peak to peak) so any distortion products produced in the signal generator would not be resolvable. The PSD estimates obtained from this test on the system using Sprengnether seismometers are shown in Figures 6.10 through 6.12. An identical test was made on the system using Teledyne Geotech long-period seismometers which are operated at several of the DWWSSN stations, and the results are shown in Figures 6.13 and 6.14. The second- and third-order distortion products are clearly related to the seismometers with little contribution from the IP filters. The Sprengnether vertical has third-order but almost no second-order distortion, while the Sprengnether horizontals produce both second- and third-order distortion. The SL 210 (vertical) seismometer appears to have a strong quadratic nonlinearity when driven through a large amplitude and the SL 220 (horizontal) produces very little distortion. In this test, the long-period seismometers are driven to about the amplitude at which the IP channels clip during normal operation. Hence, the distortion shown in the figures should represent full-scale distortion. The distortion level is about -60 dB for the Sprengnether system, -52 dB for the SL 210, and -72 dB for the SL 220 system.

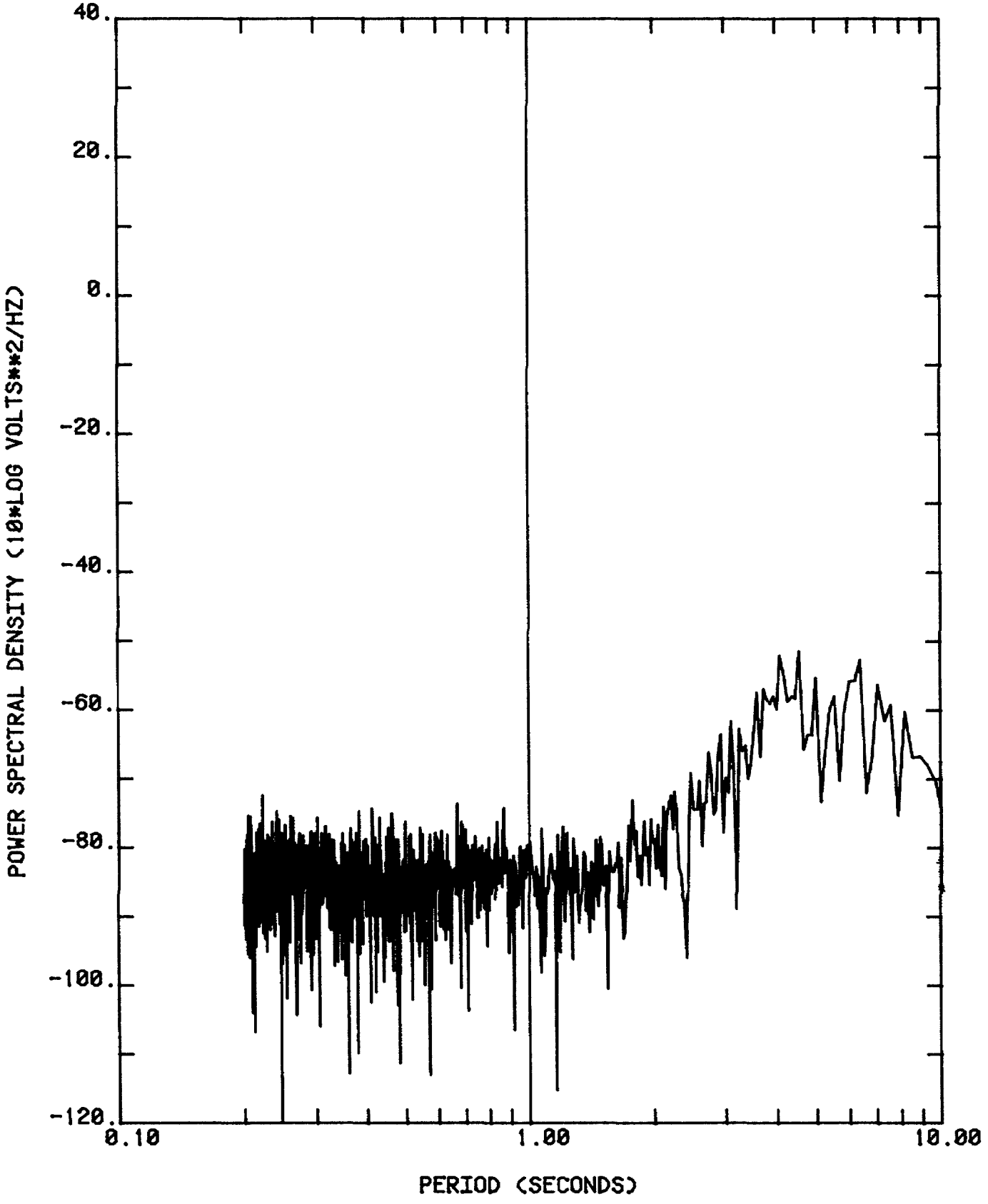

Figure 6.6.--Typical intermediate-period background noise at ALO as seen at the input to the ADC.

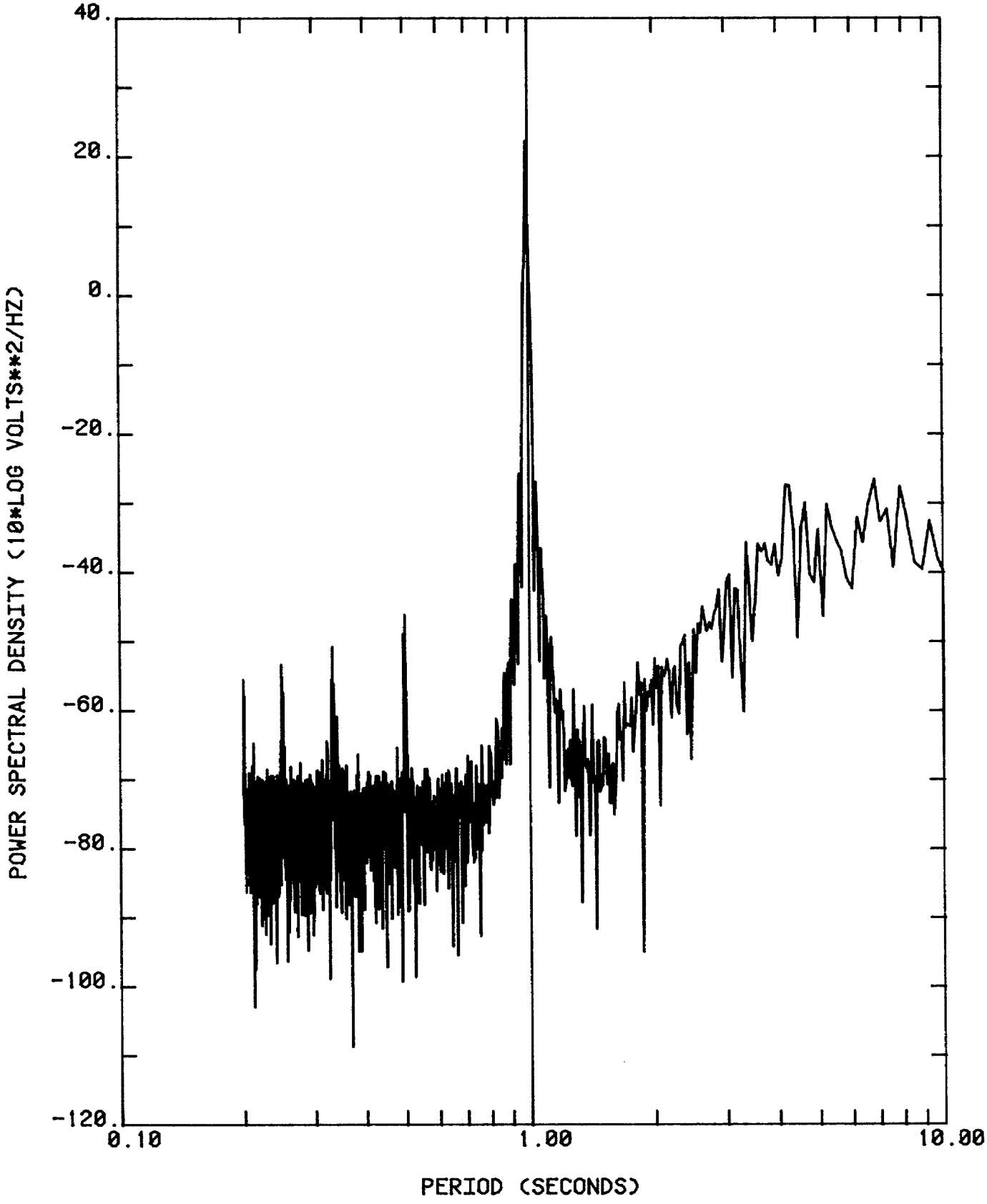

Figure 6.7.--Power spectral density computed from IPZ waveform containing a 1-Hz sine wave applied through calibrator.

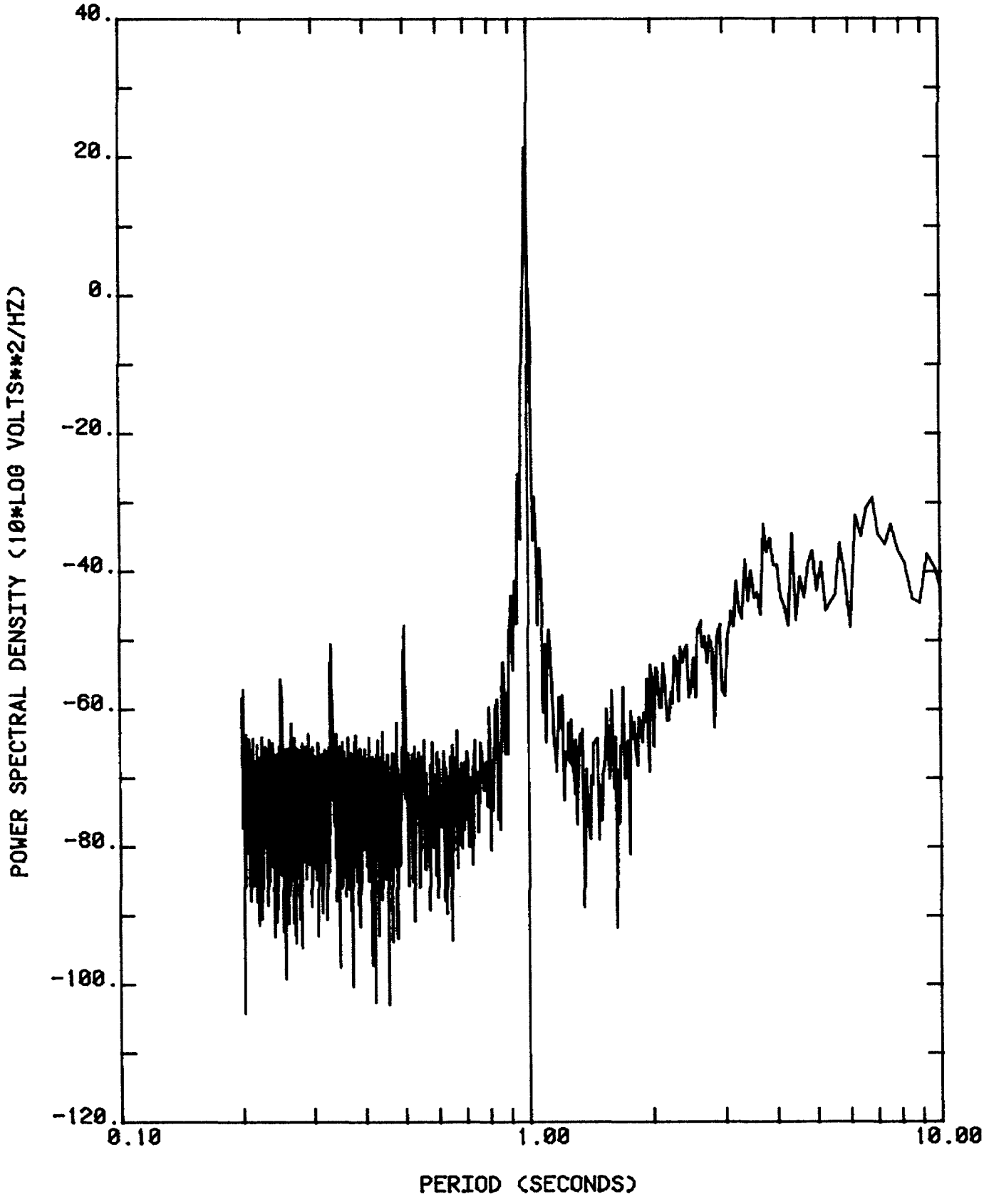

Figure 6.8.--Power spectral density computed from IPN waveform containing a 1-Hz sine wave applied through calibrator.

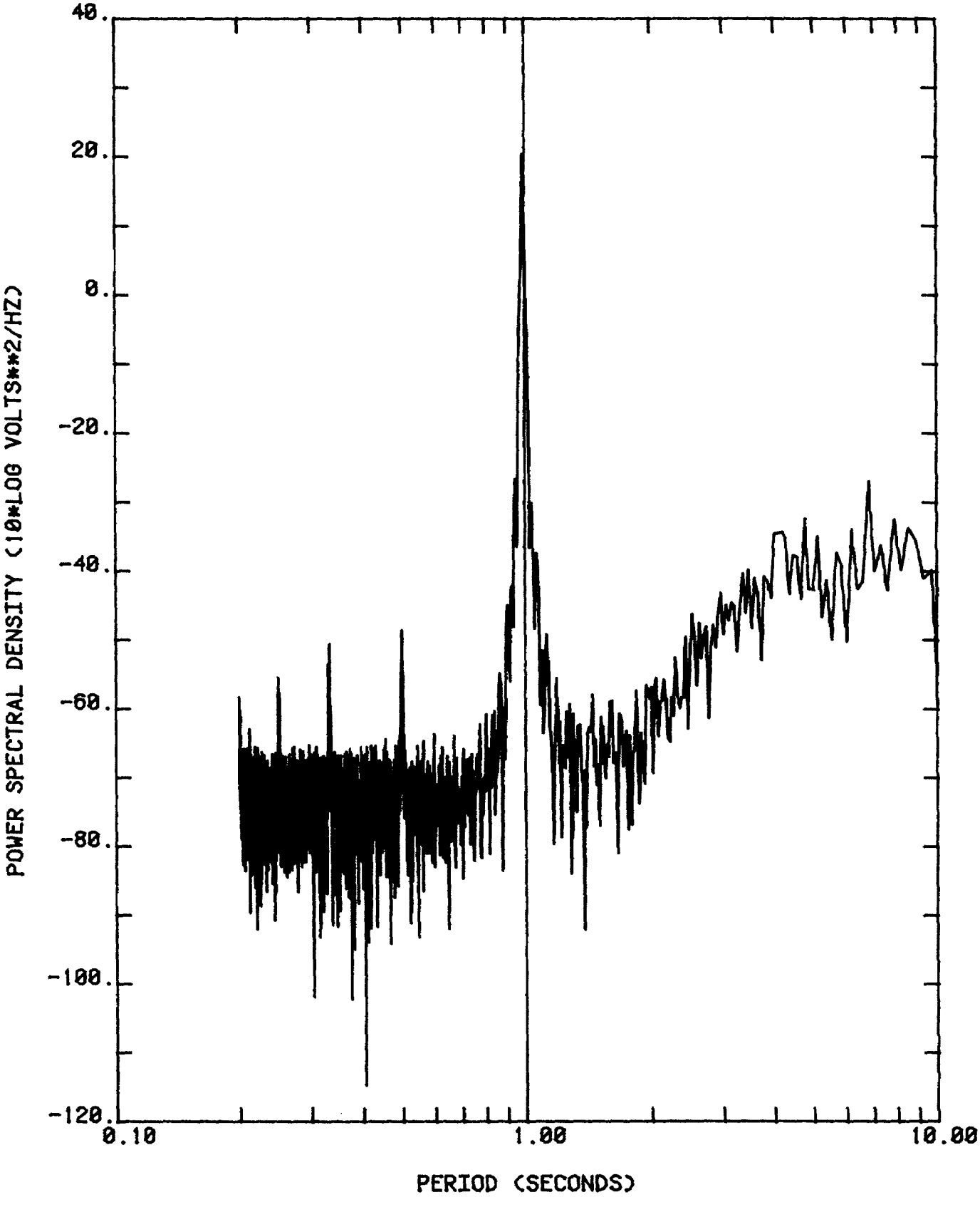

Figure 6.9.--Power spectral density computed from IPE waveform containing a 1-Hz sine wave applied through calibrator.

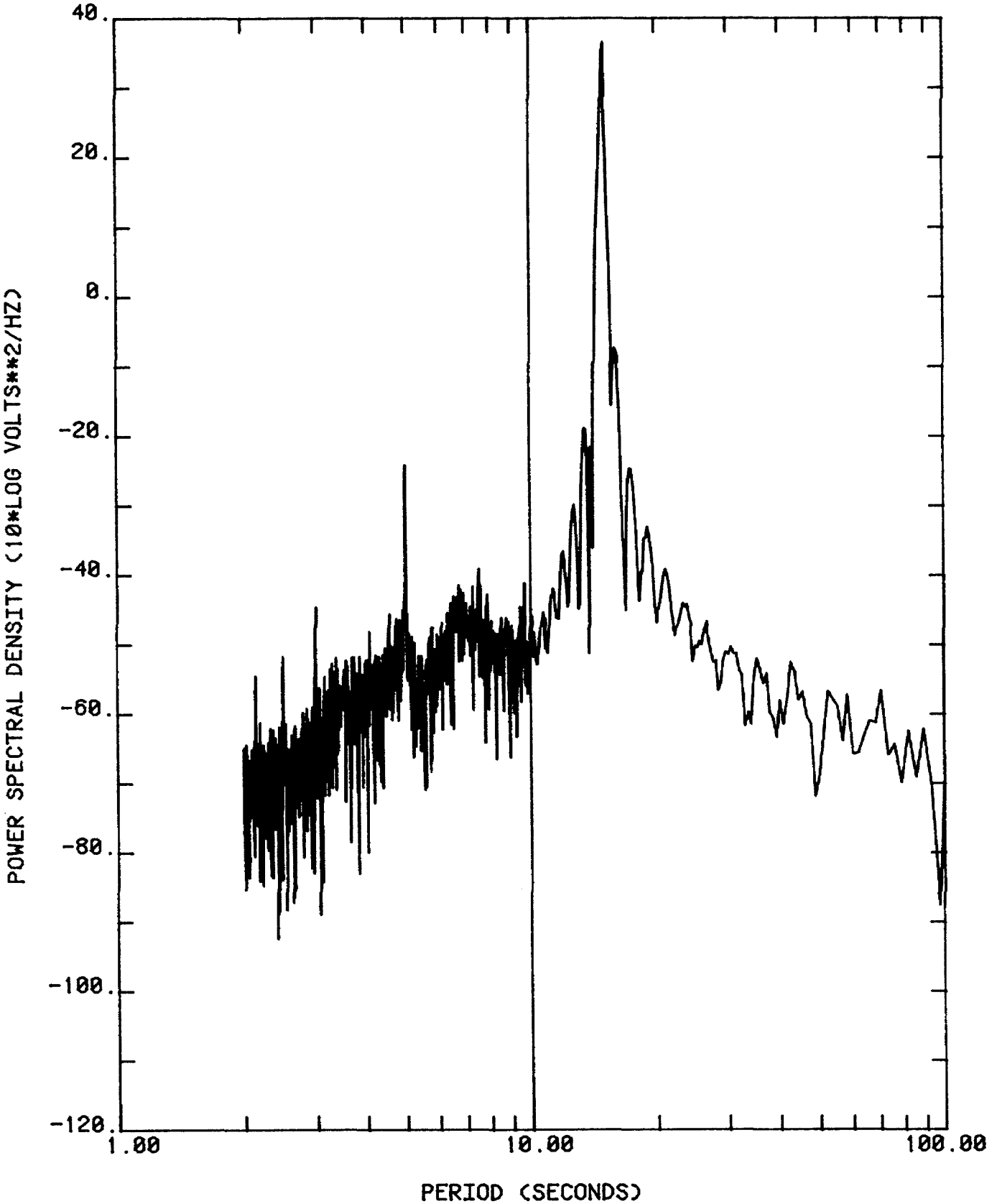

Figure 6.10.--Power spectral density computed from IPZ waveform when Sprengnether seismometer is oscillating in free period.

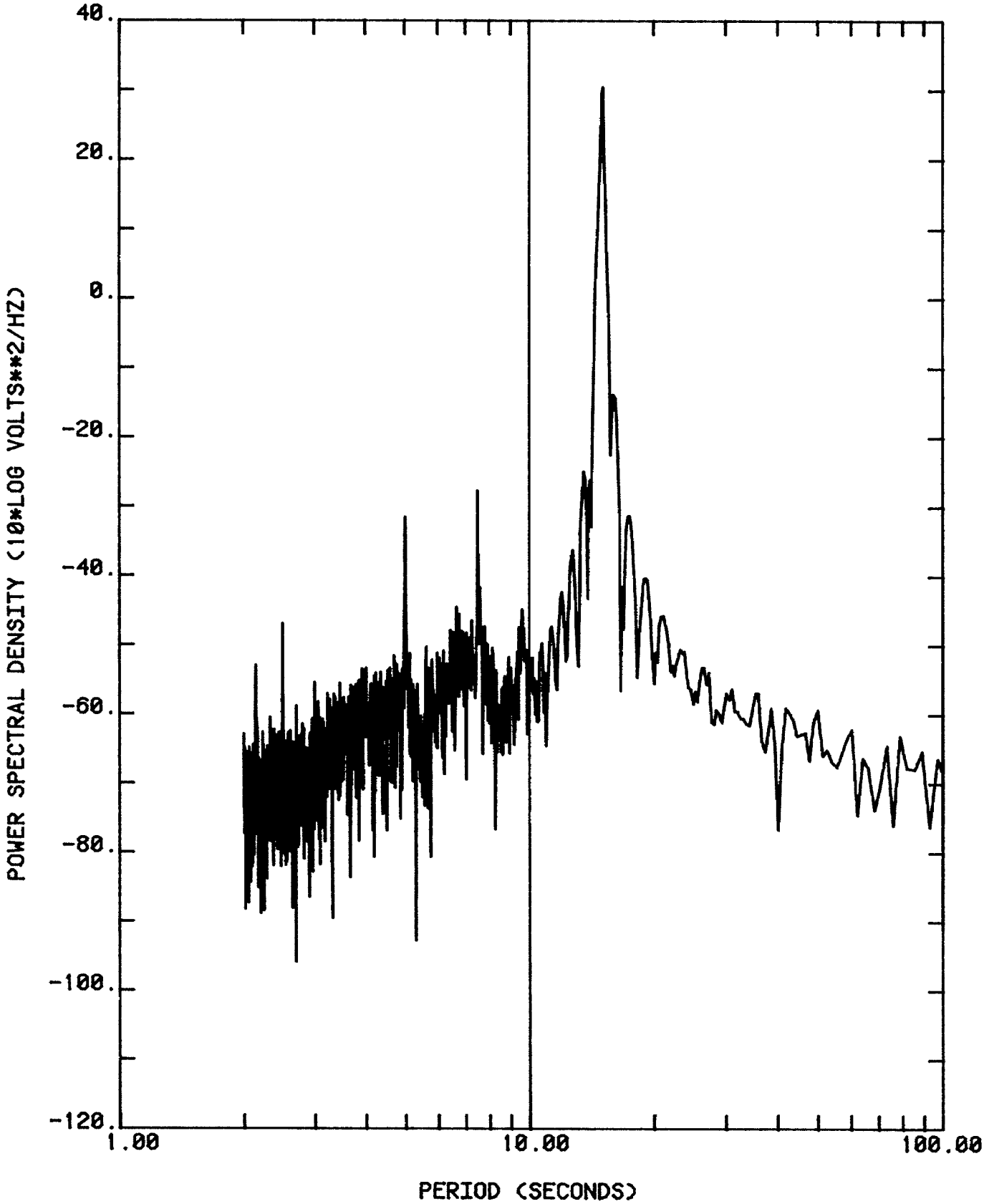

Figure 6.11.--Power spectral density computed from IPN waveform when Sprengnether seismometer is oscillating in free period.

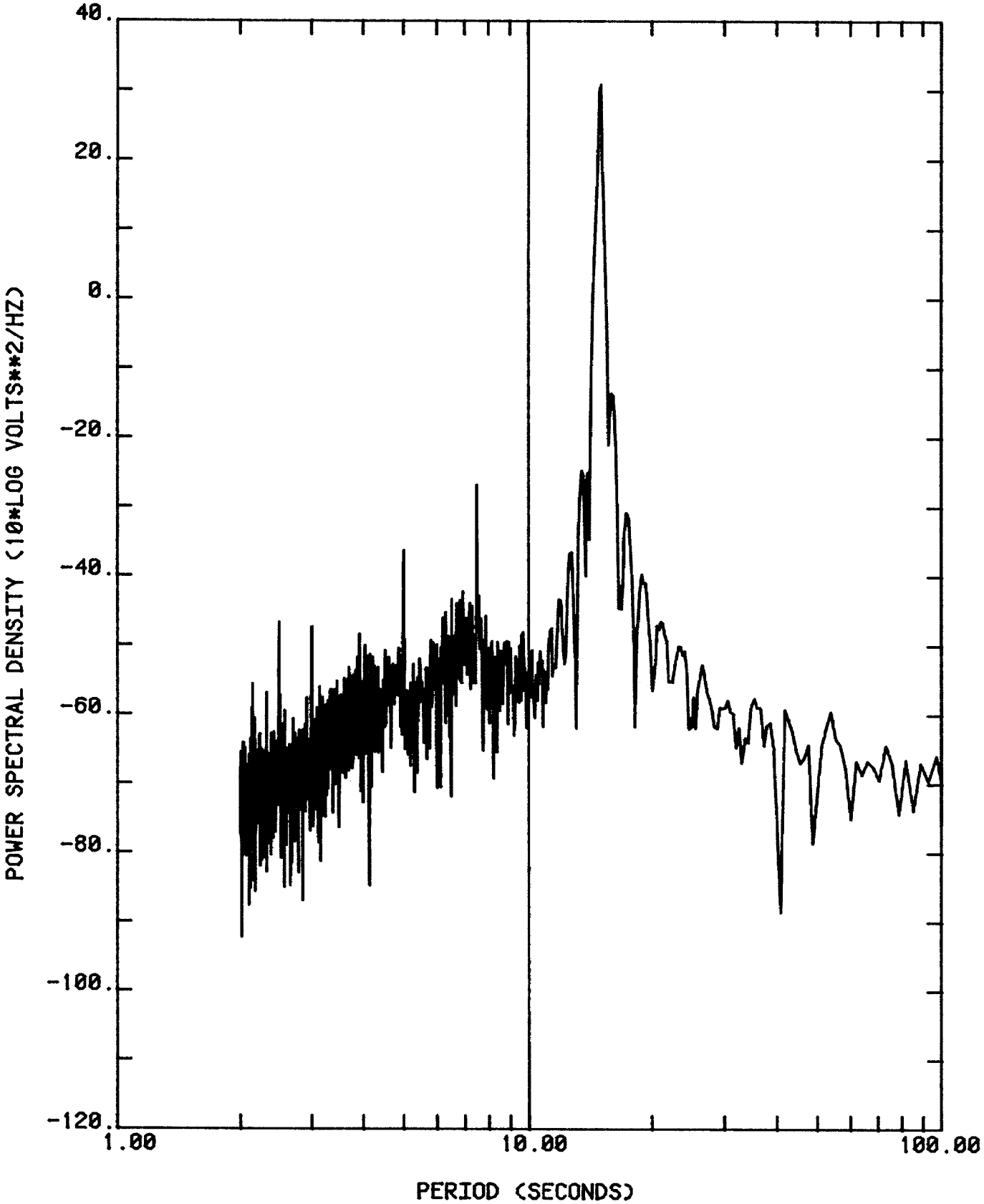

Figure 6.12.--Power spectral density computed from IPE waveform when Sprengnether seismometer is oscillating in free period.

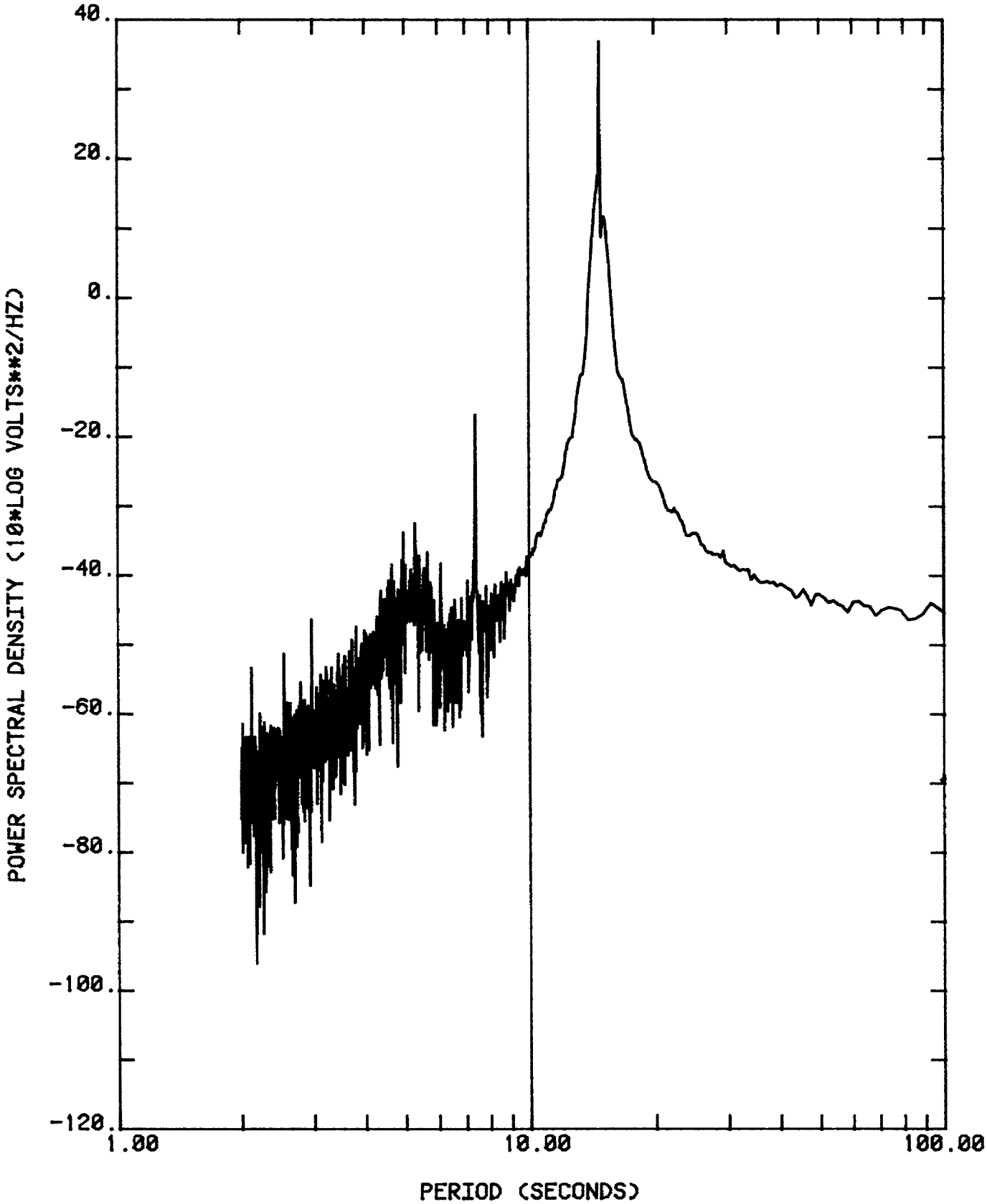

Figure 6.13.--Power spectral density computed from IPZ waveform when SL 210 seismometer is oscillating in free period.

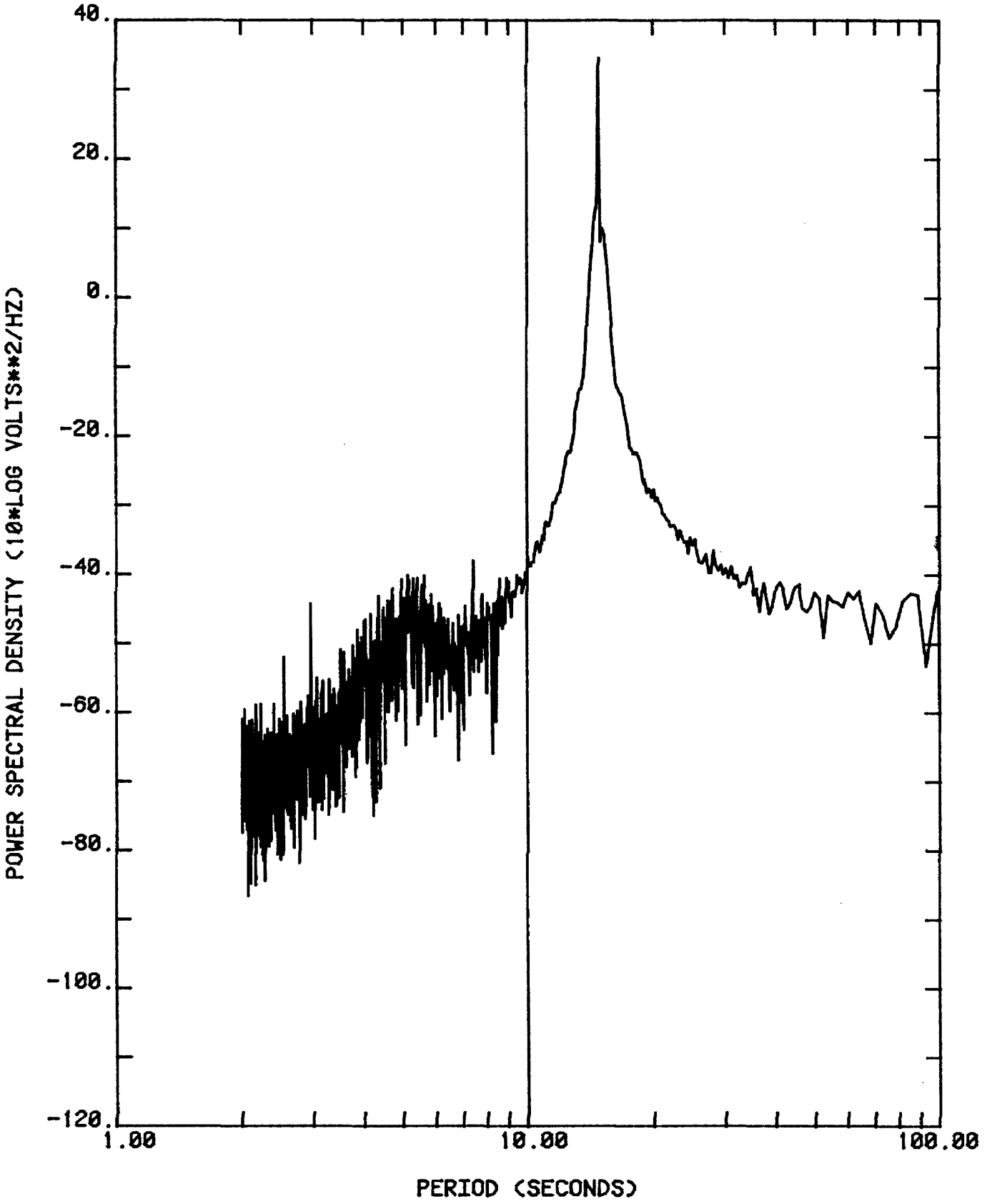

Figure 6.14.--Power spectral density computed from IPH waveform when SL 220 seismometer is oscillating in free period.

6.4 Long-Period Test Results

Only the free-period test was performed on the DWWSS long-period system. A very small dither signal was used to sustain the oscillations; the dither signal was of much smaller amplitude than in the IP tests. The test results are shown in Figures 6.15 through 6.17 for the long-period system using the Sprengnether seismometers and in Figures 6.18 and 6.19 for the system using the SL 210 and SL 220 seismometers. The observed distortion is due mostly to third and higher order terms. The level is about -80 dB in all of the tests. This translates to a full-scale distortion level of -68 dB.

6.5 Conclusions

The linearity tests described in this report are not precise measurements, but they have produced reasonable estimates of the distortion levels that may be observed when signal levels approach full scale. Equipment being developed by Gould, Inc. (1982), including a very low distortion oscillator and a high resolution (120 dB) encoder, should make it possible to routinely and accurately measure the linearity of seismographs. Clearly, this is an important test that should become a standard procedure in the test and evaluation of digital seismographs.

The distortion levels observed in the SP, IP, and LP tests are higher than one would hope to see but not unexpected in view of the fact that the DWWSS seismometers were designed long before high resolution digital recording became available. The distortion measured in these tests would not have been observed in an analog record and may not have been observed in a digital record with only 11-bit resolution. The fact that we can see the distortion in the DWWSS system (whenever the signal is within approximately 30 dB of full scale) leads one to question the value of using a 16-bit fixed-point data word, as opposed to a gain-ranged data word with less resolution but greater recording range. The higher resolution is only exploitable when the signal level is within 20 to 30 dB of full scale, yet, in the case of the DWWSS system and probably most conventional seismographs, this is the region in which intermodulation distortion appears as a self-generating noise. The point is illustrated in Figure 6.20, which shows the effective signal resolution of the DWWSS SP channel as a function of the signal level at the input to the ADC. Usable resolution is the difference between instrument noise

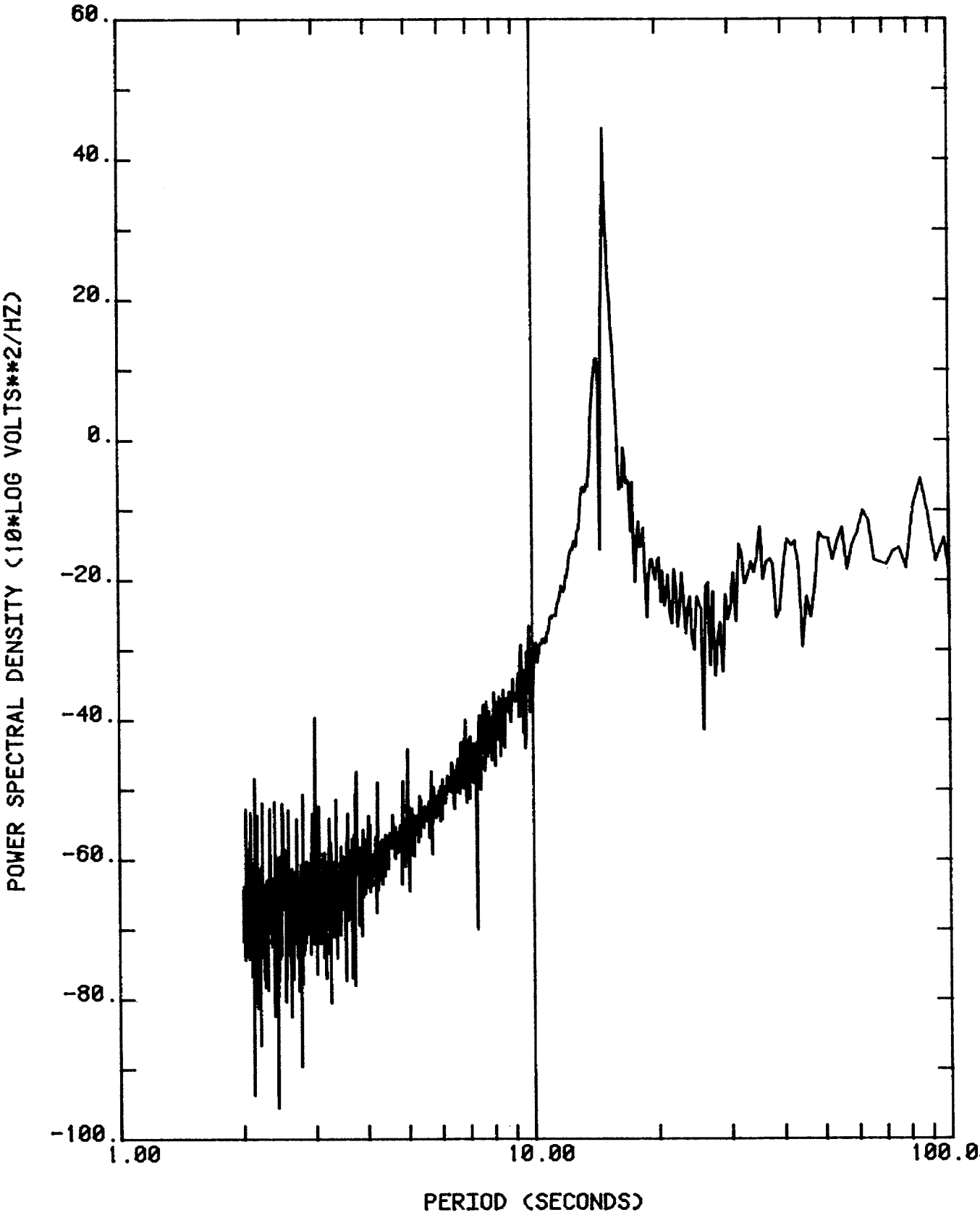

Figure 6.15.--Power spectral density computed from LPZ waveform when Sprengnether seismometer is oscillating in free period.

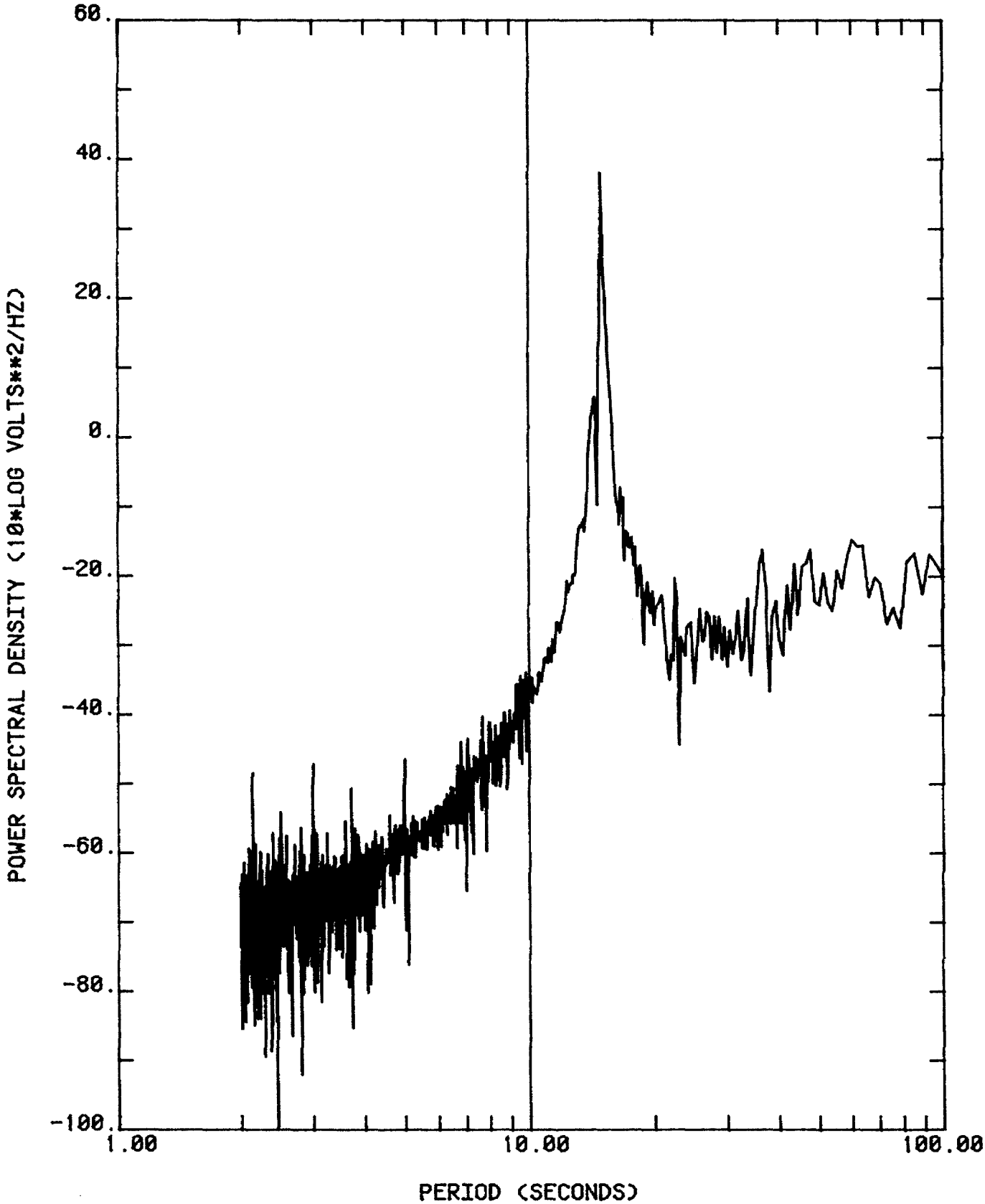

Figure 6.16.--Power spectral density computed from LPN waveform when Sprengnether seismometer is oscillating in free period.

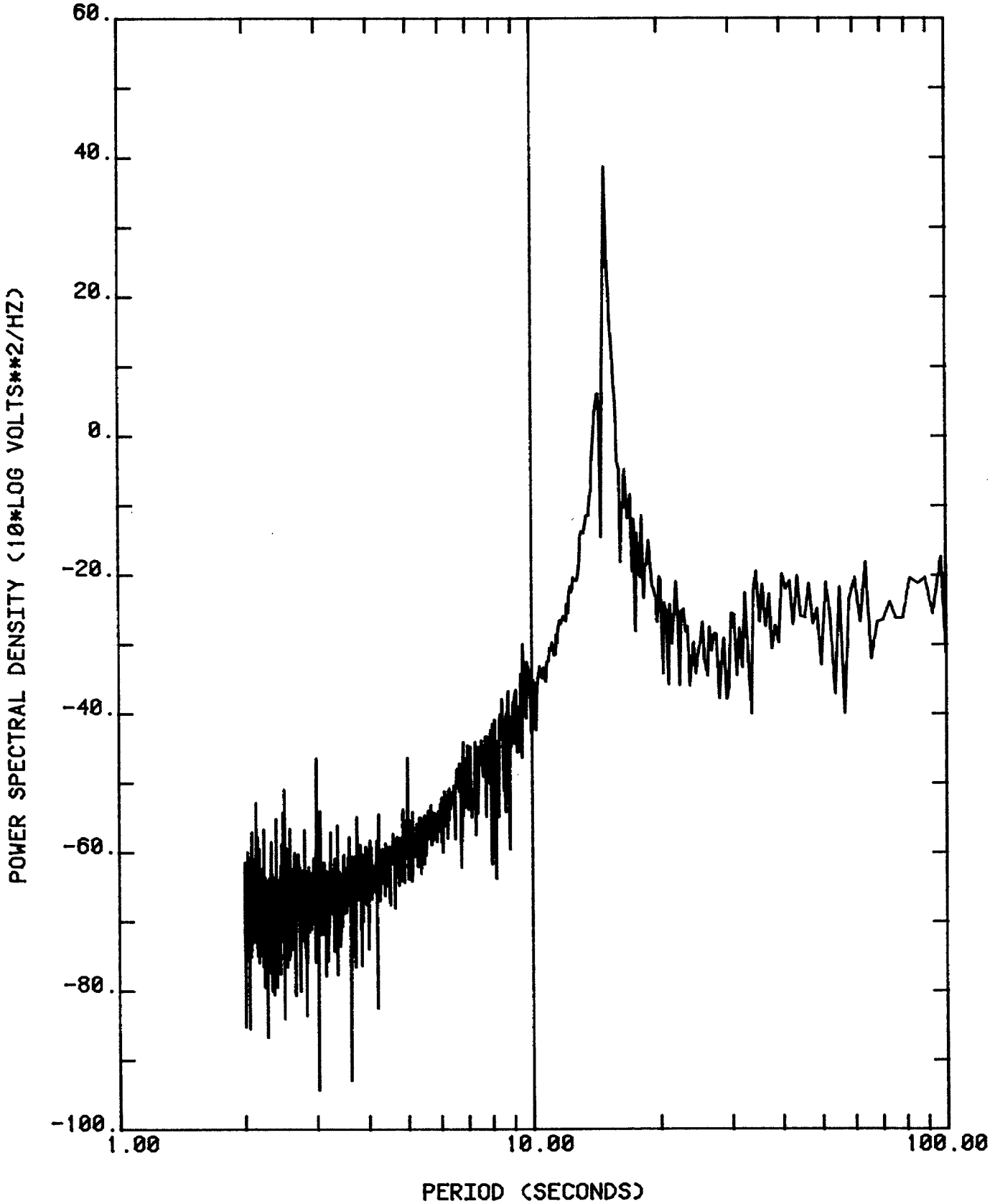

Figure 6.17.--Power spectral density conputed from LPE waveform when Sprengnether seismometer is oscillating in free period.

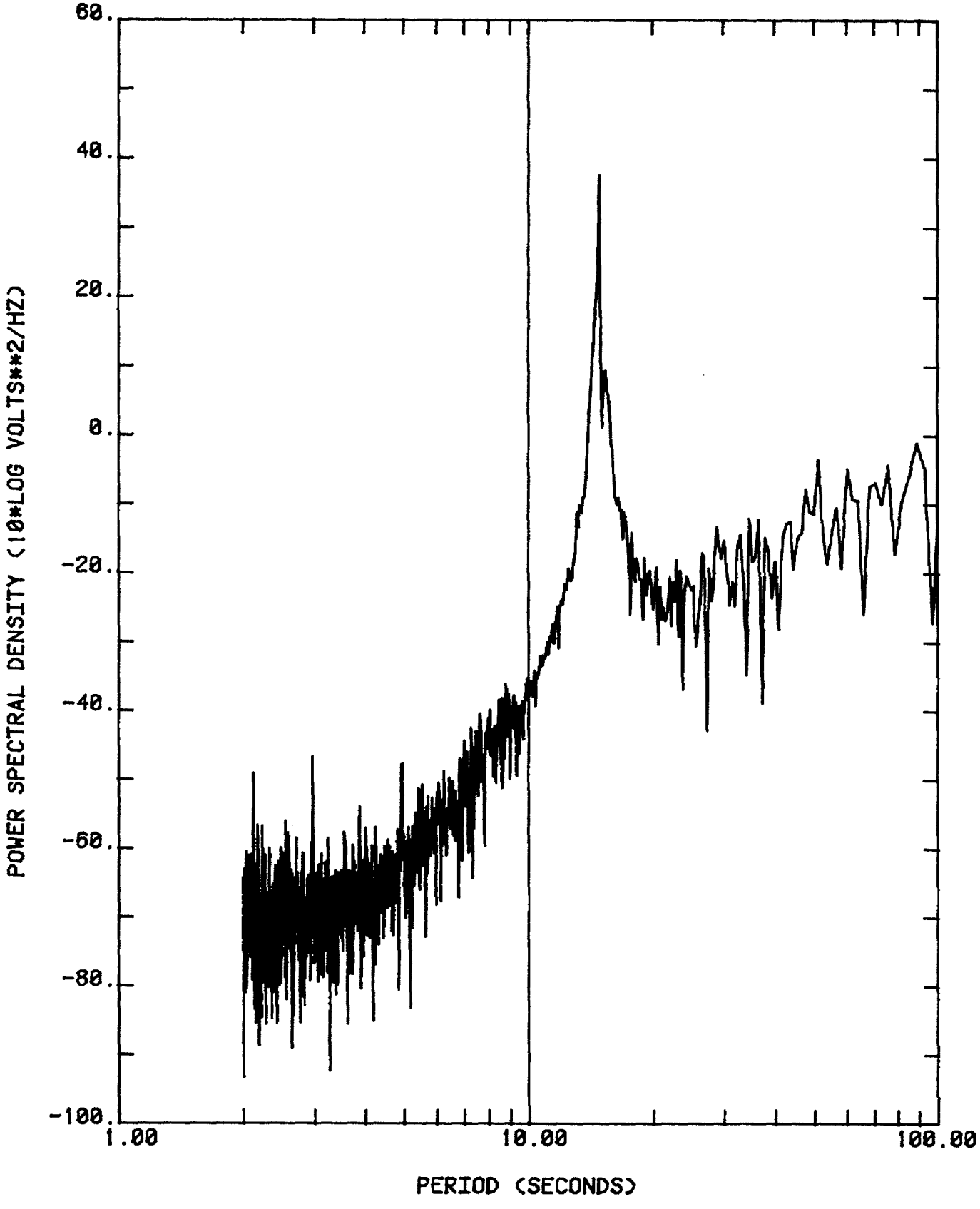

Figure 6.18.--Power spectral density computed from LPZ waveform when SL 210 seismometer is oscillating in free period.

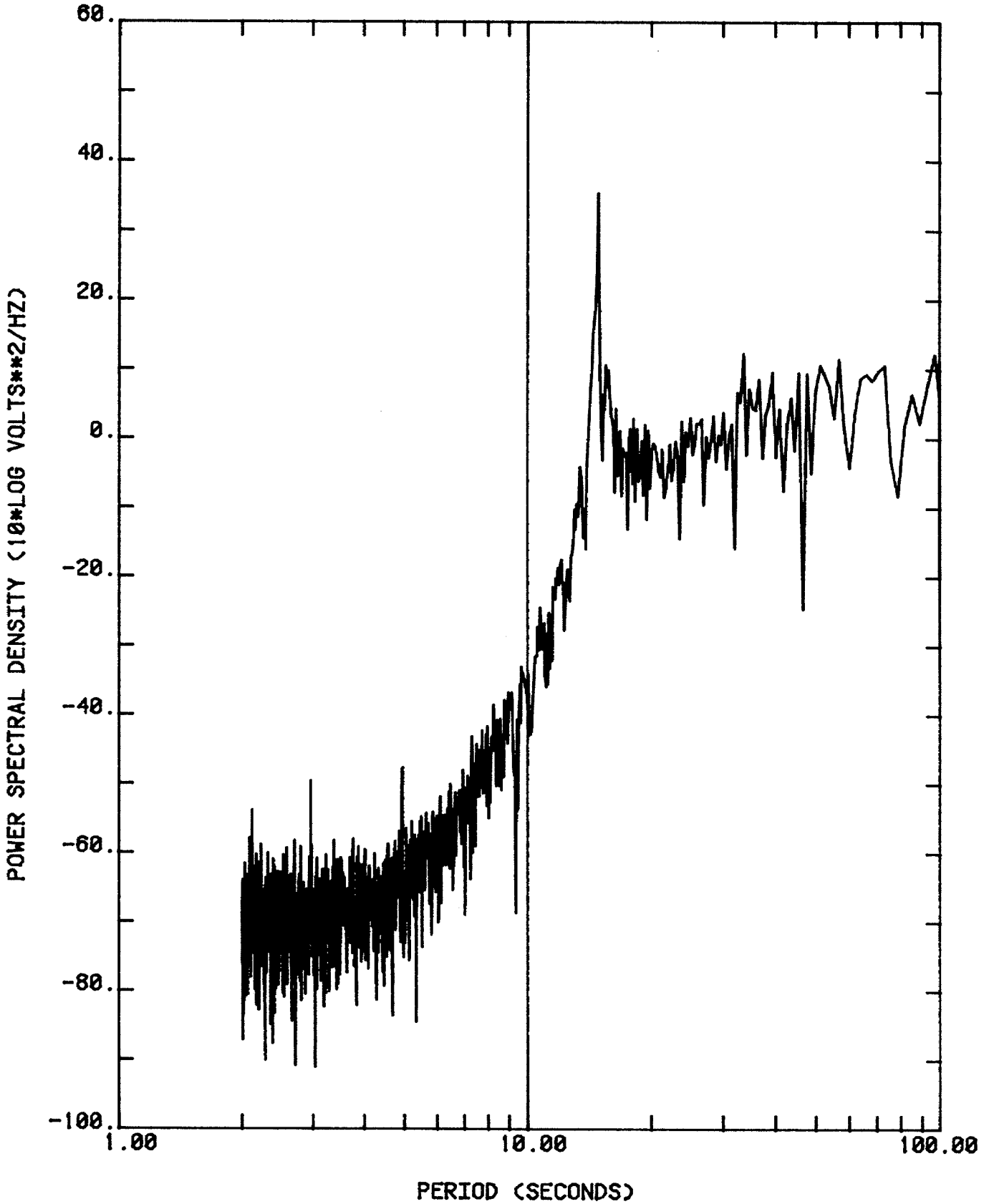

Figure 6.19.--Power spectral density computed from LPH waveform when SL 220 seismometer is oscillating in free period.

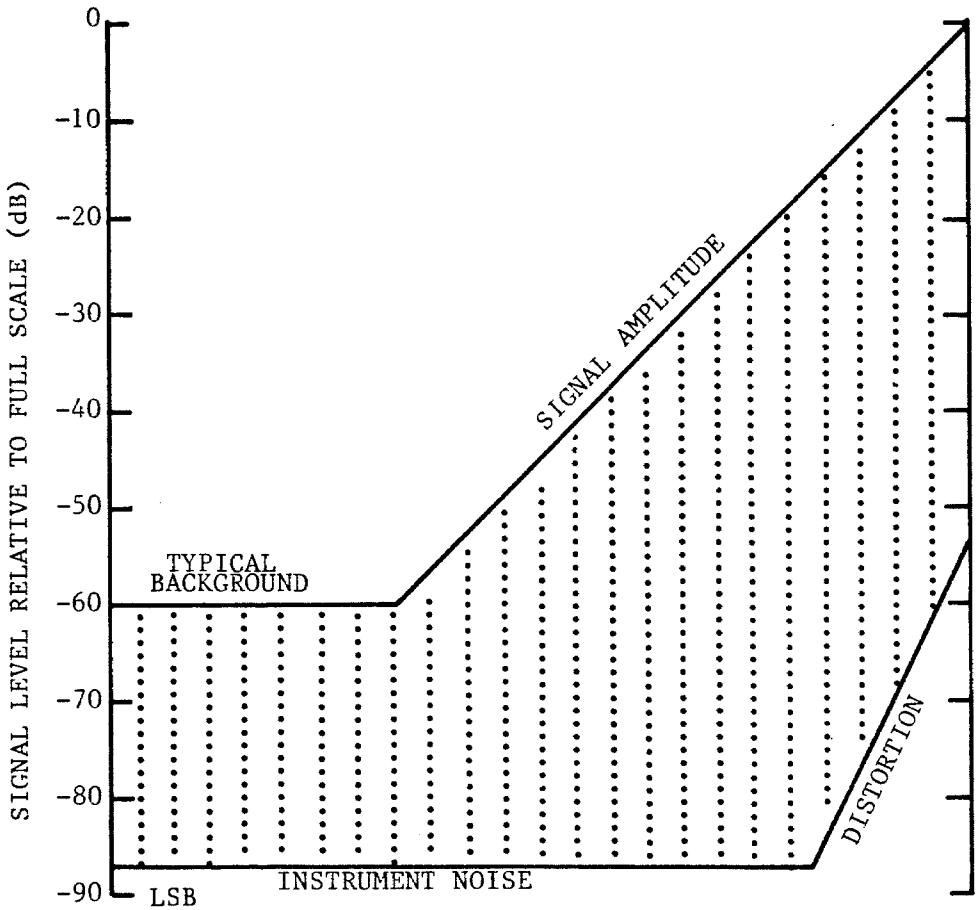

Figure 6.20.--Effective signal resolution (stippled area) for DWWSS short-period channel as function of signal level at input to the ADC.

and total signal amplitude. Over most of the range, the effective resolution is considerably less than the 90 dB resolution of the encoder. In the upper 20 dB of signal range, the effective resolution is limited by distortion. An optimally designed gain-ranged encoder could provide nearly the same effective resolution over the entire signal range plus an additional 30 dB of operating range. On the other hand, without the 15-bit resolution of the DWWSS encoder, we would have been unable to measure the distortion and arrive at this conclusion.

7. REFERENCES

Agnew, D.C. and J. Berger, 1978. Vertical seismic noise at very low frequencies, *J. Geophys. Res.*, 83, 5420-5424.

Berg, E. and D.M. Chesley, 1976. Automated high-precision amplitude and phase calibration of seismic systems, *Bull. Seism. Soc. Am.*, 66, 1413-1424.

Durham, H.B., 1982. Incoherence of seismic signals from closely spaced KS-36000 seismometers, *Sandia National Laboratories System Research Report*, 68 p.

Engdahl, E.R., Chairman, 1977. *Global earthquake monitoring: its uses, potentials, and support requirements*, report of the Panel on Seismograph Networks, Committee on Seismology, National Research Council, Washington, D.C., 75 p.

Espinosa, A.F., G.H. Sutton, and H.J. Miller, 1962. A transient technique for seismograph calibration, *Bull. Seism. Soc. Am.*, 52, 767-780.

Espinosa, A.F., G.H. Sutton, and H.J. Miller, 1965. A transient technique for seismograph calibration - manual and standard set of theoretical transient responses, Geophysics Laboratory, Institute of Science and Technology, University of Michigan.

Gould, Inc., 1982. Enhanced delta modulation encoder - its design, capabilities, and usage, Gould, Inc. Defense Electronics Division, Glen Burnie, Md.

Hoffman, J.P., 1980. The global digital seismograph network-day tape, *U.S. Geological Survey Open-File Report* 80-289, 37 p.

Jarosch, H. and A.R. Curtis, 1973. A note on the calibration of the electromagnetic seismograph, *Bull. Seism. Soc. Am.*, 63, 1145-1155.

Kolesnikov, Yu. A., and M.N. Toksoz, 1981a. Estimation of long-period seismic noise based on its correlation with pressure and temperature (in Russian), *Computational Seismology*, 14, 170-183.

Kolesnikov, Yu. A., and M.N. Toksoz, 1981b. Instrumental reduction of atmospheric noise for long-period vertical seismometers (in Russian), *Computational Seismology*, 14, 183-189.

Li, T., 1981. Lajitas quiet site noise study, Teledyne Geotech Technical Report 81-10.

McConigle, R.W. and P.W. Burton, 1980. Accuracy in LP electromagnetic seismograph calibration by least-squares inversion of the calibration pulse, *Bull. Seism. Soc. Am.*, 70, 2261-2273.

Mitchell, B.J. and M. Landisman, 1969. Electromagnetic seismograph constants by least-squares inversion, *Bull. Seism. Soc. Am.*, 59, 1335-1348.

Mitronovas, W., 1976. Accuracy in phase determination of LP electromagnetic seismographs based on transient calibration pulse, *Bull. Seism. Soc. Am.* 66, 97-104.

Peterson, J., 1980. Preliminary observations of noise spectra at the SRO and ASRO stations, *U.S. Geological Survey Open-File Report* 80-992, 25 p.

Peterson, J., C.R. Hutt, and L.G. Holcomb, 1980. Test and calibration of the seismic research observatory, *U.S. Geological Survey Open-File Report* 80-187, 86 p.

Russell, G.M., 1962. *Modulation and coding in information systems,* Prentice Hall, Inc., New York.

Sunde, E.D., 1979. *Communications systems engineering theory,* John Wiley & Sons, Inc., New York, 512 p.

Stearns, S.D., 1979. Applications of the coherence function in comparing seismometers, *Sandia National Laboratories Report* 79-1633, 33 p.

Teledyne Geotech, 1980a. Operation and maintenance manual: seismic amplifier/filter assembly model 43490, Teledyne Geotech, Inc., Garland, Texas.

Teledyne-Geotech, 1980b. Operation and maintenance manual: preamplifier and galvanometer interface model 43310, Teledyne Geotech, Inc., Garland, Texas.

Teledyne Geotech 1980c. Operation and maintenance manual: long-period filter model 43480, Teledyne Geotech, Inc., Garland, Texas.

Zirbes, M. and R.P. Buland, 1981. Network-day tape software users guide, *U.S. Geological Survey Open-File Report* 81-666, 213 p.